



Graduate School in Civil Engineering
Dottorato di Ricerca in Ingegneria Civile

Sede: Facoltà di Ingegneria - Università di Pavia - via Ferrata 1 - 27100 Pavia - Italy

Dottorato di Ricerca in Ingegneria Civile XVII Ciclo

Damage Detection and Localization
in the Space of the Observed Variables

Ph.D. Thesis

Eng. Sara Casciati

Advisor:

Dr. Eng. George Magonette

Revisor:

Prof. Armando Gobetti

February, 2005

To all my family:

Fabio & Lucia,

Thomas,

Aldo & Celestina.

Dottorato di Ricerca in Ingegneria Civile

| | |
|--|--|
| Settore: | Ingegneria |
| Sede Amministrativa non consortile: | Università degli Studi di PAVIA |
| Durata del dottorato in anni: | 3 |
| Numero studenti: | 3 ogni anno |
| Periodo formativo estero in mesi: | come previsto dal regolamento del Dottorato di Ricerca |
| Numero minimo di corsi: | 6 |

Recapiti



Dipartimento di Meccanica Strutturale
via Ferrata 1 - 27100 Pavia - Italy
Tel. 0382 / 505450 Fax 0382 / 528422



Dipartimento di Ingegneria Idraulica e Ambientale
via Ferrata 1 - 27100 Pavia - Italy
Tel. 0382 / 505300 Fax 0382 / 505589

Coordinatore

CASCIATI Fabio - Professore Ordinario di Scienza delle Costruzioni (H07A)

Dipartimento di Meccanica Strutturale
via Ferrata 1 - 27100 Pavia – Italy Tel. 0382 / 505458 Fax 0382 / 528422
e-mail: fabio@dipmec.unipv.it

Collegio dei Docenti

- CAUVIN Aldo - Professore Ordinario di Teoria e Progetto delle Costruzioni in Calcestruzzo Armato e Precompresso (H07B)
- CIAPONI Carlo - Professore Associato di Idraulica (H01A)
- FARAVELLI Lucia - Professore Ordinario di Sicurezza e Affidabilità delle Costruzioni (H07A)
- FUGAZZA Mario - Professore Associato di Sistemazione dei Bacini Idrografici (H01B)
- GOBETTI Armando - Professore Associato di Dinamica delle Strutture (H07A)
- MACCHI Giorgio - Professore Ordinario di Tecnica delle Costruzioni (H07B)
- MOISELLO Ugo - Professore Ordinario di Idrologia (H01B)
- PAPIRI Sergio - Professore Associato di Infrastrutture Idrauliche (H01B)
- SALA Roberto - Professore Associato di Macchine (H04C)

Organizzazione del corso

Il dottorato di ricerca in *Ingegneria Civile* presso la Facoltà di Ingegneria dell'Università degli Studi di Pavia è stato istituito nell'anno accademico 1994/95 (X ciclo).

Il corso consente al dottorando di scegliere tra due curricula: idraulico o strutturale. Egli svolge la propria attività di ricerca rispettivamente presso il Dipartimento di Ingegneria Idraulica e Ambientale o quello di Meccanica Strutturale.

Durante i primi due anni sono previsti almeno sei corsi, seguiti da rispettivi esami, che il dottorando è tenuto a sostenere. Il Collegio dei Docenti, composto da professori dei due Dipartimenti, organizza i corsi con lo scopo di fornire allo studente di dottorato opportunità di approfondimento su alcune delle discipline di base per entrambe le componenti, idraulica e strutturale. Corsi e seminari vengono tenuti da docenti di Università nazionali ed estere.

Il Collegio dei Docenti, cui spetta la pianificazione della didattica, si è orientato ad attivare ad anni alterni corsi sui seguenti temi:

- Meccanica dei solidi e dei fluidi
- Metodi numerici per la meccanica dei solidi e dei fluidi
- Rischio strutturale e ambientale
- Metodi sperimentali per la meccanica dei solidi e dei fluidi
- Intelligenza artificiale

più corsi specifici di indirizzo.

Al termine dei corsi del primo anno il Collegio dei Docenti assegna al dottorando un tema di ricerca da sviluppare sotto forma di tesina entro la fine del secondo anno; il tema, non necessariamente legato all'argomento della tesi finale, è di norma coerente con il curriculum, scelto dal dottorando (idraulico o strutturale).

All'inizio del secondo anno il dottorando discute con il Coordinatore l'argomento della tesi di dottorato, la cui assegnazione definitiva viene deliberata dal Collegio dei Docenti.

Alla fine di ogni anno i dottorandi devono presentare una relazione particolareggiata (scritta e orale) sull'attività svolta. Sulla base di tale relazione il Collegio dei Docenti, "previa valutazione della assiduità e dell'operosità dimostrata dall'iscritto", ne propone al Rettore l'esclusione dal corso o il passaggio all'anno successivo.

Il dottorando può svolgere attività di ricerca sia di tipo teorico che sperimentale, grazie ai laboratori di cui entrambi i Dipartimenti dispongono, nonché al Laboratorio Numerico di Ingegneria delle Infrastrutture.

Il "Laboratorio didattico sperimentale" del Dipartimento di Meccanica Strutturale dispone di:

1. una tavola vibrante che consente di effettuare prove dinamiche su prototipi strutturali;
2. opportuni sensori e un sistema di acquisizione dati per la misura della risposta strutturale;
3. strumentazione per la progettazione di sistemi di controllo attivo e loro verifica sperimentale;
4. strumentazione per la caratterizzazione dei materiali, attraverso prove statiche e dinamiche.

Il laboratorio del Dipartimento di Ingegneria Idraulica e Ambientale dispone di:

1. un circuito in pressione che consente di effettuare simulazioni di moto vario;
2. un tunnel idrodinamico per lo studio di problemi di cavitazione;
3. canalette per lo studio delle correnti a pelo libero.

A partire dall'anno accademico 1997/98 al dottorando viene data la possibilità di frequentare la "Scuola Avanzata di Formazione Integrata" dell'Istituto Universitario Studi Superiori, che si articola in tre anni e la cui finalità è quella di integrare le attività post-laurea di tipo specialistico con studi a carattere interdisciplinare adatti ad assicurare un più ampio bagaglio culturale.

Sommario

L'argomento trattato in questa tesi riguarda la diagnostica di patologie strutturali, con speciale riferimento alla doppia necessità di individuare situazioni danneggiate e di localizzare il danno stesso. Lo studio è incentrato su metodi che lavorano nello spazio delle variabili osservate, dove misure globali di informazione possono essere utilizzate per individuare il danno. La presenza di questo ultimo può essere evidenziata tramite il calcolo di quantità scalari, quali l'entropia, o vettoriali, come gli esponenti di Lyapunov. Il confronto di queste misure calcolate in sottospazi delle variabili osservate o in loro espansioni consente di realizzare una sorta di analisi di sensitività sul ruolo di ciascuna delle variabili coinvolte nel problema.

Le precedenti misure globali di informazione sono in grado di individuare, ma non di localizzare il danno. Per questo ultimo proposito un nuovo procedimento è formulato e implementato sfruttando le tecniche delle superficie di risposta per approssimare le relazioni tra le variabili osservate. Il confronto tra i modelli che risultano in diverse situazioni danneggiate e non danneggiate identifica le differenti risposte strutturali e le cause delle differenze.

Il procedimento che si basa sulla costruzione della superficie di risposta è descritto a partire dai suoi aspetti teorici di base sino alle caratteristiche della sua implementazione numerica. Inoltre, le misure globali introdotte precedentemente consentono di giudicare se il problema sia effettivamente ben

posto, ovvero se l'insieme delle quantità misurate nel caso specifico consenta di individuare il danno e di localizzarlo.

La validazione del metodo proposto è dapprima sviluppata in ambito numerico, con particolare riferimento al “benchmark” proposto dal Comitato di Controllo Strutturale dell'ASCE (la società statunitense degli ingegneri civili). Il procedimento viene successivamente applicato a due diverse situazioni sperimentali. Mentre la prima, riferendosi a una struttura intelaiata in acciaio, riproduce in scala reale le caratteristiche del problema studiato nel “benchmark”, il secondo studio riguarda una situazione strutturale di natura monumentale, dove il danno si identifica con fessure più o meno estese. Il potenziale di sviluppo evidenziato da questo ultimo caso consente di prospettare svariate applicazioni nell'individuazioni di patologie strutturali del patrimonio strutturale esistente.

Abstract

The general topic investigated in this thesis is “structural health monitoring”, with special care being devoted to damage detection and localization. The study is focused on methods which work in the space of the observed variables, where the global information measures can be used to detect the damage. In this context damage detection is demanded to global measures such as entropy or Lyapunov exponents. The comparison of these measures computed in subspaces of the observed variables or in their expansions, allows one to perform a sort of sensitivity analysis on the role of the variables involved in the problem.

Such global measures are able to detect but not to directly localize damage. For this purpose, a new approach to detect and localize the damage is formulated and implemented. It exploits response surface techniques to approximate the relationship among the observed variables. Comparing the resulting models in different damaged and undamaged situations identifies the response differences and their causes.

The response surface procedure is described from its basic theoretical aspects up to the features of its numerical implementation. Additionally, the global measures introduced above drive the analyst in establishing whether or not the problem is well posed, i.e., whether or not the set of measured quantities are able to detect the specific damage to be localized.

The validation of the proposed methodology is first numerically pursued by applying it to the benchmark case set up by the Structural Health Monitoring Panel of the American Society of Civil Engineering (ASCE). The procedure is then tested on two different experimental situations. While the first study of a three-dimensional steel frame reproduces the features of the benchmark problem, the second investigation covers a monumental structure situation, where damage is represented by more or less extended cracks in the masonry. The potential expressed by the procedure also in this second application seems to promise interesting exploitation possibilities.

Acknowledgements

First of all, I would like to thank Dr. Eng. Georges Magonette, director of the ELSA Laboratory at JRC Ispra, for his advises along the entire development of the thesis, for the stimulating discussions engaged with him, and for providing access to the experimental database which was used to validate the proposed methodology.

I also would like to thank Prof. Armando Gobetti who revised the thesis and always supported me during my education.

Finally, let me thank my friends Enrico Colabrese, Marco Domaneschi, Francesco Marazzi, and Roberto Rossi, who collaborated with me in developing some peculiar aspects of the thesis.

Table of Contents

| | |
|--|-----|
| Corso di Dottorato in Ingegneria Civile..... | I |
| Organizzazione del corso..... | III |
| Sommario..... | V |
| Abstract..... | VII |
| Acknowledgements..... | IX |
| Table of Contents..... | X |

Chapters

| | |
|--|----------|
| 1. Introduction..... | 1 |
| 2. Dynamic Systems and their Observability..... | 5 |
| 2.1 Dynamic Systems..... | 6 |
| 2.2 State-Variables Model..... | 9 |
| 2.3 Similarity Transformations..... | 12 |
| 2.4 Observability and Controllability..... | 14 |

| | |
|---|-----------|
| 2.5 The Ideal System Identification Process..... | 16 |
| 2.6 Operative Identification Procedures..... | 18 |
| 2.6.1 Observer and Kalman Filter Identification (OKID)..... | 19 |
| 2.6.2 Subspace Based Identification Method..... | 20 |
| 2.7 An Exemplification Case of Study..... | 21 |
| References for Chapter 2..... | 30 |

3. Structural Health Monitoring (SHM) in Civil

| | |
|--|-----------|
| Engineering Applications: a Brief Survey..... | 31 |
| 3.1 Operational Evaluation..... | 33 |
| 3.1.1 Economic and Life Safety Issues..... | 33 |
| 3.1.2 Definition of Damage..... | 38 |
| 3.1.3 Environmental and/or Operational Conditions..... | 42 |
| 3.2 Sensing the Response of a Structure..... | 45 |
| 3.3 Excitation Methods..... | 47 |
| References for Chapter 3..... | 53 |

4. The Long-Term Research Framework and

| | |
|------------------------------------|-----------|
| Goals..... | 57 |
| 4.1 The Damage Detection Goal..... | 58 |
| 4.2 Monitoring Capability..... | 61 |

| | | |
|-----------|---|------------|
| 4.3 | Wireless Sensors Network..... | 62 |
| 4.4 | Board Implementation toward a Smart Sensor..... | 67 |
| | References for Chapter4..... | 69 |
| 5. | Damage Detection Algorithms..... | 71 |
| 5.1 | Mapping the State-Space..... | 74 |
| 5.2 | Information Entropy and Kolmogorov Entropy..... | 75 |
| 5.3 | Lyapunov Exponents..... | 81 |
| 5.4 | Building Input-Output Relationships for Damage Localization..... | 87 |
| 5.4.1 | Genetic Algorithms..... | 88 |
| 5.4.2 | Wavelet Theory..... | 90 |
| 5.4.3 | Artificial Neural Networks..... | 91 |
| 5.4.4 | Response Surface Techniques..... | 93 |
| | References for Chapter 5..... | 95 |
| 6. | The SHM Response Surface Methodology..... | 101 |
| 6.1 | Basic Principles..... | 104 |
| 6.1.1 | Model Fitting..... | 108 |
| 6.1.2 | Estimate of the Variance of the Error | 110 |
| 6.2 | Application to Damage Diagnosis..... | 112 |
| 6.3 | The Static Problem of a Bridge under a Stationary | |

| | |
|--|------------|
| Queue of Traffic..... | 115 |
| 6.3.1 Numerical Example..... | 119 |
| 6.3.2 Including Noise into Measurements..... | 129 |
| 6.3.3 Decrease of the Number of Measurements..... | 131 |
| 6.3.4 Inferring Damage to the Structure..... | 133 |
| 6.4 Generalization and Formalization of the <i>SSE</i> -Approach | 140 |
| References for Chapter 6..... | 142 |

7. Analytical Studies Using the ASCE SHM

| | |
|--|------------|
| Benchmark Problem..... | 145 |
| 7.1 The ASCE SHM Benchmark Statement..... | 147 |
| 7.2 Application of the Method..... | 152 |
| 7.3 Results for the Benchmark Structure..... | 156 |
| References for Chapter 7..... | 164 |

8. Experimental Analyses..... 165

| | |
|--------------------------------------|------------|
| 8.1 The JRC-ELSA Laboratory..... | 166 |
| 8.2 The “Babyframe” Specimen..... | 168 |
| 8.3 The Test Setup..... | 170 |
| 8.4 Results..... | 174 |
| References for Chapter 8..... | 178 |

| | |
|---|------------|
| 9. The Palazzo Geraci Case of Study..... | 179 |
| 9.1 The Damaged Model of the Palazzo Geraci Façade..... | 180 |
| 9.2 Data Acquisition..... | 183 |
| 9.2.1 The Monitoring System Installation..... | 185 |
| 9.2.2 The Excitation Methods..... | 188 |
| 9.2.3 The First Set of Tests on the Damaged Structure..... | 190 |
| 9.2.4 The Retrofit of the Specimen by Mortar Injections..... | 193 |
| 9.2.5 The Second Set of Tests on the Undamaged Structure..... | 195 |
| 9.3 Damage Detection by Global Measures..... | 197 |
| 9.4 Damage Localization via SHM Response Surface Method..... | 198 |
| 9.4.1 Results from the Environmental Vibration Tests..... | 202 |
| 9.4.2 Results from the Tests with the Hammer..... | 204 |
| References for Chapter 9..... | 208 |
| | |
| 10. Conclusions and Future Developments..... | 209 |
| References for Chapter 10..... | 212 |

Appendices

| | |
|---|------------|
| A. Multivariate Regression Analysis..... | 213 |
| B.1 Estimation of the Parameters in Linear Regression Models..... | 213 |
| B.2 Properties of the Least Square Estimators and Estimation of σ^2 | 219 |
| B.3 Hypothesis Testing in Multiple Regression..... | 221 |
| B.4 Test for Significance of Regression..... | 222 |
| | |
| B. The Palazzo Geraci Façade Specimen..... | 227 |
| B.1 The Construction of the Specimen..... | 227 |
| B.2 The Pseudo-Dynamic Tests..... | 233 |

References

| | |
|--------------------------|------------|
| References..... | 237 |
| | |
| Other Theses..... | 245 |

Chapter 1

Introduction

The research activity summarized in this thesis deals with the topic of structural identification, with special care being devoted to its applications for damage detection and localization. Furthermore, the activity is framed in a general-purpose, long-term research program aiming to the realization of smart sensors suitably designed for Civil Engineering applications. Thence, the results achieved throughout the study were pursued with the final objective of implementing them in a software simple enough to be downloaded in the micro-processor which, coupled with the sensor, realizes the smart sensor device.

To determine a damage detection algorithm which best matches these requirements, several methods found in literature were investigated, applied, and compared. Many of the theoretical methods available show a very modest efficiency when implemented in practical situations This remark led the

research to be focused on the methods that work in the space of the observed variables, where global information measures are used to detect damage. Then the relationships among the observed variables are approximated by response surface techniques which allow one to localize the damage. As a result a new approach to damage detection is developed. The new method showed to be reliable and robust when applied to both the results of numerical simulation and experimental data.

Under these premises, the thesis is organized in nine further chapters after this short introduction. The next three chapters have the purpose to define the operation framework. In particular, Chapter 2 provides the basic governing relations, introducing the concepts of dynamic systems and their observability. Chapter 3 provides a brief survey on the applications of the structural health monitoring techniques to Civil Engineering structures. This task is pursued following the guidelines identified by the Los Alamos National Laboratory (LANL) in New Mexico, USA, as a result of its tremendous effort in summarizing and updating the wide state-of-the-art on the subject. Chapter 4, eventually, opens the perspective to the long-term ultimate goals of the research activity, explaining its motivations, illustrating its current solutions, and depicting the system architecture of the pursued operation scheme.

Chapters 5 and 6 represent the core of the thesis. Chapter 5 provides, as a consequence of the critical overview of the current practice provided in Chapter 3, a different rationale in approaching the damage detection problem. The space of the observed variables is selected as working space and some global information measures are shown to be able to detect (but not directly to localize) the damage. The algorithms which represent the best candidates to be implemented in the system architecture sketched in Chapter 4 in view of

damage localization, are then introduced and briefly discussed. One of them, based on the response surface theory, is selected, theoretically developed and implemented in Chapter 6. In particular, the SHM response surface methodology is described, and the attempts of its application to damage diagnosis are reported as found in literature and as developed in the early stage of this research. The results obtained from a first numerical example led to the abandon of the method proposed in literature, and to the development of a brand new one, which is the most suitable to the objectives of the ongoing research program.

The applicability of this method for damage detection and localization in several civil engineering structures is then investigated in the following three chapters. Three cases of study are selected for investigation, because they are representative of a wide range of situations and applications. Chapter 7 approaches the complex problem which was set up as benchmark case-study by the American Society of Civil Engineering (ASCE) committee on Structural Identification. Some of the cases proposed by the benchmark oblige the adoption of special preliminary data treatments which are illustrated in details. The validation pursued in this chapter belongs to the class of numerical simulations, but includes some degree of sophistication as accounting for the 3D nature of the structural system, the sensor noise, and the presence of damages not typically classified as of a structural nature. On the other side, Chapters 8 and 9 deal with existing laboratory models implemented at the Joint Research Center in Ispra, thus providing a direct window on professional applications. Chapter 8 considers a three story steel frame excited by a shaker, and Chapter 9 presents the results obtained from cracked, continuous, masonry tested by both ambient and hammer excitation.

Chapter 10 finally lists the further actions to be carried out in order to further test and improve the robustness of the approach developed and implemented along the thesis. A summary of the main conclusions achieved throughout the research activity ends the report.

Chapter 2

Dynamic Systems and their Observability

Many literature works show how system identification procedures can be applied for both the control and the monitoring of a structure. In this Chapter, dynamic systems are introduced, and their representations by transfer functions and state-variable models are presented. For the solutions of the control and observation problems to exist, the conditions of system controllability and observability need to be determined. In particular, the observability of a structure should be studied when deciding on the sensors placement.

The ideal system identification procedure is then summarized with the purpose of fault isolation and detection. Its practical implementation into dedicated softwares is discussed by introducing several operative algorithms. Among these, the Subspace Based Identification method is selected and its application to an exemplification case of study is illustrated.

2.1 Dynamic Systems

The operational principles of real-life systems are governed by physical laws whose modeling requires the use of nonlinear and/or time varying equations, which are usually difficult to solve. However, the commercial tools of analysis and design are commonly based on the linear systems theory. The justification of this choice is based either on the remark that the system is operated in the linear region, or on a linearization about a nominal operating point. In the latter case, the analysis is applicable only for the range of variables where the linearization is valid.

Dynamic systems can be defined as mappings of input signals into output signals, provided that the initial conditions are assigned. For linear time-invariant systems, and only for them, the associated transfer function can be defined.

One distinguishes four cases: i) a single input - single output (SISO) system with just one input signal $u(t)$ and one output signal $y(t)$, where t denotes the time, is characterized by a scalar transfer function G ; ii) a multiple input - single output (MISO) system sees G becoming a row vector; iii) a single input - multiple output (SIMO) system has as G a column vector; and iv) a multiple input - multiple output (MIMO) system is characterized by G becoming a matrix.

Given a linear time-invariant SISO system, if the input $u(t)$ is the unit-impulse function $\delta(t)$, then the output $y(t)$ is denoted as $g(t)$ and it is named the impulse response. The effects superposition principle then guarantees that the output $y(t)$ can be found for any input $u(t)$. The transfer function is defined as

the Laplace transform of the impulse response $g(t)$ when all the initial conditions are set to zero

$$G(s) = \ell[g(t)] = \int_0^{\infty} g(t) \exp(-st) dt. \quad (2.1)$$

In Equation (2.1), s is a complex variable and it is denoted as the Laplace operator.

The transfer function is related to the Laplace transforms of $y(t)$ and $u(t)$ by

$$G(s) = \frac{\ell[y(t)]}{\ell[u(t)]}. \quad (2.2)$$

The input-output relationship of a linear time-invariant system is usually described by an n -th order differential equation with constant real coefficients

$$\begin{aligned} \frac{d^n y(t)}{dt^n} + a_{n-1} \frac{d^{n-1} y(t)}{dt^{n-1}} + \dots + a_1 \frac{dy(t)}{dt} + a_0 y(t) = \\ = b_m \frac{d^m u(t)}{dt^m} + b_{m-1} \frac{d^{m-1} u(t)}{dt^{m-1}} + \dots + b_1 \frac{du(t)}{dt} + b_0 u(t). \end{aligned} \quad (2.3)$$

The transfer function results from taking the Laplace transform of both sides with zero initial conditions

$$\begin{aligned}
& (s^n + a_{n-1}s^{n-1} + \dots + a_1s + a_0)\ell[y(t)] = \\
& = (b_ms^m + b_{m-1}s^{m-1} + \dots + b_1s + b_0)\ell[u(t)],
\end{aligned} \tag{2.4}$$

and hence

$$G(s) = \frac{b_ms^m + b_{m-1}s^{m-1} + \dots + b_1s + b_0}{s^n + a_{n-1}s^{n-1} + \dots + a_1s + a_0}. \tag{2.5}$$

The equation obtained by setting the denominator of the r.h.s. of Equation (2.5) equal to zero, is called the characteristic equation. Its roots govern the stability of the linear SISO.

An “ideal sampler” collects continuous data with a given sampling period, say Δt : the result is an impulse train. The “zero-order hold” (ZOH) simply holds the signal carried by the incoming impulse at a given instant, multiple of Δt , until the next impulse arrives, thus introducing a staircase approximation of the input to the ideal sampler.

Assuming now to have a discrete data system, the previous relationships still hold, provided that the Laplace transform is replaced by the z -transform, with $z = e^{s\Delta t}$. Therefore, the transfer function depends now on the complex variable z ,

$$G(z) = \mathcal{Z}[g(k\Delta t)] = \sum_{k=0}^{\infty} g(k\Delta t)z^{-k}. \tag{2.6}$$

The inverse of z represents the unitary delay operator

$$z^{-1}Z[y(k\Delta t)] = Z[y((k-1)\Delta t)]. \quad (2.7)$$

2.2 State-Variables Model

The identification problems in mechanics can be approached following schemes which can be classified into traditional and modern control theory methods. The first ones are based on the previous concept of transfer function, while the latter approach relies on the so called state-variables models. The basic feature of the state-variables formulation is that linear and nonlinear systems, time invariant and time varying systems, can all be modeled in a unified manner as follows

$$\begin{aligned} \frac{dx_i(t)}{dt} &= f_i[x_1(t), x_2(t), \dots, x_n(t), u_1(t), u_2(t), \dots, u_p(t), w_1(t), w_2(t), \dots, w_v(t)], \\ y_j(t) &= F_j[x_1(t), x_2(t), \dots, x_n(t), u_1(t), u_2(t), \dots, u_p(t), w_1(t), w_2(t), \dots, w_v(t)]. \end{aligned} \quad (2.8)$$

Equation (2.8) forms the dynamic equations: the first row collects the state equations in number of n for an n -th order dynamic system, where n is also the number of the state variables $x_i(t)$; the second row represents the output equations, in number of q , where q is also the number of the output variables $y_j(t)$. The number of input functions $u_h(t)$ is p , and v is the number of disturbance input functions $w_k(t)$.

For ease of expression and manipulation, it is convenient to express Equation (2.8) in a vector-matrix notation, for which the bold format is adopted

$$\frac{d\mathbf{x}(t)}{dt} = \mathbf{f}[\mathbf{x}(t), \mathbf{u}(t), \mathbf{w}(t)], \quad (2.9)$$

$$\mathbf{y}(t) = \mathbf{F}[\mathbf{x}(t), \mathbf{u}(t), \mathbf{w}(t)].$$

For a linear time-invariant systems, one can write

$$\frac{d\mathbf{x}(t)}{dt} = \mathbf{A}\mathbf{x}(t) + \mathbf{B}\mathbf{u}(t) + \mathbf{E}\mathbf{w}(t), \quad (2.10)$$

$$\mathbf{y}(t) = \mathbf{C}\mathbf{x}(t) + \mathbf{D}\mathbf{u}(t) + \mathbf{H}\mathbf{w}(t),$$

where the six matrices \mathbf{A} , \mathbf{B} , \mathbf{C} , \mathbf{D} , \mathbf{E} , and \mathbf{H} have sizes $n \times n$, $n \times p$, $q \times n$, $q \times p$, $n \times v$, and $q \times v$, respectively.

The solution of the homogeneous state equations (first row of Equation (2.10), with $\mathbf{B} = \mathbf{E} = \mathbf{0}$), given the initial state vector $\mathbf{x}(t_0)$, is written as

$$\mathbf{x}(t) = \boldsymbol{\phi}(t)\mathbf{x}(t_0), \quad (2.11)$$

where $\boldsymbol{\phi}(t)$ is the $n \times n$ state-transition matrix, i.e., the matrix that satisfies the equation

$$\frac{d\boldsymbol{\phi}(t)}{dt} = \mathbf{A}\boldsymbol{\phi}(t), \quad (2.12)$$

resulting into

$$\boldsymbol{\phi}(t) = \ell^{-1}[(s\mathbf{I} - \mathbf{A})^{-1}] = e^{\mathbf{A}t} = \mathbf{I} + \mathbf{A}t + \frac{1}{2!}\mathbf{A}^2t^2 + \dots \quad (2.13)$$

The general solution of the state equations can easily be written in its Laplace transform form

$$\ell[\mathbf{x}(t)] = (s\mathbf{I} - \mathbf{A})^{-1}\mathbf{x}(t_0) + (s\mathbf{I} - \mathbf{A})^{-1}[\mathbf{B}\ell[\mathbf{u}(t)] + \mathbf{E}\ell[\mathbf{w}(t)]], \quad (2.14)$$

leading to write

$$\mathbf{x}(t) = \boldsymbol{\phi}(t - t_0)\mathbf{x}(t_0) + \int_{t_0}^t \boldsymbol{\phi}(t - \tau)[\mathbf{B}\mathbf{u}(\tau) + \mathbf{E}\mathbf{w}(\tau)]d\tau \quad t \geq t_0, \quad (2.15)$$

from which the output vector is determined by simply substituting the expression found for $\mathbf{x}(t)$ in the second row of Equation (2.10).

From the Laplace transform of the output vector with initial conditions set to zero, i.e., $\mathbf{x}(t_0) = \mathbf{0}$, one can find the relationship between the two representations of a linear time-invariant system by transfer functions and dynamic equations, being

$$\begin{aligned} \mathbf{G}_{\mathbf{u}}(s) &= \mathbf{C}(s\mathbf{I} - \mathbf{A})^{-1}\mathbf{B} + \mathbf{D}, \\ \mathbf{G}_{\mathbf{w}}(s) &= \mathbf{C}(s\mathbf{I} - \mathbf{A})^{-1}\mathbf{E} + \mathbf{H}. \end{aligned} \quad (2.16)$$

the $q \times p$ and $q \times v$ transfer function matrices between $\mathbf{u}(t)$ and $\mathbf{y}(t)$ when $\mathbf{w}(t) = \mathbf{0}$, and between $\mathbf{w}(t)$ and $\mathbf{y}(t)$ when $\mathbf{u}(t) = \mathbf{0}$, respectively.

Since the inverse of a matrix can be expressed as the ratio between its adjoint and its determinant, by substituting $(s\mathbf{I} - \mathbf{A})^{-1} = \text{adj}(s\mathbf{I} - \mathbf{A})/|s\mathbf{I} - \mathbf{A}|$ in Equation (2.18), one can see that the denominator of the transfer function matrix $\mathbf{G}_{\mathbf{u}}(s)$ equated to zero, i.e., the system characteristic function, is

$$|s\mathbf{I} - \mathbf{A}| = s^n + a_{n-1}s^{n-1} + \dots + a_1s + a_0 = 0. \quad (2.17)$$

and it is equal to the one obtained from Equation (2.5). Hence, the roots of the characteristic equation are the eigenvalues of the state matrix \mathbf{A} . The state matrix \mathbf{A} can be non-symmetric and show multiple-order eigenvalues. We assume that among its n eigenvalues, $r < n$ are distinct.

2.3 Similarity Transformations

Let us introduce a SISO, i.e., $p = 1$ and $q = 1$, in a deterministic context ($\mathbf{w} = \mathbf{0}$). The dynamic equations are transformed into another set of equations of the same dimension by the transformation

$$\mathbf{x}(t) = \mathbf{P}\bar{\mathbf{x}}(t) \Leftrightarrow \bar{\mathbf{x}}(t) = \mathbf{P}^{-1}\mathbf{x}(t), \quad (2.18)$$

which requires that \mathbf{P} is an $n \times n$ non-singular matrix.

The transformation \mathbf{P} alters the matrices \mathbf{A} , \mathbf{B} , \mathbf{C} , and \mathbf{D} , but it is called a similarity transformation because in the transformed system the characteristic

equation, the eigenvalues, the eigenvectors, and the transfer function are all preserved by the transformation.

Let us define the controllability matrix as

$$\mathbf{S} = [\mathbf{B} \quad \mathbf{AB} \quad \mathbf{A}^2\mathbf{B} \quad \dots \quad \mathbf{A}^{n-1}\mathbf{B}], \quad (2.19)$$

and build the matrix

$$\mathbf{M} = \begin{bmatrix} a_1 & a_2 & \dots & a_{n-1} & 1 \\ a_2 & a_3 & \dots & 1 & 0 \\ \vdots & \vdots & \ddots & \vdots & \vdots \\ a_{n-1} & 1 & \dots & 0 & 0 \\ 1 & 0 & \dots & 0 & 0 \end{bmatrix}, \quad (2.20)$$

having all the elements of each anti-diagonal equal to each other. This matrix is called a Hankel matrix. The transformation,

$$\mathbf{P} = \mathbf{SM}, \quad (2.21)$$

transforms the dynamic equations into the controllability canonical form (CCF).

The observability matrix is defined as

$$\mathbf{V} = \begin{bmatrix} \mathbf{C} \\ \mathbf{CA} \\ \mathbf{CA}^2 \\ \vdots \\ \mathbf{CA}^{n-1} \end{bmatrix}. \quad (2.22)$$

The transformation,

$$\mathbf{P} = (\mathbf{MV})^{-1}, \quad (2.23)$$

transforms the dynamic equations into the observability canonical form (OCF).

It is worth noting that, for each selection of \mathbf{P} , one obtains a new model characterized by a different quadruple of matrices and a different state vector $\mathbf{x}(t)$. Nevertheless, the new transfer function coincides with the original one.

The quadruple of matrices arising from a given transfer function $\mathbf{G}(s)$, are regarded as a realization of $\mathbf{G}(s)$. Here the order of the model is the dimension of the vector $\mathbf{x}(t)$. The concept of minimal realization requires that there is no other realization with a state vector of lower size.

2.4 Observability and Controllability

Arguing on the minimal nature of a realization requires the introduction of the concepts of observability and controllability. The system is said to be observable when there are not two different initial states such that the corresponding output values are the same, for any time subsequent to the initial

one. The system is observable if and only if the observability matrix \mathbf{V} has rank n .

The system is said to be controllable if, for any value ξ of \mathbf{x} , there is a suitable sequence of $\mathbf{u}(t)$ which produces an evolution of \mathbf{x} such that, at a time t_N after the initial one, $\mathbf{x}(t_N) = \xi$. The system is controllable when the rank of the controllability matrix \mathbf{S} is n .

A necessary and sufficient condition for having a minimal realization is that the model is controllable and observable.

The observability of a system depends on which variable is defined as the output. In any textbook of automatic control one finds examples of systems which are fully observable when the observed variable is selected in a suitable class; otherwise, these systems lose their observability. For instance, a system with three state variables and three potential observed variables, might be fully observable if either the first or the second observed variable is considered, but it might lose its observability when the third observed variable is the only one retained.

An observability study can be simply developed when the real dynamic system is known. In this case, the observability theory helps in selecting the suitable configuration of the sensors. However, given a network of sensors, one can encounter damage situations which are not detectable, just because of the unobservability of the system for that specific mock-up.

2.5 The Ideal Identification Process

With reference to a MIMO system for which a vector of observations of size p is available, one is free to assume the model (2.10), but:

- 1) the model order n is unknown;
- 2) the matrices in the state equations are unknown;
- 3) the matrices in the observation equations are unknown.

When a time discrete representation is adopted, Equation (2.10) takes the form

$$\begin{aligned}\mathbf{x}[(k+1)\Delta t] &= \mathbf{A}^\circ \mathbf{x}(k\Delta t) + \mathbf{B}^\circ \mathbf{u}(k\Delta t) + \mathbf{w}(k\Delta t), \\ \mathbf{y}(k\Delta t) &= \mathbf{C}^\circ \mathbf{x}(k\Delta t) + \mathbf{v}(k\Delta t),\end{aligned}\tag{2.24}$$

where $\mathbf{x}(t)$ denotes the state variables; \mathbf{A}° , \mathbf{B}° and \mathbf{C}° are matrices of real elements and sizes consistent with the associated vectors; $\mathbf{v}(t)$ and $\mathbf{w}(t)$ denote the noises. Either the identification of the vectors $\mathbf{v}(t)$ and $\mathbf{w}(t)$, or of the matrices \mathbf{A}° , \mathbf{B}° and \mathbf{C}° can be required. The attention is here focused on the latter problem and the disturbances are no longer taken into account.

Each anti-diagonal element of the Hankel matrix (2.20) is the discrete system impulse response

$$g(k\Delta t) = \mathbf{C}^\circ (\mathbf{A}^\circ)^{k-1} \mathbf{B}^\circ,\tag{2.25}$$

with $k = 1, 2, \dots$. But, being n unknown, one ignores how large the Hankel matrix is; thus he needs to write

$$1, \quad (2.26)$$

where the last two matrices are the observability and the controllability matrices for a system of infinite order.

In the framework depicted above, the identification problem is ideally solved by:

- 1) assessing the impulsive response of the system, $g(t)$;
- 2) building, for the Hankel matrix, a truncated version of large size, \mathbf{M}_{tr} ;
- 3) determining the order of the Hankel matrix, which coincides with the order of the model for minimal realization;
- 4) factorizing the truncated Hankel matrix into the product $\mathbf{V}_{ex} \mathbf{S}_{ex}$, where the rows of \mathbf{V}_{ex} (with n columns) are in number of those of \mathbf{M}_{tr} , and the columns of \mathbf{S}_{ex} (with n rows) are in number of the ones of \mathbf{M}_{tr} . They are called the extended observability and controllability matrices.

Consider a matrix \mathbf{V}_{ex}^{par} obtained by j partitions of \mathbf{V}_{ex} in blocks of p rows, with q the size of $\mathbf{y}(t)$ and j any integer. The first block of \mathbf{V}_{ex}^{par} is an estimation of the matrix \mathbf{C}° . The matrix \mathbf{A}° is given by

$$\mathbf{A}^\circ = [\mathbf{V}_{ex}^{parT} \mathbf{V}_{ex}^{par}]^{-1} \mathbf{V}_{ex}^{parT} \mathbf{V}_{ex}^{UP}, \quad (2.27)$$

where \mathbf{V}_{ex}^{UP} is obtained from \mathbf{V}_{ex}^{par} by deleting the first q rows and by adding a $(j+1)$ -th block at the bottom. Finally, \mathbf{B}° is obtained as the first columns of \mathbf{S}_{ex} .

In summary, the observation matrix \mathbf{C}° is either given or assessed. Then the problem is to identify and to monitor the observed system eigenstructure, which is the collection of n pairs (λ, ϕ_λ) , where λ ranges over the set of eigenvalues of the state matrix \mathbf{A}° ; if φ_λ are the corresponding eigenvectors, then $\phi_\lambda = \mathbf{C}^\circ \varphi_\lambda$.

If the system has no multiple eigenvalues, this collection does not depend on the state space basis. The pair (λ, ϕ_λ) is called a mode, and the set of n modes is considered as the system parameter θ ,

$$\theta = \begin{Bmatrix} \Lambda \\ \text{vec}\Phi \end{Bmatrix}. \quad (2.28)$$

Here, Λ is the vector whose elements are the eigenvalues λ , Φ is the matrix whose columns are the ϕ_λ , and vec is the column stacking operator. The resulting θ has size $(r + 1) n$.

The Fault Detection and Isolation (FDI) consists of detecting and isolating the changes in the parameter vector θ . By isolation one means to decide which mode(s) has(have) changed. This procedure is quite sensitive to numerical errors, which make it infeasible, but it underlines that the goal is to obtain a reliable estimate of the observability matrix from which the system matrices are then derived. Its feasible implementation can be found in OKID and in the Subspace Based Identification Method.

2.6 Operative Identification Procedures

In 1992, the Langley Research Center of NASA (National Aeronautics and Space Administration) released, within the COSMIC program, the Technical Memorandum 107566, which is a manual for a system/observer/controller

identification toolbox. Herein, several system identification algorithms were defined and implemented. Among these, it is worth mentioning

1. the “Eigensystem Realization Algorithm with Data Correlation” (ERA/DC), which identifies a state space model from pulse response time histories, using a data correlation technique;
2. the “State Vector Realization Algorithm” (SVRA), which identifies a state space from input and output data, using a state vector realization technique;
3. the “Observer and Kalman filter Identification” (OKID), which simultaneously identifies a state space model and an observer gain from input and output data.

This terminology became of reference in the literature of the Nineties, and it is introduced here to support a literature review of its applications for fault detection in Civil Engineering structures. In the following of this section, brief summaries of the OKID and of the Subspace Based Identification Method are provided.

2.6.1 Observer and Kalman Filter Identification (OKID)

The input/output time histories are stored as column matrices, whose number of rows is equal to the number of sampled points.

The identification of the pulse response (also referred to as Markov parameters, since autoregressive models are often implemented to find the model dimension) is obtained by using the singular value decomposition sketched in Section 2.5. It is pursued for an auxiliary system (observer) rather than for the system itself.

Initially, an estimate of the number of Markov parameters must be specified. A plot of the Hankel matrix singular values is shown to aid the selection of the correct system order.

Theoretically, there is only a specific number of independent Markov system parameters for a finite set of Markov observer parameters. Therefore, a minimum number of Markov system parameters may be used in the ERA routine to minimize the computational time in identifying the system.

The identified system matrices are eventually returned by the algorithm.

2.6.2 Subspace Based Identification Method

In view of the exemplification illustrated in the next section, Equation (2.10) can be rewritten either as

$$\begin{aligned}\mathbf{x}(t+1) &= \mathbf{A}\mathbf{x}(t) + \mathbf{B}\mathbf{u}(t), \\ \mathbf{y}(t) &= \mathbf{C}\mathbf{x}(t) + \mathbf{D}\mathbf{u}(t) + \mathbf{v}(t),\end{aligned}\tag{2.29}$$

or

$$\begin{aligned}\mathbf{x}(t+1) &= \mathbf{A}\mathbf{x}(t) + \mathbf{B}\mathbf{u}(t) + \mathbf{K}\mathbf{e}(t), \\ \mathbf{y}(t) &= \mathbf{C}\mathbf{x}(t) + \mathbf{D}\mathbf{u}(t) + \mathbf{e}(t).\end{aligned}\tag{2.30}$$

The state-space matrices \mathbf{A} , \mathbf{B} , \mathbf{C} , \mathbf{D} , and \mathbf{K} in Equation (2.30) can be estimated directly (without specifying any particular parameterization) by efficient subspace methods. The idea behind these methods can be explained as follows. If the sequence of the state vectors $\mathbf{x}(t)$ were known together with $\mathbf{y}(t)$ and $\mathbf{u}(t)$,

Equation (2.30) would be a linear regression, and the matrices \mathbf{C} and \mathbf{D} could be estimated by the least squares method (see Appendix A). Hence, the vector $\mathbf{e}(t)$ could be determined and treated as a known signal in Equation (2.30), which would then be another linear regression model for \mathbf{A} , \mathbf{B} and \mathbf{K} . One could also treat Equation (2.29) as a linear regression for \mathbf{A} , \mathbf{B} , \mathbf{C} , and \mathbf{D} , with $\mathbf{y}(t)$ and $\mathbf{x}(t+1)$ as simultaneous outputs, and find the joint process and the measurement noises as the residuals from this regression. The Kalman gain, \mathbf{K} , could then be computed from the Riccati equation.

Thus, once the states are known, the estimation of the state-space matrices would become easy. How to find the states $\mathbf{x}(t)$? All states in representations like Equation (2.30) can be formed as linear combinations of the k -steps ahead predicted outputs ($k = 1, 2, \dots, n$). It is therefore a matter of finding these predictors and then selecting a basis among them. The subspace methods provide an efficient and numerically reliable way to determine the predictors by direct projections on the observed data. Further information can be found in Sections 7.3 and 10.6 of the book [Ljung, 1999].

2.7. An Exemplification Case of Study

A case of study was selected to give a numerical evidence to the previous theoretical expressions. For this purpose, one needs the structural response time histories of the quantity of interest (e.g., acceleration) to be recorded by different sensors. Some of them can be regarded as inputs and the remaining ones as outputs. In particular, adopting the results of the full scale tests

described in Chapter 8 also in this preliminary phase, seems to be pertinent. In this section, it is enough to specify the following main characteristics:

- 1) Every test is performed by applying 12 times a random excitation for a short period of time, and by recording each time the structural response until the rest is reached again;
- 2) for each test, 20 files of measurements are available;
- 3) the first file consists of the time sequence: the recorded times are equally spaced with an acquisition frequency of 200 samples per second (s.p.s.), i.e., with a sampling time interval $\Delta t = 0.005$ s; a total duration of 252.39 s is recorded;
- 4) the second file, say the column vector named “input”, contains the force-time history, from which one can recognize the 12 excitation pulses in a sequence;
- 5) a third file contains the measures of a reference channel which is not considered in the analysis;
- 6) the remaining 17 response channels are available as outputs, and they can be organized in a matrix of 17 columns, which represents the “signal”.

Since each file consists of 12 pulses, attention is focused on a single pulse per file, i.e., all the records are divided into 12 replications. The analysis below is pursued on one single replication, starting from the first one.

MATLAB[®] is the selected software environment. The analysis is carried out by manually giving the following commands (the user-friendly interface GUI is also available, but it does not allow one to find the direct counterpart in the theory as the sequence of commands does).

a) “`Z = iddata(signal, input, 0.005)`”

creates an object “Z” which in the present case is a SIMO (single input - multiple output) system recorded with a time step of 0.005 s;

- b) `mod_basic = n4sid(iddata, [9:20], 'Cov', 'None')` estimates the state-space models using a subspace method. The assignment of no covariance matrix blocks all the calculations of the uncertainty measures, since these may take the major part of the computational time. On the other side, asking the model order to fall in the range [9, 20] implies that the calculations are carried out for all the orders in the indicated interval. As a result, the plot in Figure 2.1a is obtained. It shows the relative importance of the dimension of the state vector. More precisely, the singular values of the Hankel matrices of the impulse response are graphed for the different orders. One is prompted to select the order based on this plot, or better on its zoom in Figure 2.1b. The idea is to choose an order such that the singular values for higher orders are comparatively small.

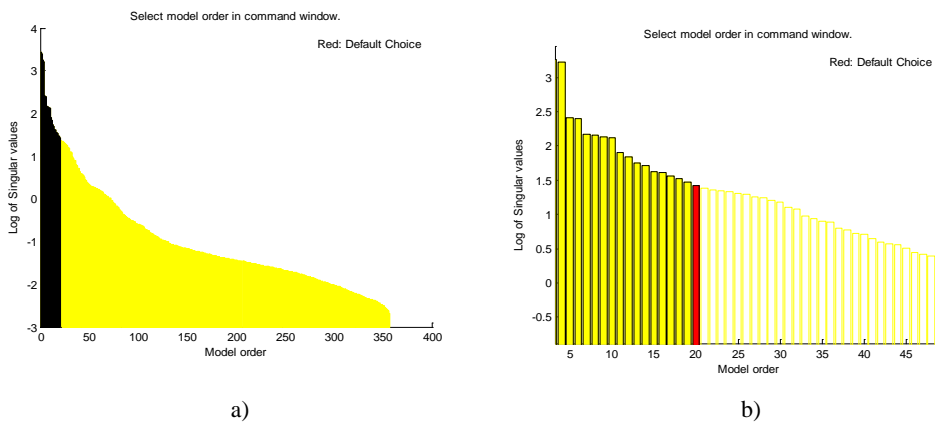


Figure 2.1 (a) Graph of the singular values of the Hankel matrices of the impulse response for different orders of the state space model. (b) Zoom of Figure 2.1a.

- c) The value 16 is first selected for the order and the model at the top of Figure 2.2 is estimated.
- d) The state space matrix (of size 16×16) is characterized by eigenvalues which can be obtained by the command
`“lambda=eig(mod_basic.A)”`,
 which results into:

```

-0.2831 + 0.9394i
-0.2831 - 0.9394i
-0.5295 + 0.8239i
-0.5295 - 0.8239i
-0.5036 + 0.6709i
-0.5036 - 0.6709i
-0.7977 + 0.5254i
-0.7977 - 0.5254i
-0.6617 + 0.6536i
-0.6617 - 0.6536i
-0.6304
 0.9487 + 0.3062i
 0.9487 - 0.3062i
 0.8225
 0.7291 + 0.0198i
 0.7291 - 0.0198i

```

- e) The commands:

```
“obb = obsv(mod_basic.A, mod_basic.C);”
```

```
“rank(obb)”
```

compute the observability matrix (of size 272×16) and its rank, which is 16 for the present model.

The results which are obtained by choosing different options than those above are now discussed.

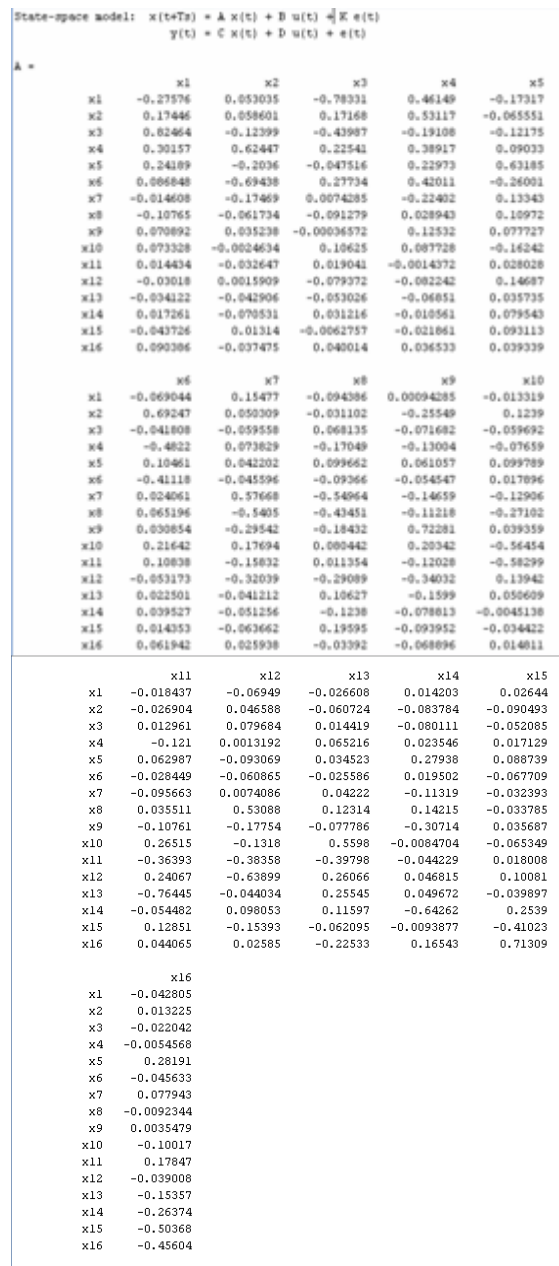
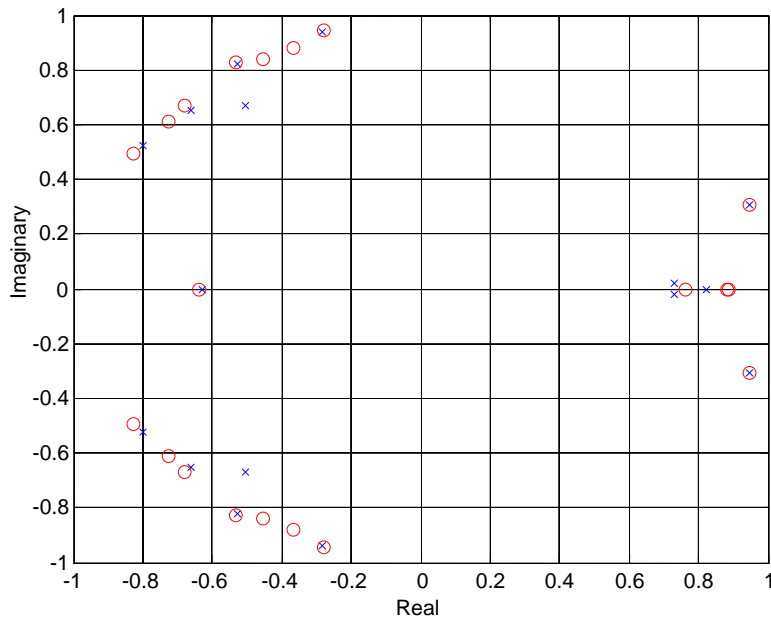


Figure 2.2 Matrix A of the estimated state space model for order number 16.

- i) Which would have been the result of selecting the default value of 20 instead of 16 as model order? A complete different model would result in terms of matrices, but some eigenvalues (six) would be preserved, as shown in Figure 2.3.
- ii) Since 12 replications are available, one can repeat the above calculations on the second pulse of the excitation. The results are compared in Figures 2.4 a and b for the models of order 16 and 20, respectively.
- iii) The previous models were derived with a non-zero \mathbf{K} matrix in Equation (2.30), but one can also search for the model with no disturbance by:
- ```
“mod_nodis = n4sid(z,16, 'Cov', 'None',
'DisturbanceModel', 'None')”
```
- This provides the new plot of Figure 2.5 instead of the one of Figure 2.1, while Figure 2.4 is replaced by Figure 2.6. Here three replications are drawn and a better agreement of the eigenvalues is found at least for the case of the model of order 16 (Figure 2.6a).
- iv) The software adopted for the numerical examples and developed in this section also works when no input is specified. To repeat the calculations for such a case, however, is out of the scope of this study.

Assume now that the considered record of input and output signals was associated to a damaged state of the structure, and that for the same system a set of undamaged records is also available. The Fault Detection and Isolation (FDI), which consists of detecting and isolating the changes in the parameter vector  $\theta$ , is performed by moving from Figure 2.6a to Figure 2.7, where the largest circles denotes the eigenvalues computed from the damaged case.



**Figure 2.3** Eigenvalues of the state space matrix  $A$  for the models of order 16 ( $\times$ ) and 20 ( $o$ ).

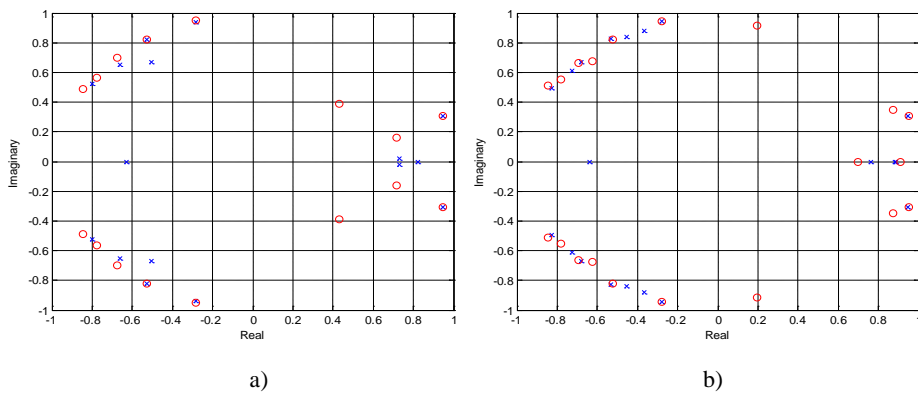


**Figure 2.4** Eigenvalues of the state space matrix  $A$  from the first two replications, for the models of order: (a) 16 and (b) 20.

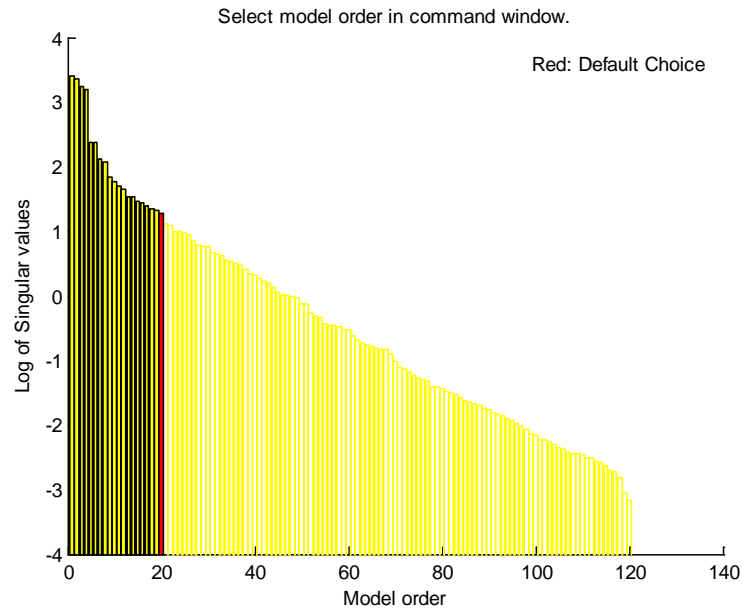


Figure 2.5 Model selection graph when the no-disturbance option is set.

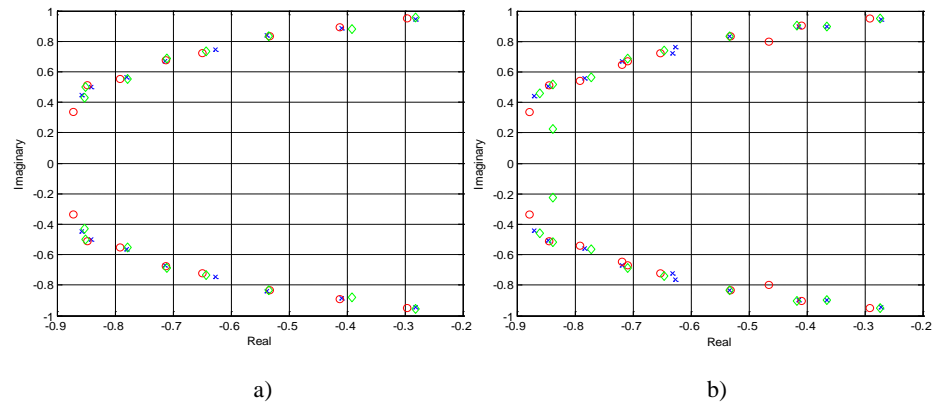
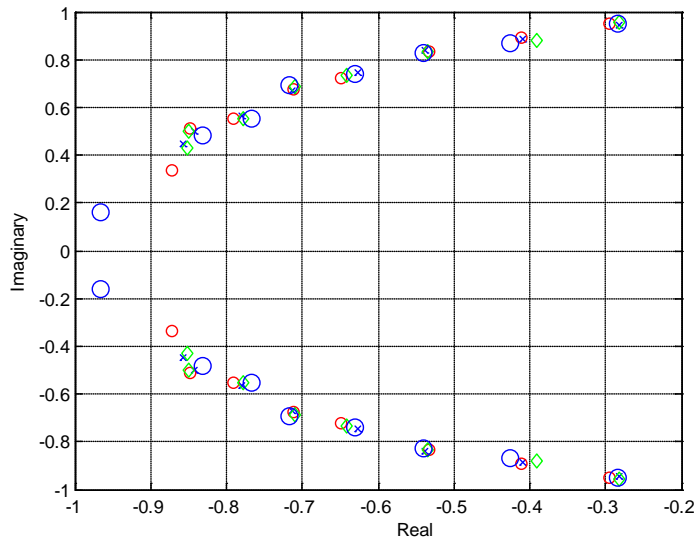


Figure 2.6 Eigenvalues of the state space matrix  $A$  from the first three replications, with the no-disturbance option and for the models of order (a) 16 and (b) 20.



**Figure 2.7** Eigenvalues of the undamaged system (largest circles), and comparison with those calculated for the three different replications of the previously considered damaged system (model order 16).

The damaged case is distinguished from the undamaged one by the presence of a pair of eigenvalues on the left hand side. However, no localization of the damage can be achieved.

## References for Chapter 2

- Basseville M., Abdelghani M. and Benveniste A. (1997). “Subspace-based Fault Detection and Isolation – Application to Vibration Monitoring”, INRIA 3299, Rennes.
- Bittanti S. (1993). *Teoria della Predizione e del Filtraggio*, Pitagora, Bologna (in Italian).
- Bittanti S. (1997). *Identificazione dei Modelli e Controllo Adattivo*, Pitagora, Bologna, (in Italian).
- Brogan W.L. (1985). *Modern Control Theory*, Prentice Hall Int., Englewood Cliffs.
- Juang J.N. (1992). *Applied System Identification*, Prentice Hall Int., Englewood Cliffs.
- Juang J.N., Horta L.G., and Phan M. (1992). “System/Observer/Controller Identification Toolbox”, NASA Technical Memorandum 107566.
- Kuo B.C. (1995). *Automatic Control Systems*, Prentice Hall Int., Englewood Cliffs.
- Ljung L. (1999). *System Identification - Theory for the User*, Prentice Hall, Upper Saddle River, N.J., 2nd edition.
- Matworks Inc. (2004). *MATLAB User's guide*.
- Peeters B. (2000). *System Identification and Damage Detection in Civil Engineering*, PhD Thesis, K.U. Leuven Civil Engineering Department.
- Pisano A.A. (1999). *Structural System Identification: Advanced Approaches and Applications*, Ph.D. Thesis, Graduate School of Civil Engineering, University of Pavia, n. 4.

## **Chapter 2**

### **Dynamic Systems and their Observability**

Many literature works show how system identification procedures can be applied for both the control and the monitoring of a structure. In this Chapter, dynamic systems are introduced, and their representations by transfer functions and state-variable models are presented. For the solutions of the control and observation problems to exist, the conditions of system controllability and observability need to be determined. In particular, the observability of a structure should be studied when deciding on the sensors placement.

The ideal system identification procedure is then summarized with the purpose of fault isolation and detection. Its practical implementation into dedicated softwares is discussed by introducing several operative algorithms. Among these, the Subspace Based Identification method is selected and its application to an exemplification case of study is illustrated.

## 2.1 Dynamic Systems

The operational principles of real-life systems are governed by physical laws whose modeling requires the use of nonlinear and/or time varying equations, which are usually difficult to solve. However, the commercial tools of analysis and design are commonly based on the linear systems theory. The justification of this choice is based either on the remark that the system is operated in the linear region, or on a linearization about a nominal operating point. In the latter case, the analysis is applicable only for the range of variables where the linearization is valid.

Dynamic systems can be defined as mappings of input signals into output signals, provided that the initial conditions are assigned. For linear time-invariant systems, and only for them, the associated transfer function can be defined.

One distinguishes four cases: i) a single input - single output (SISO) system with just one input signal  $u(t)$  and one output signal  $y(t)$ , where  $t$  denotes the time, is characterized by a scalar transfer function  $G$ ; ii) a multiple input - single output (MISO) system sees  $G$  becoming a row vector; iii) a single input - multiple output (SIMO) system has as  $G$  a column vector; and iv) a multiple input - multiple output (MIMO) system is characterized by  $G$  becoming a matrix.

Given a linear time-invariant SISO system, if the input  $u(t)$  is the unit-impulse function  $\delta(t)$ , then the output  $y(t)$  is denoted as  $g(t)$  and it is named the impulse response. The effects superposition principle then guarantees that the output  $y(t)$  can be found for any input  $u(t)$ . The transfer function is defined as

the Laplace transform of the impulse response  $g(t)$  when all the initial conditions are set to zero

$$G(s) = \ell[g(t)] = \int_0^{\infty} g(t) \exp(-st) dt. \quad (2.1)$$

In Equation (2.1),  $s$  is a complex variable and it is denoted as the Laplace operator.

The transfer function is related to the Laplace transforms of  $y(t)$  and  $u(t)$  by

$$G(s) = \frac{\ell[y(t)]}{\ell[u(t)]}. \quad (2.2)$$

The input-output relationship of a linear time-invariant system is usually described by an  $n$ -th order differential equation with constant real coefficients

$$\begin{aligned} \frac{d^n y(t)}{dt^n} + a_{n-1} \frac{d^{n-1} y(t)}{dt^{n-1}} + \dots + a_1 \frac{dy(t)}{dt} + a_0 y(t) = \\ = b_m \frac{d^m u(t)}{dt^m} + b_{m-1} \frac{d^{m-1} u(t)}{dt^{m-1}} + \dots + b_1 \frac{du(t)}{dt} + b_0 u(t). \end{aligned} \quad (2.3)$$

The transfer function results from taking the Laplace transform of both sides with zero initial conditions

$$\begin{aligned}
& (s^n + a_{n-1}s^{n-1} + \dots + a_1s + a_0)\ell[y(t)] = \\
& = (b_ms^m + b_{m-1}s^{m-1} + \dots + b_1s + b_0)\ell[u(t)],
\end{aligned} \tag{2.4}$$

and hence

$$G(s) = \frac{b_ms^m + b_{m-1}s^{m-1} + \dots + b_1s + b_0}{s^n + a_{n-1}s^{n-1} + \dots + a_1s + a_0}. \tag{2.5}$$

The equation obtained by setting the denominator of the r.h.s. of Equation (2.5) equal to zero, is called the characteristic equation. Its roots govern the stability of the linear SISO.

An “ideal sampler” collects continuous data with a given sampling period, say  $\Delta t$ : the result is an impulse train. The “zero-order hold” (ZOH) simply holds the signal carried by the incoming impulse at a given instant, multiple of  $\Delta t$ , until the next impulse arrives, thus introducing a staircase approximation of the input to the ideal sampler.

Assuming now to have a discrete data system, the previous relationships still hold, provided that the Laplace transform is replaced by the  $z$ -transform, with  $z = e^{s\Delta t}$ . Therefore, the transfer function depends now on the complex variable  $z$ ,

$$G(z) = Z[g(k\Delta t)] = \sum_{k=0}^{\infty} g(k\Delta t)z^{-k}. \tag{2.6}$$

The inverse of  $z$  represents the unitary delay operator

$$z^{-1}Z[y(k\Delta t)] = Z[y((k-1)\Delta t)]. \quad (2.7)$$

## 2.2 State-Variables Model

The identification problems in mechanics can be approached following schemes which can be classified into traditional and modern control theory methods. The first ones are based on the previous concept of transfer function, while the latter approach relies on the so called state-variables models. The basic feature of the state-variables formulation is that linear and nonlinear systems, time invariant and time varying systems, can all be modeled in a unified manner as follows

$$\begin{aligned} \frac{dx_i(t)}{dt} &= f_i[x_1(t), x_2(t), \dots, x_n(t), u_1(t), u_2(t), \dots, u_p(t), w_1(t), w_2(t), \dots, w_v(t)], \\ y_j(t) &= F_j[x_1(t), x_2(t), \dots, x_n(t), u_1(t), u_2(t), \dots, u_p(t), w_1(t), w_2(t), \dots, w_v(t)]. \end{aligned} \quad (2.8)$$

Equation (2.8) forms the dynamic equations: the first row collects the state equations in number of  $n$  for an  $n$ -th order dynamic system, where  $n$  is also the number of the state variables  $x_i(t)$ ; the second row represents the output equations, in number of  $q$ , where  $q$  is also the number of the output variables  $y_j(t)$ . The number of input functions  $u_h(t)$  is  $p$ , and  $v$  is the number of disturbance input functions  $w_k(t)$ .

For ease of expression and manipulation, it is convenient to express Equation (2.8) in a vector-matrix notation, for which the bold format is adopted

$$\frac{d\mathbf{x}(t)}{dt} = \mathbf{f}[\mathbf{x}(t), \mathbf{u}(t), \mathbf{w}(t)], \quad (2.9)$$

$$\mathbf{y}(t) = \mathbf{F}[\mathbf{x}(t), \mathbf{u}(t), \mathbf{w}(t)].$$

For a linear time-invariant systems, one can write

$$\frac{d\mathbf{x}(t)}{dt} = \mathbf{A}\mathbf{x}(t) + \mathbf{B}\mathbf{u}(t) + \mathbf{E}\mathbf{w}(t), \quad (2.10)$$

$$\mathbf{y}(t) = \mathbf{C}\mathbf{x}(t) + \mathbf{D}\mathbf{u}(t) + \mathbf{H}\mathbf{w}(t),$$

where the six matrices  $\mathbf{A}$ ,  $\mathbf{B}$ ,  $\mathbf{C}$ ,  $\mathbf{D}$ ,  $\mathbf{E}$ , and  $\mathbf{H}$  have sizes  $n \times n$ ,  $n \times p$ ,  $q \times n$ ,  $q \times p$ ,  $n \times v$ , and  $q \times v$ , respectively.

The solution of the homogeneous state equations (first row of Equation (2.10), with  $\mathbf{B} = \mathbf{E} = \mathbf{0}$ ), given the initial state vector  $\mathbf{x}(t_0)$ , is written as

$$\mathbf{x}(t) = \boldsymbol{\phi}(t)\mathbf{x}(t_0), \quad (2.11)$$

where  $\boldsymbol{\phi}(t)$  is the  $n \times n$  state-transition matrix, i.e., the matrix that satisfies the equation

$$\frac{d\boldsymbol{\phi}(t)}{dt} = \mathbf{A}\boldsymbol{\phi}(t), \quad (2.12)$$

resulting into

$$\phi(t) = \ell^{-1}[(s\mathbf{I} - \mathbf{A})^{-1}] = e^{\mathbf{A}t} = \mathbf{I} + \mathbf{A}t + \frac{1}{2!}\mathbf{A}^2t^2 + \dots \quad (2.13)$$

The general solution of the state equations can easily be written in its Laplace transform form

$$\ell[\mathbf{x}(t)] = (s\mathbf{I} - \mathbf{A})^{-1}\mathbf{x}(t_0) + (s\mathbf{I} - \mathbf{A})^{-1}[\mathbf{B}\ell[\mathbf{u}(t)] + \mathbf{E}\ell[\mathbf{w}(t)]], \quad (2.14)$$

leading to write

$$\mathbf{x}(t) = \phi(t - t_0)\mathbf{x}(t_0) + \int_{t_0}^t \phi(t - \tau)[\mathbf{B}\mathbf{u}(\tau) + \mathbf{E}\mathbf{w}(\tau)]d\tau \quad t \geq t_0, \quad (2.15)$$

from which the output vector is determined by simply substituting the expression found for  $\mathbf{x}(t)$  in the second row of Equation (2.10).

From the Laplace transform of the output vector with initial conditions set to zero, i.e.,  $\mathbf{x}(t_0) = \mathbf{0}$ , one can find the relationship between the two representations of a linear time-invariant system by transfer functions and dynamic equations, being

$$\begin{aligned} \mathbf{G}_{\mathbf{u}}(s) &= \mathbf{C}(s\mathbf{I} - \mathbf{A})^{-1}\mathbf{B} + \mathbf{D}, \\ \mathbf{G}_{\mathbf{w}}(s) &= \mathbf{C}(s\mathbf{I} - \mathbf{A})^{-1}\mathbf{E} + \mathbf{H}. \end{aligned} \quad (2.16)$$

the  $q \times p$  and  $q \times v$  transfer function matrices between  $\mathbf{u}(t)$  and  $\mathbf{y}(t)$  when  $\mathbf{w}(t) = \mathbf{0}$ , and between  $\mathbf{w}(t)$  and  $\mathbf{y}(t)$  when  $\mathbf{u}(t) = \mathbf{0}$ , respectively.

Since the inverse of a matrix can be expressed as the ratio between its adjoint and its determinant, by substituting  $(s\mathbf{I} - \mathbf{A})^{-1} = \text{adj}(s\mathbf{I} - \mathbf{A})/|s\mathbf{I} - \mathbf{A}|$  in Equation (2.18), one can see that the denominator of the transfer function matrix  $\mathbf{G}_{\mathbf{u}}(s)$  equated to zero, i.e., the system characteristic function, is

$$|s\mathbf{I} - \mathbf{A}| = s^n + a_{n-1}s^{n-1} + \dots + a_1s + a_0 = 0. \quad (2.17)$$

and it is equal to the one obtained from Equation (2.5). Hence, the roots of the characteristic equation are the eigenvalues of the state matrix  $\mathbf{A}$ . The state matrix  $\mathbf{A}$  can be non-symmetric and show multiple-order eigenvalues. We assume that among its  $n$  eigenvalues,  $r < n$  are distinct.

## 2.3 Similarity Transformations

Let us introduce a SISO, i.e.,  $p = 1$  and  $q = 1$ , in a deterministic context ( $\mathbf{w} = \mathbf{0}$ ). The dynamic equations are transformed into another set of equations of the same dimension by the transformation

$$\mathbf{x}(t) = \mathbf{P}\bar{\mathbf{x}}(t) \Leftrightarrow \bar{\mathbf{x}}(t) = \mathbf{P}^{-1}\mathbf{x}(t), \quad (2.18)$$

which requires that  $\mathbf{P}$  is an  $n \times n$  non-singular matrix.

The transformation  $\mathbf{P}$  alters the matrices  $\mathbf{A}$ ,  $\mathbf{B}$ ,  $\mathbf{C}$ , and  $\mathbf{D}$ , but it is called a similarity transformation because in the transformed system the characteristic

equation, the eigenvalues, the eigenvectors, and the transfer function are all preserved by the transformation.

Let us define the controllability matrix as

$$\mathbf{S} = [\mathbf{B} \quad \mathbf{AB} \quad \mathbf{A}^2\mathbf{B} \quad \dots \quad \mathbf{A}^{n-1}\mathbf{B}], \quad (2.19)$$

and build the matrix

$$\mathbf{M} = \begin{bmatrix} a_1 & a_2 & \dots & a_{n-1} & 1 \\ a_2 & a_3 & \dots & 1 & 0 \\ \vdots & \vdots & \ddots & \vdots & \vdots \\ a_{n-1} & 1 & \dots & 0 & 0 \\ 1 & 0 & \dots & 0 & 0 \end{bmatrix}, \quad (2.20)$$

having all the elements of each anti-diagonal equal to each other. This matrix is called a Hankel matrix. The transformation,

$$\mathbf{P} = \mathbf{SM}, \quad (2.21)$$

transforms the dynamic equations into the controllability canonical form (CCF).

The observability matrix is defined as

$$\mathbf{V} = \begin{bmatrix} \mathbf{C} \\ \mathbf{CA} \\ \mathbf{CA}^2 \\ \vdots \\ \mathbf{CA}^{n-1} \end{bmatrix}. \quad (2.22)$$

The transformation,

$$\mathbf{P} = (\mathbf{MV})^{-1}, \quad (2.23)$$

transforms the dynamic equations into the observability canonical form (OCF).

It is worth noting that, for each selection of  $\mathbf{P}$ , one obtains a new model characterized by a different quadruple of matrices and a different state vector  $\mathbf{x}(t)$ . Nevertheless, the new transfer function coincides with the original one.

The quadruple of matrices arising from a given transfer function  $\mathbf{G}(s)$ , are regarded as a realization of  $\mathbf{G}(s)$ . Here the order of the model is the dimension of the vector  $\mathbf{x}(t)$ . The concept of minimal realization requires that there is no other realization with a state vector of lower size.

## 2.4 Observability and Controllability

Arguing on the minimal nature of a realization requires the introduction of the concepts of observability and controllability. The system is said to be observable when there are not two different initial states such that the corresponding output values are the same, for any time subsequent to the initial

one. The system is observable if and only if the observability matrix  $\mathbf{V}$  has rank  $n$ .

The system is said to be controllable if, for any value  $\xi$  of  $\mathbf{x}$ , there is a suitable sequence of  $\mathbf{u}(t)$  which produces an evolution of  $\mathbf{x}$  such that, at a time  $t_N$  after the initial one,  $\mathbf{x}(t_N) = \xi$ . The system is controllable when the rank of the controllability matrix  $\mathbf{S}$  is  $n$ .

A necessary and sufficient condition for having a minimal realization is that the model is controllable and observable.

The observability of a system depends on which variable is defined as the output. In any textbook of automatic control one finds examples of systems which are fully observable when the observed variable is selected in a suitable class; otherwise, these systems lose their observability. For instance, a system with three state variables and three potential observed variables, might be fully observable if either the first or the second observed variable is considered, but it might lose its observability when the third observed variable is the only one retained.

An observability study can be simply developed when the real dynamic system is known. In this case, the observability theory helps in selecting the suitable configuration of the sensors. However, given a network of sensors, one can encounter damage situations which are not detectable, just because of the unobservability of the system for that specific mock-up.

## 2.5 The Ideal Identification Process

With reference to a MIMO system for which a vector of observations of size  $p$  is available, one is free to assume the model (2.10), but:

- 1) the model order  $n$  is unknown;
- 2) the matrices in the state equations are unknown;
- 3) the matrices in the observation equations are unknown.

When a time discrete representation is adopted, Equation (2.10) takes the form

$$\begin{aligned}\mathbf{x}[(k+1)\Delta t] &= \mathbf{A}^\circ \mathbf{x}(k\Delta t) + \mathbf{B}^\circ \mathbf{u}(k\Delta t) + \mathbf{w}(k\Delta t), \\ \mathbf{y}(k\Delta t) &= \mathbf{C}^\circ \mathbf{x}(k\Delta t) + \mathbf{v}(k\Delta t),\end{aligned}\tag{2.24}$$

where  $\mathbf{x}(t)$  denotes the state variables;  $\mathbf{A}^\circ$ ,  $\mathbf{B}^\circ$  and  $\mathbf{C}^\circ$  are matrices of real elements and sizes consistent with the associated vectors;  $\mathbf{v}(t)$  and  $\mathbf{w}(t)$  denote the noises. Either the identification of the vectors  $\mathbf{v}(t)$  and  $\mathbf{w}(t)$ , or of the matrices  $\mathbf{A}^\circ$ ,  $\mathbf{B}^\circ$  and  $\mathbf{C}^\circ$  can be required. The attention is here focused on the latter problem and the disturbances are no longer taken into account.

Each anti-diagonal element of the Hankel matrix (2.20) is the discrete system impulse response

$$g(k\Delta t) = \mathbf{C}^\circ (\mathbf{A}^\circ)^{k-1} \mathbf{B}^\circ,\tag{2.25}$$

with  $k = 1, 2, \dots$ . But, being  $n$  unknown, one ignores how large the Hankel matrix is; thus he needs to write

$$1, \quad (2.26)$$

where the last two matrices are the observability and the controllability matrices for a system of infinite order.

In the framework depicted above, the identification problem is ideally solved by:

- 1) assessing the impulsive response of the system,  $g(t)$ ;
- 2) building, for the Hankel matrix, a truncated version of large size,  $\mathbf{M}_{tr}$ ;
- 3) determining the order of the Hankel matrix, which coincides with the order of the model for minimal realization;
- 4) factorizing the truncated Hankel matrix into the product  $\mathbf{V}_{ex} \mathbf{S}_{ex}$ , where the rows of  $\mathbf{V}_{ex}$  (with  $n$  columns) are in number of those of  $\mathbf{M}_{tr}$ , and the columns of  $\mathbf{S}_{ex}$  (with  $n$  rows) are in number of the ones of  $\mathbf{M}_{tr}$ . They are called the extended observability and controllability matrices.

Consider a matrix  $\mathbf{V}_{ex}^{par}$  obtained by  $j$  partitions of  $\mathbf{V}_{ex}$  in blocks of  $p$  rows, with  $q$  the size of  $\mathbf{y}(t)$  and  $j$  any integer. The first block of  $\mathbf{V}_{ex}^{par}$  is an estimation of the matrix  $\mathbf{C}^\circ$ . The matrix  $\mathbf{A}^\circ$  is given by

$$\mathbf{A}^\circ = [\mathbf{V}_{ex}^{parT} \mathbf{V}_{ex}^{par}]^{-1} \mathbf{V}_{ex}^{parT} \mathbf{V}_{ex}^{UP}, \quad (2.27)$$

where  $\mathbf{V}_{ex}^{UP}$  is obtained from  $\mathbf{V}_{ex}^{par}$  by deleting the first  $q$  rows and by adding a  $(j+1)$ -th block at the bottom. Finally,  $\mathbf{B}^\circ$  is obtained as the first columns of  $\mathbf{S}_{ex}$ .

In summary, the observation matrix  $\mathbf{C}^\circ$  is either given or assessed. Then the problem is to identify and to monitor the observed system eigenstructure, which is the collection of  $n$  pairs  $(\lambda, \phi_\lambda)$ , where  $\lambda$  ranges over the set of eigenvalues of the state matrix  $\mathbf{A}^\circ$ ; if  $\varphi_\lambda$  are the corresponding eigenvectors, then  $\phi_\lambda = \mathbf{C}^\circ \varphi_\lambda$ .

If the system has no multiple eigenvalues, this collection does not depend on the state space basis. The pair  $(\lambda, \phi_\lambda)$  is called a mode, and the set of  $n$  modes is considered as the system parameter  $\theta$ ,

$$\theta = \begin{Bmatrix} \Lambda \\ \text{vec}\Phi \end{Bmatrix}. \quad (2.28)$$

Here,  $\Lambda$  is the vector whose elements are the eigenvalues  $\lambda$ ,  $\Phi$  is the matrix whose columns are the  $\phi_\lambda$ , and  $\text{vec}$  is the column stacking operator. The resulting  $\theta$  has size  $(r + 1) n$ .

The Fault Detection and Isolation (FDI) consists of detecting and isolating the changes in the parameter vector  $\theta$ . By isolation one means to decide which mode(s) has(have) changed. This procedure is quite sensitive to numerical errors, which make it infeasible, but it underlines that the goal is to obtain a reliable estimate of the observability matrix from which the system matrices are then derived. Its feasible implementation can be found in OKID and in the Subspace Based Identification Method.

## 2.6 Operative Identification Procedures

In 1992, the Langley Research Center of NASA (National Aeronautics and Space Administration) released, within the COSMIC program, the Technical Memorandum 107566, which is a manual for a system/observer/controller

identification toolbox. Herein, several system identification algorithms were defined and implemented. Among these, it is worth mentioning

1. the “Eigensystem Realization Algorithm with Data Correlation” (ERA/DC), which identifies a state space model from pulse response time histories, using a data correlation technique;
2. the “State Vector Realization Algorithm” (SVRA), which identifies a state space from input and output data, using a state vector realization technique;
3. the “Observer and Kalman filter Identification” (OKID), which simultaneously identifies a state space model and an observer gain from input and output data.

This terminology became of reference in the literature of the Nineties, and it is introduced here to support a literature review of its applications for fault detection in Civil Engineering structures. In the following of this section, brief summaries of the OKID and of the Subspace Based Identification Method are provided.

### **2.6.1 Observer and Kalman Filter Identification (OKID)**

The input/output time histories are stored as column matrices, whose number of rows is equal to the number of sampled points.

The identification of the pulse response (also referred to as Markov parameters, since autoregressive models are often implemented to find the model dimension) is obtained by using the singular value decomposition sketched in Section 2.5. It is pursued for an auxiliary system (observer) rather than for the system itself.

Initially, an estimate of the number of Markov parameters must be specified. A plot of the Hankel matrix singular values is shown to aid the selection of the correct system order.

Theoretically, there is only a specific number of independent Markov system parameters for a finite set of Markov observer parameters. Therefore, a minimum number of Markov system parameters may be used in the ERA routine to minimize the computational time in identifying the system.

The identified system matrices are eventually returned by the algorithm.

### 2.6.2 Subspace Based Identification Method

In view of the exemplification illustrated in the next section, Equation (2.10) can be rewritten either as

$$\begin{aligned}\mathbf{x}(t+1) &= \mathbf{A}\mathbf{x}(t) + \mathbf{B}\mathbf{u}(t), \\ \mathbf{y}(t) &= \mathbf{C}\mathbf{x}(t) + \mathbf{D}\mathbf{u}(t) + \mathbf{v}(t),\end{aligned}\tag{2.29}$$

or

$$\begin{aligned}\mathbf{x}(t+1) &= \mathbf{A}\mathbf{x}(t) + \mathbf{B}\mathbf{u}(t) + \mathbf{K}\mathbf{e}(t), \\ \mathbf{y}(t) &= \mathbf{C}\mathbf{x}(t) + \mathbf{D}\mathbf{u}(t) + \mathbf{e}(t).\end{aligned}\tag{2.30}$$

The state-space matrices  $\mathbf{A}$ ,  $\mathbf{B}$ ,  $\mathbf{C}$ ,  $\mathbf{D}$ , and  $\mathbf{K}$  in Equation (2.30) can be estimated directly (without specifying any particular parameterization) by efficient subspace methods. The idea behind these methods can be explained as follows. If the sequence of the state vectors  $\mathbf{x}(t)$  were known together with  $\mathbf{y}(t)$  and  $\mathbf{u}(t)$ ,

Equation (2.30) would be a linear regression, and the matrices  $\mathbf{C}$  and  $\mathbf{D}$  could be estimated by the least squares method (see Appendix A). Hence, the vector  $\mathbf{e}(t)$  could be determined and treated as a known signal in Equation (2.30), which would then be another linear regression model for  $\mathbf{A}$ ,  $\mathbf{B}$  and  $\mathbf{K}$ . One could also treat Equation (2.29) as a linear regression for  $\mathbf{A}$ ,  $\mathbf{B}$ ,  $\mathbf{C}$ , and  $\mathbf{D}$ , with  $\mathbf{y}(t)$  and  $\mathbf{x}(t+1)$  as simultaneous outputs, and find the joint process and the measurement noises as the residuals from this regression. The Kalman gain,  $\mathbf{K}$ , could then be computed from the Riccati equation.

Thus, once the states are known, the estimation of the state-space matrices would become easy. How to find the states  $\mathbf{x}(t)$ ? All states in representations like Equation (2.30) can be formed as linear combinations of the  $k$ -steps ahead predicted outputs ( $k = 1, 2, \dots, n$ ). It is therefore a matter of finding these predictors and then selecting a basis among them. The subspace methods provide an efficient and numerically reliable way to determine the predictors by direct projections on the observed data. Further information can be found in Sections 7.3 and 10.6 of the book [Ljung, 1999].

## 2.7. An Exemplification Case of Study

A case of study was selected to give a numerical evidence to the previous theoretical expressions. For this purpose, one needs the structural response time histories of the quantity of interest (e.g., acceleration) to be recorded by different sensors. Some of them can be regarded as inputs and the remaining ones as outputs. In particular, adopting the results of the full scale tests

described in Chapter 8 also in this preliminary phase, seems to be pertinent. In this section, it is enough to specify the following main characteristics:

- 1) Every test is performed by applying 12 times a random excitation for a short period of time, and by recording each time the structural response until the rest is reached again;
- 2) for each test, 20 files of measurements are available;
- 3) the first file consists of the time sequence: the recorded times are equally spaced with an acquisition frequency of 200 samples per second (s.p.s.), i.e., with a sampling time interval  $\Delta t = 0.005$  s; a total duration of 252.39 s is recorded;
- 4) the second file, say the column vector named “input”, contains the force-time history, from which one can recognize the 12 excitation pulses in a sequence;
- 5) a third file contains the measures of a reference channel which is not considered in the analysis;
- 6) the remaining 17 response channels are available as outputs, and they can be organized in a matrix of 17 columns, which represents the “signal”.

Since each file consists of 12 pulses, attention is focused on a single pulse per file, i.e., all the records are divided into 12 replications. The analysis below is pursued on one single replication, starting from the first one.

MATLAB<sup>®</sup> is the selected software environment. The analysis is carried out by manually giving the following commands (the user-friendly interface GUI is also available, but it does not allow one to find the direct counterpart in the theory as the sequence of commands does).

a) “`Z = iddata(signal, input, 0.005)`”

- creates an object “Z” which in the present case is a SIMO (single input - multiple output) system recorded with a time step of 0.005 s;
- b) `“mod_basic = n4sid(iddata, [9:20], 'Cov', 'None')”` estimates the state-space models using a subspace method. The assignment of no covariance matrix blocks all the calculations of the uncertainty measures, since these may take the major part of the computational time. On the other side, asking the model order to fall in the range [9, 20] implies that the calculations are carried out for all the orders in the indicated interval. As a result, the plot in Figure 2.1a is obtained. It shows the relative importance of the dimension of the state vector. More precisely, the singular values of the Hankel matrices of the impulse response are graphed for the different orders. One is prompted to select the order based on this plot, or better on its zoom in Figure 2.1b. The idea is to choose an order such that the singular values for higher orders are comparatively small.

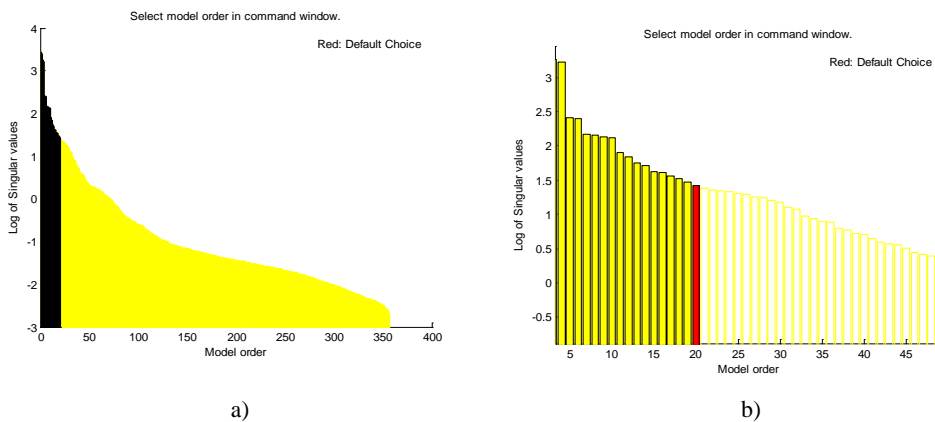


**Figure 2.1** (a) Graph of the singular values of the Hankel matrices of the impulse response for different orders of the state space model. (b) Zoom of Figure 2.1a.

- c) The value 16 is first selected for the order and the model at the top of Figure 2.2 is estimated.
- d) The state space matrix (of size  $16 \times 16$ ) is characterized by eigenvalues which can be obtained by the command  
`“lambda=eig(mod_basic.A)”`,  
 which results into:

```

-0.2831 + 0.9394i
-0.2831 - 0.9394i
-0.5295 + 0.8239i
-0.5295 - 0.8239i
-0.5036 + 0.6709i
-0.5036 - 0.6709i
-0.7977 + 0.5254i
-0.7977 - 0.5254i
-0.6617 + 0.6536i
-0.6617 - 0.6536i
-0.6304
 0.9487 + 0.3062i
 0.9487 - 0.3062i
 0.8225
 0.7291 + 0.0198i
 0.7291 - 0.0198i

```

- e) The commands:

```
“obb = obsv(mod_basic.A, mod_basic.C);”
```

```
“rank(obb)”
```

compute the observability matrix (of size  $272 \times 16$ ) and its rank, which is 16 for the present model.

The results which are obtained by choosing different options than those above are now discussed.

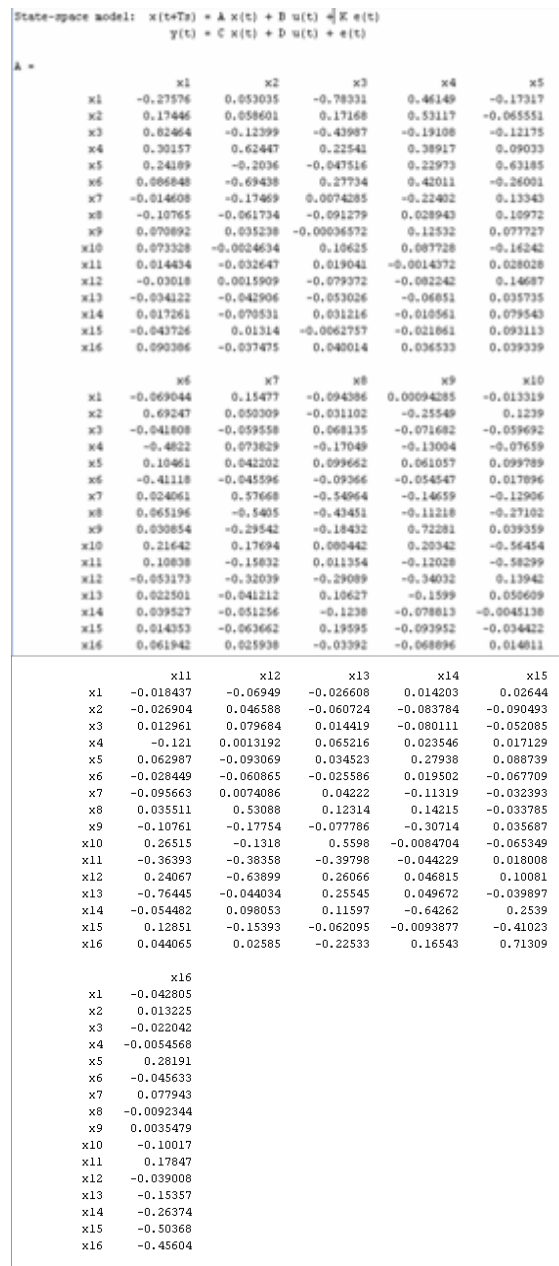


Figure 2.2 Matrix A of the estimated state space model for order number 16.

- i) Which would have been the result of selecting the default value of 20 instead of 16 as model order? A complete different model would result in terms of matrices, but some eigenvalues (six) would be preserved, as shown in Figure 2.3.
- ii) Since 12 replications are available, one can repeat the above calculations on the second pulse of the excitation. The results are compared in Figures 2.4 a and b for the models of order 16 and 20, respectively.
- iii) The previous models were derived with a non-zero  $\mathbf{K}$  matrix in Equation (2.30), but one can also search for the model with no disturbance by:
- ```
“mod_nodis = n4sid(z,16, 'Cov', 'None',
'DisturbanceModel', 'None')”
```
- This provides the new plot of Figure 2.5 instead of the one of Figure 2.1, while Figure 2.4 is replaced by Figure 2.6. Here three replications are drawn and a better agreement of the eigenvalues is found at least for the case of the model of order 16 (Figure 2.6a).
- iv) The software adopted for the numerical examples and developed in this section also works when no input is specified. To repeat the calculations for such a case, however, is out of the scope of this study.

Assume now that the considered record of input and output signals was associated to a damaged state of the structure, and that for the same system a set of undamaged records is also available. The Fault Detection and Isolation (FDI), which consists of detecting and isolating the changes in the parameter vector $\boldsymbol{\theta}$, is performed by moving from Figure 2.6a to Figure 2.7, where the largest circles denotes the eigenvalues computed from the damaged case.

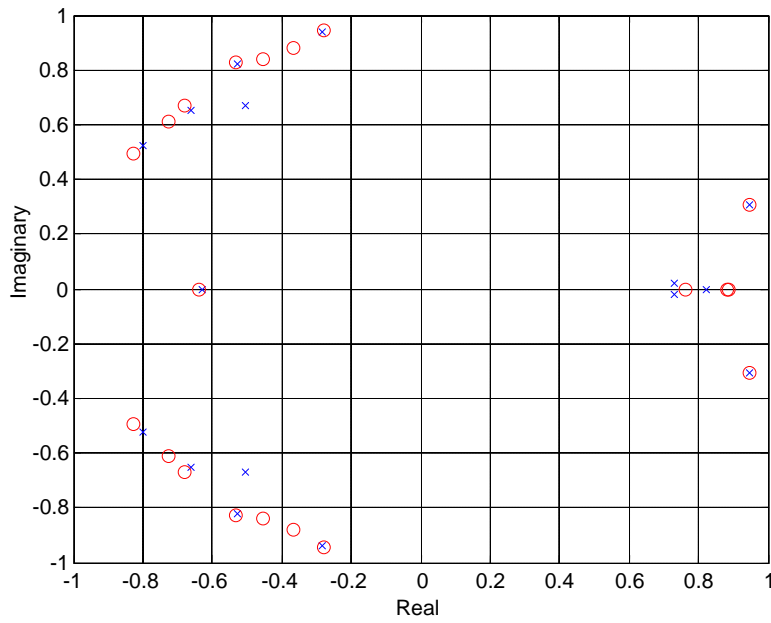


Figure 2.3 Eigenvalues of the state space matrix A for the models of order 16 (\times) and 20 (\circ).

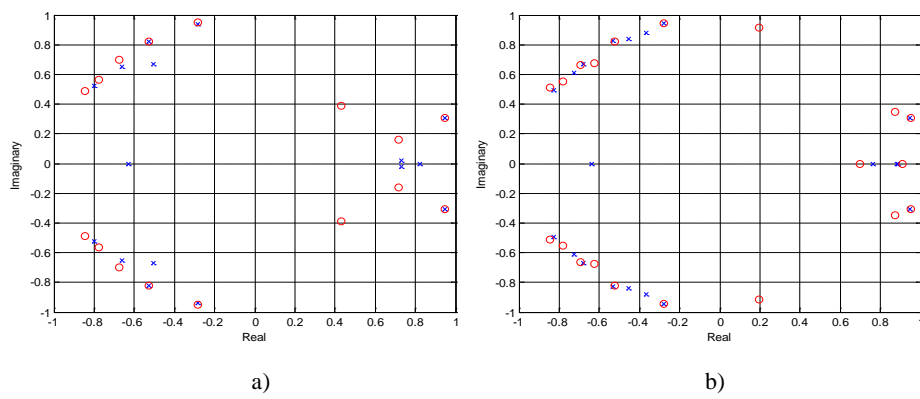


Figure 2.4 Eigenvalues of the state space matrix A from the first two replications, for the models of order: (a) 16 and (b) 20.

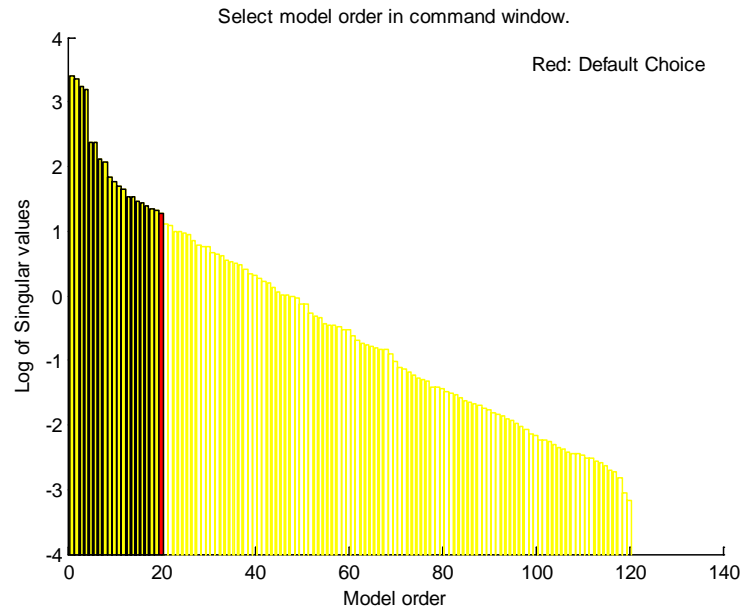


Figure 2.5 Model selection graph when the no-disturbance option is set.

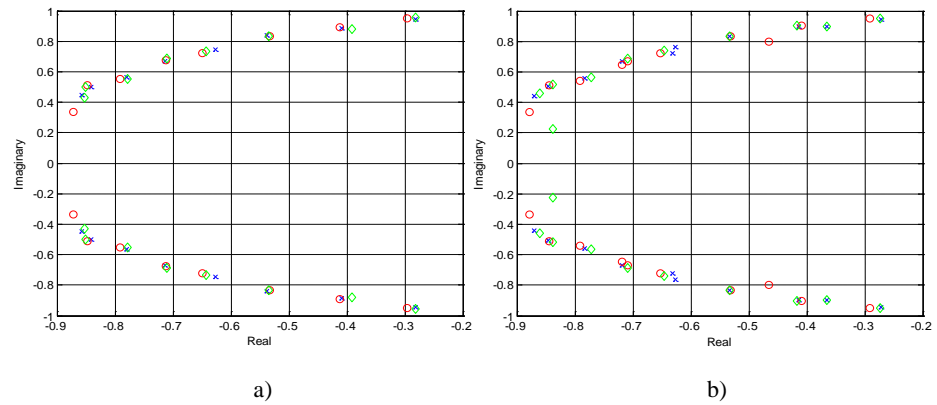


Figure 2.6 Eigenvalues of the state space matrix \mathbf{A} from the first three replications, with the no-disturbance option and for the models of order (a) 16 and (b) 20.

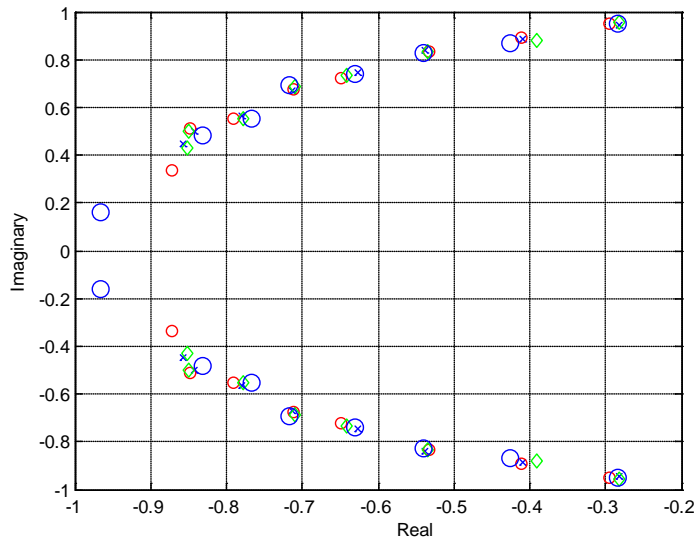


Figure 2.7 Eigenvalues of the undamaged system (largest circles), and comparison with those calculated for the three different replications of the previously considered damaged system (model order 16).

The damaged case is distinguished from the undamaged one by the presence of a pair of eigenvalues on the left hand side. However, no localization of the damage can be achieved.

References for Chapter 2

- Basseville M., Abdelghani M. and Benveniste A. (1997). “Subspace-based Fault Detection and Isolation – Application to Vibration Monitoring”, INRIA 3299, Rennes.
- Bittanti S. (1993). *Teoria della Predizione e del Filtraggio*, Pitagora, Bologna (in Italian).
- Bittanti S. (1997). *Identificazione dei Modelli e Controllo Adattivo*, Pitagora, Bologna, (in Italian).
- Brogan W.L. (1985). *Modern Control Theory*, Prentice Hall Int., Englewood Cliffs.
- Juang J.N. (1992). *Applied System Identification*, Prentice Hall Int., Englewood Cliffs.
- Juang J.N., Horta L.G., and Phan M. (1992). “System/Observer/Controller Identification Toolbox”, NASA Technical Memorandum 107566.
- Kuo B.C. (1995). *Automatic Control Systems*, Prentice Hall Int., Englewood Cliffs.
- Ljung L. (1999). *System Identification - Theory for the User*, Prentice Hall, Upper Saddle River, N.J., 2nd edition.
- Matworks Inc. (2004). *MATLAB User’s guide*.
- Peeters B. (2000). *System Identification and Damage Detection in Civil Engineering*, PhD Thesis, K.U. Leuven Civil Engineering Department.
- Pisano A.A. (1999). *Structural System Identification: Advanced Approaches and Applications*, Ph.D. Thesis, Graduate School of Civil Engineering, University of Pavia, n. 4.

Chapter 3

Structural Health Monitoring (SHM) in Civil Engineering Applications: a Brief Survey

The main literature reviews on structural health monitoring can be found in [Doebbling et al., 1997] and [Sohn et al., 2003]. These reports are part of the Damage Identification Project ongoing at the Engineering Sciences and Applications Division, Weapon Response Group, of the Los Alamos National Laboratory (LANL), and they are updated every five or six years.

Structural Health Monitoring (SHM) is, in general, defined as the process of implementing a damage detection strategy for aerospace, civil and mechanical engineering.

Usage Monitoring (UM) is the attempt to measure the input to, and the response of a structure prior to damage so that regression analysis can be used to predict the onset of damage and deterioration in the structural conditions.

Prognosis is the coupling of information from SHM, UM, the current environmental and operational conditions, the previous component and system level testing, and the numerical modeling, to estimate the remaining useful life of the system.

In general, the SHM process consists of the observation of a system over time using periodically sampled dynamic response measurements from an array of sensors, the extraction of damage-sensitive features from these measurements, and the statistical analysis of these features to determine the current state of the system health.

For long-term SHM, the output of this process is a periodically updated information regarding the ability of the structure to perform its intended function, in light of the inevitable aging and degradation resulting from the operational environment.

After extreme events, such as earthquakes or blast loading, SHM is used for rapid condition screening and it aims to provide, in near real time, reliable information regarding the integrity of the structure.

According to the LANL statistical pattern recognition paradigm defined in [Farrar and Doebling, 1999], the SHM process can be described in four steps:

1. Operational Evaluation;
2. Data Acquisition, Fusion, and Cleansing;
3. Feature Extraction and Information Condensation;
4. Statistical Model Development for Feature Discrimination.

The focus of the present thesis regards items 3 and 4, namely information condensation and feature discrimination. However, in any practical applications, it is always necessary to start from 1 and 2, as Chapters 8 and 9, which report the experimental activity, will show. Therefore, this Chapter provides a synthesis for items 1 and 2 as a natural premise to the thesis developments. In particular, the motivations of this thesis are explained, and the guidelines following which the experimental analyses need to be carried out are provided.

3.1 Operational Evaluation

The operational evaluation begins to define why the monitoring is to be done, and it begins to tailor the monitoring to the unique aspects of the system and to the unique features of the damage that is to be detected. In this preliminary phase, the economic and/or life safety motives for performing the monitoring are considered; the definition of damage for the system being monitored is given; the operational and environmental conditions under which the system functions are monitored, and the eventual limitations in acquiring data in the operational environment are addressed.

3.1.1 Economic and Life Safety Issues

The economic and life safety issues are the primary driving force behind the development of structural health monitoring technology in various fields. The first studies on the topic trace down to the early sixties, but only special structures applications were considered, such as nuclear power plants and

offshore oil platforms. For example, the oil industry needed rapid fatigue analysis in the 80's, when large jacket platforms were being designed and the fatigue of these structures was an important issue. Frequency-based methods were investigated, because the dynamic wave and wind loads frequency data were readily available. A monitoring system was operated for six years by the British Petroleum, and the result was that the structure was designed too conservatively. Subsequent structures were therefore designed less conservatively with consistent cost savings.

The spread of SHM techniques to common types of civil and/or aerospace structures is now one of the main tasks of the worldwide research activity, and it is motivated by the aging of the structures and by the consequent increase of the costs of their maintenance or replacement, which are necessary to guarantee the life safety. The fast development of new technologies could make this task feasible in the near future, also thanks to the decrease of the price of the necessary equipment. However, two critical issues first need to be solved: if on one hand the hardware must be adapted to the conditions suitable to civil infrastructure applications as depicted in this and in the next Chapters, on the other hand the software to be implemented for damage detection still does not find an agreement in the research community. It is starting from these two considerations that this thesis took its first steps within the project framework depicted in Chapter 4, where the technological aspects under development are presented. The rest of the thesis is then focused on the complex issue of solving the damage detection problem. In this Chapter, the motivations of these studies are emphasized on the base of the literature sources.

Considering the number of structures reaching a critical age, innovative test and assessment tools as well as methods are required in order to avoid an

infrastructure breakdown. In particular, the peak of construction of the European transportation infrastructure happened in the 70's of the last century. The critical age when rehabilitation and retrofit works at bridges become essential starts after 30 years of service. Considering the time of construction, a huge peak of repair and retrofit investments are therefore expected for the years 2005 onward, as shown by Figure 3.1. The need for the maintenance of bridges and civil infrastructures is of fundamental importance due to the fact that the society depends on the transportation infrastructure for economic, environmental, life-quality, safety and employment protection reasons. The failure of a single bridge can cause a huge loss to the society.

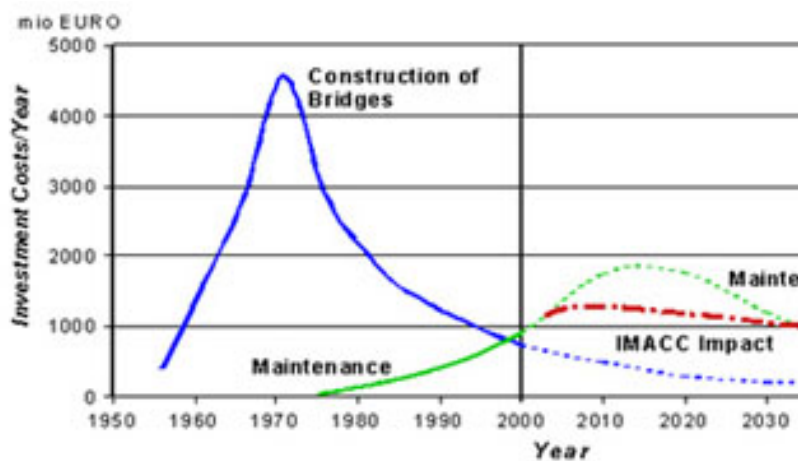


Figure 3.1 Construction-cost versus maintenance-estimate and monitoring-impact.

Furthermore, the seismic resistant construction methods are of fundamental importance for disaster prevention. Not only a loss of life can be minimized, but also the heavy toll in injuries, the economic loss of infrastructure assets, and the burdening of the environment by large amounts of debris, can be reduced by implementing seismic resistant design and construction processes. For this purpose, the methodologies for the assessment of structures and the consequent strengthening requirements following an earthquakes are necessary.

Together with the life safety issues, several economic reasons are pushing the research toward the implementation of structural health monitoring systems. A study developed by [Helmicki et al., 1997] in the United States of America showed that the inadequacies in their national transportation system may be reducing the annual growth rate in the gross domestic product by as much as the 1%. This means that the annual compounding economic impact of the non-optimal operation and maintenance of the civil infrastructures may reach a significantly higher level than that of a major natural disaster. The Federal Highway Administration estimates that nearly the 35% of all bridges in the United States (236000 out of 576000) are either structurally or functionally deficient, as reported in [Wang et al., 1997]. The cost of repair or rebuild lies in the billion of dollars. Effective SHM methods could reduce this cost while providing higher levels of safety for the users during repair or assessment.

Similar conclusions were achieved by the American Association of State Highway and Transportation Officials (AASHTO) and the California Department of Transportation (CALTRANS). The latter one developed an evaluation system for the reliability, the durability, and the serviceability of a structure. This system enables the upper management to assess the costs of repair and maintenance of bridges and highways, and to allocate the resources

efficiently. A loss function, L_{ij} , represents an expected loss when the j th system component fails to resist the i th failure mode or hazard, and it is a function of the structure's change in stiffness or boundary conditions

$$L_{ij} = m_i [k_j^{current} - k_j^{baseline}], \quad (3.1)$$

where m_i is a loss coefficient related to the i th failure mode or i th hazard; $k_j^{current}$ and $k_j^{baseline}$ are the current and baseline stiffness of the j th element, respectively. This formula allows one to evaluate the economic loss in quantitative terms when a structure is repaired or monitored for damage. Then, when deciding on whether or not to implement a SHM scheme, the following Corporate Performance Measure (CPM) of the SHM scheme can be used

$$CPM = \frac{Capacity}{\sum_{i=1}^n \sum_{j=1}^m [C_{ij} + L_{ij}]}, \quad (3.2)$$

where the term *Capacity* in the numerator gives a measure of the structure's remaining usage, and C_{ij} represents the cost of the structure's component j to resist to the i th failure mode or hazard. The result is a methodology that provides a logical connection between the allocation of resources and the structural deterioration. Further details can be found in [Sikorsky, 1999].

Although this thesis considers only the applications of structural health monitoring to civil engineering structures, it must be mentioned that a lot of studies on the topic refer also to different application fields. The SHM systems

are becoming even more important for those structures which have reduced strength capacity as a trade-off with weight reduction. In particular, the aerospace industry and the shipbuilding industry concentrate a lot of their efforts in design optimization to reduce the weight of some structures, and yet still provide the required strength. The increasing demands for lightweight structures and high strength-to-weight ratio materials have motivated the use of anisotropic reinforced laminated composites. Delamination is one of the most important failure modes for these composite materials. Such defect might be caused by poor process control during manufacturing, impact loading, or other hazardous service environment. The delamination substantially reduces the stiffness and the buckling load capacity, which, in turn, influences the structure's stability characteristics.

The pipeline corrosion is instead the major problem for the oil, chemical and petro-chemical industries. The cost associated with the removal of the pipe insulation for visual inspection is prohibitive, thus motivating any sort of smart innovation in that field.

As one may notice, the damage definition varies depending on the case-specific situation. Therefore, any practical SHM application should specify a priori what kind of damage needs to be detected.

3.1.2 Definition of Damage

In general, damage is defined as the changes introduced into a system that adversely affect its current or future performance. In structural and mechanical systems, the changes to the material and/or geometric properties, including the changes to the boundary conditions and to the system connectivity, are considered as damage.

Implicit in this definition is the concept that damage is not meaningful without a comparison between two different states of the system, one of which is assumed to represent the initial, and often undamaged state. However, in many situations damage detection must be performed in an unsupervised learning mode, which occurs when data from damaged systems are not available. To overcome this problem, in many studies the damage is intentionally introduced into a structure, in an effort to simulate damage without having to wait for such a damage to occur. In other cases, a damage-sensitive feature is postulated, and then an experiment is developed to demonstrate the effectiveness of this feature. In these cases there is no need to formally define the damage. Most laboratory investigations fall into this category. On the other hand, when a SHM system is deployed on an in-situ structure, it is imperative that the investigators first clearly define and quantify the damage that they are looking for. Then, they can increase the likelihood that the damage will be detected and make optimal use of their sensing resources.

A critical issue in the implementation of a SHM system is the length scale of the damage. Indeed, all damages begin at the material level and then, under appropriate loading scenarios, they progress to the component and system levels at various rates. At the early stage, damage is typically a local phenomenon and it may not significantly influence the lower-frequency global response of a structure that is normally measured during the vibration tests. There is a need to capture the system response on widely varying length scales, and such system model has proven difficult.

The time scale may also vary with respect to the type, the size, and the location of the damage under investigation. The adverse effects of the damage can be either immediate, or may take some time before they alter the system

performance. For example, a crack that forms in a mechanical part produces a change in the geometry which alters the stiffness characteristics of that part. The period of time in which this damage will affect the system performance depends on the size and location of the crack, and on the loads applied to the system. The damage associated with fatigue and corrosion can accumulate over long periods of time. Damage can also result from scheduled discrete events, such as an aircraft landing, and from unscheduled discrete events, such as an earthquake or the enemy fire on a military vehicle.

The basic premise of most damage detection methods is that the damage will alter the stiffness, the mass, or the energy dissipation properties of a system, which, in turn, alter the measured dynamic response of the system.

In many studies, the damage in beams is simply defined as a reduction in the bending stiffness, EI , where I is the moment of inertia of the beam cross-section and E is the elastic modulus. For multi-story buildings undergoing earthquake loads, the stiffness reduction of beams and columns are usually investigated.

For example, to calculate the stiffness degradation of a damaged reinforced concrete beam, a sensitivity-based model updating technique was developed by [Maeck et al., 1998]:

$$S \Delta P = \Delta \theta, \quad (3.3)$$

where $\Delta \theta$ is the discrepancy between the analytical and experimental modal parameters; ΔP is the perturbation of the design parameters to be estimated; S is the Jacobean or sensitivity matrix consisting of the first derivative of the analytical modal parameters with respect to the design parameters. To simplify the above sensitivity-based updating technique, a damage function which

describes the damage pattern along the beam length using only few representative parameters is identified. In particular, the stiffness degradation is assumed to be of the following form

$$E = E_0[1 - (1 - \alpha)\cos^2 t] \quad , \quad t = \frac{\pi}{2} \left(\frac{x}{\beta L/2} \right)^n \quad , \quad (3.4)$$

where E_0 is the initial Young modulus; L is the length of the beam; x is the distance along the beam measured from the center line; α , β , and n are the damage parameters to be updated. α represents the level of stiffness reduction at the center of the beam: no damage is present when α is equal to 1. β characterizes the relative length of the damaged zone with respect to the length of the beam. The exponent n characterizes the variation of the Young modulus from the beam center to the end of the damaged zone. If n is larger than 1, a flat damage pattern is produced. Otherwise, a steep pattern is obtained.

In another approach [Onate et al., 2000], the complex behavior of concrete, including concrete cracking, tension stiffening, and nonlinear multi-axial material properties is considered to detect the cracks in concrete and reinforced concrete structures. In particular, the finite element techniques are developed to permit a more rational analysis of the cracking. Based on a local damage index, a modified constitutive equation between stress and strain can be formulated. The modified constitutive model accounts for the reduction of the moment resisting area caused by the cracking, and for the different response in tension and compression.

Although several methods are available to detect a single crack in a concrete test beam, only few of them were employed for multiple cracking.

3.1.3 Environmental and/or Operational Conditions

The road traffic is recorded when monitoring the operational conditions of a bridge. Different vehicle types with varying axles and suspension systems, various pavement roughness, and different traffic loads with varying traffic speeds are considered. The traffic loads are measured by means of a weight-in-motion roadway scale. The thermal stresses caused by the variation in temperature throughout the day are also to be measured, because they can far exceed the environmental stresses and the traffic-induced stresses, but they are not explicitly considered in the bridge design. A bridge under construction should be monitored from the initial phase to verify the fabrication stresses induced in the bridge members before usage.

When a structure is monitored over a long period of time, it is possible to have multiple baseline configurations. That is the structures under test can be subjected to alterations during the normal operating conditions, such as changes in the mass. To cope with this situation, a damage detection model based on singular value decomposition (SVD) is proposed by [Ruotolo and Surace, 1997] to distinguish between changes in the working conditions and the onset of damage. Let \mathbf{v}_i the feature vector collected at n different normal configurations ($i = 1, 2, \dots, n$). When a new feature vector \mathbf{v}_c is collected, the whole feature vectors can be arranged in a matrix, $\mathbf{M} = [\mathbf{v}_1 \mathbf{v}_2 \dots \mathbf{v}_n \mathbf{v}_c]$. If the structure is intact, the new feature vector, \mathbf{v}_c , will be close to one of the feature vectors \mathbf{v}_i , and the rank of the matrix \mathbf{M} estimated by SVD should remain unchanged by

adding \mathbf{v}_c to \mathbf{M} . On the other hand, if the structure experienced damage, the rank of the matrix \mathbf{M} will increase by one.

Practical issues are associated with making accurate and repeatable dynamic response measurements on complex structures, at a limit number of locations and often operating in adverse environments. The operational constraints of a bridge testing can obscure the damage detection results. In particular, the bridge testing using traffic excitation suffers from the lack of sufficient instrumentation. Indeed, when normal traffic is used as an excitation source, only the exterior sides of the bridge main span can be instrumented, whereas other places, such as the locations under the vehicle path or on the bottom of the deck, are rarely accessible unless a truck with a special crane is available. The limitation of measurement points becomes a bigger problem when closely spaced modes exist. Accurate numerical models are needed for bridge applications in which some modal frequencies are closely spaced. The closely spaced frequencies can be obscured during the modal analysis of measurement data from limited measurements on the bridge span sides and can lead to poor analysis results.

When using modal parameters for damage detection, one must also take into account that the environmental variations may cause changes in these parameters. Therefore, the environmental and operational variations such as varying temperature, moisture, and loading conditions affecting the dynamic response of the structures, can often mask the subtler structural changes caused by damage. Several studies that addressed this issue are reported below.

[Farrar et al., 1994] performed a vibration test on the I-40 bridge in New Mexico, USA, to investigate if the modal parameters can be used to identify structural damage within the bridge. Four different levels of damage are

introduced to the bridge by gradually cutting one of the bridge girders. Because the magnitude of the bridge's natural frequency is proportional to its stiffness, the decrease of the frequency is expected as the damage progresses. However, the frequency value increases for the first two damage levels, and then eventually decreases for the remaining two damage cases. Later investigations revealed that, beside the artificially introduced damage, the ambient temperature of the bridge played a major role in the variation of the bridge's dynamic characteristics.

Temperatures are therefore measured in [Doebling and Farrar, 1997] to ascertain their effects on the modal properties of the Alamosa Canyon Bridge in New Mexico. A total of 52 data sets are recorded during the six days of testing. A series of modal tests are conducted every 2 hours over a 24 hour period to assess the change of modal properties as a function of the environmental conditions. A statistical procedure that propagates the variability in the measured frequency response function (FRF) data and estimates the uncertainty bounds of the corresponding modal properties is developed. In addition, various levels of attempted damage are introduced to the bridge, but the permitted alternation in the bridge does not result in noticeable changes in the modal properties. Based on the obtained experimental data, it is therefore observed that the effects of environmental changes can often mask subtler structural changes caused by damage. In particular, the first modal frequency is shown to vary approximately 5% during the 24 hours cycle and to be closely related to the temperature differential across the deck of the bridge. Because the bridge is approximately aligned in the north and south direction, there was a large temperature gradient between the east and west sides of the bridge deck throughout the day.

A linear adaptive filter is examined in [Sohn et al., 1998] to discriminate the changes of modal parameters due to temperature changes from those caused by structural damage or other environmental effects. Experimental study from the Alamosa Canyon Bridge indicate that a linear filter of four temperature inputs (two time and two spatial dimensions) can reproduce the variation of the frequencies with respect to the time of the day. From this linear filter, a confidence interval of the fundamental frequency for a new temperature profile is established to discriminate the natural variation due to temperature from other effects.

In conclusion, SHM based on vibration signature will not be accepted in practical applications unless robust techniques are developed to explicitly account for the environmental and operational constraints/conditions. Although the researchers are aware of the importance of these issues when the SHM system is deployed in field, there are little proven techniques able to properly address these issues.

3.2 Sensing the Response of a Structure

The process of sensing the response of a structure involves the data acquisition, fusion and cleansing through signal processing techniques. The actual implantation of a structural health monitoring system typically starts with designing a proof-of-concept experiment. First, an excitation mechanism for vibration testing is determined. Then, the physical quantities to be measured, the type and number of sensors, the sensors resolution, the bandwidth, and the sensor placement are decided. The data acquisition/storage/transmittal hardware

is selected, and the issues of data acquisition are addressed, such as how to select the resolution and the dynamic ranges of the measured quantities, which anti-aliasing filter should be applied, and how often the data should be collected. If fatigue crack growth is the failure mode of concern, it is necessary to collect data almost continuously at relatively short time intervals; in other cases data may be collected immediately before and at periodic intervals after a severe event. Finally, the recorded data are transmitted safely to the central monitoring facilities or to the interested users of the data.

The process is application-specific and the economic considerations play a major role in these decisions. A proper selection and design of the data acquisition system and of the signal processing procedures should be eventually based on a prior numerical simulation of the test system.

Because data can be measured under varying conditions, it is important to perform a data normalization, i.e., a procedure to “normalize” the data sets such that the signal changes caused by the operational and environmental variations of the system can be separated from the structural changes of interest, such as the structural deterioration or degradation. One of the most common procedures is to normalize the measured response by the measured inputs. When environmental or operating condition variability is an issue, the need can arise to normalize the data in some temporal fashion to facilitate the comparison of the data measured at similar times of an environmental or operational cycle. An alternative is to normalize the data by the direct measurements of the varying environmental or operational parameters.

The sources of variability in the data acquisition process and with the system being monitored need to be identified and minimized at the possible extent. In general, not all the sources of variability can be eliminated. Therefore, it is

necessary to make the appropriate measurements such that these sources can be statistically identified.

The data fusion is the procedure for integrating the information (data) from disparate sources (a multitude of sensors) with the objective of making a more robust decision than it is possible with any one sensor alone [Klein, 1999]. It can be performed in an unsophisticated manner by examining the relative information between various sensors; or complex analyses of the information from sensor arrays such as those provided by artificial neural networks can be used.

The data cleansing is the process of selectively choosing the data to accept for, or to reject from, the feature selection process. For this purpose, many signal processing techniques, such as filtering and decimation, can be applied to the data acquired during the dynamic tests. The data cleansing process is usually based on the knowledge gained by the individuals directly involved with the data acquisition.

These practical issues need to be addressed for any damage detection method being adopted. Their application in the study cases treated in this thesis is described in Chapters 8 and 9.

3.3 Excitation Methods

The excitation methods are grouped in two categories: the forced excitation methods and the ambient excitation methods.

In the forced excitation testing of structures, a wide variety of forcing techniques is used including actuators, shakers, step relaxation, and various

methods of measured impact (Figure 3.2). For most of the forced vibration tests the input forcing function is well characterized since the excitation forces are applied in a controlled manner and measured. Furthermore, the system identification techniques for determining the modal characteristics (resonant frequencies, mode shapes, and modal damping ratios) of structures subjected to measured inputs are well established. One advantage of the forced vibration test is that the input force is usually strong enough to dominate other noise disturbance, resulting in a strong signal to noise ratio.

Local excitation methods, such as excitation using a piezoelectric actuator (Figure 3.3), are a subset of the forced excitation techniques which can be employed to excite only a localized region of the whole system. This facilitates the extraction of features sensitive to local structural responses rather than the global behavior of the system, and often mitigates the environmental and operational effects, which tend to be global phenomena. The nature of high frequency excitation, which is typically above 30 Hz, makes this technique very sensitive to local changes within the structure. The small flaws in the early stages of damage are often undetectable through global vibration signature methods, but these flaws can be detected using the PZT sensor-actuators, provided the PZT sensor-actuators are near the incipient damage.

The ambient excitation is the excitation experienced by the structure under its normal operating conditions. All structures are constantly subject to ambient excitation from various sources (Figure 3.4). The input force is generally not recorded or cannot be measured during the dynamic tests that utilize ambient excitation. Because the input is not measured, it is not known if this excitation source provides the input at the frequencies of interest, how stationary the input is, or how uniform the input is over a particular frequency range. Even when

measured input excitation (forced excitation) is used, ambient vibration sources are often still present producing undesirable and often unavoidable extraneous input to the structure.

Whether or not the measurements of the excitation forces are available make a difference for the subsequent system identification procedures. Many structural parameters, such as modal frequencies, modal damping and mode shapes, can be generally identified without the need for a precise measurement of the excitation forces. However, these situations usually require the nature of the excitation to be well characterized (e.g., a broadband white noise, an impulse, etc.) even if the actual loading event is not measured. On the other hand, there are many other structural parameters, such as the mode participation factors, that require the excitation to the system to be monitored.

The decision regarding the measuring of the excitation forces is determined by both the damage-sensitive features that will be identified, and the practicality of measuring the excitation force on a particular structure. There are many situations where measuring the excitation forces on a structure are both practical and useful, and there are other situations where it is both impractical and not useful. In either case, some meaningful information with respect to the structures can be extracted from the data, but whether the trade of additional testing cost for the additional information is worthwhile is a case-specific decision. For example, during the modal test of a frame structure in a laboratory, the applied loads from an impact hammer, a shaking table, or a shaker are readily measured using the standard instrumentation. However, during a field test of a highway bridge under loading from high-speed traffic, it is far less clear how to measure all the loads imparted to the structure from the traffic. Additionally, the bridge will undergo environmental loads such as wind

and thermal gradients that may be difficult to characterize. For the development of on-line real-time SHM, the use of ambient excitation provides an attractive means of exciting the structure. This type of excitation is particularly a very attractive alternative to forced vibration tests during dynamic testing of bridge structures, because bridges are consistently subject to ambient excitation from sources such as traffic, wind, wave propagation, pedestrians, and seismic excitation. Except for the seismic excitation, the input force is generally not recorded or cannot be measured during the dynamic tests that utilize ambient excitation. However, the use of ambient excitation often provides a means of evaluating the response of the structure to the actual vibration environment of interest.



(a) A hydraulic shaker: larger force capacity than electro-dynamic shaker but limited high frequency capability.



(b) Mechanical eccentric mass shaker: generates sinusoidal excitation, but difficult to apply in vertical direction.



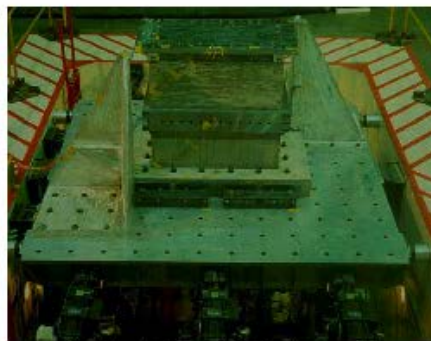
(c) An electro-dynamic shaker:



(d) Impact excitation with an impact hammer



(e) Step-relaxation applied to a wind turbine



(f) A hydraulic multi-axis shake table

Figure 3.2 Different types of forced excitation methods.

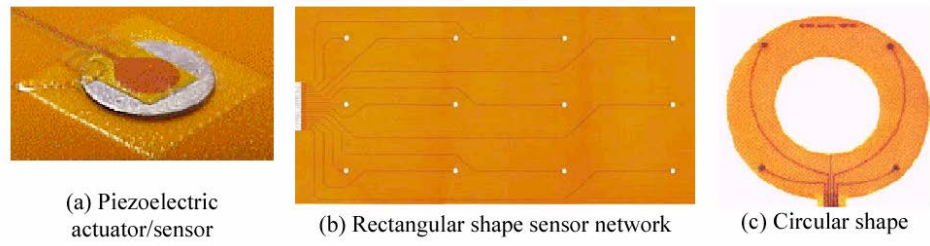


Figure 3.3 An embedded network of distributed piezoelectric actuators/sensors: this thin film of sensor/actuator network can be either surface mounted or embedded into composite structures.

(Courtesy of Agilent Technologies, Inc.)



Figure 3.4 Examples of ambient excitations.

References for Chapter 3

- Balageas D., ed. (2002). *Structural Health Monitoring 2002*, Destec Publications, Lancaster.
- Boller C. and Staszewski W.J., eds. (2004). *Structural Health Monitoring 2004*, Destec Publications, Lancaster.
- Casciati F., ed. (2003). *Proceedings 3rd World Conference on Structural Control*, John Wiley & Sons, Chichester.
- Chang F-K., ed. (1997). *Structural Health Monitoring*, Technomic, Lancaster.
- Chang F-K., ed. (2000). *Structural Health Monitoring 2000*, Technomic, Lancaster.
- Chang F-K., ed. (2001). *Structural Health Monitoring 2001*, CRC Press, Boca Raton.
- Chang F-K., ed. (2003). *Structural Health Monitoring 2003*, Destech Publications, Lancaster.
- Doebling S.W., Farrar C.R., Prime M.B., and Shevitz D.W. (1997). "Damage Identification and Health Monitoring of Structural and Mechanical Systems from Changes in their Vibration Characteristics: a Literature Review",
- Doebling S.W. and Farrar C.R. (1997). "Using Statistical Analysis to Enhance Modal-Based Damage Identification", *Proceedings of DAMAS '97, Structural Damage Assessment Using Advanced Signal Processing Procedures*, University of Sheffield, UK, pp.199-210.
- Farrar C. R., Baker W. E., Bell T. M., Cone K. M., Darling, T.W., Duffey T.A., Eklund A., and Migliori A. (1994). "Dynamic Characterization and

- Damage Detection in the I-40 Bridge Over the Rio Grande,” Los Alamos National Laboratory Report: LA-12767-MS.
- Farrar C.R. and Doebling S.W. (1999). “Vibration-Based Structural Damage Identification”, accepted for publication on *Philosophical Transactions: Mathematical, Physical and Engineering Sciences*, Royal Society, London, UK.
- Farrar C.R., Sohn H., Hemez F.M., Anderson M.C., Bement M.T., Cornwell P.J., Doebling S.W., Schultze J.F., Lieven N., and Robertson A.N. (2003). “Damage Prognosis: Current Status and Future Needs”, Los Alamos National Laboratory report LA-14051-MS.
- Helmicki A., Hunt V., Shell M., Lenett M., Turer A., Dalal V., and Aktan A. (1999). “Multidimensional Performance Monitoring of a Recently Constructed Steel-Stringer Bridge”, *Proceedings of the 2nd International Workshop on Structural Health Monitoring*, Stanford University, Palo Alto, CA, pp.408-416.
- Klein L.A. (1999). *Sensor and Data Fusion: Concepts and Application*, Second Edition, TT35, SPIE Press.
- Maeck J., Abdel-Wahab M., and De Roeck G. (1998). “Damage Detection in Reinforced Concrete Structures by Dynamic System Identification”, *Proceedings of ISMA23, Noise and Vibration Engineering*, Leuven, Belgium.
- Onate E., Hanganu A., and Miquel J. (2000). “Prediction of Damage and Failure in Civil Engineering Structures Using a Finite Element Model”, *European COST F3 Conference on System Identification and Structural Health Monitoring*, Madrid, Spain, pp.53-70.

- Ruotolo R. and Surace C. (1997). "Damage Detection Using Singular Value Decomposition", *Proceedings of DAMAS '97, Structural Damage Assessment Using Advanced Signal Processing Procedures*, University of Sheffield, UK, pp.87-96.
- Sikorsky C., (1999). "Development of a Health Monitoring System for Civil Structures Using a Level IV Non-destructive Damage Evaluation Method", *Proceedings of the 2nd International Workshop on Structural Health Monitoring*, Stanford University, Palo Alto, CA, pp.68-81.
- Sohn, H., Dzwonczyk M., Straser E.G., Law K.H., Meng T., and Kiremidjian A.S. (1998). "Adaptive Modelling of Environmental Effects in Modal Parameters For Damage Detection in Civil Structures," *Proceedings of SPIE, Smart Systems for Bridges, Structures, and Highways*, Vol. 3325, pp. 127-138.
- Sohn H., Farrar C. R., Hemez F.M., Czarnecki J. J., Shunk D.D., Stinemates D.W., and Nadler B.R.. (2003). "A Review of Structural Health Monitoring Literature: 1996-2001", Los Alamos National Laboratory Report, LA-MS, distributed at the SAMCO Summer School held in Cambridge, UK.
- Wang, M.L. , Satpathi D., and Heo G. (1997). "Damage Detection of a Model Bridge Using Modal Testing," *Proceedings of the 1st International Workshop on Structural Health Monitoring, Current Status and Perspectives*, Stanford University, Palo Alto, CA, pp.589-600.
- Wu Z. and Abe M. (eds., 2003). *Structural Health Monitoring and Intelligent Infrastructures*, Balkema, Lisse.

Chapter 4

The Long-term Research Framework and Goals

Chapter 3 showed how broad is the spectrum of structural monitoring and structural identification. Large monitoring facilities (see [Wong, 2004]) mainly rely on wired equipment, which of course turns out to be limited in terms of sensor deployment and for the number of channels simultaneously collected.

This chapter starts from the identification of real structural damage detection goals, and results in a system network architecture which is the frame of reference for the developments of the following Chapters 5 and 6.

4.1 The Damage Detection Goal

The need for quantitative, global damage detection methods applicable to complex structures is yielding the structural engineering research toward the development of processes that are able to outline changes in the system response. Indicators of the onset and progress of structural damage should also be coupled with approaches able to identify and diagnose the nature of the damage.

The key-point in any practical application of the structural health assessment procedures is the ability to detect damage. This starts the decision making process leading to repair, rehabilitation or replacement. In aerospace engineering a heuristic approach, based on periodical inspections with different depth of assessment, was developed and coded. A similar scheme was inferred for systems associated with high risks as ships, transportation vehicles, dams, skyscrapers, and extremely long bridges. In general, any civil structure requires a periodic examination for assessing its functionality and/or for maximizing its service life.

Most currently used damage detection methods consist of visual inspection followed by local in-depth examination [Chang, 2002; Van der Auweraer and Peeters, 2003]. These two steps are referred to as global and local diagnosis, respectively. Global diagnosis for large structures is often labour intensive, costly and possibly subjective. Indeed, techniques for global diagnosis have not reached yet a satisfactory stage for routine applications [Chase and Washer, 1997], even if the efforts to develop a physical testing technique to improve, supplement, and/or even replace visual inspection, by means of expert systems,

neural networks and other Artificial Intelligence (AI) tools, are producing promising results [Wong, 2004].

By contrast, non-destructive testing techniques for local diagnosis have been noticeably advanced. These techniques, which commonly use acoustic, ultrasonic, magnetic field, X-ray or thermal principles, are generally referred to as Non-Destructive Evaluation (NDE) methods. The NDE schemes work adequately provided that the damage is located within a sufficiently restricted, accessible, and a priori known volume of the structural component under investigation. An important issue in utilizing the inspection results is that the quality of the applied inspection method must be appropriately modelled [Faber et al., 2003; Stahl and Gagnon, 1995].

Moving back from this approach to the goal of a global structural integrity assessment, the research focuses either on signal-based methods or model-based methods. The studies involve both the sensor technologies [Faravelli and Spencer, 2003], and the damage detection and localization methods [Doebbling et al., 1996 and 1999].

The breakthrough in this area was represented by the increasing monitoring facilities, which posed the following problem: how can the results of a monitoring systems be used to detect and localize damage? The general answer is simply to use the monitored data to build up a model of the structural system; the model changes are then identified as the index of structural modification, i.e., damage. The adoption of modal analysis is an early solution proposed in this framework [Peeters, 2000].

However, the present gap existing between the research achievements and the end-user deployment has several motivations.

- The proposed non-destructive testing methods for bridges diagnosis, for instance, have been overwhelmingly based on dynamic modal testing using accelerometers. The sensors are assumed to be located at a limited number of points on the structure, since covering a large area using many accelerometers is still regarded as very expensive, but there are no techniques able to provide an effective diagnosis using measurements from only a few points. In particular, in the area of activity of the author (Civil and Infrastructure Engineering), modal analysis was shown to identify damages only when deterioration is rather evident [Casciati S. and Faravelli, 2002].
- The measurement data inevitably contain noise and this noise makes it difficult to identify the signal, especially when local and small damages are concerned. In other words, the effectiveness of using global testing to diagnose and locate small damage still needs to be established and quantified.
- The approaches which also include numerical modelling as a dominant or complementary tool (e.g., finite element model updating) can result costly for a large number of structures (for instance bridges in a transportation network). The modelling errors inherent in the FE methods also need to be considered in their applicability. The approaches to global diagnosis using high resolution images [Fu and Moosa, 2001; Shinozuka, 2003] could result much more convenient and effective.

4.2 Monitoring Capability

Long term structural health monitoring (SHM) can provide a benchmark to improve the fidelity of subjective visual inspections, reduce the inspection costs by focusing the inspection efforts where damage may be located, and decrease the manual inspection periods.

Today's conventional monitoring systems (Figure 4.1) are characterized as having instrumentation points wire-connected to the centralized data acquisition system through coaxial cables. Common sensors output analogue signals that need to be sampled and digitized for use in modern discrete signal processing systems. When the analogue signals arrive at the centralized data acquisition system, an analogue-to-digital converter discretizes the analogue waveforms. At this stage, the user of the monitoring system can take the raw digitized data and extract the relevant engineering quantities from the data. As the number of instruments increases, the degree of sophistication in the instrumentation and the computational data processing needs become far greater.



Figure 4.1 Today's conventional wired monitoring system.

The distance from the sensors to the data acquisition system can range from 10 to 300 m in practice. As the signal travel distance becomes longer, the analogy signals may become noisy and degrade because of coupled noise sources near the cable path. The cost of installation of all the instrumentations approaches 25% of the total cost of a monitoring system, and the installation time consumes over 75% of the total testing time for large scale structures. With the monitoring system installed, the concern shifts to the cost of maintenance. For in-situ testing, the repeated changes in temperature and humidity, exposure to rain and direct sunlight rapidly deteriorate the sensors and the cables.

These prohibitive factors prevent from the wide diffusion of the long term structural health monitoring technique for many civil infrastructures. However, the quick development of new technology provides tools that can be employed to eliminate these difficulties.

In particular, wireless communication can remedy the recurring cabling problem of the conventional monitoring system. Smart Sensors (sensor + microprocessor) with embedded microprocessors or microcontrollers can allow distributed computational power and data processing. MEMS (i.e., Micro Electronic Mechanical Systems) accelerometers can provide compelling performance and attractive unit price. With the combination of these technologies, it is possible to move the data acquisition and a portion of the data processing toward the sensors.

4.3 Wireless Sensors Network

For this purpose, a two layers system architecture (Figures 4.2 and 4.3) was selected for the development of a wireless sensor network. The wireless key design factors are the ease of installation, a low cost per unit, and a broad functionality. In particular, the fundamental parameters to perform the choice of a wireless modem are the available bandwidth, the power consumption, the transmission reliability, the transmission range, and the cost. Based on these considerations, the components of the sensor and computational units were selected and are summarized in Table 4.I.

Frequency selection and choosing a low-cost distributed power supply are the major steps to be taken when planning and implementing a modular, wireless sensors system. According to the law regulations, the “Industrial, Scientific, Medical” (ISM) frequency band can be adopted, which consists of several frequency intervals, mainly:

- 433.05 MHz – 434.79 MHz;
- 865 MHz – 870 MHz (only in Europe);
- 902 MHz – 928 MHz (only in USA);
- 2.4000 GHz – 2.4835 GHz (~79 MHz usable BW);
- 5.725 GHz – 5.875 GHz;
- other open standards.

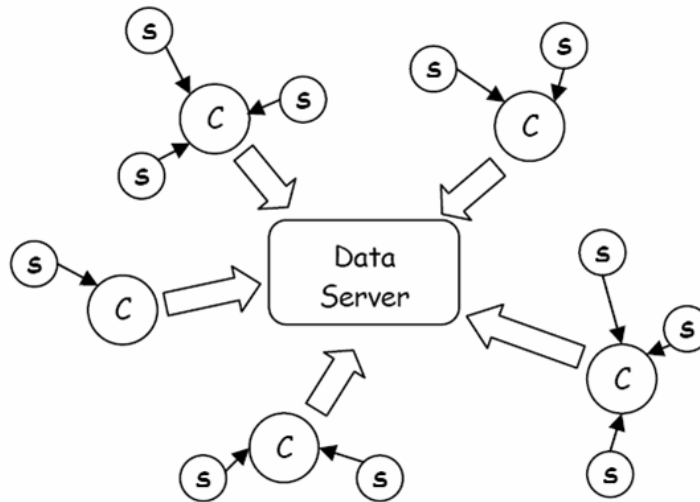


Figure 4.2 Two layers wireless architecture.

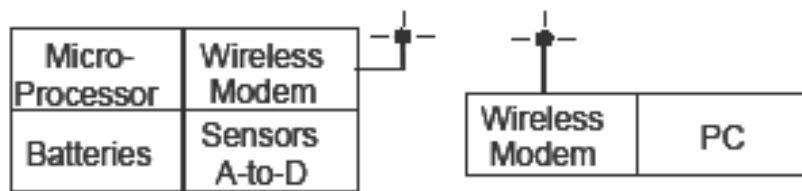


Figure 4.3 Wireless monitoring system.

TABLE 4.I SYSTEM ARCHITECTURE UNDER DEVELOPMENT.

| S = SENSING UNIT | C = COMPUTATIONAL NODE |
|---|--|
| MEMS Accelerometer (Crossbow); Micro-converter (Analog device); RF Transceiver (Aurel). | RF Transceiver (Aurel); CPU; 2.4 GHz modem with TCP/IP protocol. |

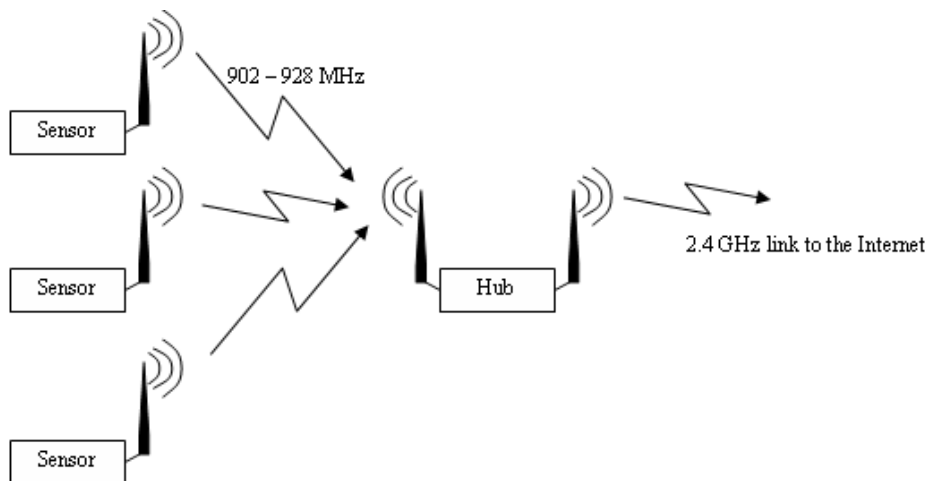


Figure 4.4 Hybrid wireless sensor network.

The goal is to combine long-range and low-power. Therefore, for the radio links between the sensors and some higher-level acquisition device, attention is focused on the ISM frequency bands lower than 1 GHz, as they combine a good range and a low power. For the remaining parts of the wireless network, the 2.4 GHz frequency band could be a very good candidate. For example, a Wi-Fi 2.4 GHz could be used. The clear advantage of such a hybrid architecture lies in using common, off-the-shelf network components wherever possible and in using special, custom wireless links only where necessary (i.e., at the sensor level). Figure 4.4 shows an example of such a tiered network architecture.

Each sensor, actuator or associated printed circuit board requires an adequate power supply; hence, the need for very low-power systems and for some power harvesting technique. The following solutions are available:

- Microwave beams are of common use in aerospace applications, but they are not suitable for civil structures monitoring due to the presence of people.
- Electromagnetic induction could be interesting but, unfortunately, in the presence of human beings it is not a viable solution except for ultra-low power applications (e.g.: smartcards).
- Solar power: can allow some freedom in the placement of sensors, but a fully wireless solution is not possible because cables are still needed for power distribution.
- Vibration power harvesting is under investigation.

Electromagnetic induction is the production of an electrical potential (or voltage) difference across a conductor located in a variable magnetic field. The idea is to create a powered volume where the sensors draw power from electromagnetic induction. This technique cannot work for SHM applications because, when working at 100 kHz, a magnetic field of 100 μ T must be used to produce 10 mW (which is a suitable value for a sensor with uninterrupted operation). But this field is well beyond the limits enforced by the law. By contrast, a sensor with very low duty cycle (one transmission per day and the rest of the day in sleep mode) could become feasible if coupled with a rechargeable battery.

A 15 cm by 15 cm solar panel supplies a power of 500mW in full sunlight. This peak value can drop by 80% depending on the weather conditions, but it would still be enough for a sensor with low duty cycle. Careful sizing, backup batteries, low power electronics, Sun Hours Per Day tables, etc., must be considered when adopting this solution. Strictly speaking, a fully wireless solution is not possible because cables are still needed for power distribution. Nevertheless, solar power allows some freedom in the placement of sensors.

Vibration power harvesting is the most fascinating candidate presently under investigation.

4.4 Board Implementation toward a Smart Sensor

A smart sensor comes with a microprocessor installed on a suitable board. A software can be transferred to the board of Figure 4.5, by downloading a suitable C-language code from a PC.

The board uses the serial port in order to communicate with a second unit. The link between the two units can either be a standard serial cable or a wireless network.

Communication errors are possible, especially when the link is provided by a wireless network. The most common error is when the wireless network gets close to congestion and some bytes are lost. In this case, the slave board discards the corrupted data so that their impact is minimized.

For the wireless link between the two boards, two MaxStream RF transceivers were used (Figure 4.5). They were configured as a plain cable replacement. In other words, it was as the cable had been simply replaced by two antennas and some empty space between them.

The great advances in sensors technology make the continuous distributed monitoring of civil infrastructure a feasible task. In particular, a wireless sensor network made of clusters of sensors wireless communicating to a computational core is under development [Casciati et al., 2004]. In parallel, an efficient damage detection algorithm needs to be implemented in the sensors microprocessor. This algorithm must be simple, low-power consuming, and

low-memory taking to avoid an over wealth of information. A method meeting these requirements was formulated in [Faravelli and Casciati, 2004] on the basis of the response surface approximation theory. The method was tested experimentally on laboratory structures. The results are reported in Chapters 8 and 9. A thorough numerical study of a benchmark problem is discussed in Chapter 7. Preliminarily, Chapter 5 and 6 provide the suitable theoretical framework.

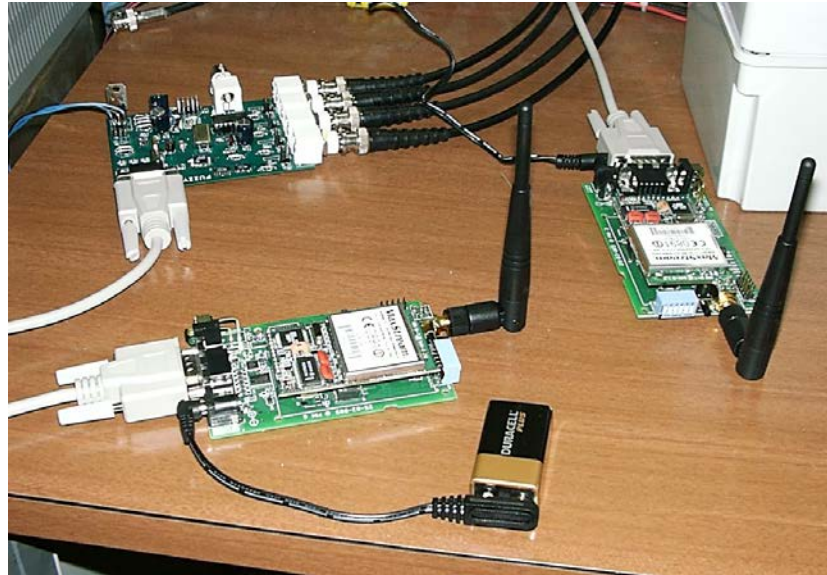


Figure 4.5 Units with wireless communication.

References for Chapter 4

- Casciati F., Casciati S., Faravelli L., and Rossi R. (2004). "Hybrid Wireless Sensors Network", *Proceedings SPIE04*, SPIE.
- Casciati S. and Faravelli L. (2002). "Structural Damage Detection Based on Dynamic Response Identification", *Structural Health Monitoring 2002*, D. Balageas (ed.), DEStech Publications Inc., Lancaster, 1081-1090.
- Chang P. (2002). "The Role of Health Monitoring in Infrastructure Management", *Structural Health Monitoring 2002*, D. Balageas (ed.), DEStech Publications Inc., Lancaster, 21-30.
- Chase S.B. and Washer G. (1997). "Nondestructive Evaluation for Bridge Management in the Next Century", *Public Roads*, July-August, 16-25.
- Doebling S.W., Farrar C.R., Prime M.B., and Shevitz D.W. (1996). "Damage Identification and Health Monitoring of Structural and Mechanical Systems for Changes in Their Vibration Characteristics: a Literature Review", LA-13070-MS Report, Los Alamos National Laboratory.
- Doebling S.W., Farrar C.R., Prime M.B., and Shevitz D.W. (1999). "Damage Identification and Health Monitoring of Structural and Mechanical Systems for Changes in Their Vibration Characteristics", *Shock and Vibration Digest*, 30, 2.
- Faber M.H., Engelund S., and Racwitz R. (2003). "Aspect of Parallel Wire Cable Reliability", *Structural Safety*, 25, 2, 201-225
- Faravelli L. and Casciati S. (2004). "Structural Damage Detection and Localization by Response Change Diagnosis", *Progress in Structural Engineering and Materials*, 6, 2, 104-115.

- Faravelli L. and Spencer J.B. (eds., 2003). *Proceedings of the US-Europe Workshop on Sensor and Smart Structures Technology*, John Wiley & Sons, Chichester, UK.
- Fu G. and Moosa A.G. (2001). "Structural Damage Diagnosis using High Resolution Images", *Structural Safety*, 23, 4, 281-295
- Peeters B. (2000). *System Identification and Damage Detection in Civil Engineering*, PhD Thesis, K.U. Leuven Civil Engineering Department.
- Stahl F.L. and Gagnon C.C. (1995). *Cable Corrosion in Bridges and Other Structures*, ASCE Press.
- Van der Auweraer H. and Peeters B. (2003). "International Research Projects on Structural Health Monitoring: an Overview", *Structural Health Monitoring*, 2 (4), 341-358.
- Wong K-Y. (2004). "Instrumentation and Health Monitoring of Cable-Supported Bridges", *Journal of Structural Control and Health Monitoring*, 11, 2.

Chapter 5

Damage Detection Algorithms

The previous three chapters emphasize some gaps between the practical goals and the theoretical algorithms in the current approaches to structural damage identification.

- 1) The goal is to identify changes in the response correlations; the algorithms pursue the identification of the whole system in the two cases of no-damage and damage.
- 2) When damage occurs, the state space where the dynamic system is described may vary. For example, the removal of a brace in a frame is just a stiffness matrix modification, but the opening of a hinge in a continuous beam requires a state space enlargement.

In order to manage these concepts, different representations are usefully introduced. The one usually adopted for dynamic systems requires to operate in

the whole state-space of dimension n . It is worth noting that for a mechanical system ruled by a second order differential equation, n is twice the number of degrees of freedom ν , i.e., $n = 2 \nu$. The evolution of the motion in this space is described by the trajectory of a single point, and the time is a relevant parameter. Indeed, this representation is the projection of the system trajectory from a full space of size $n+1$, which also includes the time.

An alternative representation is obtained by the Poincaré maps. Here the point representing the motion is not recorded continuously, but at finite time steps. This representation is the only available when considering a monitoring system, since the data acquisition is carried out with an assigned sampling rate.

The construction of a Poincaré map starts from the representation of the motion at given times, each of which is represented by a dot in the state space. Let h the number of time instants used to build the Poincaré map. If the available data are larger than h , say jh , with j a positive integer, one can represent j Poincaré maps, assuming that the system underwent j different experiments. But the same data can also be regarded as the simultaneous evolution of j different systems. At a given time each of them is a point in the state space, but their collection represents, by definition, a Gibbs set. The evolution of these systems in time is then followed by building different plots, each of which is associated to a subsequent instant. If one initially selects the Gibbs set systems all in a single cell of the grid in which the state-space is discretized, then the geometric features of the graphical representation at the successive time instants will denote a more or less order in the evolution. Figure 5.1 gives an example of three different possible ways of evolution of the same Gibbs set.

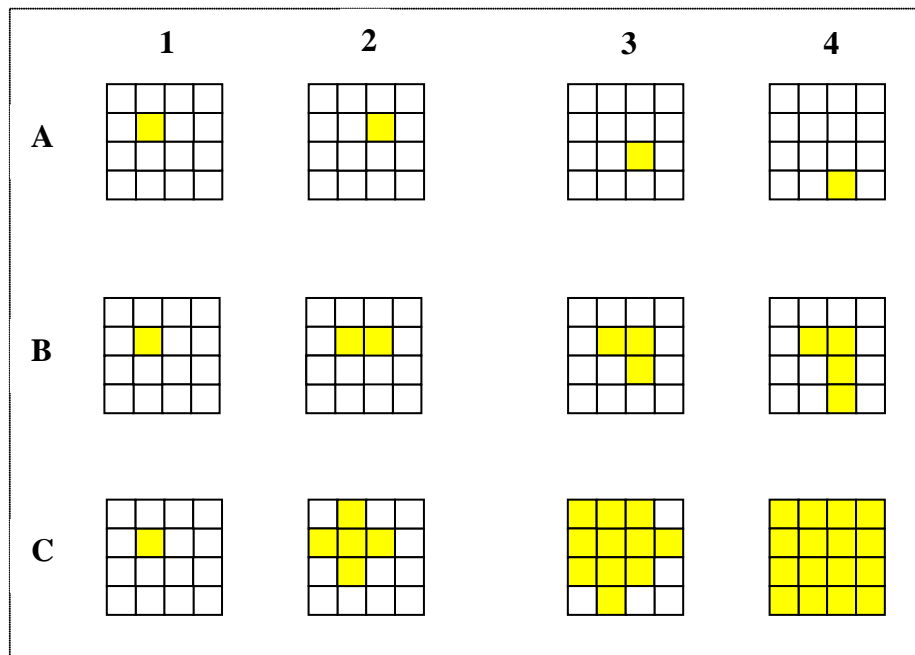


Figure 5.1 Top row: the Gibbs set, whose representing points are originally in a single cell, evolves with all the points remaining grouped into a single cell.
 Middle row: the previous Gibbs set evolves by invading a slowly increasing number of cells.
 Bottom row: the Gibbs set evolves by quickly invading all the state space.

In order to follow the evolution of a Gibbs set, several quantitative measures were proposed, such as the Lyapunov exponents, the entropy, Kolmogorov entropy, the space dimensions and so on. In this chapter, the different measures are applied to the data obtained from a monitoring system.

For this purpose, a further step first needs to be taken: the mapping of the Gibbs set from the state space into the space of the observed variables. This aspect is discussed in the next section. The advantage achieved by the mapping is that, in this way, one does not need to know the dimension of the state space,

but only the size N of the observed variable space (denoted by q in the developments of Chapter 2), which is selected by the analyst. A further advantage is that damages that introduce new degrees of freedom can be managed without modifications, provided that the problem is still well-posed, i.e., that the available measurements allow one to observe the new situation according to the observability principle discussed in Chapter 2.

5.1 Mapping the State-Space

The numerical example developed at the end of Chapter 2 outlined the bottleneck of the current structural damage identification techniques, i.e., the identification of the system state space matrices. Recall Equation (2.10)

$$\begin{aligned}\frac{d\mathbf{x}(t)}{dt} &= \mathbf{A}\mathbf{x}(t) + \mathbf{B}\mathbf{u}(t) + \mathbf{E}\mathbf{w}(t), \\ \mathbf{y}(t) &= \mathbf{C}\mathbf{x}(t) + \mathbf{D}\mathbf{u}(t) + \mathbf{H}\mathbf{w}(t).\end{aligned}\tag{5.1}$$

When the excitation \mathbf{u} is ignored and the number of rows of \mathbf{C} is greater than the size of \mathbf{A} , \mathbf{C} can be partitioned into two matrices \mathbf{C}_1 and \mathbf{C}_2 ,

$$\begin{aligned}\mathbf{y}_1(t) &= \mathbf{C}_1\mathbf{x}(t) + \mathbf{I}_1\mathbf{w}_1(t) \\ \mathbf{y}_2(t) &= \mathbf{C}_2\mathbf{x}(t) + \mathbf{I}_2\mathbf{w}_2(t)\end{aligned},\tag{5.2}$$

with the first \mathbf{C}_1 matrix of the same size of \mathbf{A} and non-singular. Here \mathbf{H} is regarded as the identity matrix \mathbf{I} .

If the inverse of \mathbf{C}_1 exists, then

$$\mathbf{y}_2(t) = \mathbf{C}_2[\mathbf{C}_1^{-1}(\mathbf{y}_1(t) - \mathbf{I}_1 \mathbf{w}_1(t))] + \mathbf{I}_2 \mathbf{w}_2(t), \quad (5.3)$$

or equivalently,

$$\mathbf{y}_2(t) = \mathbf{\Omega} \mathbf{y}_1(t) - \mathbf{\omega}(t), \quad (5.4)$$

which indirectly explicitates a mapping between the state-space and the observation space. This mapping formally allows one to introduce in the observation space, the representations and the measures which are usually defined in the state-space.

Figure 5.2 shows the sections of the Poincaré maps for the signals used as examples in Chapter 2. In particular, a section of the full space of the observations is reported in the plane of signals 5 and 14. As the lag of the representation increases, one can detect a trend in the motion. By drawing together the responses in the damaged and undamaged conditions, one can notice their different features and regard the plots as a qualitative tool for damage detection. Of course, the localization of damage would require a comparative analysis of all the sections that one can draw.

In order to manage the whole state-space, or observation space (after the mapping), global measures as the ones described in the next two sections are needed.

5.2 Information Entropy and Kolmogorov Entropy

Either in the state-space, or in the observation space after the mapping, one can introduce a discretization in cells by means of a grid as, for instance, the one in Figure 5.2. The i -th cell can then be associated to a probability mass p_i of being visited, which is roughly estimated by the ratio between the number of points in the cell and the total number of systems in the studied Gibbs set.

The entropy $I(t)$ is a scalar function which measures the disorder associated with the evolution of a dynamic system and it is given by

$$I(t) = -\sum_i [p_i(t) - \ln_2(p_i(t))], \quad (5.5)$$

where the sum covers all the cells that are actually visited, i.e., the ones of non-null probability. Such a quantity is a function of time, but it also depends on the size and number of cells. The logarithm of base 2 is related to the common practice of measuring the information in bits.

The entropy rate, i.e., the time derivative of the entropy function $I(t)$, is referred to as Kolmogorov entropy or K -entropy

$$K(t) = \frac{\partial I}{\partial t} \quad (5.6)$$

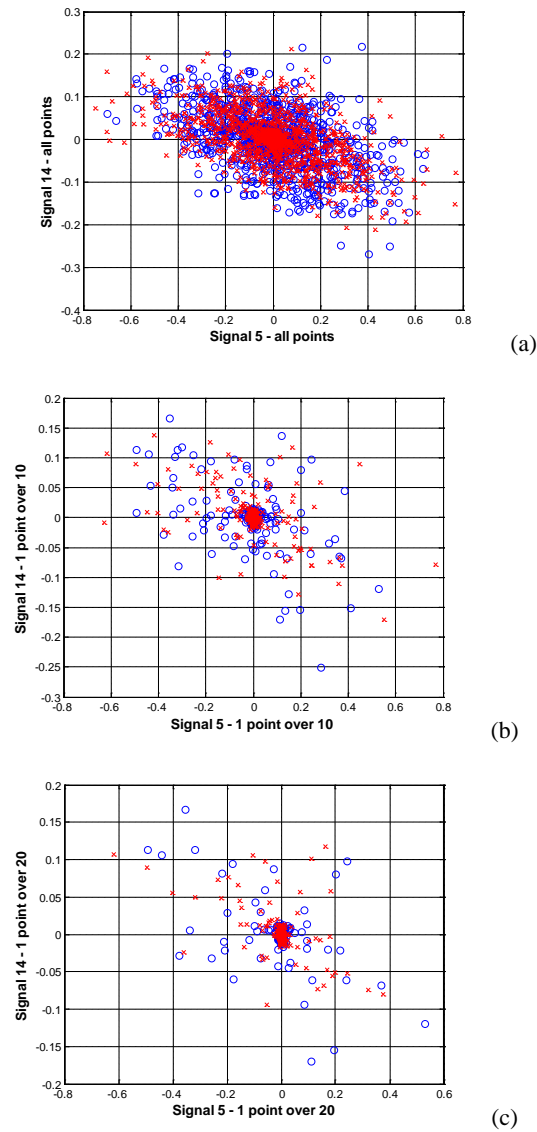


Figure 5.2 Sections of the Poincaré maps drawn for the two sets of signals introduced in Chapter 2, Section 2.7: “o” denotes the undamaged signals and “x” the damaged ones. (a) In the first map, all the points recorded during the first shaker pulse (nearly 4000) are shown. (b) In the second map, 1 point over 10, and (c) in the third map, 1 point over 20 are considered.

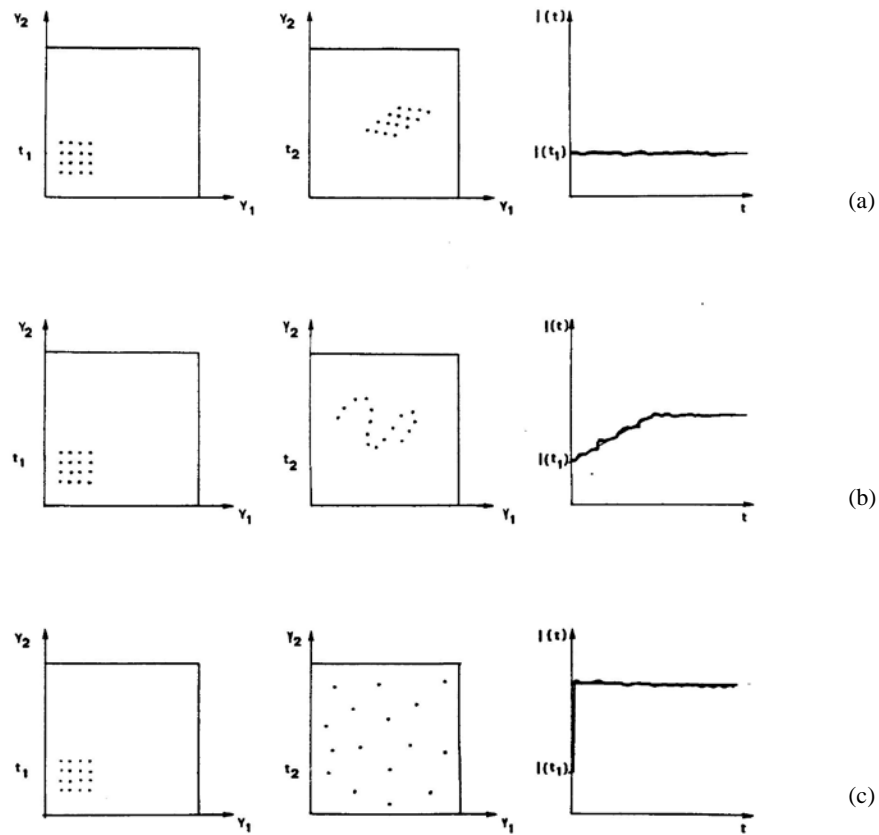


Figure 5.3 Classification of a dynamic system based on Kolmogorov entropy: a) regular, b) stochastic or chaotic, and c) fully random.

The numerical evaluation of the function $I(t)$ usually gives a strongly irregular result. This suggests not to compute the Kolmogorov entropy as a derivative. As illustrated in Figure 5.3, for many dynamic systems the entropy shows a nearly linear increase of the form

$$I(t) = I(t_0) + K(t - t_0), \quad (5.7)$$

and then it reaches a stationary state where it remains constant, so that the corresponding Kolmogorov entropy is null.

This rationale allows one to compute the Kolmogorov entropy as the slope,

$$K = \frac{I(t) - I(t_0)}{t - t_0}. \quad (5.8)$$

Coming back to the signal sets of Chapter 2, one must operate in a space of dimension $17!$ Even by adopting only 5 classes of cells, corresponding to large negative, negative, zero, positive and large positive values, means to introduce $5^{17} = 7.63 \cdot 10^{11}$ cells. Therefore, it is more convenient to work in a Lagrangian scheme by following the single dynamic system, rather than in an Eulerian form by scanning the all space. Furthermore, the range of each axis is divided into 11 parts so that, for each axis, cell 1 collects the first 4 ranges, cell 2 is built on range 5, cell 3 on range 6, cell 4 on range 7 and cell 5 groups the remaining 4 ranges. As it will be shown in the next section, this procedure gives quite inaccurate results; nevertheless, the required information is conveniently achieved for comparison purposes.

Under these assumptions, Figure 5.4 provides the entropy plots computed for the 12 pulses of the damaged case. The maximum entropy value is 3.219 for all the 12 pulses, while the average entropy in the stationary range (between 10 and 90 steps) is 2.8333. The average of the Kolmogorov entropy scalar results to be $2.7866/\Delta t$, with $\Delta t = 0.005$ s.

Considering the signal set available for the undamaged case, one obtains the plot of Figure 5.5, where the maximum value of the entropy is again equal to 3.219 for all the 12 pulses, while its average in the stationary range (between 10 and 90 steps) is 3.1274. The average of the Kolmogorov entropy scalar is now $3.0823/\Delta t$.

This simple example shows how the average values of the computed entropy and of the computed Kolmogorov entropy can help in detecting damage. Damage is characterized by lower values of both these means. Once again, damage is detected but it is not localized.

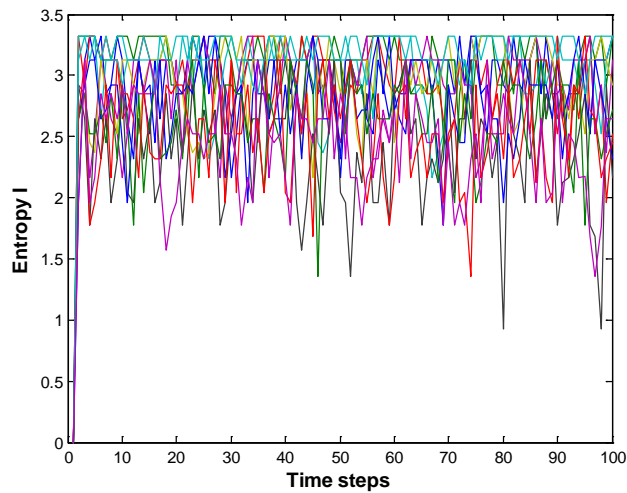


Figure 5.4 Entropy evolution from the central cell for the 12 pulses: set of damaged case signals.

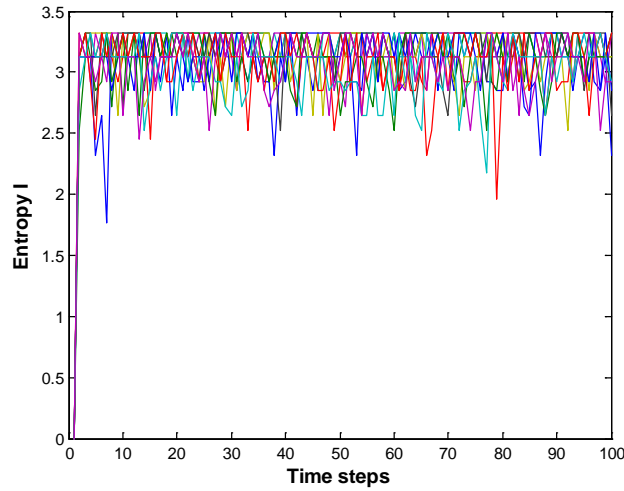


Figure 5.5 Entropy evolution from the central cell for the 12 pulses: set of undamaged case signals.

5.3 Lyapunov Exponents

The Lyapunov exponents represent a measure of the divergence in time of trajectories which were initially close to each other. Consider a small test volume around an initial point in the state space or in the observation space after mapping: for instance, a sphere of radius ε and centre in (y_1, y_2) as illustrated in Figure 5.6. As driven by the dynamic equation of motion, this sphere becomes an ellipsoid of different radii at subsequent instants.

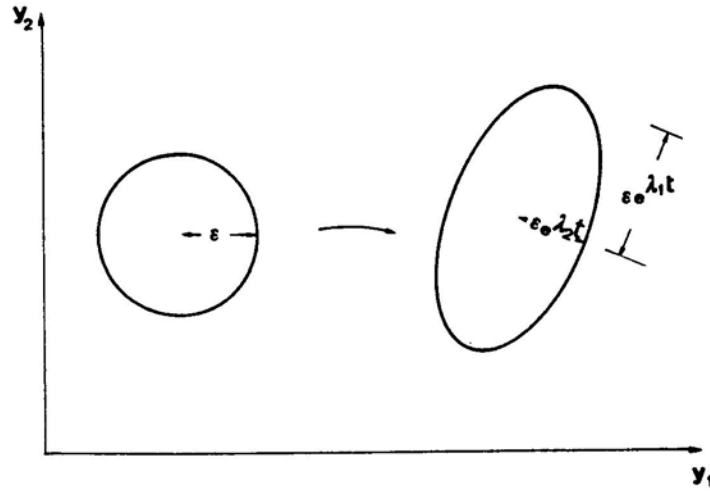


Figure 5.6 Illustration of the concept of Lyapunov exponent.

Let N the dimension of the space, one writes N equations of evolution for such radii

$$\varepsilon_i = \varepsilon \cdot 2^{\lambda_i t} \quad i = 1, \dots, N, \quad (5.9)$$

which provide the mathematic expression of the i -th Lyapunov exponent

$$\lambda_i = \frac{1}{t} \ln_2 \left(\frac{\varepsilon_i}{\varepsilon} \right). \quad (5.10)$$

For dissipative systems, the sum of the Lyapunov exponents must be negative; null for Hamiltonian (conservative) systems. A positive value of any exponent denotes a stretching direction which, for a Gibbs set formed by the

same nonlinear dynamic system, emphasizes the sensitivity to the initial condition (chaos).

The idea is to work in the observation space (after mapping) and to form three different Gibbs sets of damaged, undamaged and mixed damaged and undamaged systems, respectively: the trajectories should diverge and the Lyapunov exponents should detect this behavior. To link the anomalous exponent(s) with the damage location(s) is something to be further investigated.

The Wolf algorithm initially suggested for the numerical evaluation of the Lyapunov exponents, is not very robust and can easily lead to wrong results. Indeed, the algorithm does not allow to test for the presence of exponential divergence, but just assumes its existence and thus yields a finite exponent also for stochastic data, where the exponent is infinite.

The algorithm on which attention could be focused, tests directly for the exponential divergence of nearby trajectories and thus allows to decide whether it really makes sense to compute a Lyapunov exponent for a given data set. It is referred to as the Kantz algorithm and it computes the maximum Lyapunov exponent. Unfortunately, at present, no multivariate implementations are available in the literature. But, as the example below will show, the knowledge of just the maximum exponent is not satisfactory for the purpose of damage detection.

The computation of the full Lyapunov spectrum, which requires considerably more effort than just the maximal exponent, was implemented in a beta routine within the “TISEAN package” [Hegger et al., 1999] and it also works in the multivariate case. An essential feature is the estimate of the local Jacobians \mathbf{J} , i.e., of the linearized dynamics which governs the growth of infinitesimal perturbations. It can be obtained from the direct fits of local linear

models of the type $\mathbf{y}_{n+1} = \mathbf{a}_n \mathbf{y}_n + \mathbf{b}_n$, where the first row of the Jacobian is the vector \mathbf{a}_n , and $(\mathbf{J})_{ij} = \delta_{i-1j}$, for $i = 2, \dots, m$, where m is the embedding dimension. When working in the observed variable space, m coincides with the number of observed variables N . The vector \mathbf{a}_n is given by the least squares minimization over the vectors $\{\mathbf{y}_1\}$ which form the set of neighbors of \mathbf{y}_n [Sano and Sawada, 1985]. Alternatively, one could construct a global nonlinear model and compute its local Jacobians by taking the derivatives.

In both cases, the Jacobians are multiplied one by one following the trajectory by as many different vectors \mathbf{u}_k in the tangent space as the number of Lyapunov exponents that need to be computed. Every few steps, a Gram-Schmidt orthonormalization procedure is applied to the set of \mathbf{u}_k , and the logarithms of their rescaling factors are cumulated. Their average, in the order of the Gram-Schmidt procedure, gives the Lyapunov exponents in descending order.

The routine “`lyap_spec`” applies this method employing local linear fits. Apart from the problem of spurious exponents, this method contains some other pitfalls: it assumes that well defined Jacobians exist, and it does not test for their relevance. Then the result can suffer from these bad estimates and the exponents are correspondingly wrong. But for the purpose of a comparison to detect damage, its accuracy should not affect the results.

The calculations were carried out on the following measurements: a) 2 shaker pulses in the undamaged case, b) 2 shaker pulses in the damaged case and c) 1 shaker pulse in the undamaged case followed by 1 shaker pulse in the damaged case. Since 17 channels are available, using a global embedding dimension of 17, 17 Lyapunov exponents are computed in Table 5.I, where all

the iterations that the code prints every ten seconds of computations are reported. Thus, a higher number of the iterations denotes a longer global execution time. The longest run was the one on the damaged and undamaged data together. This represents a first flag for damage detection. In addition, one can see that all the Lyapunov exponents of the damaged case at convergence are lower than those obtained for the undamaged case (while the mixed case lies in between the two), and that the undamaged case shows seven positive Lyapunov exponents versus the six of the damaged case.

It is worth noting that the adopted computer code has a limitation on the length of each analyzed signal. This suggested to work with no more than 7500 time steps. When more data are available, subsequent windows of the global data can be considered, and the computations are repeated for the different windows.

Furthermore, the knowledge of the Lyapunov exponent spectrum allows one to compute the following estimates:

- 1) Pesin's inequality states that the sum of all the positive Lyapunov exponents is an upper-bound for the Kolmogorov entropy. Thence, the last column in Table 5.I gives the sum of the positive exponents, and shows that the lowest value is achieved in the damaged case. Here one can also realize how rough are the Kolmogorov estimates computed in the previous section, where nearly doubled values were estimated. But, despite that grid approximation was quite inaccurate, both here and in the previous section the comparison of values which allow one to achieve a decision on the undamaged/damaged state, works.
- 2) The Lyapunov dimension (or Kaplan-Yorke dimension) is defined by the expression

$$D_L = k - \frac{\sum_{i=1}^k \lambda_i}{\lambda_{k+1}}, \quad (5.11)$$

where k is the order number of the last (in decreasing order) Lyapunov exponent for which the numerator sum is positive. Roughly speaking it is the minimal fractal dimension of the space where the dynamics is preserved. The values of this dimension are also reported in Table 5.I, and it is evident how the damaged situation corresponds to a lower value of the Lyapunov dimension.

As a final remark of this section, it can be concluded that there are several quantitative approaches for the differentiation of the response signals. Although, the weaker (damaged) cases are successfully detected, no information is however collected on the cause of such e weakness (damage localization).

5.4 Building Input-Output Relations for Damage Localization

Despite the debate is still ongoing, there is evidence that input-output relationships independent of, or not fully based on the mechanical understanding of the problem, can be conveniently adopted in view of damage localization. The relationship identifiers can be of different nature: neural networks, genetic algorithms, wavelet theory, or statistics.

TABLE 5.I Lyapunov exponents (by Δt) computed for the 3 investigated situations.

| Iteration | Positive Lyapunov exponents * Δt | | | | | | | Kolm. entropy estimate* Δt |
|------------------|--|--------------|--------------|--------------|--------------|--------------|--------------|--|
| Undamaged | 1 | 2 | 3 | 4 | 5 | 6 | 7 | |
| 953 | 0.466 | 0.378 | 0.287 | 0.215 | 0.138 | 0.066 | | 1.55 |
| 1417 | 0.432 | 0.355 | 0.266 | 0.204 | 0.125 | 0.064 | | 1.45 |
| 1602 | 0.434 | 0.358 | 0.271 | 0.208 | 0.130 | 0.058 | | 1.46 |
| 1798 | 0.445 | 0.363 | 0.274 | 0.211 | 0.135 | 0.060 | | 1.49 |
| 2022 | 0.456 | 0.372 | 0.286 | 0.217 | 0.136 | 0.063 | | 1.53 |
| 2318 | 0.472 | 0.384 | 0.295 | 0.228 | 0.140 | 0.065 | | 1.59 |
| 2703 | 0.494 | 0.401 | 0.306 | 0.232 | 0.148 | 0.074 | 0.002 | 1.67 |
| 3230 | 0.511 | 0.418 | 0.321 | 0.247 | 0.153 | 0.080 | 0.009 | 1.74 |
| 4014 | 0.533 | 0.435 | 0.333 | 0.257 | 0.159 | 0.087 | 0.016 | 1.82 |
| 4748 | 0.509 | 0.417 | 0.319 | 0.243 | 0.152 | 0.080 | 0.010 | 1.73 |
| 5412 | 0.499 | 0.409 | 0.315 | 0.239 | 0.149 | 0.079 | 0.007 | 1.70 |
| 5904 | 0.508 | 0.413 | 0.320 | 0.243 | 0.150 | 0.078 | 0.008 | 1.72 |
| 6537 | 0.518 | 0.421 | 0.325 | 0.246 | 0.154 | 0.080 | 0.010 | 1.76 |
| 7282 | 0.526 | 0.432 | 0.332 | 0.252 | 0.158 | 0.083 | 0.012 | 1.80 |
| 7499 | 0.528 | 0.434 | 0.336 | 0.253 | 0.158 | 0.084 | 0.013 | 1.81 |

#estimated KY-Dimension= 13.061959

| Iteration | Positive Lyapunov exponents * Δt | | | | | | | Kolm. entropy estimate* Δt |
|----------------|--|--------------|--------------|--------------|--------------|--------------|----------|--|
| Damaged | 1 | 2 | 3 | 4 | 5 | 6 | 7 | |
| 851 | 0.433 | 0.341 | 0.279 | 0.210 | 0.121 | 0.063 | | 1.45 |
| 1451 | 0.392 | 0.313 | 0.241 | 0.186 | 0.098 | 0.044 | | 1.28 |
| 1734 | 0.390 | 0.312 | 0.240 | 0.184 | 0.098 | 0.041 | | 1.27 |
| 1989 | 0.392 | 0.315 | 0.244 | 0.188 | 0.097 | 0.046 | | 1.28 |
| 2266 | 0.398 | 0.318 | 0.248 | 0.190 | 0.101 | 0.052 | | 1.31 |
| 2559 | 0.405 | 0.323 | 0.256 | 0.192 | 0.111 | 0.055 | | 1.34 |
| 2885 | 0.413 | 0.330 | 0.261 | 0.196 | 0.116 | 0.059 | | 1.38 |
| 3263 | 0.425 | 0.337 | 0.269 | 0.201 | 0.124 | 0.059 | | 1.42 |
| 3715 | 0.432 | 0.346 | 0.278 | 0.208 | 0.130 | 0.062 | | 1.46 |
| 4301 | 0.435 | 0.348 | 0.278 | 0.209 | 0.130 | 0.062 | | 1.46 |
| 5070 | 0.425 | 0.342 | 0.272 | 0.201 | 0.126 | 0.056 | | 1.42 |
| 5714 | 0.421 | 0.343 | 0.273 | 0.199 | 0.126 | 0.053 | | 1.42 |
| 6192 | 0.425 | 0.346 | 0.274 | 0.201 | 0.127 | 0.054 | | 1.43 |
| 6682 | 0.427 | 0.350 | 0.278 | 0.204 | 0.128 | 0.056 | | 1.45 |
| 7182 | 0.431 | 0.354 | 0.281 | 0.206 | 0.130 | 0.057 | | 1.46 |
| 7499 | 0.434 | 0.356 | 0.283 | 0.208 | 0.132 | 0.059 | | 1.47 |

#estimated KY-Dimension= 12.185942

TABLE 5.I Lyapunov exponents (by Δt) computed for the 3 investigated situations (cont.).

| Iteration | Positive Lyapunov exponents * Δt | | | | | | | Kolm. entropy estimate * Δt |
|---------------------------|--|--------------|--------------------|--------------|--------------|--------------|-------|--|
| | 1 | 2 | 3 | 4 | 5 | 6 | 7 | |
| Mixed sequence | | | | | | | | |
| 963 | 0.424 | 0.340 | 0.268 | 0.208 | 0.121 | 0.066 | 0.001 | 1.43 |
| 1381 | 0.417 | 0.330 | 0.255 | 0.194 | 0.114 | 0.048 | | 1.36 |
| 1512 | 0.415 | 0.328 | 0.249 | 0.190 | 0.113 | 0.047 | | 1.34 |
| 1641 | 0.414 | 0.327 | 0.247 | 0.191 | 0.115 | 0.043 | | 1.34 |
| 1777 | 0.416 | 0.331 | 0.249 | 0.191 | 0.115 | 0.042 | | 1.34 |
| 1927 | 0.420 | 0.334 | 0.250 | 0.194 | 0.114 | 0.042 | | 1.35 |
| 2089 | 0.422 | 0.336 | 0.254 | 0.198 | 0.116 | 0.044 | | 1.37 |
| 2270 | 0.427 | 0.341 | 0.260 | 0.199 | 0.118 | 0.049 | | 1.39 |
| 2480 | 0.437 | 0.346 | 0.266 | 0.204 | 0.121 | 0.050 | | 1.42 |
| 2731 | 0.445 | 0.355 | 0.269 | 0.209 | 0.127 | 0.057 | | 1.46 |
| 3021 | 0.455 | 0.367 | 0.278 | 0.213 | 0.132 | 0.062 | | 1.51 |
| 3387 | 0.464 | 0.375 | 0.285 | 0.219 | 0.137 | 0.065 | | 1.55 |
| 3866 | 0.472 | 0.386 | 0.298 | 0.228 | 0.142 | 0.067 | | 1.59 |
| 4537 | 0.467 | 0.381 | 0.297 | 0.226 | 0.141 | 0.068 | | 1.58 |
| 5401 | 0.449 | 0.365 | 0.280 | 0.212 | 0.131 | 0.063 | | 1.50 |
| 6161 | 0.444 | 0.359 | 0.277 | 0.209 | 0.128 | 0.059 | | 1.48 |
| 6766 | 0.446 | 0.360 | 0.279 _e | 0.211 | 0.130 | 0.058 | | 1.48 |
| 7356 | 0.449 | 0.365 | 0.281 | 0.213 | 0.132 | 0.059 | | 1.50 |
| 7499 | 0.451 | 0.366 | 0.282 | 0.214 | 0.133 | 0.060 | | 1.56 |

#estimated KY-Dimension= 12.356568

In a more general framework, i.e., in view of structural safety assessment, it is necessary to quantify and compare the importance of each one of the variables which characterize the structural engineering problems, such as the material properties, the loads and the member dimensions. The Response Surface (RS) and the Artificial Neural Network (ANN) techniques, are good candidates to solve complex and elaborated problems [Faravelli, 1994; Gomes and Awruch, 2004]. Indeed, in problems where the computational cost of

structural evaluations is high, these two techniques may provide feasible structural relationships.

This section, for the sake of completeness, pays also attention to the potential offered by the genetic algorithms and the wavelet theory.

5.4.1 Genetic Algorithms

Let a data set to be given in the form of a function $z = f(x, y)$, of the two parameters x and y . An approximation of the function $z = f(x, y)$ in the form of a polynomial $p(x, y)$ can be written as follows

$$z = p(x, y) = c_1 x^{e_{11}} y^{e_{12}} + c_2 x^{e_{21}} y^{e_{22}} + \dots \quad (5.12)$$

Here, c_i and e_{ij} are the coefficients and exponents of the polynomial, respectively, and they are often determined on the basis of a minimal squared distance criterion. The optimization method can be implemented by adopting genetic algorithms [Faravelli, 2000]. The genetic algorithms conduct a computational simulation of the natural selection process. For this purpose, the survival of the best fitting individuals is assumed to be similar to an optimization process. In this analogy, the possible solutions of the optimization problem form a population: each member of the population is judged according to the optimality of the solution that it represents. The natural selection is then simulated by eliminating from the population those members which represent bad solutions.

Note that any single solution is described by a set of genes forming a chromosome, which is usually a binary string of 1's and 0's representing the variables of the solution. In the case of Equation (5.12) these variables are the

coefficients of the approximating polynomial. As said, such variables are used to evaluate their corresponding fitness value, which is the objective function of the associated optimization problem. In the next step, the chromosomes are selected for reproduction and the individuals with higher fitness will receive more copies. Then, new generations of solutions are performed by crossover (mating). The crossover points are selected randomly. In this way, some portions between the selected chromosomes (parents) are exchanged and two new strings (children) are created. During this process, mutations are possible, i.e., a particular gene in a particular chromosome is randomly changed with some small probability, to ensure that the algorithm does not get stuck starting from a bad initial population [Gen and Cheng, 2000].

A signal-based approach relies on measurements of the dynamic responses as underlined in the previous sections of this Chapter, as well as in Section 2.6. The measured values are compared with the values obtained from the calculations carried out for various locations and sizes of the defect (crack, damage, and so on). The form of the objective function depends on the number of points, n , in which the dynamic responses are measured

$$\Psi = 1 - (w_1 + \dots + w_n)/n \quad (5.13)$$

where w_i denotes a scalar which is equal to zero when the measured calculated data show an exact match, and one in the case of no correlation. The minimum value of the objective function determines the predicted location (and size) of the defect [Krawczuc and Ostachowicz, 2001]. Genetic operations with continuous variables can be carried in a same way, except for the crossover and the mutation during the reproduction. Actually they can be derived by looking

into the operation of a binary-coded genetic algorithm [Yi and Feng, 2003]. The direct application of genetic algorithms to structural damage detection is discussed in [Chou and Ghaboussi, 2001].

5.4.2 Wavelet Theory

Following [Escudié et al., 2001], one builds the wavelet of basis

$$\Psi_{a,b}(t) = \frac{1}{\sqrt{|a|}} \Psi\left(\frac{t-b}{a}\right), \quad (5.14)$$

from analyzing a wavelet which satisfies some due constraints of a general nature or specific for the problem under investigation. Then for a given signal $y(t)$, the wavelet coefficients are defined as

$$C_{a,b} = \int_{-\infty}^{+\infty} y(t) \Psi_{a,b}(t) dt. \quad (5.15)$$

The wavelet transform is eventually the function $Y(a, b)$ which associates to the parameters a and b the value of the coefficient $C_{a,b}$ of the wavelet $\Psi_{a,b}$ in the signal decomposition. The parameter b represents the temporal localization, while $1/a$ is the frequency parameter.

The wavelet transform provides a signal analysis at different scale, as well as an useful time-frequency representation in the (a, b) plane. Indeed, the coefficient (5.15) is very small where the analysed signal $y(t)$ is quite regular over a rather long interval. The coefficient has significant values for short high

frequency signal fragments, and in particular this occurs for $1/a$ of the order of magnitude of the frequency.

Wavelet analysis was successfully employed in shape recognition and texture analysis. This is the rationale which leads one to its adoption in structural damage identification problems [Venini, 2003].

5.4.3 Artificial Neural Networks

Artificial neural networks provide a useful tool for their ability to learn from experience by extracting from previous examples conclusions for successive cases of study, and to select the essential characteristics from the available data by neglecting the irrelevant ones [Pisano, 1997; Faravelli and Pisano, 1997]. The basic elements of a neural network are the neurons, the layers, and the activation functions. Moreover, each network has its own architecture characterized by one or more layers placed between the input and the output layers. Each neuron receives information from all the neurons in the next layer, but it is not allowed to communicate with neurons in the same layer. A multi-layer neural network possesses a strong ability to map non-linear problems. Indeed, the Kolmogorov theorem states that any continuous function of n variables x_i defined in the unit closed interval can be expressed in the form:

$$f(x_1, x_2, \dots, x_n) = \sum_{j=1, 2n+1} [w_j (\sum_{i=1, n} \phi_{ij}(x_i))], \quad (5.14)$$

with w_j continuous functions of a single variable and ϕ_{ij} monotone functions independent of f . A further theorem by Hecht-Nielsen theoretically proves that any function can be reproduced by a three-layer neural network. However, there

are many solution surfaces that are extremely difficult to model using just one hidden layer, and the use of more hidden layers is recommended in these cases. The functions in Equation (5.14) apply to weighed combinations of the input. Then learning means, for a neural network, to change the weights of the neuron connections until the optimal performance of the network is reached.

The techniques using neural networks have attracted the interest of civil engineers for both identification and control of structural systems [Nakamura et al., 1998; Masri et al., 2000].

The non-parametric damage detection approach proposed in [Nakamura et al., 1998] adopts a feed-forward multi-layer network trained by using the random search method. The root-mean-square errors are evaluated to compare the results obtained from the damaged and undamaged cases. The methodology requires that a reference state of the structure is established by training a suitable neural network only once, whenever the monitoring system is originally installed. A continuous monitoring is then activated. The changes (damage) in the system may be detected just by observing the output error of the trained network. Such a two steps procedure locates the changes in the global measures, while the actual damaged structural component and the amount of the damage are not identified.

Some researchers have extended the neural network approach to detect, localize, and quantify the damage in structures. [Xu et al., 2003] adopt a four steps procedure. A neural network emulator is first trained using the dynamic responses of the healthy structure; the damage occurrence alarm results then from the error between the dynamic response forecast by the emulator and the observed one. A third step builds up a parametric neural network for the proper selection of the evaluation index and, eventually, it is used in step 4 to quantify

the damage. Alternatively, [Zheng et al., 2003] train a neural network with simulated values of modal parameters in order to recognize the behaviour of the damaged as well as the undamaged structure. It turns out to be able to detect location and size of the damage.

Probabilistic neural networks were also adopted for fault identification in [Marwala, 2001].

5.6.4 Response Surface Techniques

The response surface method, as originally proposed by [Box and Wilson, 1954], represents a statistical tool able to find the operating conditions of a chemical process so that some response is optimized. The subsequent generalizations made such a method being used to develop approximating functions that can be used as an alternative to long running computer codes. Some books [Myers, 1971; Khuri and Cornell, 1987] and recent papers [Romero et al., 2004] provide modern perspectives on this subject in light of emerging computational power.

Typically, in an n -dimensional random variable space, the response surface is assumed to be a (often quadratic) function of the space coordinates where the constants are determined by evaluating the function at certain specified sampling points [Gupta and Manohar, 2004].

Various techniques have been explored to select the sampling points and to determine the coefficients of the function [Petersen, 1985; Casciati and Faravelli, 1991]. It may be noted that, in the existing literature, the term response surface is being used for studies that are essentially rooted in the statistical sampling theory [Wong, 1984 and 1985; Faravelli, 1989 and 1992]. However, response surface methods which bypass some of the mathematical

requirements inspired from the statistical sampling theory as in [Myers and Montgomery, 1995; Faravelli, 1989; Breitung and Faravelli, 1996], can be found in studies that combine the theories of reliability indices with the sampling procedures [Bucher and Borgund, 1990; Rajashekhar and Ellingwood, 1993; Liu and Moses, 1994; Kim and Na, 1997; Guan and Melchers, 2001]. Indeed, when closed form mechanical models of complex structural systems are not available, the number of analyses required by a trivial Monte Carlo simulation can be minimized by using polynomial approximations of the actual limit states in the reliability analysis.

In synthesis [Gayton et al., 2003], the Response Surface Method (RSM) represents a convenient way to achieve a deal between the reliability algorithms and the numerical methods used to model the mechanical behaviour. The special feature of such a method is that the user is allowed to choose and check the computed mechanical experiments, but the optimal choice is not often an easy task.

Since the Response Surface methods basically provide an approximation for a complex input-output relationship, they can be used for damage detection when the attention is focused on the changes in the estimated approximations. An early application can be found in [Inada et al., 1999], where however data come from the simulation carried out on an analytical models, rather than from the actual measurements. The idea is developed in the next Chapter.

References for Chapter 5

- Baker G.L. and Gollub J.P. (1996). *Chaotic Dynamics*, Cambridge University Press, 2nd. Edition.
- Bontempi F. (1993). *Transizione al Caos in Problemi di Dinamica Strutturale* (in Italian), PhD Thesis, Graduate School in Structural Engineering, Polytechnic of Milan-University of Pavia.
- Breitung K. and Faravelli L. (1996). “Response Surface Methods and Asymptotic Approximations”, Chapter 6 in F. Casciati and J.B. Roberts (eds.), *Mathematical Models for Structural Reliability Analysis*, CRC Press, Boca Raton, USA, 227-285.
- Bucher C.G. and Borgund U.A. (1990). “A Fast and Efficient Response Surface Approach for Structural Reliability Problems”, *Structural Safety*, 7, 57-66
- Box G.E.P. and Wilson K.B. (1954) “The Exploration and Exploitation of Response Surfaces: Some General Considerations and Examples”, *Biometrics*, 10, 16-60.
- Casciati F. and Faravelli L. (1991). *Fragility Analysis of Complex Structural Systems*, Research Studies Press, Taunton, UK.
- Chou and Ghaboussi (2001). “Genetic Algorithm in Structural Damage Detection”, *Computers & Structures*, 79, 1335-1353.
- Escudié B., Gazanhes C., Tachoire H and Torra V. (2001). *Des Cordes aux Ondelles* (in French), Publications de l’Univerversité de Provence.
- Faravelli L., (1989). “Response Surface Approach for Reliability Analysis”, *Journal of Engineering Mechanics, ASCE*, 115, (12), 2763-2781

- Faravelli L. (1994) "Blocking Problems in the Analysis of Random Fields", *Probabilities and Materials*, D. Breyse (ed.), NATO-ASI Series 269, Kluwer Academic Publishers, Dordrecht, The Netherlands, 177-196.
- Faravelli L. (1992). "Structural Reliability via Response Surface", *Stochastic Mechanics, Proc. IUTAM Symposium on Nonlinear*, N. Bellomo N. F. Casciati (eds.), Springer Verlag, 213-223,.
- Faravelli L., (2000). "Modelling the Response of an Elastomeric Base Isolator", *Journal of Structural Control*, 8, 1, 17-30.
- Faravelli L. and Casciati S. (2004). "Structural Damage Detection and Localization by Response Change Diagnosis", *Progress in Structural Engineering and Materials*, 6, 2, 104-115.
- Faravelli L. and Pisano A. (1997). "Damage Assessment Toward Performance Control", *Proceedings of DAMAS'97*, University of Sheffield, UK, 185-198.
- Gayton N., Bourinet J.M. and Lemaire M. (2003). "CQ2RS: a New Statistical Approach to the Response Surface Method for Reliability Analysis", *Structural Safety*, 25, 1, 99-121
- Gen M. and Cheng R. (2000). *Genetic Algorithms and Engineering Optimization*, John Wiley and Sons, New York.
- Gomes H.M. and Awruch A.M. (2004). "Comparison of Response Surface and Neural Network with Other Methods for Structural Reliability Analysis", *Structural Safety*, 26, 1, 49-58
- Guan X.L. and Melchers R.E. (2001). "Effect of Response Surface Parameters Variation on Structural Reliability Estimation", *Structural Safety*, 23, 4, 429-444.

- Gupta S. and Manohar C.S. (2004). "An Improved Response Surface Method for the Determination of Failure Probability and Importance Measures", *Structural Safety*, 26, 2, 123-139
- Habarbanel H.D.I. (1995). *Analysis of Observed Chaotic Data*, Springer Verlag.
- Hegger R., Kantz H., and Schreiber T., (1999). "Practical implementation of nonlinear time series methods: The TISEAN package", *Chaos* 9, 413-435.
- Inada T., Shimamura Y., Todoroki A., Kobayashi H., and Nakamura H., (2000). "Damage Identification Method for Smart Composite Cantilever Beam with Piezoelectric Materials", *Proceedings Structural Health Monitoring 2000*, F-K. Chang (ed.), DEStech, Lancaster, 986-994.
- Kantz H. and Schreiber T. (1997). *Nonlinear Time Series Analysis*, Cambridge University Press.
- Kim S-H. and Na S-W. (1997). "Response Surface Method Using Vector Projected Sampling Points", *Structural Safety*, 19, 1, 3-19.
- Krawczuc M. and Ostachowicz W. (2001). "Spectral Beam Finite Element and Genetic Algorithm for Crack Detection in Beams", *Structural Health Monitoring 2001*, F-K. Chang (ed.), DEStech Publications Inc., Lancaster, 889-898.
- Khuri A.I. and Cornell J.A. (1987). *Response Surfaces: Design and Analyses*, Marcel and Decker, New York.
- Liu Y.W. and Moses F.A. (1994). "A Sequential Response Surface Method and its Application in the Reliability Analysis of Aircraft Structural Systems", *Structural Safety*, 16, 39-46.

- Marwala T. (2001). "Probabilistic Fault Identification using a Committee of Neural Networks and Vibration Data", *AIAA, Journal of Aircraft*, 38, ,1 38-146.
- Masri S.F., Smyth A.W., Chassiakos A.G., Caughey T.K., and Hunter N.F. (2000). "Application of Neural Networks for Detection of Changing in Nonlinear Systems", *J. Eng. Mech., ASCE*, 126, 7., 666-683.
- Myers R.H. (1971). *Response Surface Methodology*, Allyn and Bacon, Boston.
- Myers R.H. and Montgomery D.C. (1995). *Response Surface Methodology: Process and Product Optimization using Design Experiments*, John Wiley & Sons.
- Nakamura M., Masri S.F., Chassiakos A.G., and Caughey T.K. (1998). "A Method for Non-parametric Detection through the Use of Neural Networks", *Earthquake Engineering and Structural Dynamics*, 27, 997-1010.
- Petersen R.G., (1985). *Design and Analysis of Experiments*, Marcel Decker, New York.
- Pisano A. (1997). *Structural System Identification: Advanced Approaches and Applications*, PhD Thesis, University of Pavia, Dept. of Structural Mechanics.
- Romero V.J., Swiler L.P., and Giunta A.A. (2004). "Construction of Response Surfaces Based on Progressive-Lattice-Sampling Experimental Design with Application to Uncertainty Propagation", *Structural Safety*, 26, 2, 201-219.
- Rajashekhhar M.R. and Ellingwood B.R. (1993). "A New Look at the Response Surface Approach for Reliability Analysis", *Structural Safety*, 12, , 205-220.

- Sano M. and Sawada Y. (1985), Measurement of the Lyapunov spectrum from a chaotic time series, *Phys. Rev. Lett.* 55, 1082.
- Venini P. (2003). "Some Thoughts on Identification and Control in Wavelet Space", in Casciati F. (ed.), *Proceedings of the 3rd World Conference on Structural Control*, John Wiley & Sons, Chichester, Vol 3., 515-520.
- Wong F.S. (1984). "Uncertainties in Dynamic Soil-Structure Interaction", *J. Eng. Mech., ASCE*, 110, 308-324
- Wong F.S. (1985), "Slope Reliability and Response Surface Method", *J. Geo Eng., ASCE*, 111, , 32-53.
- Xu B., Wu Z.S., and Yokoyama K. (2003). "Response Time Series Based Structural Parametric Assessment Approach with Neural Networks", *Structural Health Monitoring and Intelligent Infrastructures*, Z. Wu and M. Abe (eds.), Balkema, Lisse, The Netherlands, Vol. 1, 601-609.
- Yi J-H. and Feng M.Q. (2003). "Stochastic Optimization Techniques for NDE of Bridges using Vibration Signatures", *Smart Structures and Materials 2003*, SPIE 5057, S-C. Liu (ed.), SPIE, Bellingham, 582-593.
- Zheng H.T., Xue S.T., Qian Y.Y., Xie L.Y., and Mita A (2003). "Structural Damage Identification by Neural Networks and Modal Analysis", *Structural Health Monitoring and Intelligent Infrastructures*, Z. Wu and M. Abe (eds.), Balkema, Lisse, The Netherlands, Vol. 1, 635-639.

Chapter 6

The SHM Response Surface Methodology

In many technical fields, the experimenters can identify a response variable of interest, y , and a set of predictor variables, x_1, x_2, \dots, x_k . In some systems the nature of the relationship between y and the x 's might be known "exactly", based on the underlying engineering, chemical, or physical principles. Then one could write a model of the form $y = g(x_1, x_2, \dots, x_k) + \eta$, where the term η represents the "error" in the system. This type of relationship is often called a mechanistic model. In the more common situation where the underlying mechanism is not fully understood, the experimenter must approximate the unknown function g with an appropriate empirical model $y = f(x_1, x_2, \dots, x_k) + \varepsilon$, where ε also accounts for the lack of fit error η_L introduced in the model by the assumed form of $f(\cdot)$. Usually, the function f is a first-order or second-order

polynomial in the basic predictors or their transformations. This empirical model is called a response surface model.

Identifying and fitting from experimental data an appropriate response surface model requires some knowledge of statistical experimental design fundamentals, regression modelling techniques, and elementary optimization methods. All three of these topics are generally integrated into the so called response surface methodology (RSM).

The most extensive applications of RSM are in the industrial world, particularly in situations where several input variables potentially influence some performance measure or quality characteristic (the response) of the product or process. For example, y might be the viscosity of a polymer and x_1 , x_2 , and x_3 might be the reaction time, the reactor temperature, and the catalyst feed rate in the process. Clearly, if we could easily construct the graphical display of the relationship between the response and the predictors (the response surface), the optimization of this process would be very straightforward. By inspection of the plot, we could identify the values of the process variables which yield to the desired value of the response variable of interest. Unfortunately, in most practical situations, the true response function is unknown. In this case, the field of response surface methodology consists of the experimental strategy for exploring the space of the process variables, empirical statistic modelling to develop an appropriate approximating relationship, and optimization methods for finding the levels or values of the process variables that produce desirable values of the response.

In the applications to damage diagnosis, the experimental strategy consists of the monitoring of the structure in time. Each output of this process can be regarded alternatively as response or predictor. When the measurement of one

sensor is considered as the response, the response surface model is the relationship between that measurement and those recorded at the same time by the other sensors on the structure. In some cases, this relationship is known, for example by computing the influence line of a bridge in a static problem in so many points that the load distribution can be inferred from the response measurements. When dynamic problems or more complex structures are considered, an approximation is needed. The change in the statistical distribution of the error involved in these problems can be considered as a damage indicator. This strategy is herein discussed, and its application to a numerical example leads to the formulation of a new method for damage detection and localization. The testing of the method on more thorough examples is then the objective of the following three chapters.

It must be preliminarily said that the nature of a monitoring system itself prevents one from applying the statistical experimental design techniques, which ensure that the approximating function is close to the real unknown model by performing the experiments in the most representative design points. However, as opposite to the industrial applications, here the concern is not building the most reliable approximation function to identify the process optimal conditions, but finding a feature which can detect a change in the model. This feature is not related to the intensity of the error, but to its statistical distribution. Therefore, the approximating function is just a mean for feature extraction. To distinguish this method from the classical approach, we will denote it as structural health monitoring response surface methodology (SHM-RSM). The general theory which is common between the two methods is reported in detail in Appendix A, while the following section summarizes only the aspects strictly necessary for the damage diagnosis application.

6.1 Basic Principles

In general, an experiment involves a response y that depends on other variables $\xi_1, \xi_2, \dots, \xi_k$. The variables $\xi_1, \xi_2, \dots, \xi_k$ are usually called the natural variables, because they are expressed in the natural units of measurements. In many RSM works, it is convenient to transform the natural variables to coded variables x_1, x_2, \dots, x_k , which are usually defined to be dimensionless with mean zero and the same spread or standard deviation. In terms of the coded variables, the response surface function is written as

$$y = f(x_1, x_2, \dots, x_k) + \varepsilon \quad (6.1)$$

In most practical applications, the underlying true response surface is typically driven by some unknown physical mechanism which may be very complicated. It is therefore necessary to develop an approximating model based on the observed data from the system, i.e., an empirical model. The resulting form assigned to $f(\cdot)$ introduces a systematic lack of fit error η_L into the system, which is included in the global error term $\varepsilon = \eta_L + \eta$, where η is the random error, or pure error. The latter error [Breitung-Faravelli, 1996] arises from the remark that, if the same experiment is run r times for the same values of the x 's, the resulting outcomes y_1, \dots, y_r may result different due to the randomness of the variables. Thus, the term ε in Equation (6.1) represents all the other sources of variability not accounted for in $f(\cdot)$, and it includes effects such as measurement error on the response, other sources of variation that are inherent in the process or system (background noise, or common cause variation in the

language of statistical process control), the effect of other variables, and so on. We will treat ε as a statistical error, and we will assume it to have a normal distribution with mean zero and variance σ^2 . Therefore, determining the probability distribution of the variance σ^2 completely defines, in a statistical fashion, the error ε .

Usually, a low-order polynomial in some relatively small region of the variable space is appropriate to model the response surface function $f(\cdot)$. In many cases, either a first-order or second-order model is used. The general motivation for a polynomial approximation for the true response function g is based on its Taylor-series expansion around the point $x_{01}, x_{02}, \dots, x_{0k}$. For example, the first-order model is developed from the first-order Taylor expansion

$$g \cong f = g(x_{01}, x_{02}, \dots, x_{0k}) + \left. \frac{\partial g}{\partial x_1} \right|_{\mathbf{x}=\mathbf{x}_0} (x_1 - x_{01}) + \left. \frac{\partial g}{\partial x_2} \right|_{\mathbf{x}=\mathbf{x}_0} (x_2 - x_{02}) + \dots + \left. \frac{\partial g}{\partial x_k} \right|_{\mathbf{x}=\mathbf{x}_0} (x_k - x_{0k}) \quad (6.2)$$

where \mathbf{x} refers to the vector of regressor variables and \mathbf{x}_0 is that vector of variables at the specific point $x_{01}, x_{02}, \dots, x_{0k}$. Because in Equation (6.2) we have included only the first-order terms of the expansion, it can be rewritten as

$$y = \beta_0 + \beta_1 x_1 + \beta_2 x_2 + \dots + \beta_k x_k + \varepsilon \quad (6.3)$$

If we were to include second-order terms in Equation (6.2), this would lead to the second-order approximating model

$$y = \beta_0 + \sum_{j=1}^k \beta_j x_j + \sum_{j=1}^k \beta_{jj} x_j^2 + \sum_{i < j} \sum_{j=2}^k \beta_{ij} x_i x_j \quad (6.4)$$

It can be noted that there is a close connection between RSM and multiple linear regression analysis. The β 's in Equations (6.3) and (6.4), respectively, are sets of unknown parameters. To estimate the values of these parameters, we must collect data on the system that we are studying. Multiple regression analysis is a branch of statistical model building that uses these data to estimate the β 's. Because, in general, polynomial models are linear function of the unknown β 's, we refer to the technique as multiple linear regression analysis.

The model (6.3) is therefore called a multiple linear regression model with k regressor variables, and the parameters β_j , $j = 0, 1, \dots, k$, are the regression parameters. This model describes a hyperplane in the k -dimensional space of the regressor variables $\{x_j\}$. The parameter β_j represents the expected change in y per unit change in x_j , when all the remaining variables x_i ($i \neq j$) are held constant.

The first-order model is likely to be appropriate when the experimenter is interested in approximating the true response surface over a relatively small region of the variables space, in a location where there is a little curvature in g . Sometimes the curvature in the true response surface is strong enough that the first-order model is inadequate. A second-order model will likely be required in these situations. This model would likely be useful as an approximation to the

true response surface in a relatively small region around a point where there is a substantial curvature in the true response function g . A mound-shaped response surface and elliptical contours are generated by this model. Such a response surface could arise in approximating a response such yield, where we would expect to be operating near a maximum point on the surface. The second-order model is widely used in the classic response surface methodology because it is very flexible and it can take on a wide variety of functional forms, so it will often work well as an approximation to the true response surface. However, in some situations, approximation polynomial of order greater than two are used.

In SHM applications, a polynomial degree of the first order is often sufficient, as we will see further ahead. Common structures, except for suspended bridges and tall antennas, are designed to provide a linear response in their operational conditions, and hence a response surface built on the monitored data is likely to be linear. However, the basic theory of the damage detection approach still holds and it can be easily adapted also to the cases where higher-order polynomials are needed. Indeed, models that are more complex in appearance than Equation (6.3) may often still be analyzed by multiple linear regression techniques since, in general, any regression model that is linear in the parameters (the β -values) is a linear regression model, regardless of the shape of the response surface that it generates. The damage detection method is theoretically based on the principle of response surface, but it practically makes use of the multiple linear regression techniques to extract the damage sensitive feature from the data, regardless of the accuracy of the response surface approximation in representing the real one. Therefore, in the following sections the essential steps of multiple linear regression analysis are recalled.

TABLE 6.I DATA FOR MULTIPLE LINEAR REGRESSION

| y | x₁ | x₂ | ... | x_k |
|----------------|----------------------|----------------------|-----|----------------------|
| y ₁ | x ₁₁ | x ₁₂ | ... | x _{1k} |
| y ₂ | x ₂₁ | x ₂₂ | ... | x _{2k} |
| ⋮ | ⋮ | ⋮ | | ⋮ |
| y _n | x _{n1} | x _{n2} | ... | x _{nk} |

6.1.1 Model Fitting

Model fitting is the method for estimating the regression coefficients in multiple linear regression models. For this purpose, the least squares method is typically used. A detailed description of the method is provided in Appendix A, while here only the equations that are the results of this procedure are summarized.

Suppose that $n > k$ observations on the response variable are available, say y_1, y_2, \dots, y_n . Along with each observed response y_i , we will have an observation on each regressor variable, and let x_{ij} denote the i -th observation or level of variable x_j . The data will appear as in Table 6.I.

We may write the model in Equation (6.3) in terms of the observations in Table 6.I as

$$\begin{aligned}
 y_i &= \beta_0 + \beta_1 x_{i1} + \beta_2 x_{i2} + \dots + \beta_k x_{ik} + \varepsilon_i \\
 &= \beta_0 + \sum_{j=1}^k \beta_j x_{ij} + \varepsilon_i, \quad i = 1, 2, \dots, n
 \end{aligned}
 \tag{6.5}$$

or in matrix notation as

$$\mathbf{y} = \mathbf{A}\boldsymbol{\beta} + \boldsymbol{\varepsilon} \tag{6.6}$$

where

$$\mathbf{y} = \begin{bmatrix} y_1 \\ y_2 \\ \vdots \\ y_n \end{bmatrix}, \mathbf{A} = \begin{bmatrix} 1 & x_{11} & x_{12} & \dots & x_{1k} \\ 1 & x_{21} & x_{22} & \dots & x_{2k} \\ \vdots & \vdots & \vdots & & \vdots \\ 1 & x_{n1} & x_{n2} & \dots & x_{nk} \end{bmatrix}, \boldsymbol{\beta} = \begin{bmatrix} \beta_1 \\ \beta_2 \\ \vdots \\ \beta_{k+1} \end{bmatrix}, \text{ and } \boldsymbol{\varepsilon} = \begin{bmatrix} \varepsilon_1 \\ \varepsilon_2 \\ \vdots \\ \varepsilon_n \end{bmatrix}.$$

In general, \mathbf{y} is the $n \times 1$ vector of the response variables, \mathbf{A} is the $n \times (k+1)$ matrix of the levels of the regressor variables, $\boldsymbol{\beta}$ is the $(k+1) \times 1$ vector of the regression coefficients, and $\boldsymbol{\varepsilon}$ is the $n \times 1$ vector of the total errors. We assume that the error term $\boldsymbol{\varepsilon}$ in the model has $E(\boldsymbol{\varepsilon}) = 0$ and $\text{Var}(\boldsymbol{\varepsilon}) = \sigma^2$, and that the $\{\varepsilon_i\}$ are uncorrelated random variables.

The method of the least squares chooses the β 's in Equation (6.5) so that the sums of the squares of the errors, ε_i , are minimized. In matrix notation, the vector of least squares estimators \mathbf{b} is the $\boldsymbol{\beta}$ vector that minimizes the function $L = \boldsymbol{\varepsilon}^T \boldsymbol{\varepsilon} = (\mathbf{y} - \mathbf{A}\boldsymbol{\beta})^T (\mathbf{y} - \mathbf{A}\boldsymbol{\beta})$, and it results to be given by

$$\mathbf{b} = (\mathbf{A}^T \mathbf{A})^{-1} \mathbf{A}^T \mathbf{y} \tag{6.7}$$

The fitted regression model is then

$$\hat{\mathbf{y}} = \mathbf{A}\mathbf{b} \tag{6.8}$$

The difference between the observation \mathbf{y} and the fitted model $\hat{\mathbf{y}}$ is the $n \times 1$ vector of the residuals

$$\mathbf{e} = \mathbf{y} - \hat{\mathbf{y}} = \mathbf{y} - \mathbf{A}\mathbf{b} \quad (6.9)$$

6.1.2 Estimate of the Variance of the Error

To develop an estimator of the variance of the error σ^2 , consider the sum of the squares of the residuals,

$$SSE = \sum_{i=1}^n (y_i - \hat{y}_i)^2 = \sum_{i=1}^n e_i^2 = \mathbf{e}^T \mathbf{e} \quad (6.10)$$

Substituting Equation (6.9) and using $\mathbf{A}^T \mathbf{A}\mathbf{b} = \mathbf{A}^T \mathbf{y}$ yields

$$SSE = \mathbf{y}^T \mathbf{y} - \mathbf{b}^T \mathbf{A}^T \mathbf{y} \quad (6.11)$$

Equation (6.11) is called the error or residual sum of squares, and it has $n-k-1$ degrees of freedom associated with it. It can be shown that an unbiased estimator of σ^2 is given by

$$s^2 = \frac{SSE}{n-k-1} \quad (6.12)$$

The estimate of σ^2 produced by Equation (6.12) is model-dependent. That is, its value depends on the form of the model that is fit to the data. For

example, if we fit a quadratic model to the data, the estimate of σ^2 may result to be larger than the estimate obtained from a first-order model, suggesting that the first-order model is superior than the quadratic in that there is less unexplained variability resulting from the first-order fit. If replicate runs are available (that is, more than one observation on y at the same x -levels), then a model-independent estimate of σ^2 can be obtained. Indeed, when replicates of a single experiment are possible, i.e., when one can associate to the same matrix \mathbf{A} different response vectors \mathbf{y} , this subset of experiments provides an estimate of the pure error variance. The variance of the lack of fit error is then obtained by subtracting this estimate to s^2 . In the particular case under investigation, the measurements are collected in a continuous monitoring. This prevents one from collecting replicates able to estimate the pure error variance and, hence, the lack of fit and the pure error cannot be distinguished one from the other.

It is worth noting again that the above summarized approach just makes use of regression analysis: to rigorously speak of response surface, the levels of the predictors should be selected by the operator according to a preliminary assigned experiment plan. This is not the case, since the whole decision-making procedure is based on a continuous monitoring of the response variables. But, as already mentioned, it is accepted in the literature that the term response surface also applies to methods which bypass some of the mathematical requirements inspired from the statistical sampling theory.

6.2 Application to Damage Diagnosis

[Kullaa, 2004] uses the above methodology to eliminate from the data the effects of the environmental and operational conditions, which are not measured but unknown underlying factors. The variables in the response surface model of Equation 6.6 are the monitored quantities of interest (e.g., the modal frequency), while the unknown model coefficients β can be regarded as the underlying factors, which are estimated by Equation (6.7). By computing the residuals from Equation (6.10), these factors can be extracted from the data. The resulting residual vector e is called the vector of the unique factors, because it is insensitive to the operational and environmental conditions. These unique factors are therefore used for damage detection.

[Iwasaki et al., 2001] first applied the response surface theory to develop a simple, low-cost method for damage diagnosis, which does not require a finite elements model (FEM) of the entire structure. First, the system identification of a structure in its intact state is performed using the response surface, that is, a response surface is created from the measured sensor data obtained from the initial state. The response surface is named as initial response surface. For example, the data from a sensor are selected as the response and the data obtained from the adjacent sensors are selected as the predictors. During the training process, a set of every sensor data is periodically obtained by cycling measurements several times. After the training process, a damage monitoring process is started. From the measured set of data, the system identification of the structure is performed and a response surface is recreated. The response surface is named as recreated response surface. The recreated response surface

is compared with the initial one using a statistical similarity test, or F -test, as follows.

Consider two response surfaces that are created from two different sets of experiments

$$\begin{aligned} \mathbf{y}_1 &= \mathbf{A}_1 \boldsymbol{\beta}_1 + \boldsymbol{\varepsilon}_1 \\ \mathbf{y}_2 &= \mathbf{A}_2 \boldsymbol{\beta}_2 + \boldsymbol{\varepsilon}_2 \end{aligned} \quad (6.13)$$

where the number of experiments for regression are n_1 and n_2 , respectively. In order to investigate the similarity of the two response surfaces, a null-hypothesis test is introduced. The hypothesis definition is

$$H_0 : \boldsymbol{\beta}_1 = \boldsymbol{\beta}_2 \quad (6.14)$$

The error terms $\boldsymbol{\varepsilon}_1$ and $\boldsymbol{\varepsilon}_2$ are assumed to be vectors of independent random variables and to have the same distributions in the two sets of experiments. In this case, the F -statistic value, F_0 , is defined as

$$F_0 = \frac{SSE_0 - SSE_{12}}{SSE_{12}} \cdot \frac{n - 2p}{p} \quad (6.15)$$

where $p = k + 1$ (with k number of predictors), $n = n_1 + n_2$, $SSE_{12} = SSE_1 + SSE_2$, and SSE_0 is the residual sum of squares of the response surface obtained by considering the global set of measurements. Under the null-hypothesis H_0 , the F -statistic value, F_0 , follows an F -distribution of degrees of

freedom ($p, n-2p$). When the two response surfaces are similar to each other, F_0 assumes a small value. The critical limit for the rejection of the hypothesis H_0 is therefore

$$F_0 > F_{\alpha, p, n-2p} \quad (6.16)$$

That is, the similarity between the response surfaces is rejected when F_0 is greater than $F_{\alpha, p, n-2p}$, where α is the significance level.

When the system identified from the monitoring process (i.e., the recreated response surface) is discriminated from the system identified from the initial state (i.e., the initial response surface), it means that the relation among the sensors data is changed, and it can be concluded that something happened to the structure. This does not always mean damage initiation, but it can provide a low cost solution for damage diagnosis of the structure to decide the necessity of precise investigation.

The method was applied to detect delamination in a CFRP cantilever beam specimen, instrumented with three conventional strain gages on its surface. A delamination crack of various lengths was introduced under the middle gage. In this study, the strain data of the middle gage were assumed as the response, while the strain data of the adjacent two sensors were regarded as the predictors. Quadratic polynomials were selected as the response surfaces approximation function. By statistically comparing the initial response surface obtained from the strain data of the undamaged beam with the one that has been recreated after delamination, the delamination cracks longer than 6 mm were successfully detected since the rejection of the null hypothesis H_0 was achieved by F -test.

The method presents the advantage that it does not require tests of the damaged structure to define the limit between the intact and damaged states. However, the main criticism to the F -test scheme illustrated above concerns its validation only in cases of study where the problems related to the sensor sensitivity and the associated measurement errors are ignored, and where the loading condition is the same for any set of the replicated experiments. Indeed, the variability introduced by these two sources implies a greater uncertainty in the undamaged approximation, and this could make difficult the detection of damages to which the model is not sufficiently sensitive.

6.3 The Static Problem of a Bridge under a Stationary Queue of Traffic

The method proposed by [Iwasaki et al., 2001] is applied to the static problem of a bridge which needs to withstand, together with its self-weight, \mathbf{W} , a random moving load of vehicles, $\mathbf{Q}(z,t)$, where t denotes the time and z is the spatial coordinate along the bridge longitudinal axis.

The exact solution in terms of vertical displacements can be easily computed for all the bridge sections, and the actual relationship between the vertical displacement of one section and those of the other sections is in this case known by computing the so called influence line. The development of this relationship is discussed in the following and its analogy to a linear regression model is then the basis on which the damage detection method is applied.

Let $k + 1$ the number of known vertical displacements, $\Delta_1(t), \Delta_2(t), \dots, \Delta_{k+1}(t)$, and k the number of loaded sections of the bridge. Therefore, the dependence of $\mathbf{Q}(z,t)$ on z is eliminated by fixing the sections where the load is applied at time t .

Assuming, for example, the vertical displacement of section $k + 1$ as the response variable of interest and the vertical displacements of the remaining k sections as the predictors, we wish to find their relationship, i.e., the response surface function $f(\cdot)$ that satisfies

$$\Delta_{k+1}(t) = f[\Delta_1(t), \Delta_2(t), \dots, \Delta_k(t), t] + \varepsilon(t) \quad (6.17)$$

where the dependence on time is due to both the loading time variability and the potential of damage. The goal is to write a function without the first dependence.

The function which provides the value of the displacement Δ_i in section i due to a unit load in section j is the well known influence line, $L_{ij}(t)$. Its dependence on time accounts for the potential of damage. Therefore, at each point in time, t , one can write

$$\Delta_i(t) = \Delta_{W_i}(t) + \sum_{j=1}^k L_{ij}(t) Q_j(t) \quad (6.18)$$

where $i = 1, \dots, k + 1$, and $\Delta_{W_i}(t)$ is the contribution to $\Delta_i(t)$ of the dead load \mathbf{W} (again depending on time to account for the potential of damage). By rewriting

Equation (6.18) in matrix notation, one finds that the following general equation applies

$$\mathbf{\Delta}(t) = \mathbf{\Delta}_W(t) + \mathbf{L}(t)\mathbf{Q}(t) \quad (6.19)$$

To express the displacement at section $k + 1$ as a function of the other k displacements, we first need to express $\mathbf{Q}(t)$ as a function of them. For a non singular $k \times k$ square matrix \mathbf{L} , one obtains

$$\mathbf{Q}(t) = \mathbf{L}^{-1}(t)[\mathbf{\Delta}(t) - \mathbf{\Delta}_W(t)] \quad (6.20)$$

where $\mathbf{\Delta}_Q(t) = \mathbf{\Delta}(t) - \mathbf{\Delta}_W(t)$ is the $k \times 1$ vector of the contributions to the k vertical displacements $\mathbf{\Delta}(t)$ of the $k \times 1$ moving load of vehicles $\mathbf{Q}(t)$ applied to those k sections.

Writing Equation (6.19) for the contribution of $\mathbf{Q}(t)$ to the vertical displacement at section $k + 1$ and substituting Equation (6.20), give

$$\Delta_{k+1}(t) - \Delta_{Wk+1}(t) = \mathbf{L}_{k+1}(t)\mathbf{Q}(t) = \mathbf{L}_{k+1}(t)\mathbf{L}^{-1}(t)[\mathbf{\Delta}(t) - \mathbf{\Delta}_W(t)] \quad (6.21)$$

where \mathbf{L}_{k+1} is the $1 \times k$ row-vector of vertical displacements of section $k + 1$ due to a unit vertical point load in the other k sections. It is therefore convenient to assume $\Delta_{Qk+1}(t) = \Delta_{k+1}(t) - \Delta_{Wk+1}(t)$ as response and $\mathbf{\Delta}_Q(t) = \mathbf{\Delta}(t) - \mathbf{\Delta}_W(t)$ as predictors, i.e., to consider the contribution of $\mathbf{Q}(t)$ to the vertical displacements instead of the total vertical displacements.

The result is a linear dependence of the response on the predictors. Given a set of measurements collected at n different times, the previous relationship can be synthesized into Equation (6.6) with

$$\mathbf{y} = \begin{Bmatrix} y_1 \\ y_2 \\ \vdots \\ y_n \end{Bmatrix} = \begin{Bmatrix} \Delta_{k+1}(t_1) - \Delta_{Wk+1}(t_1) \\ \Delta_{k+1}(t_2) - \Delta_{Wk+1}(t_2) \\ \vdots \\ \Delta_{k+1}(t_n) - \Delta_{Wk+1}(t_n) \end{Bmatrix}, \quad \mathbf{A} = \begin{Bmatrix} \mathbf{A}_1 \\ \mathbf{A}_2 \\ \vdots \\ \mathbf{A}_n \end{Bmatrix} = \begin{Bmatrix} [\Delta(t_1) - \Delta_W(t_1)]^T \\ [\Delta(t_2) - \Delta_W(t_2)]^T \\ \vdots \\ [\Delta(t_n) - \Delta_W(t_n)]^T \end{Bmatrix},$$

$$\boldsymbol{\beta} = \begin{Bmatrix} \beta_1 \\ \beta_2 \\ \vdots \\ \beta_k \end{Bmatrix} = \begin{Bmatrix} [\mathbf{L}_{k+1}(t_1)\mathbf{L}^{-1}(t_1)]^T \\ [\mathbf{L}_{k+1}(t_2)\mathbf{L}^{-1}(t_2)]^T \\ \vdots \\ [\mathbf{L}_{k+1}(t_n)\mathbf{L}^{-1}(t_n)]^T \end{Bmatrix}.$$

Hence, one can see that the resulting matrices sizes are $n \times 1$ for \mathbf{y} , $n \times k$ for \mathbf{A} , and $k \times 1$ for $\boldsymbol{\beta}$, because the constant term of the first-order response surface model of Equation (6.5) is null.

The linear regression parameter $\boldsymbol{\beta}$ in Equation (6.6) can also be estimated by applying the previously described least squares method. If the available measurements are the computed values of the vertical displacements, the obtained estimate \mathbf{b} is practically equal to the theoretic values given by the influence lines product of Equation (6.21). The value of SSE for this linear regression model is negligible, because the error is only of a numerical nature. A first significant contribution to the error term $\boldsymbol{\varepsilon}$ in Equation (6.6) can be introduced by adding a random noise to the computed displacements. A further level of approximation can be achieved by considering also a number of

regressors lower than the k displacements required by the model. In these cases, the vector \mathbf{b} estimated by Equation (6.7) as the result of the linear regression analysis is no longer the one of Equation (6.21).

The n measurements leading to the estimate of Equation (6.7) can be repeated several times, with different random traffic loads and different random noises added to the exact solution. The result is a population of SSE -values and of corresponding F -values, from which histograms can be drawn. In the next section a numerical example of this procedure is provided. The F -test method proposed by [Iwasaki et al., 2001] is first applied to the undamaged states of a simple schematization of a bridge structure, to test if the method is able to recognize, under varying excitation, that no structural changes occur into the model when adding noise to the measurements and when reducing the number of sensors on the structure. A damage is then introduced into the model, but the F -test seems to be insensitive to the slight modifications in the displacement values associated with significant damage when noise is present in the measurements. The correct information about damage can, however, be emphasized by a statistic comparison of the samples of the estimates s of the standard deviations of the errors which result from subsequent clusters of experiments, in the undamaged and damaged states. This observation leads to the abandon of the [Iwasaki et al., 2001] F -test method and to the formulation of a new damage-sensitive feature.

6.3.1 Numerical Example

The bridge model under consideration has three spans, two lateral ones of length $L_1 = L_3 = 8$ m each, and a main span which is $L_2 = 24$ m long. For the purpose of this study, the rough schematization of a simply supported beam in

Figure 6.1 is adopted. The model is discretized into $N_e = 40$ beam elements of length $l = 1$ m each, and $N = 41$ nodes. The elements cross-section has a moment of inertia $I = 0.1$ m⁴ with respect to the horizontal in-plane axis, and an area $A = 1.69$ m². The given material properties are the Young modulus $E = 30000000$ kN/m² and the mass density $\rho = 2500$ kg/m³. The calculations are carried out in MATLAB[®] environment.

Under the assumption of irrelevant axial deformations, each node has two degrees of freedom, a rotation and a vertical displacement, except for the four supports that block the vertical displacements, but not the rotations. The four supports are assumed with no settlement, and hence only $N-4 = 37$ vertical displacements are allowed. Therefore, the system has a total of $D = N+(N-4) = 78$ degrees of freedom.

The 4×4 element stiffness matrices of the form

$$\mathbf{K}_{el} = EI \begin{bmatrix} \frac{12}{l^3} & -\frac{6}{l^2} & -\frac{12}{l^3} & -\frac{6}{l^2} \\ -\frac{6}{l^2} & \frac{4}{l} & \frac{6}{l^2} & \frac{2}{l} \\ \frac{12}{l^3} & \frac{6}{l^2} & \frac{12}{l^3} & \frac{6}{l^2} \\ -\frac{6}{l^2} & \frac{2}{l} & \frac{6}{l^2} & \frac{4}{l} \end{bmatrix} \quad (6.22)$$

are assembled in a 78×78 global stiffness matrix \mathbf{K}_{glob} , following the standard finite element procedures.

The self-weight is included by applying a vertical (downward) point force of intensity $W = (\rho A l) g = 42.25$ kN in $N-4 = 37$ nodes.

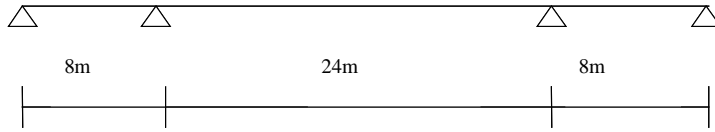


Figure 6.1 Undamaged state of the structure.

Collecting the weights is a 78×1 vector, \mathbf{F}_W , where zeros are placed where no forces are present, one can compute the 78×1 vector of displacements due to the self weight alone as

$$\mathbf{D}_W = \mathbf{K}_{\text{glob}}^{-1} \mathbf{F}_W \quad (6.23)$$

from which the vertical displacements are extracted and arranged in a 41×1 vector, Δ_W , containing zeros in correspondence of the four supports.

In addition to the dead load, a random train of vehicles crossing the bridge is considered as live load, and it is modelled by a vertical (downward) point force of random intensity that can be applied to $k = 20$ given nodes. The index i of the potentially loaded nodes does not vary in the range $[1,37]$, but only a single node in each couple of subsequent nodes is considered, starting from the first node after the l.h.s. support. Namely, the nodes that could be loaded have an assigned coordinate z equal to:

- 1m, 3m, 5m, 7m, and 33m, 35m, 37m, 39m in the two lateral bays;
- 9m, 11m, 13m, 15m, 17m, 19m, 21m, 23m, 25m, 27m, 29m, 31m in the central span.

For each of these potential nodes, the random nature of the force is represented by generating a random number \tilde{P} using the function “rand”, which is implemented in MATLAB[®] and returns a scalar in the interval (0,1) whose value changes each time that it is referenced. Assigning the following probabilities of having, at time t , a load $Q(t,i)$ of a certain intensity in node i :

$$P[Q(t,i) = 0] = 0.5$$

$$P[Q(t,i) = 10 \text{ kN}] = 0.25 \quad (6.24)$$

$$P[Q(t,i) = 150 \text{ kN}] = 0.25$$

the value \tilde{P} determines the intensity of load $Q(t,i)$ as follows

$$Q(t,i) = \begin{cases} 0 \text{ kN}, & \text{if } \tilde{P} < 0.5 \\ 10 \text{ kN}, & \text{if } 0.75 < \tilde{P} \\ 150 \text{ kN}, & \text{otherwise} \end{cases} \quad (6.25)$$

When node i shows the highest load value of 150 kN, the same value occurs at node $i+2$. It is easy to recognize in this load assignment a rough stationary sequence of cars and trucks.

By repeating this assignment $n = 70$ times, one obtains (for different values \tilde{P}) the 70 different load distributions representing the structure loading conditions at 70 different times t_1, t_2, \dots, t_{70} .

If we collect the live loads values in a 78×70 matrix, \mathbf{F}_Q (where zeros are placed in correspondence of the unloaded nodes), the corresponding 78×70 displacements can be computed as

$$\mathbf{D}_Q = \mathbf{K}_{\text{glob}}^{-1} \mathbf{F}_Q \quad (6.26)$$

from which the vertical displacements are extracted and arranged in a 41×70 matrix, Δ_Q .

In an analogous manner, the $N = 41$ total vertical displacements of the structure at $n = 70$ different times can be extracted from the 78×70 matrix

$$\mathbf{D} = \mathbf{D}_w + \mathbf{D}_Q = \mathbf{K}_{\text{glob}}^{-1} (\mathbf{F}_w + \mathbf{F}_Q) \quad (6.27)$$

or they can be directly computed as a 41×70 matrix from

$$\Delta = \Delta_w + \Delta_Q \quad (6.28)$$

The previous calculations provide the exact solution of the static problem by standard finite elements procedures. Let us now assume that only $k + 1 = 21$ vertical displacements out of the 37 computed non-null ones are known, as it is most likely to happen when actual measurements are taken from a bridge. Namely, the vertical displacements in the $k = 20$ sections where the live loads are prescribed and in the middle-span (section of coordinate 20 m) are extracted from the solution of Equation (6.28), and they are considered as the ideal

measurements when no noise is present. Based on these measurements, one can build a first-order response surface model, where, for example, the response variable of interest is the vertical displacement at mid-span, and the predictors are the other $k = 20$ measurements. For consistence with the previous section, consider the vertical displacements due to the live load alone and given by the transpose of Equation (6.26), in the response surface model

$$\Delta_{Q20}^T = \beta_0 + \sum_{j=1}^{20} \beta_j \Delta_{Q2j-1}^T + \boldsymbol{\varepsilon} \quad (6.29)$$

That is, Δ_{Qi} is the 1×70 i -th row of the 41×70 matrix Δ_Q , i is the node number or section coordinate, $\boldsymbol{\varepsilon}$ is a 70×1 vector, and $\beta_0, \beta_1, \dots, \beta_k$ are the $k + 1 = 21$ unknown scalar linear regression coefficients. Collecting them in a 21×1 vector $\boldsymbol{\beta}_{20}$ and setting

$$\mathbf{y}_{20} = \Delta_{Q20}^T \quad (6.30)$$

and

$$\mathbf{A}_{20} = \begin{bmatrix} \mathbf{1} & \Delta_{Q1}^T & \dots & \Delta_{Q2j-1}^T & \dots & \Delta_{Q39}^T \end{bmatrix} \quad (6.31)$$

where $\mathbf{1}$ is a 70×1 vector of ones so that the resulting matrix \mathbf{A}_{20} has size 70×21 , allow one to write

$$\mathbf{y}_{20} = \mathbf{A}_{20}\mathbf{b}_{20} + \boldsymbol{\varepsilon}_{20} \quad (6.32)$$

The suffix “₂₀” underlines that the values contained in the matrices depend on the node whose $n = 70$ vertical displacements are considered as the response vector \mathbf{y} in the response surface model.

By applying the least square method (i.e., Equation (6.7)), one obtains an estimate \mathbf{b}_{20} of the 21×1 vector of the linear regression coefficients, and computes the *SSE* value from Equation (6.11). Since in this case the first-order response surface model corresponds to the actual relationship between response and predictors, the error in Equation (6.32) is only of numerical nature and the associated *SSE* is estimated to be of the order of 10^{-5} cm^2 .

The influence line is computed as the displacements due to an unitary vertical point force which is moved along the same $k = 20$ beam sections to which the live load is assigned. When the unitary force is applied to section i , the 78 consequent displacements are given by

$$\mathbf{D}_{Li} = \mathbf{K}_{\text{glob}}^{-1} \mathbf{F}_{Li} \quad (6.33)$$

where \mathbf{F}_{Li} is a 78×1 vector of zeros, except for a 1 corresponding to the current force position. Repeating for all the k sections and storing each time the computed vertical displacements in a 41×20 matrix (with zeros in correspondence of the four supports), we can extract a 20×20 matrix \mathbf{L}_k by considering only the rows of the displacements in the $k = 20$ loaded sections, and a 1×20 row-vector \mathbf{L}_{20} corresponding to the vertical displacements at mid-span due to a unitary force in each of the $k = 20$ sections. The live load

contribution to the vertical displacement at mid-span can therefore be computed also by applying Equation (6.21), which in this case becomes

$$\Delta_{Q20} = \mathbf{L}_{20} \mathbf{L}_k^{-1} \Delta_{Qk} \quad (6.34)$$

where Δ_{Qk} is the 20×70 matrix extracted from the 41×70 matrix Δ_Q by considering only the columns of the vertical displacements in the $k = 20$ loaded sections. Note that the so obtained Δ_{Q20} is equal to row 20 of matrix Δ_Q and it is the transpose of \mathbf{y}_{20} in Equation (6.32). The 21×1 difference vector $\mathbf{b}_{20} - [0 \quad \mathbf{L}_{20} \mathbf{L}_k^{-1}]^T$ results to be of the order of 10^{-7} or lower, so that in this case the regression and the exact model are practically the same, when considering ideal measurements without noise. Therefore, in this case, the null-hypothesis H_0 defined by Equation (6.14) holds.

Under the null-hypothesis H_0 , the F -statistic value, F_0 , follows an F -distribution of degrees of freedom $(p, m-2p)$, where $p = 21$, $m = n_1 + n_2 = 2n = 140$, and $m-2p = 98$. Hence, for this problem, one finds

$$F_{\alpha, p, m-2p} = \text{finv}(1-0.01, 21, 98) = 2.047 \quad (6.35)$$

where the function “`finv(P, V1, V2)`”, available in the MATLAB[®] Statistics Toolbox, computes the inverse of the F -cdf (cumulative distribution function) with numerator degrees of freedom $V1 = p$ and denominator degrees of freedom $V2 = m-2p$ for the corresponding probability in $\mathbb{P} = 1-\alpha$, and the significance level α set to 1%.

Let us now compute the F -value defined by Equation (6.15) for two sets of $n = 70$ measurements each, obtained by considering the undamaged state of the structure under two different sets of $n = 70$ loading conditions each. For this purpose, the coefficients \mathbf{b} of the three linear regression models built on each of the two sets of measurements and on the global one which includes both sets, respectively, need to be estimated. The values of SSE_1 , SSE_2 , and SSE_0 used in Equation (6.15) are then computed by applying Equation (6.11) for the three cases, respectively. To obtain a representative population of F -values which allows to appreciate a significance level $\alpha = 1\%$, the analysis is repeated 100 times. The result is the histogram in Figure 6.2, which has the F -values on the horizontal axis, and the number of occurrence of these values during the 100 experiments on the vertical axis. The mean of the F -histogram is equal to 9.5798 and it is much beyond the limit value computed in Equation (6.35), thus showing that the F -method does not recognize that no structural change occurs when the loading conditions are varied and no noise is present.

Note that for a significant number of measurements ($n = 70$) compared to the number of predictor variables in the response surface model ($k = 20$), the variance of the error in the global linear regression model, and its correspondent SSE_0 , are approximately twice the ones computed on each single set of measurements, i.e., $SSE_0 \cong 2SSE_1 \cong 2SSE_2$. Figure 6.3 provides, for example, a comparison of the histograms of the two quantities SSE_0 and $2SSE_1$. No significant statistical differences can be observed between the two distributions. The non-dimensional difference of the two means given by

$$ADM = \{E[SSE_0] - E[SSE_1]\} / E[SSE_0] \quad (6.36)$$

is in this case equal to 1.3822.

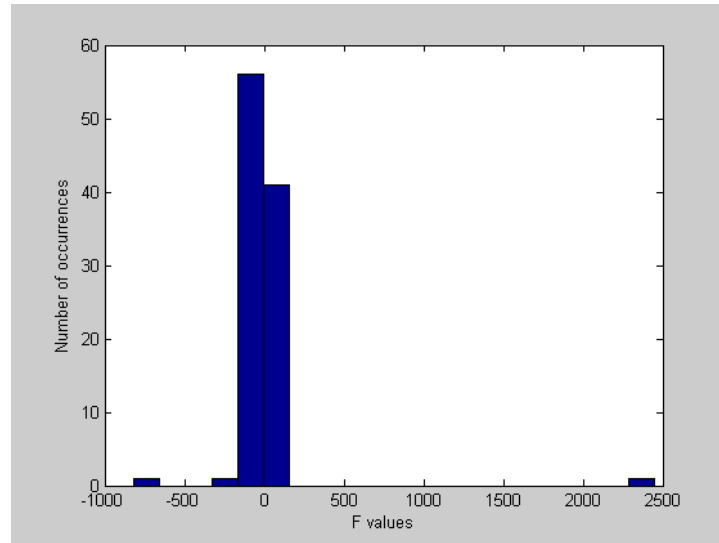


Figure 6.2 *F*-histogram for the undamaged state of the structure under different load conditions.

Response at 20 m, and $k = 20$ predictors.

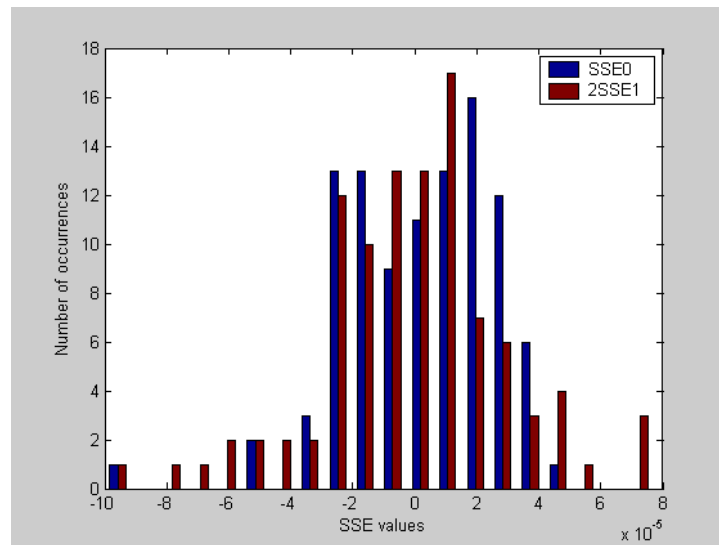


Figure 6.3 *SSE*-histograms for the undamaged state of the structure under different load conditions. Response at 20 m, and $k = 20$ predictors.

6.3.2 Including Noise into Measurements

Using the function “`randn(m, n)`” available in MATLAB[®] to generate a $m \times n$ array of random numbers whose elements are normally distributed with null mean and unitary standard deviation, the noise can be introduced in the response surface model of Equation (6.32) by setting

$$\mathbf{y}_{20} = \mathbf{\Delta}_{Q20}^T + \mathbf{n} \quad (6.37)$$

and

$$\mathbf{A}_{20} = \left[\mathbf{1} \quad \mathbf{\Delta}_{Q1}^T + \mathbf{N}(:,1) \quad \dots \quad \mathbf{\Delta}_{Q2j-1}^T + \mathbf{N}(:,j) \quad \dots \quad \mathbf{\Delta}_{Q39}^T + \mathbf{N}(:,20) \right] \quad (6.38)$$

where “ $\mathbf{n} = a \text{ randn}(70,1)$ ”, “ $\mathbf{N} = a \text{ randn}(70, 20)$ ”, and $a = 0.5$. Three different random noise levels are added to the measurements by referencing each function “`randn(m, n)`” three times and by dividing a by 10 at the end of each time. For the three levels of noise, the coefficients \mathbf{b}_{20} estimated by the least square method (Equation (6.7)) are no longer approximately equal to $[\mathbf{0} \quad \mathbf{L}_{20} \mathbf{L}_k^{-1}]^T$, but they differ of amounts of the order of 10^{-1} , and the *SSE* values computed by Equation (6.11) are of the order of 10, 10^{-1} , and 10^{-3} cm^2 , respectively.

Let us now compute the *F*-value defined by Equation (6.15), for two sets of measurements obtained by considering the undamaged state of the structure under two different sets of loading conditions, and different noises in the measurements. By again repeating the analysis 100 times for each of the three

noise levels, one obtains the three corresponding F -histograms in Figure 6.4, whose means are equal to 1.0092, 0.9765, and 1.0062, respectively. The F -values are now lower than the limit of 2.047, thus recognizing that damage has not happened yet.

The non-dimensional difference of the two means (ADM) in Equation (6.36) is in this case equal to 0.1889. A better convergence of the histograms in Figure 6.5 could be achieved either by increasing the number n of repetitions or, as we will see in the next section, by decreasing the number k of the predictors. Indeed, the most k is significant with respect to n , the best is the convergence between the two histograms.

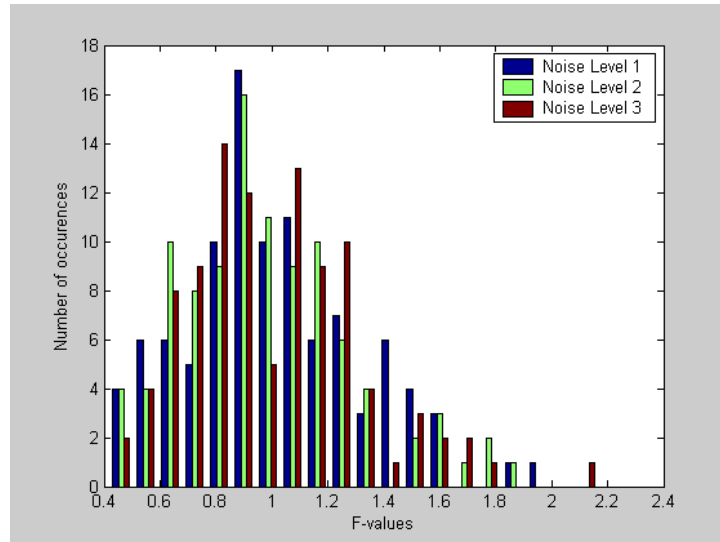


Figure 6.4 F -histograms for the undamaged state of the structure under different load conditions and for three levels of random noises in the measurements. Response at 20 m, and $k = 20$ predictors.

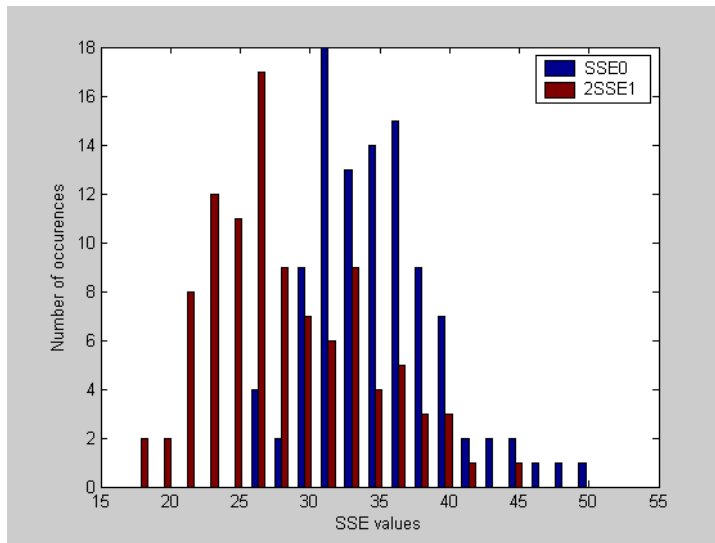


Figure 6.5 SSE-histograms for the undamaged state of the structure under different load conditions and for the highest random noises of level 1 in the measurements. Response at 20 m, and $k = 20$ predictors.

6.3.3 Decrease of the Number of Measurements

From now on, the model is estimated on the basis of only $k = 11$ measurements, instead of the 21 required by the model loads assumption. Namely, only the vertical displacements at the sections of coordinates:

- 1m, 5m and 35m, 39m in the lateral bays,
- 9m, 13m, 17m, 23m, 27m, 31m in the central span,

and the one at mid-span are considered. For $p = 11$, the limit F -value becomes

$$F_{\alpha,p,m-2p} = \text{finv}(1-0.01, 11, 118) = 2.4016 \tag{6.39}$$

The F -histograms obtained by considering two sets of measurements of the undamaged structure under different loads and random noises, are shown in Figure 6.6 for the three levels of noise. The means of the histograms are 0.4324, 0.43, and 0.9496, respectively. The F -values are lower than the new limit, 2.4016, and therefore the undamaged model is still correctly identified.

The histograms of the SSE_0 and $2SSE_1$ in Figure 6.7 are more close to each other than in the previous case and the ADM is equal to 0.0877, because the number of repetitions, $k = 70$, on which the estimates are made is more significant with respect to the number of regressors, $n = 10$.

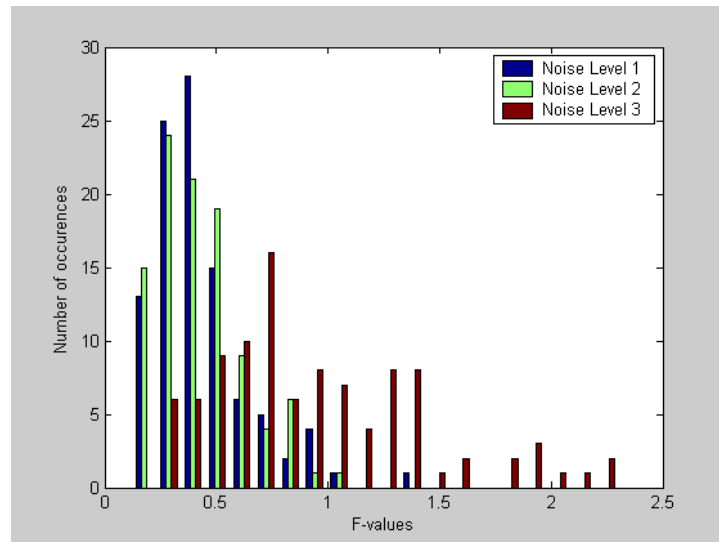


Figure 6.6 F -histograms for the undamaged state of the structure under different load conditions and for three levels of random noises in the measurements. Response at 20 m, and $k = 10$ predictors.

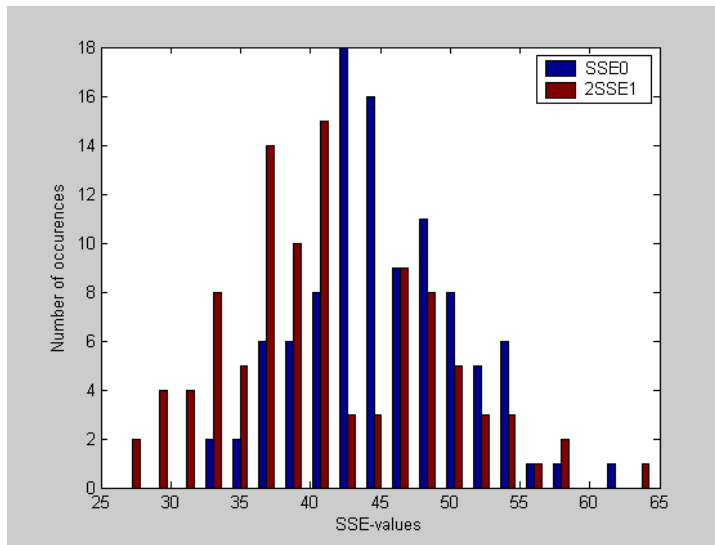


Figure 6.7 SSE-histograms for the undamaged state of the structure under different load conditions and for the highest random noises of level 1 in the measurements. Response at 20 m, and $k = 10$ predictors. $ADM = 0.0877$.

6.3.4 Inferring Damage to the Structure

Figures 6.2, 6.4, and 6.6 refer to the comparison of two undamaged states of the structure and test the ability of the F -method to identify the same model for different loading conditions, noise levels, and a reduced number of measures, respectively. The damage is now introduced by forming an internal plastic hinge in correspondence of the second l.h.s. support ($z = 8\text{m}$), so that the two elements which converge into this node can now rotate of different amounts (Figure 6.8). One degree of freedom (corresponding to this rotation) is therefore added to the structure, whose global stiffness $\mathbf{K}_{\text{glob}}^*$ becomes a 79×79 matrix. Repeating the procedure described in section 6.3.1 for this new stiffness matrix, one finds the

79×70 displacements \mathbf{D}_Q^* due to the 79×70 random live loads \mathbf{F}_Q^* which are applied to the same 20 sections as before and are null where no forces are present. Of the resulting 41×70 vertical displacements, Δ_Q^* , only the 10 corresponding to those considered in the undamaged case are used to build a response surface model. The three levels of random noises are added to these measurements. The linear regression coefficients are then estimated and the values of SSE_2 are computed for the damaged case.

The resulting F -histograms and the SSE comparison for the damaged and undamaged states of the structure are shown in Figure 6.9 and 6.10, respectively, and they are obtained by considering the vertical displacements at mid-span as response variable in the model of Equation (6.32). No information about damage can be achieved from these histograms, because no damage occurs at this location and the method is not sensitive to the small changes inferred by the damage to the vertical displacements at mid-span.

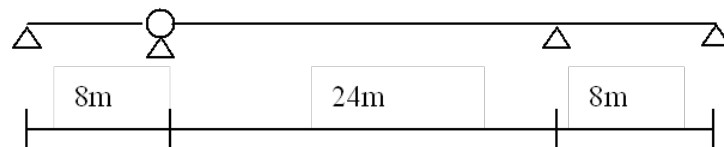


Figure 6.8 Damaged state of the structure.

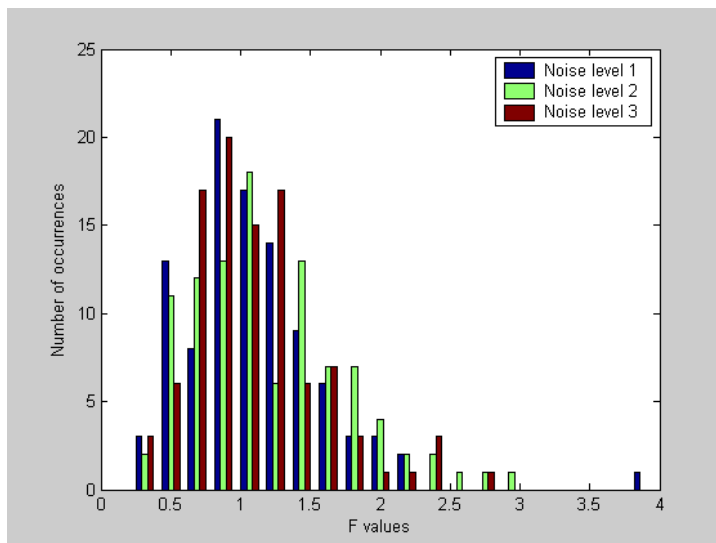


Figure 6.9 *F*-histograms for the damaged and undamaged states of the structure under different load conditions and for three levels of random noises in the measurements.

Response at 20 m, and $k = 10$ predictors.

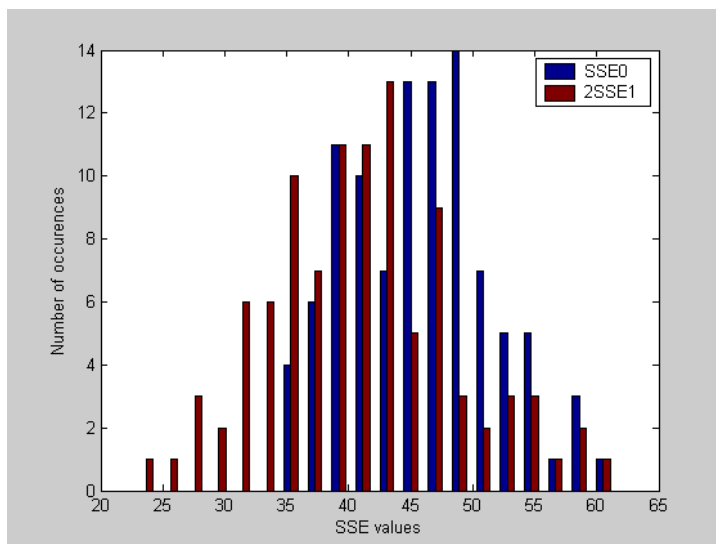


Figure 6.10 SSE-histograms for the damaged and undamaged states of the structure under different load conditions and for the highest random noises of level 1 in the measurements.

Response at 20 m, and $k = 10$ predictors.

Therefore, the analysis must be performed for all the locations in which the measurements are available by permuting the variable considered as response in the model, so that histograms can be built in correspondence of each location. In particular, the histograms shown in Figures 6.11 and 6.12 are computed at the node of coordinate $z = 9$ m, which is the closest to the damage among the nodes considered for measurements. The values of the corresponding damage indices are reported in Table 6.II together with those computed at all the other measurement locations along the beam for comparison. The sensors indices used to identify those locations are defined in Table 6.III.

By simply looking at the pictures, one can observe that the damage is univocally localized only in the case of the lowest noise level 3, for both the F -method (Figure 6.11) and the SSE comparison (Figure 6.12c). As the noise level increases, the results in Table 6.II show that the damage location may vary in a certain range. However, the SSE method is always able to detect the presence of damage, and to correctly localize it into the left hand side of the structure for all the noise levels. Furthermore, the sensor at 9 m is always identified as damaged. The F -method, instead, is not able to detect the presence of damage for the highest noise level 1, and it does not recognize the sensor at 9 m as damaged for noise level 2.

The novelty and the better performance of the SSE -comparison technique with respect to the F -method led the further work to be focused on the first. In particular, the following chapters aim to show the applicability of the method to more practical situations than the one exposed here as first simple theoretical example. To easily understand how the method is applied to the more complex cases of study, a generalization and formalization of the procedure is previously provided in the last section of this Chapter.

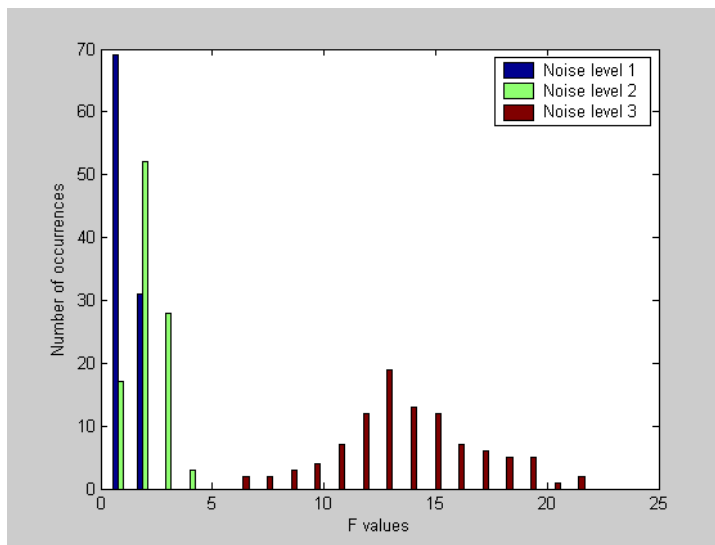
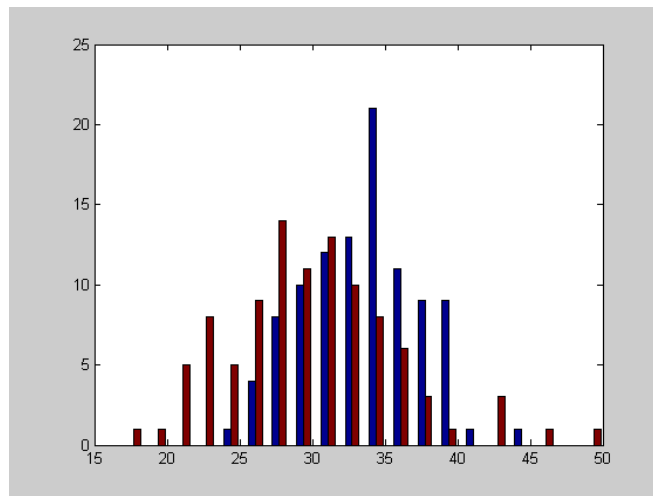


Figure 6.11 *F*-histograms for the damaged and undamaged states of the structure under different load conditions and for three levels of random noises in the measurements. Response at 9 m, and $k = 10$ predictors.



a)

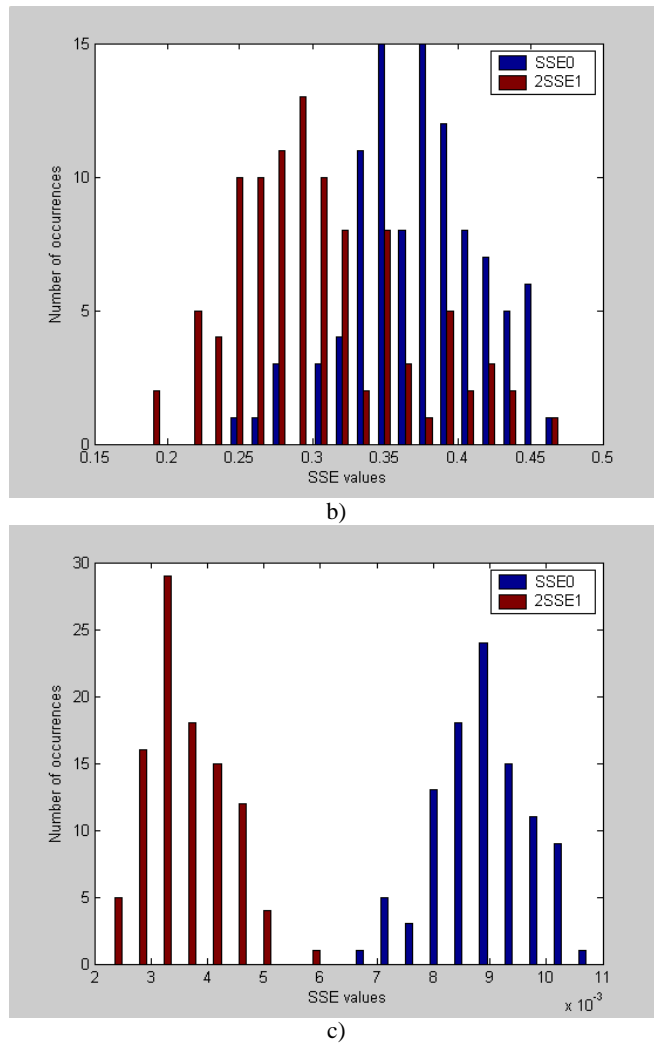


Figure 6.12 SSE-histograms for the damaged and undamaged states of the structure under different load conditions and for the random noises of (a) level 1, (b) level 2, and (c) level 3. Response at 9 m, and $k = 10$ predictors.

TABLE 6.II DAMAGE INDICES AT DIFFERENT LOCATIONS IN INCREASING ORDER.

THE COLUMNS CORRESPOND TO THE THREE LEVELS OF NOISE. FIRST ROW: MEAN VALUES OF THE F-HISTOGRAMS. SECOND ROW: ADM OF THE SSE-HISTOGRAMS. THIRD ROW: REFERENCE VALUES OF THE ADM WHICH CORRESPOND TO THE MAXIMA COMPUTED FROM TWO SETS OF MEASUREMENTS OF THE UNDAMAGED STATE.

| F1 COMPARISON = | F2 COMPARISON = | F3 COMPARISON = |
|-----------------------|-----------------------|-----------------------|
| 0.9341 8.0000 | 0.9729 9.0000 | 0.9561 9.0000 |
| 1.0167 1.0000 | 0.9981 10.0000 | 0.9572 10.0000 |
| 1.0320 9.0000 | 1.0232 8.0000 | 0.9625 8.0000 |
| 1.0523 10.0000 | 1.0573 7.0000 | 0.9754 7.0000 |
| 1.0627 7.0000 | 1.0795 6.0000 | 0.9812 6.0000 |
| 1.0679 6.0000 | 1.1673 5.0000 | 1.1099 11.0000 |
| 1.0922 11.0000 | 1.1984 11.0000 | 1.1469 5.0000 |
| 1.2071 3.0000 | 1.3609 1.0000 | 1.7994 4.0000 |
| 1.3448 2.0000 | 2.1750 3.0000 | 1.9291 1.0000 |
| 1.3892 5.0000 | 3.6065 4.0000 | 7.5973 2.0000 |
| 2.1005 4.0000 | 11.7686 2.0000 | 13.6574 3.0000 |
| ADM1 = | ADM2 = | ADM3 = |
| 0.0621 6.0000 | 0.0570 9.0000 | 0.0541 9.0000 |
| 0.0797 1.0000 | 0.0654 10.0000 | 0.0551 10.0000 |
| 0.0802 7.0000 | 0.0794 6.0000 | 0.0645 4.0000 |
| 0.0837 8.0000 | 0.0809 5.0000 | 0.0753 6.0000 |
| 0.0905 10.0000 | 0.0937 11.0000 | 0.0849 11.0000 |
| 0.0981 9.0000 | 0.0975 1.0000 | 0.0854 7.0000 |
| 0.1035 3.0000 | 0.1001 8.0000 | 0.0854 8.0000 |
| 0.1039 11.0000 | 0.1002 7.0000 | 0.0902 5.0000 |
| 0.1079 2.0000 | 0.1872 3.0000 | 0.1357 1.0000 |
| 0.1433 5.0000 | 0.3265 4.0000 | 0.5646 2.0000 |
| 0.1889 4.0000 | 0.5829 2.0000 | 0.5978 3.0000 |
| ADM1u = 0.0989 | ADM2u = 0.1005 | ADM3u = 0.0900 |

TABLE 6.III SENSOR LOCATIONS.

| | | | | | | | | | | | |
|---------|---|---|---|----|----|----|----|----|----|----|----|
| SENSOR | 1 | 2 | 3 | 4 | 5 | 6 | 7 | 8 | 9 | 10 | 11 |
| z [m] | 1 | 5 | 9 | 13 | 17 | 23 | 27 | 31 | 35 | 39 | 20 |

6.4 Generalization and Formalization of the SSE- Approach

The previous example indicates the SSE approach as a fascinating candidate for damage detection and localization. Indeed, this method meets all the requirements to be implemented in the long-term, continuous structural health monitoring system described in Chapter 3. However, the reliability and the good performance of the algorithm on real structures still needs to be validated. For this purpose, the method must be first theoretically adapted to the practical situations, so that the procedure used to achieve the results presented in the following chapters can be generalized and easily understood for all the considered study cases.

In general, let N_S the number of sensors placed on the monitored structure. The sensors measure the time histories of the quantity of interest (acceleration, strain, etc.) at different locations on the structure, for a given duration T , a given sampling frequency f , and a total number of points $N_P = T f$. Each time history is considered as a set of clusters of experiments by dividing it into N_{set} successive segments of length $n = \gamma N_S$ each, where γ is an assigned positive integer. Therefore, $N_{set} = \text{int}(N_P/n)$. The selection of γ needs to provide a

number of measurements n which is significant with respect to the number of predictors in the model, $k = N_S - 1$.

By ordering the measured time histories in a matrix of size $N_p \times N_S$, and by considering only n rows at the time, one obtains the data for multiple linear regression analysis in Table 6.I, where x_{ij} is the i -th value of the time history segment recorded by sensor j . The multiple linear regression coefficients are estimated by Equation (6.7), and the error sum of squares, which provides an estimate of the variance of the error in the model, can then be computed from Equation (6.11). By repeating for all the N_{set} clusters of n points each contained in the response time histories, one obtains a histogram of SSE -values. By permuting the sensor whose measurements are considered as function of the others (i.e., the response variable), an SSE histogram can be built in correspondence of each sensor location. The described procedure is summarized in the flow-chart of Figure 6.13, and it takes as inputs the response time histories recorded during two different tests on the structure.

If the two tests were performed during different periods of the structure lifetime, the method assumes one of the two as reference case and then plots twice its SSE -histogram together with the one obtained by considering the global set of available measurements. A damage index ADM is then defined as the non-dimensional difference of the means of the histograms (Equation 6.36), and it is used to evaluate if the other test still refers to the same structural condition, or if some modifications occurred during the period of time between the two tests.

The procedure needs to first be applied to the measurements taken from two different tests on the undamaged structure, so that the maximum value of the correspondent non-dimensional mean differences of the SSE -histograms can be

assumed as damage index threshold value, ADM_u . When the values of ADM , computed by considering the current unknown state of the structure together with its initial undamaged state, result to be greater than ADM_u , it means that the model of the structural system has changed. This change can also be localized close to the sensors at whose locations the greatest values of ADM are found.

References for Chapter 6

- Breitung K. and Faravelli L. (1996). "Response Surface Methods and Asymptotic Approximations", Chapter 6 in F. Casciati and J.B. Roberts (eds.), *Mathematical Models for Structural Reliability Analysis*, CRC Press, Boca Raton, USA, 227-285.
- Draper N. and Smith H. (1981). *Applied Regression Analysis*, Wiley, New York.
- Kullaa J. (2004). "Structural Health Monitoring under Variable Environmental or Operational Conditions", *Proceedings of the 2nd European Workshop on Structural Health Monitoring 2004*, 1262-1269.
- Iwasaki A., Todoroki A., and Sugiya T. (2002). "Remote Smart Damage Detection via Internet with Unsupervised Statistical Diagnosis", *IUTAM Symposium on Dynamics of Advanced Materials and Smart Structures*, Japan, 157-166.

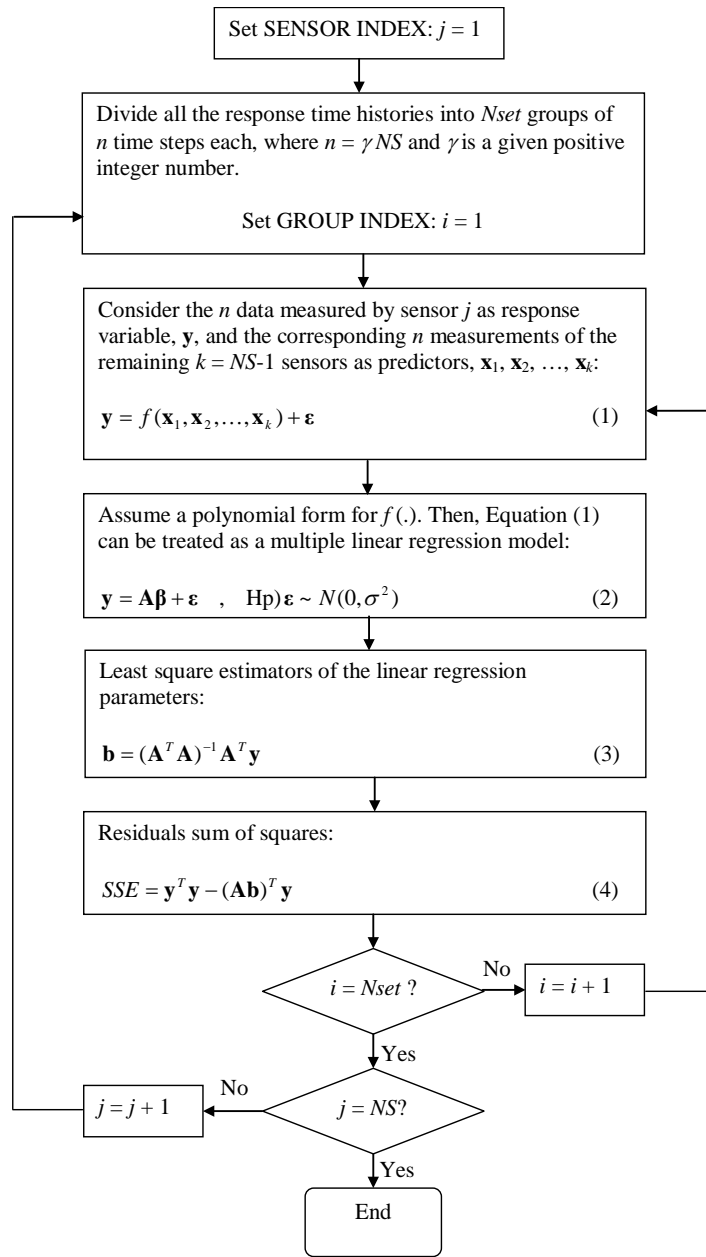


Figure 6.13 Flow chart of the proposed SHM scheme.

Chapter 7

Analytical Studies Using the ASCE SHM Benchmark Problem

In Chapter 6, a new method for damage detection and localization using the SHM-RSM via *SSE*-approach was proposed based on the results from a simple theoretical example, where the true response surface function was a priori known for the baseline case in absence of noise. The applicability of the method to an actual monitoring system needs to be validated by investigating cases of study which are close to reality. Before applying it to the measurements taken from existing structures (Chapters 8 and 9), it is appropriate to evaluate its performance when applied to response time histories which are numerically computed by classical structural dynamics algorithms, from a three-dimensional finite element model of a structure under different dynamic loads. Indeed, when

passing from static to dynamic problems, an acceleration term is added to the equation of motion, which becomes a second-order differential equation. From the solution of this equation, with given initial conditions, the acceleration time histories of the different nodes of the structural model can be computed. The relationship between the acceleration of one node of the structure and those computed for the other nodes, is not known and it may not be linear anymore. However, it can still be approximated by a first-order polynomial in a relatively small region of the observed variables. No attempt is made either to find the exact response surface function, or to approximate it with the most reliable function, since, as already mentioned in Chapter 6, the experimental design strategies are not allowed within a continuous monitoring system process. Instead, the goal is to show that, also in a dynamic context, the proposed SHM-RSM is able to extract a damage sensitive feature from the comparison of *SSE*-statistical distributions obtained by fitting first-order polynomials to the response surface variables.

For this purpose, the method is applied to the normalized relative acceleration time histories obtained from the data generated by a computer program, which was developed by the American Society of Civil Engineers (ASCE) Structural Health Monitoring (SHM) task group to provide a common investigation tool for this research field. The computer program calculates the dynamic response to different excitation loads, in terms of acceleration time histories, of the three-dimensional analytical model of an existing reference structure. The structure is a two-by-two bays, four-story, braced steel frame, with slabs on each floor. Different baseline configurations of the analytical model are considered, and different excitations are applied. In particular, the ambient excitation due to the wind load and the force applied by a shaker are

modelled. Also different damage scenarios are possible, so that one can evaluate the performance of the diagnosis method relatively to the damage intensity (Level 3). The damage is represented by the complete or partial removal of some braces, thus varying the stiffness of the structure. We would like to show that the SHM-RSM approach not only detects the structural change (Level 1), but it also locates where the braces have been removed (Level 2). The results of the method are presented in the following, in view of its application to experimental measurements.

7.1 The ASCE SHM Benchmark Statement

As previously discussed in Chapters 3 and 4, the development of algorithms able to process the vast wealth of sensors information and to provide useful and simple measures of the current health state of a structure is a crucial problem involving the worldwide ongoing research activities. The coordination of these activities toward a common task is made difficult by the fact that the various studies apply different methods to different structures, thus preventing from the possibility of a side-by-side comparison. A benchmark study, where participants apply a number of monitoring techniques to a common structure with common objectives, was therefore needed to provide a platform for consistent evaluation of the proposed SHM methods.

At the 1996 International Workshop on Structural Control [Chen, 1996], a plan was formed to create task groups to study the problem of structural health monitoring. Three task groups, one per region (Europe, Asia, USA), were to be formed. The USA task group solidified in 1999 jointly under the auspices of the

International Association for Structural Control (IASC) and the Dynamics committee of the ASCE Engineering Mechanics. The IASC-ASCE SHM Task Group has proposed a series of benchmark Structural Health Monitoring studies, beginning with a relatively simple problem and proceeding on to more realistic and more challenging cases of study, to compare and contrast the efficacy of various techniques. These problems focus on both analytical and experimental studies of an existing test structure. This work focuses on the first phase of the benchmark studies, which are based on the simulation of the test structure that forms the cornerstone of all the benchmark problems. Starting with simulated data allows to better understand the sensitivities of the method to various aspects of the problem, such as difference between the identification model and the true model, incomplete sensor information, and the presence of noise in measurement signals. The use of simulated data from the analytical structural model based on an existing structure allows for future comparisons with data taken on the actual structure.

The benchmark problem is based on the test structure shown in Figure 7.1a and located in the Earthquake Engineering Research Laboratory at the University of British Columbia (UBC). The structure is a 2-by-2 bays, 4-story, rectangular steel frame built at approximately 1:3 scale. The model is 3.6 m tall and 2.5 m wide. There is one floor slab per bay per floor: four 800 kg slabs at the first level, four 600 kg slabs at each of the second and third levels, and four 400 kg slabs at the fourth level. Details of the structural members properties (beams, columns and braces) are given in [Johnson et al., 2000].

Two finite element models based on this structure were developed to generate the simulated data. The first is a 12DOF shear-building model that constrains all motion except two horizontal translations and one rotation per

floor. The second is a 120DOF model that only requires floor nodes to have the same horizontal translation and in-plane rotation. The horizontal slab panels are assumed to contribute only towards the in-plane stiffness making the floor behave as rigid with respect to in-plane motions only. The remaining out-of-plane degrees of freedom (namely, vertical motion and pitching/rolling of the floor) are active. This more complex 120DOF model was constructed to include model error effects. Indeed, most structures are not as simple as engineers often model them, which leads to the presence of model error. The columns and floor beams are modelled as Euler-Bernoulli beams in both finite element models. The braces are bars with no bending stiffness. A diagram of the analytical model is shown in Figure 7.1b.

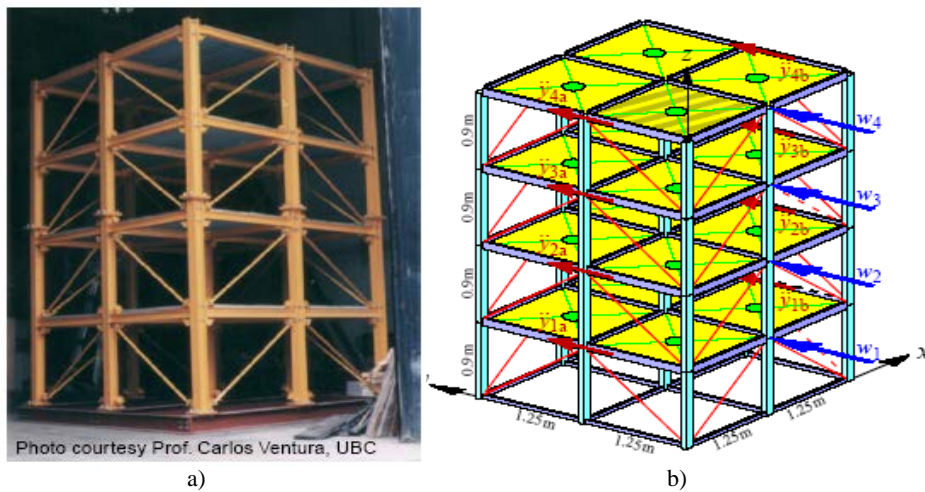


Figure 7.1 The ASCE benchmark structural system: (a) real structure at UBC; and (b) analytical model. From [Johnson et al., 2000].

The finite element models (either the 12 or 120 DOF models) represent the structural system in terms of active degrees of freedom \mathbf{q} , related to the physical degrees of freedom \mathbf{x} by

$$\mathbf{x} = \mathbf{T}\mathbf{q} \quad (7.1)$$

where \mathbf{T} is the transformation matrix for the consideration of rigid-floor effect. The equation of motion is

$$\mathbf{M}\ddot{\mathbf{q}} + \mathbf{C}_d\dot{\mathbf{q}} + \mathbf{K}\mathbf{q} = \mathbf{T}^T\mathbf{f} \quad (7.2)$$

where \mathbf{M} , \mathbf{C}_d and \mathbf{K} are the mass, damping and stiffness matrices, respectively; \mathbf{f} is a vector of forces applied to the physical degrees of freedom. Both ambient and forced excitations are considered by applying the force at each floor in the weak (y -) direction as wind loading in Cases 1 and 2, and by assuming that a shaker on the roof at the top of the centre column excites the structure in a direction $\pm(\hat{\mathbf{i}} - \hat{\mathbf{j}})$, where $\hat{\mathbf{i}}$ and $\hat{\mathbf{j}}$ are unit vectors in the x - and y -directions, respectively, in Cases 3 to 5. Although the structure is excited in two directions, only the y -direction is to be analyzed for Case 3. Cases 4 and 5 introduce asymmetry by replacing one of the 400 kg floor slabs on the roof (the one with hatched shading in Figure 7.1b) with a 550 kg slab, and are analyzed with 3-D motion of the floors. Cases 1, 3, and 4 refer to the 12DOF data generation model, while cases 2 and 5 include the model error.

The forces are modelled as filtered Gaussian white noise. The Gaussian white noise processes are passed through a 6th order low-pass Butterworth filter

with a 100 Hz cut-off. The data generation uses a discrete-time integration at 1kHz, and provides the sensor measurements at 1kHz.

Sixteen accelerometers, two in the x -direction and two in the y -direction of each floor, return noisy sensor measurements

$$\ddot{\mathbf{y}} = \mathbf{C}\mathbf{q} + \mathbf{D}\mathbf{f} + \mathbf{v} \quad (7.3)$$

where \mathbf{v} is a sensor noise vector, whose elements are Gaussian pulse processes with root mean square (rms) equal to 10% of the rms of the roof acceleration.

Damage to the structure can be simulated by removing the stiffness of various elements from the finite element models. Six damage patterns are defined for the structure: (i) all of the first floor braces are removed; (ii) all of the first and third floor braces removed; (iii) one brace is removed in first story (the one drawn as dashed line in Figure 7.1b); (iv) one brace is removed in each of the first and third stories (also drawn as dashed line in Figure 7.1b); (v) as the previous damage pattern but with the floor beam from (2.5m, 0, 0.9m) to (2.5m, 1.25m, 0.9m) partially unscrewed from the column at (2.5m, 0, 0.9m) (consequently, the beam-column connection there can only transmit forces and cannot sustain any bending moments); (vi) the area of one brace in first floor is reduced to 2/3.

7.2 Application of the Method

To compute the dynamic response of the analytical model of the benchmark structure, a data generation program called “datagen.m” was downloaded from the ASCE SHM Task Group web site (at <http://wusceel.cive.wustl.edu/asce.shm/>). This code presents the graphical user interface (GUI) in Figure 2, and allows the user to select which undamaged baseline case to run and which damage pattern to use among those described in the previous section, or to create new damage patterns. The fast Nigham-Jennings algorithm, which makes use of the MATLAB SimuLink toolbox, was selected for the responses calculation. Given a constant initial excitation level of 150 kN, different seed numbers were used for the force generation in the undamaged cases, to obtain couples of reference tests from which the threshold value ADM_u of the damage index can be estimated. The other user-defined parameters shown in Figure 7.2 were set as their default values. In particular, a noise level of 10 is included in the analyses, the sampling time interval is 0.001 s, and the total duration is 40 s.

For each simulated case, the resulting acceleration time histories of length $N_p = 40001$ points were computed at different measurement points and collected as column vectors of a measurements matrix, \mathbf{acc} , of size $N_p \times N_C$, where $N_C = 16$ is the total number of measurement points in the x and y directions. The sensor locations in Figure 9.3 are denoted by the column number of the corresponding measurements in matrix \mathbf{acc} . When performing the analyses in the weak y -direction, only the even column indices of \mathbf{acc} are considered, while the odd column indices corresponding to the measurements

along the x -direction are used only in the three-dimensional analyses of Cases 4 and 5.

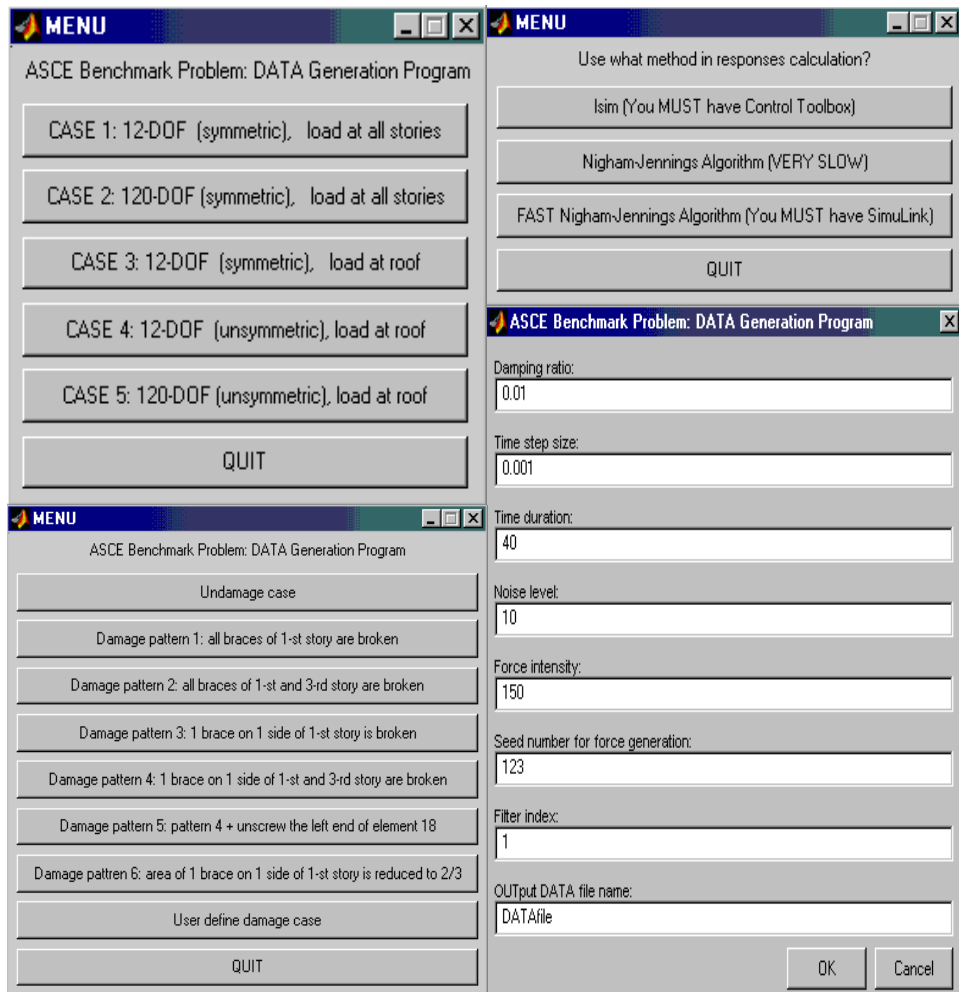


Figure 7.2 Graphic User Interface (GUI) of datagen.m (from <http://wusceel.cive.wustl.edu/asce.shm/>).

application is useful to evaluate its efficacy when compared with the other SHM techniques whose results for the benchmark problem are reported in literature.

The data obtained from “datagen.m” were used to compute the relative accelerations of one floor with respect to the one immediately below. The resulting time histories needed to be previously normalized by subtracting from each signal its mean, and by dividing it by its root mean square.

The normalized relative acceleration time histories are used as inputs to the method described in section 6.3 and summarized in Figure 6.13. In particular, for each baseline configuration of the undamaged structure, the measurements from each damage pattern were regressed together with those of the reference undamaged case, and the resulting global *SSE*-histogram was compared with twice the one obtained by considering the undamaged case alone. For the benchmark case, the parameter γ was set equal to 40; therefore, the time histories were considered as 125 clusters of $n = \gamma N_s = 320$ points each.

By permuting the response variable so that all the sensors are considered as functions of the others, a *SSE*-histograms comparison is obtained at every location. The damage index, *ADM*, is defined as the non-dimensional difference of the means of the two histograms. Since the input data were already made non-dimensional by dividing them by their rms, in this case it is not necessary to divide the means difference by the global one. The values of *ADM* are compared to the limit value, *ADM_u*, of the considered baseline configuration. This limit is obtained by applying the method to two sets of measurements of the undamaged structure under different loads (simulated by assigning different seed numbers), and by computing the corresponding maximum value of the non-dimensional means difference of the *SSE*-histograms.

7.3 Results for the Benchmark Structure

The results for the cases 1, 2, and 3 (see Figure 7.2) of the benchmark problem are given in Table 7.I, 7.II, and 7.III, respectively, for the damage patterns 1 and 2. Damage pattern 1 is correctly identified in all cases by detecting the damage at the sensors on the first floor only. The histograms comparisons at each sensor location for case 2 and damage patterns 1 and 2 are shown in Figures 7.4 and 7.5, respectively. From these pictures, it is evident that a significant shift between the histograms occurs at the sensors located on the floors where the damage is introduced (floor 1 for damage pattern 1; floors 1 and 3 for damage pattern 2). In this case, all the other regions do not seem to be affected by the damage, since the histograms stay close to each other. However, for case 1 and damage pattern 2 (see Table 7.I) a small shift of the histograms is observed also for the second floor, whose response is influenced by the removal of the braces on the third floor. This effect becomes more significant for case 3 and damage pattern 2 (see Table 7.III), where the shifts at the sensors on the second floor are larger than the ones at the sensors on the third floor. Therefore, in this case the damage could have been introduced either at the second or at the third floor. But this ambiguity also depends on the inter-story position of the bracing system, whose edges correspond to both the second and third floors.

Cases 4 and 5 and damage patterns 4, 5, and 6 introduce an asymmetry in the structure. This leads to high values of SSE , whose histograms become very narrow, i.e., with a very small variance. The change in the structural behaviour is due more to the new asymmetry than to the specific damage inferred to the structure. The ADM values are all far beyond their limit values, so that in these cases the presence of damage is detected, but it cannot be located.

As an example, the results for case 3, damage patterns 3 and 4 are given in the first row of Table 7.IV. Both damage cases give similar results, and the maxima *ADM* correspond to the first floor. To distinguish if damage occurs at the right or left hand side of the structure, one could separate the sensors on each side, and perform the analyses only on four sensors (second row of Table 7.IV). The damage is located on the side where the maxima *ADM* values are observed. The high values obtained may be due to the fact that we are comparing an asymmetric damaged condition to a symmetric baseline configuration. To distinguish damage pattern 4 from 3 we could compare them with each other (last row of Table 7.IV), thus recognizing a damage in 10.

However, this procedure is not reliable, and what we should be able to do is to compare the sensor at the damage location with the adjacent ones on the same floor. The lack of a sufficient number of sensors prevents from locating damages of small entities. We will show in the next section how it is instead possible to locate the lack of a single bracing system by a more distributed sensors placement.

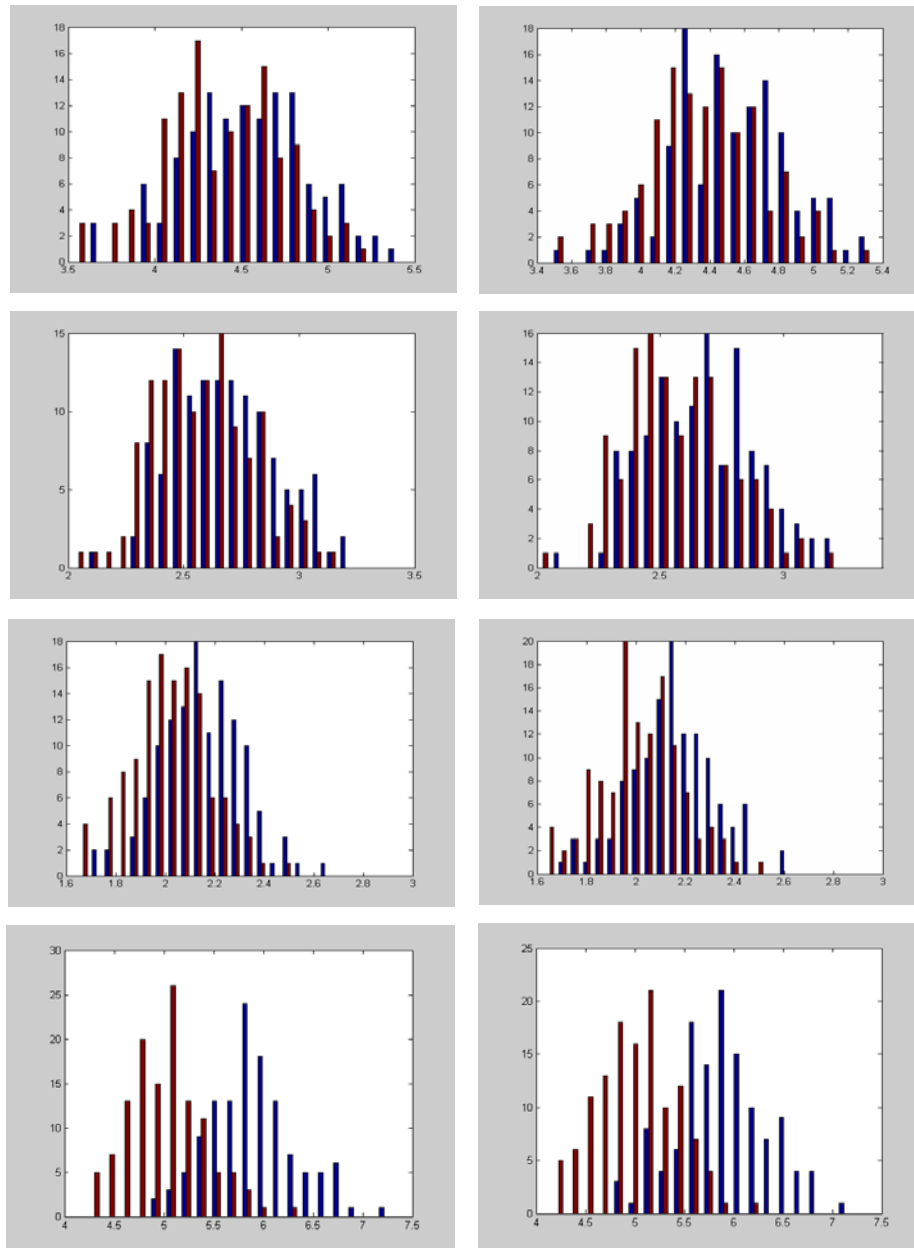


Figure 7-5: Histograms comparison at different sensor locations for CASE 2, damage pattern 1.

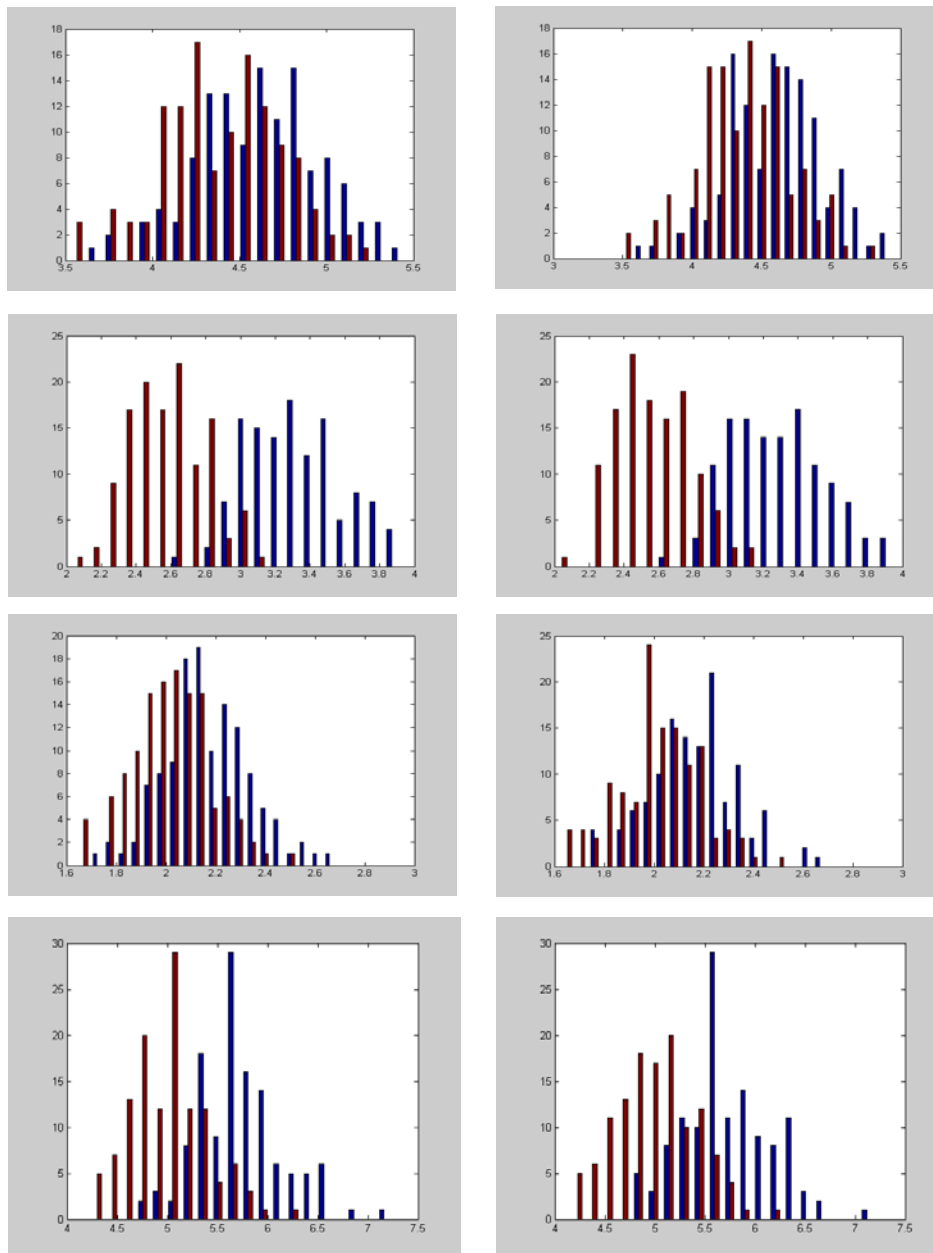


Figure 7-4: Histograms comparison at different sensor locations for CASE 2, damage pattern 2.

TABLE 7.I RESULTS FOR CASE 1 AND DAMAGE PATTERNS 1 AND 2.(THE DASHED LINE CORRESPONDS TO $ADMu = 0.2858$).

| CASE1, DAMAGE PATTERN 1 | | CASE1, DAMAGE PATTERN 2 | |
|-------------------------|----------|-------------------------|-----------|
| abs(ADM) | Sensor | abs(ADM) | Sensor |
| 0.0305 | 10 | 0.0735 | 14 |
| 0.0396 | 12 | 0.0794 | 16 |
| 0.0471 | 6 | 0.4782 | 6 |
| 0.0593 | 8 | 0.4959 | 8 |
| 0.0752 | 16 | 0.8333 | 10 |
| 0.0828 | 14 | 0.8496 | 12 |
| 1.0757 | 2 | 1.6321 | 2 |
| 1.1150 | 4 | 1.6671 | 4 |

TABLE 7.II RESULTS FOR CASE 2 AND DAMAGE PATTERNS 1 AND 2.(THE DASHED LINE CORRESPONDS TO $ADMu = 0.1958$).

| CASE2, DAMAGE PATTERN 1 | | CASE2, DAMAGE PATTERN 2 | |
|-------------------------|----------|-------------------------|-----------|
| abs(ADM) | Sensors | abs(ADM) | Sensors |
| 0.1040 | 12 | 0.1465 | 6 |
| 0.1056 | 10 | 0.1492 | 8 |
| 0.1326 | 6 | 0.2244 | 16 |
| 0.1344 | 8 | 0.2357 | 14 |
| 0.1481 | 16 | 0.7142 | 2 |
| 0.1537 | 14 | 0.7151 | 4 |
| 0.8721 | 2 | 0.7298 | 10 |
| 0.8887 | 4 | 0.7339 | 12 |

TABLE 7.III RESULTS FOR CASE 3 AND DAMAGE PATTERNS 1 AND 2.
 (THE DASHED LINE CORRESPONDS TO $ADMu = 0.5263$ IN THE y -DIRECTION,
 AND TO $ADMu = 0.31$ IN THE x -DIRECTION).

| CASE3, DAMAGE PATTERN 1 | | CASE3, DAMAGE PATTERN 2 | |
|-------------------------|----------|-------------------------|-----------|
| y-direction | | y-direction | |
| Abs(meandifference) | Sensors | Abs(meandifference) | Sensors |
| 0.0041 | 14 | 0.5813 | 14 |
| 0.0118 | 16 | 0.6023 | 16 |
| 0.0353 | 8 | 1.3998 | 12 |
| 0.0477 | 6 | 1.4100 | 10 |
| 0.0724 | 12 | 6.6094 | 8 |
| 0.0816 | 10 | 6.6256 | 6 |
| 1.2044 | 4 | 10.8644 | 4 |
| 1.2091 | 2 | 10.8765 | 2 |
| x-direction | | x-direction | |
| Abs(meandifference) | Sensors | Abs(meandifference) | Sensors |
| 0.0116 | 15 | 0.1126 | 13 |
| 0.0148 | 13 | 0.1172 | 11 |
| 0.0567 | 5 | 0.1221 | 15 |
| 0.0597 | 7 | 0.1258 | 9 |
| 0.1302 | 11 | 0.7058 | 5 |
| 0.1307 | 9 | 0.7070 | 7 |
| 0.4573 | 1 | 2.1328 | 1 |
| 0.4704 | 3 | 2.1370 | 3 |

TABLE 7.IV RESULTS FOR CASE 1 AND DAMAGE PATTERNS 3 AND 4(THE DASHED LINE CORRESPONDS TO $ADMu = 0.2858$).

| CASE1, DAMAGE PATTERN 3 | | CASE1, DAMAGE PATTERN 4 | |
|---|----------------|-------------------------|----------------|
| abs(<i>ADM</i>) | Sensor | abs(<i>ADM</i>) | Sensor |
| 1.9526 | 8 | 2.0870 | 8 |
| 2.3732 | 6 | 2.4996 | 6 |
| 2.9178 | 12 | 3.2647 | 12 |
| 3.3798 | 16 | 3.5787 | 16 |
| 3.5577 | 10 | 4.0148 | 10 |
| 3.9898 | 14 | 4.1822 | 14 |
| 4.6691 | 2 | 4.9058 | 2 |
| 4.8240 | 4 | 5.2460 | 4 |
| CASE1, Damage Pattern 3 | | CASE1, Damage Pattern 4 | |
| abs(<i>ADM</i>) | Sensor | abs(<i>ADM</i>) | Sensor |
| l.h.s. | r.h.s. | l.h.s. | r.h.s. |
| 0.9046 2.0000 | 0.7004 1.0000 | 0.8109 2.0000 | 0.4762 1.0000 |
| 1.4346 3.0000 | 1.8637 2.0000 | 1.7564 3.0000 | 1.8975 2.0000 |
| 2.1052 1.0000 | 3.4261 3.0000 | 4.0205 1.0000 | 3.5233 3.0000 |
| 4.1232 4.0000 | 13.6654 4.0000 | 4.7772 4.0000 | 13.6994 4.0000 |
| CASE1, Comparison Damage Pattern 4 and Damage Pattern 3 | | | |
| abs(<i>ADM</i>) | | Sensor | |
| 0.0103 2.0000 | | | |
| 0.0182 6.0000 | | | |
| 0.0371 8.0000 | | | |
| 0.1356 16.0000 | | | |
| 0.1498 12.0000 | | | |
| 0.1599 14.0000 | | | |
| 0.2232 4.0000 | | | |
| 0.2372 10.0000 | | | |

As a final remark, it must be reported that we applied the Lyapunov exponent approach to the ASCE benchmark cases 1, 2 and 3, focusing on the damage paths 1 and 6.

For case 1, when all the sensors are considered in the analysis a dimension larger than 10 (10.578267) is obtained. By contrast, when only the sensors in the direction of the excitation are retained, the dimension goes down to 2 (2.281453).

This testifies the quite ineffective role of the transversal sensors in this study. In other words, there are several sensors, but only a few of them provide useful information to detect the kind of damage that was introduced.

It should be also noted that to use a window of data without the initial points is more accurate in detecting damage. The damage detection is pursued by observing the decreasing value of the Lyapunov dimension (2.346864 for the undamaged case and 2.282358, and 2.284072 for damages paths 1 and 6 in case 1). But the few sensors allow one to detect just one positive Lyapunov exponent, which in this case increases with damage (from $4.940176e-02$ to $5.472561e-02$ and $5.050406e-02$ in the three situations, respectively).

This confirms that more exponents must be compared, but in this case only one of them is positive. It is hard however to distinguish damaged and undamaged conditions from the estimated oscillations.

We move now to case 2, with the following results: the Lyapunov exponent is equal to 2.378224 in the undamaged state, to 2.208108 and 2.310382 for damage paths 1 and 6, respectively. Here the only positive Lyapunov exponent decreases from $5.619954e-02$ to $4.427956e-02$ and $5.521079e-02$, respectively.

These results authorize one to expect easy damage detection in case 1, while case 6 cannot be distinguished from the undamaged case.

The results for case 3 when using all the 16 sensors give a Lyapunov dimension of 7.065286, while when considering only 8 of them the dimension becomes 2.237522 in the undamaged case and decreases to 2.165715 and 2.146255 for damage paths 1 and 6, respectively.

Here in case 3, the only positive Lyapunov exponent correctly decrease from the undamaged case value $4.846539e-02$ to $4.164272e-02$ and $4.196441e-02$, respectively.

References for Chapter 7

- Beck J.L., Yuen K-V. and Au S-K. (2002) “Probabilistic Damage Detection using Markov Chain Simulation with Application to a Benchmark Problem”, F. Casciati (ed.), *Proc. 3rd World Conference on Structural Control*, Vol. 2, John Wiley & Sons, Chichester, 1065-1070
- Chen, J.C., ed. (1996). *Proceedings of the Second International Workshop on Structural Control: Next Generation of Intelligent Structures*, Hong Kong, December 18–21, 1996. Available on the web pages of the *US Panel on Structural Control Research*:
http://cwis.usc.edu/dept/civil_eng/structural/welcome.html.
- Johnson E. A., Lam H. F., Katafygiotis L. S, and Beck J. L. (2000). “A benchmark problem for structural health monitoring and damage detection”, *ASCE 14th Engineering Mechanics Conference*, Austin, Texas.

Chapter 8

Experimental Analyses

The experimental data were obtained from two structures at the JRC-ELSA laboratory in Ispra: the “BABYFRAME” and the “Palazzo Geraci façade” specimens. The latter one is a continuous structure of nonlinear behaviour, exposed to environmental conditions. Hence, the complexity of the problem requires that it must be treated separately, in the next Chapter. To provide a first evaluation of the performance of the proposed damage detection method when applied to data recorded from real structures, the “BABYFRAME” specimen was instead selected for its simplicity. It is a steel frame with three reinforced concrete floors, which was built in a controlled laboratory environment, at scale 2/3 of a real building. The damage is in this case represented by the removal of two braces at the first floor.

Since in most practical applications one cannot infer damage to a structure, an inverse procedure was adopted to perform the experimental analyses. Assuming that the structure in its present state is damaged, the undamaged situation is restored by adding stiffness elements or by filling the cracks with mortar (in Chapter 9). The data recorded before and after the strengthening operation are then statistically compared to detect and locate the structural changes.

8.1 The JRC-ELSA Laboratory

The ELSA (European Laboratory for Structural Assessment) of the European Union Joint Research Centre (JRC) in Ispra (north of Italy), aims to the definition of precise methodologies and procedures for structural health monitoring and retrofitting/repair techniques. Particular attention is paid to seismic prevention and protection. For this purpose, a reaction wall was built to perform pseudo-dynamic tests on real scale structures. The reaction wall is 16 m high and 21 m wide, so that a four or five-story real scale building, or multiple small buildings can be tested.

The activities carried out at the laboratory cover different topic areas, among which it is worth mentioning the assessment and retrofit of reinforced concrete frames, the seismic evaluation of masonry structures, the seismic protection of structures by means of isolators and viscous-elastic dampers (passive control), and the active control of structures in the civil engineering applications.

The introduction in the code of new construction techniques which meet the seismic requirements of a particular area, and the conservation of the cultural

heritage are of main concern in Europe. Specimens of historical monuments are therefore assessed at ELSA, and innovative retrofit techniques are studied for their seismic protection. The Palazzo Geraci façade, which will be analyzed in Chapter 9, was tested with a base isolator made of eight radial C-steel elements between two octagonal plates of support. The study of the Sao Vicente de Fora monastery cloister (Lisbon), within the project COSISMO, showed the good deformability of arch-column systems under seismic loading, and the effectiveness of placing pre-stressed bars above the arches is currently under investigation. The recent retrofits of the San Giorgio in Trignano bell tower and of the lateral tympani of the upper San Francesco di Assisi Basilica, which represent the first worldwide applications of innovative anti-seismic devices based on shape memory alloys, were performed following the excellent results obtained at the ELSA laboratory, within the project ISTECH (Innovative Stability Techniques for the European Cultural Heritage). A shape memory alloy, in its austenite form, presents the advantages of a super-elastic stress-strain relationship, which is characterized by a wide hysteretic cycle (high dissipation of energy) within two plateaux of loading-unloading (constant stress at increasing strain), and small residual deformations. Comparative analyses were carried out by testing also fibre composite reinforcements. This latter retrofit technique decreases the shear collapse mechanisms and is not expensive, but it is not always applicable to monumental structures because of its anti-elasticity.

8.2 The “Babyframe” Specimen

The “BABYFRAME” specimen is a three-story steel frame with reinforced concrete slabs on each floor (Figure 8.1). The scale is $2/3$ of a real structure. The geometric features of the specimen are given in Figure 8.2. The frame has two longitudinal bays of 4 m each (in the X direction) by one transversal bay of 2.5 m (in the Y direction). The height of the each floor is 2 m. The profiles of the columns are HEB140 and those of the longitudinal and transversal beams are IPE180; all of them are made of standard steel Fe360 and welded. The details of the welded beam-column joints are shown in Figure 8.3. The reinforced concrete slabs were poured on a corrugated steel sheet, which was clamped to the beams by nails, as shown in Figure 8.4. The undulations of the steel sheet are oriented along the transversal direction. The structure was built within the ELSA laboratory and rigidly clamped to its strong floor.

The “BABYFRAME” was used for several studies, in different topic areas. For example, passive and semi-active control devices were recently applied to the structure, and their performances under seismic excitation were evaluated and compared. The devices were designed specifically for this structure, which had been previously dynamically characterized by tests with the hammer and modal analyses. The structure was strengthened by steel braces on the transversal sides, and it underwent several pseudo-dynamic tests, with and without the control devices. The braces and the devices prevented the structure from being damaged. However, after the tests the damaged braces were removed, and no braces are currently present on the structure.



Figure 8.1 BABYFRAME.

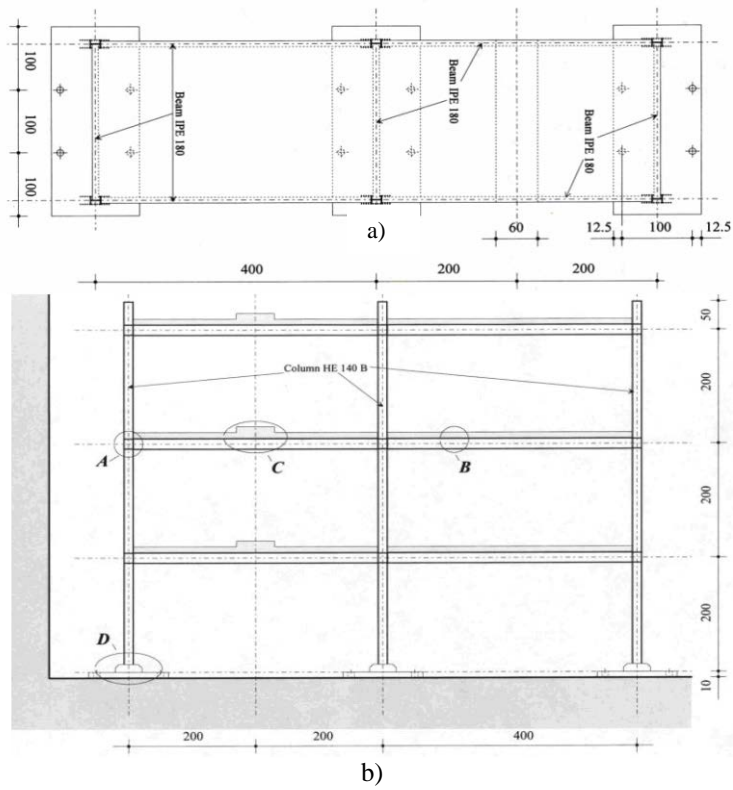


Figure 8.2 (a) Plant view and (b) Elevation of the BABYFRAME specimen.

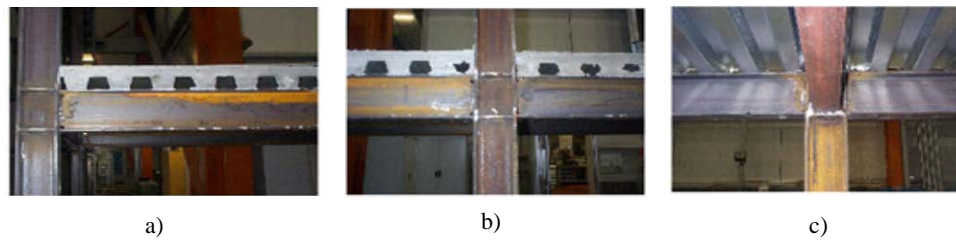


Figure 8.3 Details of the welded beam-column connections. (a) Exterior joint. (b) Interior joint. (c) Internal view of an exterior joint.

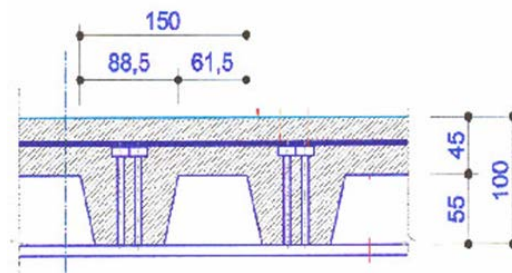


Figure 8.4 Cross-section of the reinforced concrete slab on the beam flange

8.3 The Test Setup

The test was performed by placing seventeen accelerometers on the structure, and by measuring their response while an electro-dynamic shaker, mounted on the third floor in eccentric position, was providing a random excitation. An Analogue Device ADXL05EM-1 with a sensitivity of $20 \text{ m/s}^2/\text{V}$ was used to measure the force of the shaker. The accelerometers were ten Schaevitz S05-E001 with a sensitivity of $2 \text{ m/s}^2/\text{V}$, and seven Crossbow CXL01LF1 with a sensitivity of $5 \text{ m/s}^2/\text{V}$. The position of the accelerometers and the shaker are shown in Figure 8.5.

The most of the accelerometers (nine) were placed on the first floor of the structure, so that at least the measurement of the acceleration in the longitudinal X -direction was taken at each beam-column joint. In particular, all the accelerometers Crossbow of higher sensitivity were placed here, together with two Schaevitz in node 7 (one for each horizontal direction). The upper two floors were instrumented with four Schaevitz each. Each couple of sensors was places at the opposite edges of the building with respect to the other, and it measured the acceleration in the X and Y direction, respectively.

The shaker has a mass of 30 kg and was mounted at a position of coordinates (6.575, 2.275, 6) m. The signal given to the shaker was a random signal with a frequency range from 1 to 80 Hz. Each test has 12 excitation signals with a time distance of 20 s between them. The excitation was applied in the $-X$ (longitudinal) direction, where the negative sign is assigned to the accelerations in the same direction. A technical description of the shaker is given in Figure 8.6.

The signals were collected at a PC through a TEAC GX-1 front end with 16 channels with an expansion unit, which has 16 channels. The sampling frequency was 200 Hz and a filter of 80 Hz was used in each channel.

A bracing system was then mounted at the first floor in order to change the structure's stiffness (Figure 8.7) and the same test was performed again.

Figure 8.8 provides the records of the shaker time histories (along the X axis, i.e., longitudinal) and the records at the accelerometer 3, during the unbraced and braced tests.

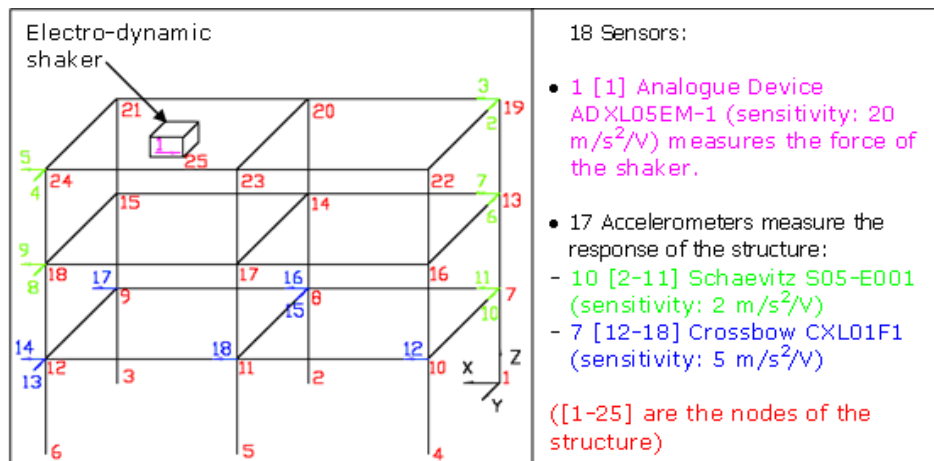
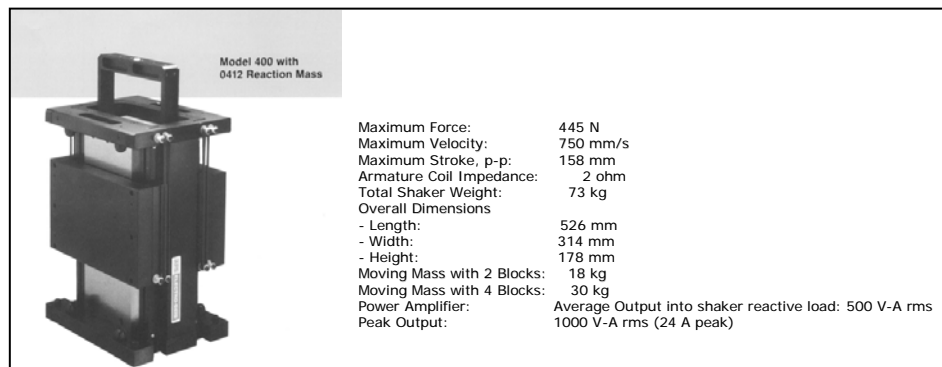


Figure 8.5 Sensors locations and types.



a)



b)

Figure 8.6 (a) Shaker installed on the top of the structure. (b) Technical description of the electro-dynamic shaker used as forced excitation.

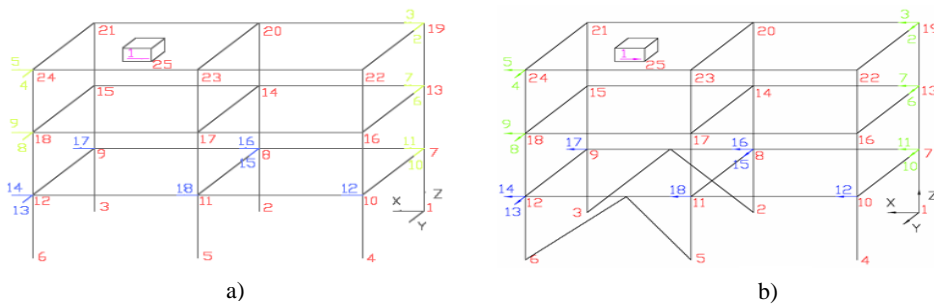


Figure 8.7 (a) Damaged state and (b) undamaged state of the structure. Note that the sensors located close to the damage are the accelerometers 17, 14, 16, and 18.

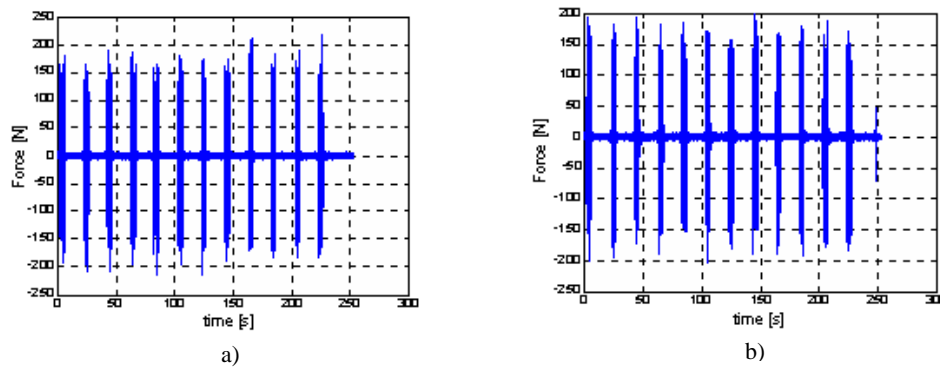


Figure 8.8 Force-time histories measured by sensor 1 during (a) the damaged and (b) the undamaged tests.

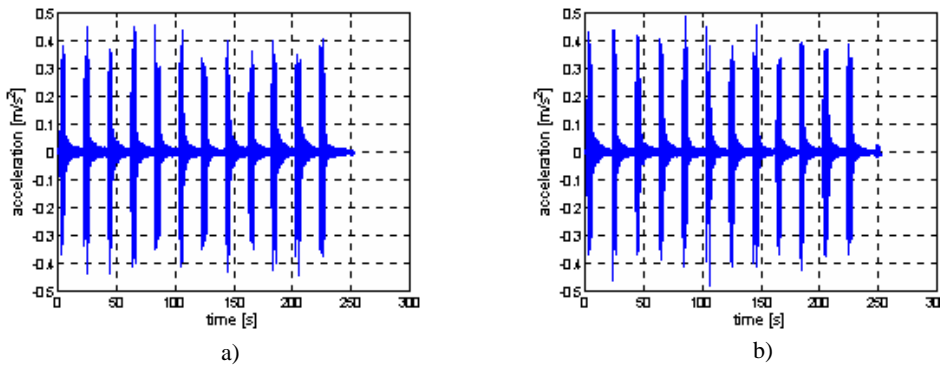


Figure 8.9 Acceleration-time histories measured by sensor 3 during (a) the damaged and (b) the undamaged tests.

8.4 Results

The data collected during this laboratory test are the same ones that were used for the exemplifications of Chapters 2 and 5. Thence, for the data sets collected in the damaged and undamaged cases, one already knows that the presence of damage can be detected by using any of the measures introduced in Chapter 5, i.e., entropy, Kolmogorov entropy, Lyapunov exponent spectrum and Lyapunov dimension (see Figures 5.4 and 5.5 and Table 5.I). The SHM-RSM method is now applied to the same data to verify that not only it can detect the damage, but it is also able to correctly localize it.

We recall that the time histories collected from the damaged and undamaged states of the structure contain 50479 points each. Before the damage detection method can be applied to the available measurements, the processes of data filtering, data cleansing and data fusion described in Chapter 3 need to be applied.

The signals are filtered in the frequency domain by taking their 2^{16} points fast Fourier transform (FFT) and by multiplying it by a function which consists of an increasing sine wave, a middle flat plateau, and a decreasing sine wave. In this way, the high and low frequencies are eliminated from the frequency contents of the signals. The corrected signals in time domain are then obtained by inverse FFT.

The points corresponding to the 20 seconds of pause between each couple of successive excitation pulses are extracted from the signals, and only the parts of time histories during which the excitation is active are used in the analyses. No data normalization is attempted.

The resulting measurements to which the damage detection method is applied are acceleration time histories, in physical units (m/s^2), with zero means and a reduced number of points, $N_p = 9827$. The force measurements obtained from sensor 1 are not used in the analyses, because we want the method to be independent of the input excitation. Hence, the total number of sensors, in the X and Y directions, is $N_s = 17$. As in the previous Chapter, we collect the acceleration time histories in a $N_p \times N_s$ matrix, from which the clusters of n measurements on which the multiple linear regression model is built are repeatedly taken until the entire length of the time histories has been considered, and then cycled according to the sensor whose measurements are considered as response. To achieve a significant number of clusters compared to the number of variables in the response surface model, a parameter $\gamma = 5$ was selected so that each of the reduced time history was divided into 115 segments of $n = 85$ points each.

Figure 8.10 shows the *SSE* histograms comparison at the sensor locations that surround the damaged area. The damage indices computed in Table 8.I show that the highest values correspond to these locations, thus correctly identifying the place where the longitudinal braces had been removed. Note that, when the method is applied to the accelerometers in the X direction, it correctly detects and localizes the damage at the first floor, and it recognizes that also the second floor response is slightly affected by the presence of damage, while the third floor response does not significantly change. In the Y direction, the damage at the first floor is detected only by accelerometer 15, while the other histograms do not significantly change. Although these accelerometers record the influence of the shaker because of its eccentric

position, no transversal braces were added or removed from the structure. Therefore, no structural change is detected in this direction.

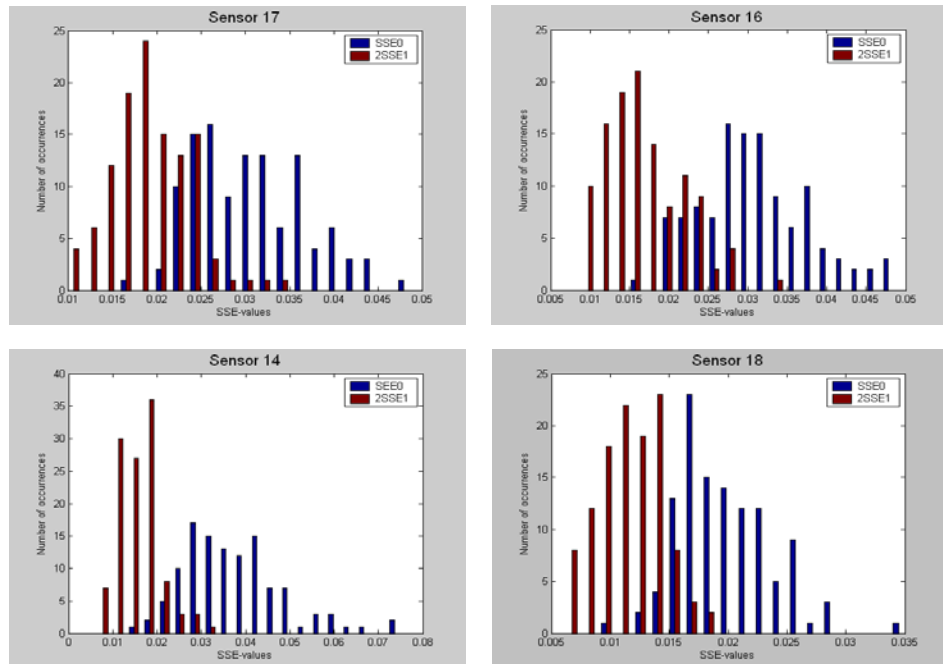


Figure 8.10 SSE comparison for the accelerometers 17, 14, 18, and 16.

TABLE 8.1 VALUES OF THE ADIMENSIONAL DIFFERENCE OF THE *SSE*-MEANS AT DIFFERENT SENSOR LOCATIONS; A DASHED LINE DIVIDES THE SENSORS WHICH DETECT DAMAGE FROM THOSE WHICH DO NOT, BY COMPARISON WITH A REFERENCE VALUE OF $ADMu = 0.2553$.

| <i>ADM</i> | SENSOR |
|---------------|-----------|
| 0.1705 | 3 |
| 0.1801 | 5 |
| 0.2163 | 4 |
| 0.2249 | 10 |
| 0.2414 | 13 |
| 0.2445 | 8 |
| 0.2677 | 9 |
| 0.2724 | 2 |
| 0.2765 | 6 |
| 0.3080 | 7 |
| 0.3129 | 12 |
| 0.3257 | 15 |
| 0.3441 | 11 |
| 0.3685 | 17 |
| 0.4057 | 18 |
| 0.4557 | 16 |
| 0.5801 | 14 |

References for Chapter 8

- Casciati S., Colabrese E., and Magonette G. (2003a). “Damage Detection and Localization by Statistical Comparison of Response Time Histories”, *Structural Health Monitoring 2003*, F.-K. Chang (ed.), DEStech, Lancaster, 733-741.
- Casciati S., Colabrese E., and Magonette G. (2003b). “Monitoring and Response Surface Methodology to detect and Locate Structural Damage, Structural Health Monitoring and Intelligent Infrastructures”, Z. Wu and M. Abe (eds.), Balkema, Lisse, The Netherlands, Vol. 1, 423-429.

Chapter 9

The Palazzo Geraci Case of Study

The last presented application of the response surface damage detection method deals with a structure close to a real-case situation. Indeed, the structure under investigation is a complex continuum exposed to environmental conditions, so that it undergoes traffic and wind loading, as well as temperature gradients. In this case, the damage is represented by the cracks in the masonry. Measurements of the dynamic response of the cracked structure were taken applying different excitation methods, including a hammer, a shaker at the top, and ambient vibrations. The specimen was then retrofitted by filling the cracks with a mortar-type material to restore the undamaged condition of the structure. Thence, the measurements acquisition was repeated to obtain data from the reference undamaged case. The response surface method is applied to the recorded data sets in order to investigate its ability to detect and locate damage.

9.1 The Damaged Model of the Palazzo Geraci Façade

Palazzo Geraci is an ancient, baroque, noble palace in Palermo, Sicily. It was first built in the seventeenth century as the residence of the prince of Roccafiiorita, and then acquired by the family of the marquesses Geraci. In 1780, the architect Venanzio Marvuglia was charged with consistently modifying the façade and re-organizing the interiors. As a result, in the nineteenth century the building presented itself as documented by Figure 9.1a.

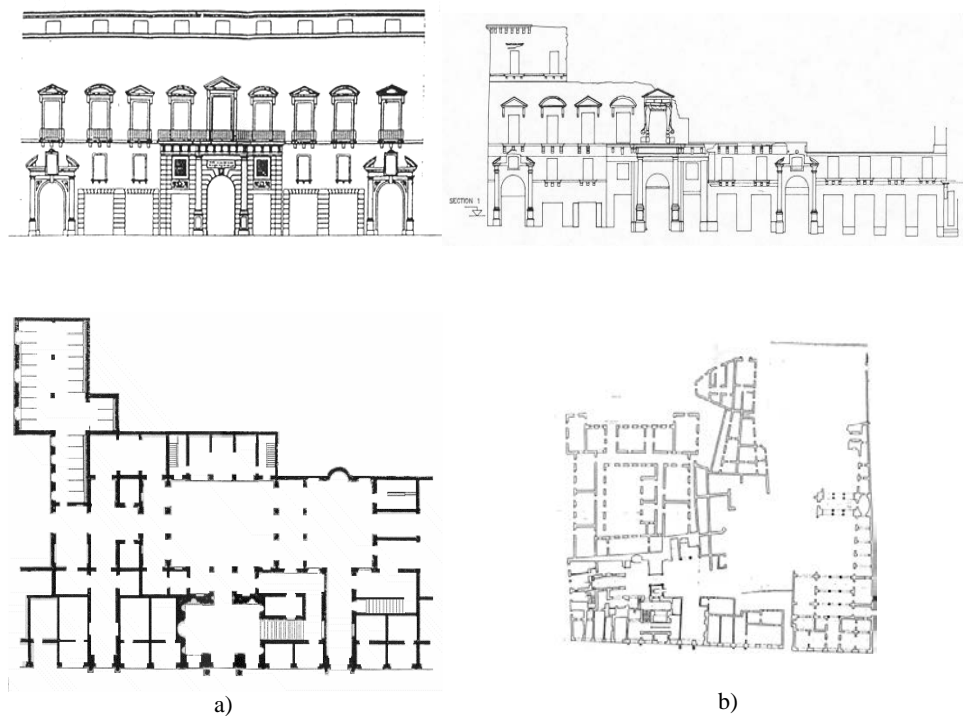


Figure 9.1 Front prospect (top) and plant (bottom) of Palazzo Geraci: (a) in the nineteenth century, and (b) at present.

The palace was built around the interior gardens and it was made of a ground floor, a split mid-floor, a noble floor, and a loft. The apartments between the ground floor and the noble floor were assigned to the servants, while the ground floor was occupied by shops. Three arch-gates, two lateral ones and the principal gate at the centre of the front façade, allowed the vehicles inside the gardens. The main central gate was between two smaller entrances for pedestrians, and it gave on a hall from where one could access the noble floor by the main stair on the left. Above the gate, the front façade was decorated by windows and balconies. The central balcony, or tribune, was supported by the two columns at the sides of the gate.

The building underwent several transformations along the centuries, and it was partially destroyed before it assumed its present configuration. In 1875, some works were made on the building façade, including the addition of some balconies at the noble floor and the wet plaster finishing. At the beginning of the twenties, when the nobles were replaced by the middle-class, the building was partitioned into several properties and the access system to the various parts was changed, thus losing the architectural integrity of the palace. To make matters worse, most of the interiors were destroyed by the bombing during Second World War, and currently the façade stands in precarious conditions, as shown in Figure 9.1b.

The retrofit studies focused on the central part of the façade (Figure 9.2), including the main arch-gate, the openings, and the tribune supported by the two columns. This portion was reproduced in a 1:2 scale model at the ELSA Laboratory, in Ispra. Photogrammetry and Laser Vibrometry were used for the geometric and mechanic characterisation of the monument. The model design was commissioned to an architectural office in Palermo. The resulting “Palazzo

Geraci façade” specimen was mounted perpendicularly to the reaction wall of the ELSA Laboratory, and it underwent a series of pseudo-dynamic tests. Details of the construction of the specimen and of the pseudo-dynamic tests are given in Appendix B.

The upper part of the wall, corresponding to the noble floor of the palace, was severely damaged by the last series of pseudo-dynamic tests, and it had to be demolished. The remaining part is 4.6 m high and 0.7 m thick, with a total of five openings. The reduced model was then transported from the laboratory to its present location outside of the building (Figure 9.4). During the move, new cracks formed in proximity of the openings.

The cracked state of the reduced model is documented by the pictures in Figure 9.5. The cracks are present on both sides of the model front façade, but on the left side they are less evident than on the right side.

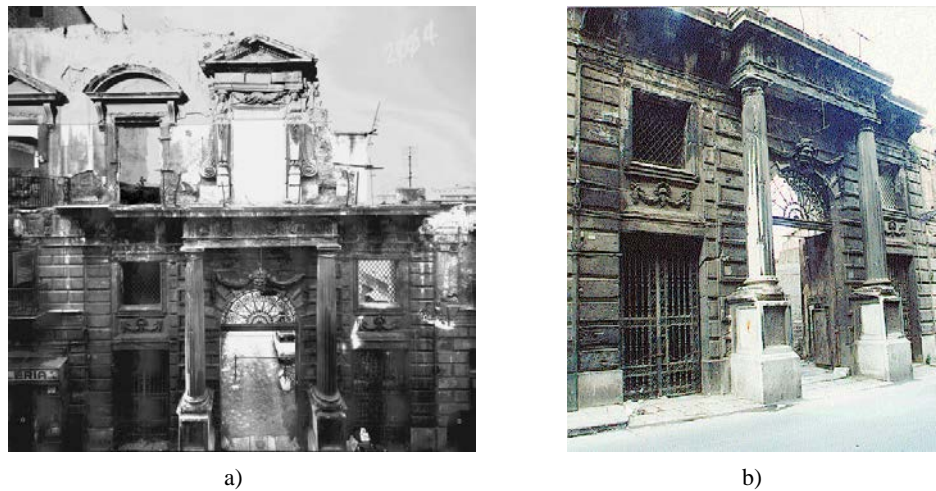


Figure 9.2 (a) The central part of the façade of Palazzo Geraci nowadays, and
(b) detail of the ground floor.

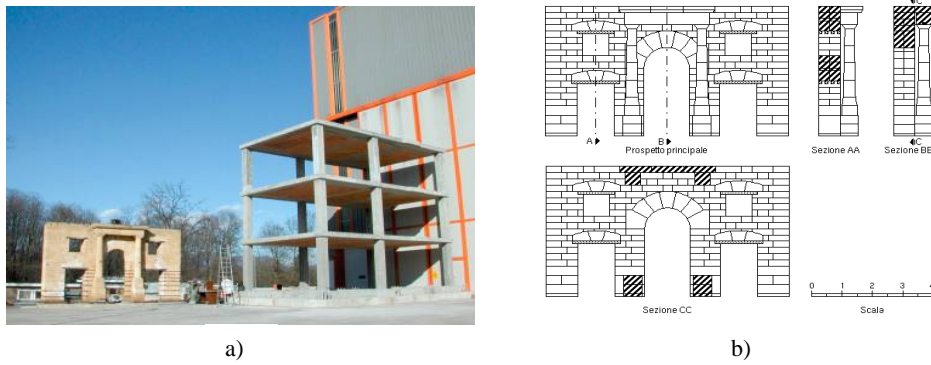


Figure 9.3 (a) The reduced model in its present location outside of the laboratory (the structure on the right is a 1:1 scale steel frame, which was assembled and then carried inside the laboratory for testing). (b) Front prospect and sections of the reduced model.

9.2 Data Acquisition

The measurements acquisition was carried out by Fabio Beni within the framework of his MS-thesis [Beni, 2000]. Modal analysis was applied for damage detection: in particular, the modal frequencies and the mode shapes were experimentally determined and compared with those computed by a two dimensional finite element model of the front facade of the structure. Therefore, the monitoring system was planned and developed with this specific task in mind. The experimental part of this thesis is reported here to understand how the measurements were taken.



Figure 9.4 Cracks at different locations of the reduced model: (a) left openings; (b) right openings; (c) central-left foot; (d) right-end foot (through cracks on the rear side).

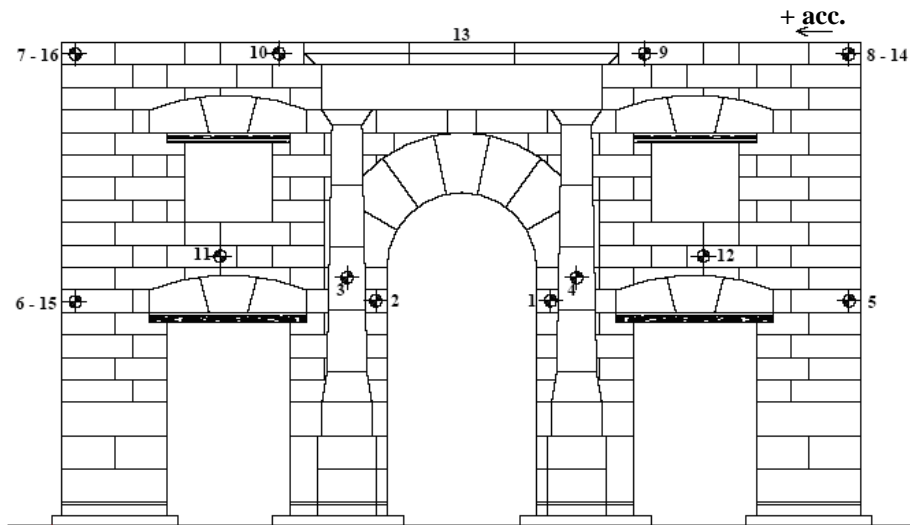


Figure 9.5 Sensors locations and id numbers. Note that the main cracks in the structure are located close to sensors 5, 8, 12, and 2.

9.2.1 The Monitoring System Installation

Assuming as principal direction of the excitation the one parallel to the plane of the façade, the sensors were placed to best identify the mode shapes in this plane. The main concern was the correct determination of the lower modes of the wall for its dynamic characterization, while less attention was paid to the portal frame supported by the columns, which were instrumented with only a few sensors. Accelerometers were placed also on the short sides of the structure to deperate the experimental frequencies from the torsional and transversal contributions. The resulting sensors number and locations are shown in Figures 9.5 and 9.6a.

The selected type of sensors is a capacitive accelerometer, which functions exploiting the same principle of a condenser: the vibration of the device causes a distance variation between two plaques embedded in a dielectric fluid, varying their electric capacity, which results in a current or voltage change. Fifteen Lucas/Schaevitz accelerometers, with sensitivity of ± 0.2 g/volt and powered at 5 Vpk, were used. In the tests with the shaker, a further sensor (sensor 13), with a sensitivity of ± 0.8 g/volt, was glued to the moving mass of the shaker at the top of the structure.

The accelerometers were mounted by cementing aluminium plates to the masonry; the sensing devices were then attached to the plates by screws (Figure 9.6b).

The signals acquisition system (Figure 9.6c) consisted of an industrial PC, on which a data acquisition software developed by the ELSA laboratory is implemented. The software requires the user to input all the information concerned with the acquisition (e.g., the number of channels, the duration of the test, the sampling frequency, etc.). Once the acquisition is started, the data recorded by the accelerometers are not saved until a trigger is switched. No low-pass filter for anti-aliasing was applied to the signals.

The industrial PC was linked to a junction box, able to receive up to 16 channels and powered at 15 V (Figure 9.6d). Each channel corresponds to a cable from an accelerometer, and all the inputs are passed to the industrial PC through one output. As one can see from Figure 9.6e, the most difficult and time-consuming part of the monitoring system installation was the cabling.

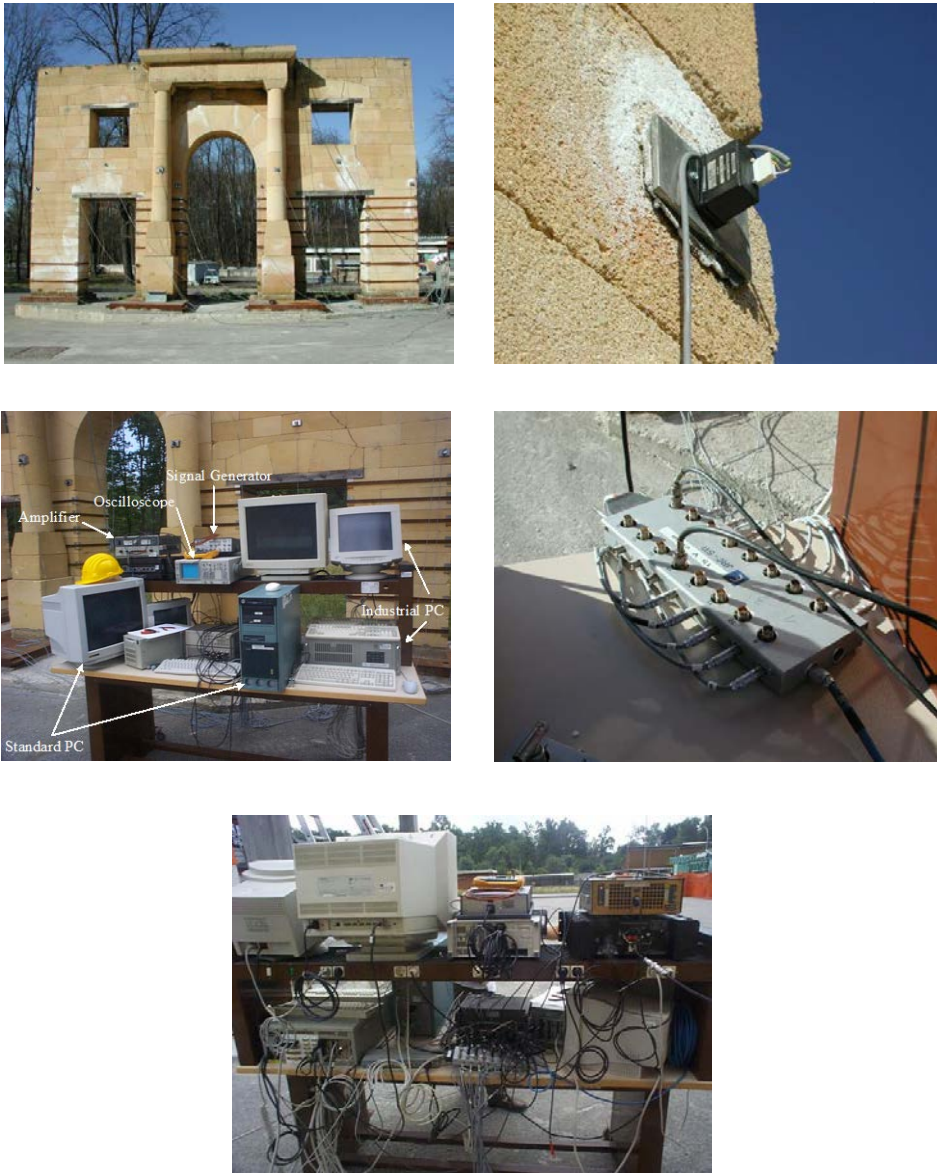


Figure 9.6 Monitoring system. (a) Sensors installation. (b) Accelerometer. (c) Data acquisition.
(d) Junction box. (e) Cabling.



Figure 9.7 Forced excitation methods. (a) Instrumented hammer. (b) Shaker at the top of the structure, in central position.

9.2.2 The Excitation Methods

To record the dynamic response of the structure to different loadings, both forced and environmental excitation methods were applied to the specimen by performing different tests.

In the ambient vibration tests, the wind was the main excitation source, since the near-by traffic is usually very low. Therefore, the results very much depended on the weather conditions of the days in which the tests were performed.

The forced excitation was applied to the structure using either an instrumented hammer or a shaker.

The size of an instrumented hammer (Figure 9.7a) depends on the mass and on the volume of the structure under investigation. Indeed, the energy transferred to the structure must be of a sufficient amount not to be absorbed by the structure, or covered by the environmental noise. In this case, the selected hammer has a mass of 5 kg and a rubber tip, appropriate to excite the low

frequencies. To correctly excite the structure, the strokes must be calibrated with intensities of the same order. Indeed, although the excited natural frequencies stay almost the same, the damping is strongly influenced by the intensities of the strokes due to the different motion mechanisms that they may generate. At the base of the hammer handle there is a BNC connection to which a cable can be linked for power supply. The cable gives current to the force cell located close to the rubber tip, and it sends the signal recorded by the force cell to the analyzer. However, the hammer can also be used as a simple excitation source, without power supply.

The same electro-dynamic shaker used for the BABYFRAME tests and described in Chapter 8, was mounted at the top of the structure, in central position (Figure 9.7b). For this purpose, a plate was fixed to the top of the structure by metal pins embedded in designated holes, and the shaker was then bolted to the plate. Two other lateral plates were added to the top of the structure in view of performing other tests with the shaker in eccentric position.

The resonance peaks of the signals vary due to the presence of the shaker on the structure. Indeed, the addition of a mass to the structure causes its resonant frequencies to decrease (accordingly to the relationship $\omega = \sqrt{k/m}$, for a single degree of freedom system of natural frequency ω , stiffness k , and mass m). This effect must be taken into account overall when dealing with structures of small dimensions, as pedestrian bridges. Also the position of the shaker affects the frequencies of the structure, modifying the frequency associated to the first in-plane mode shape more than the others. To obtain comparable results, the shaker was kept on the structure during all the tests.

9.2.3 The First Set of Tests on the Damaged Structure

All the three excitation methods were used to record the response of the structure in its damaged state. In particular, two ambient vibration tests (a01 and a13), two tests with the shaker (a09 and a10), and eleven tests with the instrumented hammer in different positions were performed, for a total of fifteen tests which are described in Table 9.I. The results were then analyzed in the frequency domain by means of the spectral power density function, in order to judge the clearness of the signals, to compare the signals obtained with the same excitation method, and to compare the different excitation methods among each others. These observations are useful to select the most reliable time histories to which apply the SHM-RSM method, and therefore they are summarized here.

The ambient vibration tests, a01 and a13, provided similar, but different results in terms of frequency content. Indeed, the spectral power densities of the signals recorded in a01 show well-defined peaks, while the ones in a13 have an irregular trend, i.e., a rich frequency content. In particular, a peak at 25 Hz is present in the signals recorded in a13 by the accelerometers located on the right hand side of the structure, thus indicating the motion of part of the structure, but the same peak is not observable in the signals of a01. These differences may be due to a change in the intensity of the excitation force, which can generate different mechanisms and excite new frequencies. During the day in which test a13 was performed, the wind was indeed blowing stronger than during the day of test a01.

The tests with the instrumented hammer (which was used only as excitation source) provided clear results, especially after erasing the initial effects of the strokes.

TABLE 9.I TESTS PERFORMED ON THE DAMAGED STATE OF THE STRUCTURE.

| TEST | EXCITATION METHOD | SAMPLING FREQUENCY [Hz] | DURATION [sec] |
|------|--------------------------------|----------------------------|-------------------|
| a01 | Ambient | 100 | 300 |
| a02 | Hammer in 5 | 100 | 100 |
| a03 | Hammer in 6 | 100 | 100 |
| a04 | Same as a02 | 500 | 100 |
| a05 | Same as a03 | 500 | 100 |
| a06 | Hammer in 17 | 500 | 100 |
| a07 | Hammer in 15 | 500 | 100 |
| a08 | Random hammer | 500 | 100 |
| a09 | Shaker chirp 0→40Hz | 100 – 500 | 360 |
| a10 | Shaker band | 100 – 500 | 300 |
| a11 | Hammer in 8 | 100 | 100 |
| a12 | Hammer in 7 | 100 | 100 |
| a13 | Ambient | 200 | 900 |
| a14 | Hammer in 7 | 100 | 100 |
| a15 | Hammer in predefined positions | 100 – 500 | 200 |

However, the accelerometers close to the impact locations recorded signals of very high amplitude with respect to the other signals, and they often gave unsatisfactory results. The duration of the signals include the stroke and the following time-decay, which is a little longer than 1 s. In practice, the part of the signals away from the stroke (after approximately 650 points) is the environmental noise and it shows the same frequency characteristics of the signals recorded by the ambient vibration tests. In particular, the tests a04 and

a05 present the same irregular trend of the ambient vibration test a13; the peak at 25 Hz is also present in the signals recorded by the accelerometers on the right side of the structure. Erasing less than 650 points, an increase of the peak at 25 Hz is observed over all signals, also where it was not present. By erasing 100 points, the trends in the frequency domain are unclear, and new frequencies appear, because at a high level of the stroke intensity there are relevant nonlinearities.

From the comparative analysis of the tests a04 and a05, one observes that the frequency contents of the spectral power densities of the signals are the same for the low levels of the excitation, but they differ as the level of the excitation increases. For example, by hitting the right side of the structure (a04), the signals recorded on the opposite side have a richer frequency content than the ones on the same side, which highlight only a particular peak. This phenomenon does not appear at the low level of the excitation. The best results for a side of the structure are therefore obtained by hitting the opposite side (i.e., to obtain good results for the right side, one needs to hit the left side, as in a05).

The tests with the hammer clarified the situation at 16 Hz, which was unclear from the ambient vibration tests. The results are more consistent with those of the test a13 than with the ones of the test a01. This also confirms that the test a13 involved more energy than the test a01. However, the tests with the hammer also revealed, in the signals 5 and 8, the presence of a peak at 14 Hz, which was not observed in the ambient vibration tests. Since only the signals 5 and 8 show this peak, it probably corresponds to a local mechanism of the structure. The cross spectral densities analysis clearly detects at this frequency a local motion of the right part of the structure, which is significant of damage. Indeed, the cross-density function of the signals 8 and 9 is null at 14 Hz,

indicating that the two sensors are not both excited at this frequency, while the cross-density functions of signals 5 and 8 show a peak at 14 Hz, thus detecting a local mode of that part of the structure. In this case, the damage could therefore be detected by non-destructive techniques and simple signals analysis.

The results obtained with the electro-dynamic shaker were difficult to analyze, probably because the intensity of the excitation was too high for the structure under investigation. By varying the intensity of the excitation applied to the structure, a change in its resonant frequencies was observed. The current intensity is related to the amplitude of the shaker motion: the longest is the path that the masses need to follow, at constant frequency, the largest is the excitation transferred to the structure. As the intensity of the excitation increased, the experimental frequencies of the structure decreased. That is, the peaks of the spectral power density functions shifted to the left as the excitation intensity increased. Also the height of the peaks varied, and they became taller as the excitation force was increased. This phenomenon was observed also in the tests with the hammer, and it is probably due to the nonlinear behaviour of the structure: indeed the increase of energy invalidates the small displacements theory. The asymmetric trend of the peaks with respect to the resonance frequency is also indicative of the nonlinear behaviour of the structure.

9.2.4 The Retrofit of the Specimen by Mortar Injections

The main cracks observed in the structure were closed by mortar injections. For this purpose, holes of 14 mm diameter and 20 cm depth were drilled in correspondence to the cracks, with a spacing of 15-20 cm. A small rubber tube of length 15 cm was then placed in each hole for a depth of 5 cm. The junctions of the tubes to the holes were sealed by filling the cracks with mortar mixed

with a low amount of water. A liquid mixture for injections was prepared using a drill and a whip for five minutes, and finally shot into the tubes by a gun and a silicone cartridge. The injection technique was carried out starting from the bottom: when the mortar reached the hole above, the entrance hole was sealed and the upper one was injected. At the end of the injections, the mortar was allowed to set for twenty days.

As a result of this retrofitting technique, the specimen now looks as shown in Figure 9.8. This state of the structure is referred to as undamaged. From the comparison of Figure 9.8 with Figure 9.5, one observes that the main repairs were performed in the proximity of the sensors 5, 8, and 12 on the right hand side (r.h.s.) of the structure, and of sensor 2 on the left hand side (l.h.s.).



Figure 9.8 Undamaged state of the structure.

Therefore, a structural change should be detected at these locations when statistically comparing the response time histories from the damaged and undamaged states of the structure. The acquisition of the latter measurements is described in the next section.

9.2.5 The Second Set of Tests on the Undamaged Structure

Based on the results of the analyses of the signals recorded on the damaged structure, it was possible to plan and to perform a reduced number of tests on the retrofitted structure. In particular, only two ambient vibration tests (x01 and x04) and four tests with the instrumented hammer in different positions, were repeated on the undamaged state of the structure, for a total of six tests which are described in Table 9.II. A couple of tests with the hammer (x02 and x05) was performed by hitting the right hand side of the structure in 5. The other couple (x03 and x06) was performed by hitting the left hand side of the structure in 6. The direction of the hammer strokes was always parallel to the structure façade. The shaker was not used anymore as excitation source, because of the unsatisfactory results that it provided for this type of structure.

The two ambient vibration tests provided equal results, and they show an increase of the first natural frequency of the structure with respect to the damaged case.

Among the tests with the hammer, the tests x05 and x06 were considered because the amplitudes of the accelerations were comparable with those recorded before the retrofit. The trends of the spectral power densities of the signals recorded in tests x05 and x06 are overlapping, and the range of the frequency variations is narrower than that observed in the damaged situation. This indicates a new monolithic behaviour of the structure, which before was

not possible due to its cracked condition. From the cross-spectral density analysis, the peak at 14 Hz is not visible anymore because the right side was successfully jointed to the rest of the structure.

Both the ambient vibration tests and the tests with the hammer showed an increase of the 14% of the first natural frequency of the structure, with respect to the damaged case. This is because a crack was located in a strategic position for the stiffness of the first mode, preventing the right-end foot from contributing to it. The mortar injections partially restored this collaboration, thus increasing the stiffness and the first fundamental frequency.

TABLE 9.II TESTS PERFORMED ON THE UNDAMAGED STATE OF THE STRUCTURE.

| TEST | EXCITATION METHOD | SAMPLING FREQUENCY [Hz] | DURATION [sec] |
|------|----------------------|----------------------------|-------------------|
| x01 | Ambient | 500 | 600 |
| x02 | Hammer in 5 | 500 | 100 |
| x03 | Hammer in 6 | 500 | 100 |
| x04 | Ambient | 500 | 600 |
| x05 | Hammer in 5 | 500 | 100 |
| x06 | Hammer in 6 | 500 | 100 |

9.3 Damage Detection by Global Measures

Let us consider, for example, only the ambient excitation tests, x04 and a13, performed on the undamaged and damaged states of the structure, respectively. Signals of length 60000 points were collected during these tests. Therefore, eight windows of 7500 points each were extracted from the signals and analysed in terms of the global measures introduced in Chapter 5.

When the analysis was conducted on the first window, the undamaged case signals gave the results reported in Table 9.III, but the damaged case signals run failed because not enough neighbours were identified. This observation gives evidence of the unreliability of such a data strip. By contrast, when window six is considered, both the damaged and undamaged case signals produce results which allow to distinguish between the two structural conditions. Indeed, a decrease in all the computed global measures is observed when passing from the undamaged to the damaged state of the structure. It can be concluded that, also for this example, all the measures of Chapter 5 are working very well in detecting damage. However, Table 9.III confirms that the maximal Lyapunov exponent can result not very efficient in detecting damage, while the whole spectrum of Lyapunov exponents does it in a clear way. Indeed, by comparing only the first column of positive Lyapunov exponents in Table 9.III, the slight change in the maxima can be undetected or considered as not significant of damage. Considering all the three columns of positive Lyapunov exponents, instead, does not leave space for doubts.

TABLE 9.III GLOBAL MEASURES COMPUTED ON THE UNDAMAGED AND DAMAGED SIGNAL SETS.

| AMBIENT EXCITATION TESTS | SIGNALS WINDOW | POSITIVE LYAPUNOV EXPONENTS $*\Delta t$ | | | KOLMOGOROV ENTROPY ESTIMATE $*\Delta t$ | LYAPUNOV DIMENSION |
|--------------------------------|-------------------|--|--------|--------|---|-----------------------|
| | | | | | | |
| x04 (Undamaged) | Window 1 | 0.2335 | 0.1300 | 0.0383 | 0.4018 | 5.426223 |
| | Window 6 | 0.2229 | 0.1326 | 0.0332 | 0.3887 | 5.377921 |
| a13 (Damaged) | Window 6 | 0.2219 | 0.1117 | 0.0068 | 0.3404 | 4.987422 |

9.4 Damage Localization via SHM Response Surface Method

The tests which were performed on both the damaged and undamaged states of the structure are summarized in Table 9.IV. In particular, four tests, a couple for each of the two structural states, were performed by applying the same excitation method: either environmental vibrations, hammer in 5, or hammer in 6. For each of these methods, the two tests referring to the undamaged state of the structure contain the same number of points and they are both considered in the analyses because they are not only useful for the comparison with a global set of measurement which includes also the damaged case, but they can also be compared one with the other to evaluate the damage index threshold value. The two tests performed on the damaged structure have, instead, different durations, and the one of lowest number of points is not suitable for the analyses, and therefore it is not considered. In conclusion, for each excitation method, we consider only one set of measurements from the damaged state of the structure,

and two from the undamaged state, for a total of three sets of measurements per excitation method (those written in bold in Table 9.IV).

The accelerometers on the short sides of the structure (sensors 14, 15, and 16 in Figure 9.5) were not used in the tests on the undamaged state of the structure, and therefore no comparison is possible in this direction. The two columns were shown to vibrate in a different manner with respect to the structure and to each other. Therefore, the corresponding sensors 3 and 4 of Figure 9.5 are not significant for regression. Furthermore, Figure 9.9 gives evidence that sensor 11 was not functioning during the tests on the undamaged structure, since the plots of the recorded accelerations are flat, especially when compared to the spikes induced by the hammer strokes on the damaged structure. The resulting number of sensors that can be used in the analyses is $N_S = 9$. Namely, sensors 1, 2, 5, 6, 7, 8, 9, 10, and 12 are considered.

Based on the previous analyses, we expect to detect damage at sensors 5 and 8, where a local mechanism was recorded in the signals frequency content. In particular, the measurements of sensor 5 should be affected by the restored collaboration of the right hand side foot of the structure, which was severely fractured in the damaged case. Additionally, cracks were repaired also near sensors 12 and 1 on the right, and near sensor 2 on the left hand side of the structure (see Figures 9.5 and 9.7). Therefore, these sensors should also be able to detect a structural change.

As for the BABYFRAME case, the experimental measurements need to be filtered before the method for damage detection and localization can be applied. The 2^{16} points fast Fourier transforms (FFT) of the signals are computed and multiplied by a function of the same form as the one used in Chapter 8 to cut the

low and high frequencies. The inverse FFT of the resulting signals is then applied to go back to the time domain. No data normalization was attempted.

The measurements from the environmental vibration tests are the easiest ones to analyze, while the ones obtained with the hammer present different number of spikes of different highest intensities depending on the test during which they were taken. Therefore, in the latter case, the process of data cleansing is fundamental to obtain comparable results. The results from the ambient excitation tests are presented in the following section, while the hammer tests need to be separately discussed.

TABLE 9.IV STATISTICALLY COMPARED RESPONSE TIME HISTORIES
(ONLY THE ONES IN BOLD WERE USED FOR THE ANALYSES).

| EXCITATION METHOD | STATE OF THE STRUCTURE | TEST NAME | SAMPLING RATE [s.p.s.] | DURATION [sec] | NUMBER OF POINTS |
|-------------------|------------------------|------------|------------------------|----------------|------------------|
| Ambient | Damaged | a01 | 100 | 300 | 30,000 |
| | | a13 | 200 | 900 | 180,000 |
| | Undamaged | x01 | 500 | 600 | 300,000 |
| | | x04 | 500 | 600 | 300,000 |
| Hammer in 5 | Damaged | a02 | 100 | 100 | 10,000 |
| | | a04 | 500 | 100 | 50,000 |
| | Undamaged | x02 | 500 | 100 | 50,000 |
| | | x05 | 500 | 100 | 50,000 |
| Hammer in 6 | Damaged | a03 | 100 | 100 | 10,000 |
| | | a05 | 500 | 100 | 50,000 |
| | Undamaged | x03 | 500 | 100 | 50,000 |
| | | x06 | 500 | 100 | 50,000 |

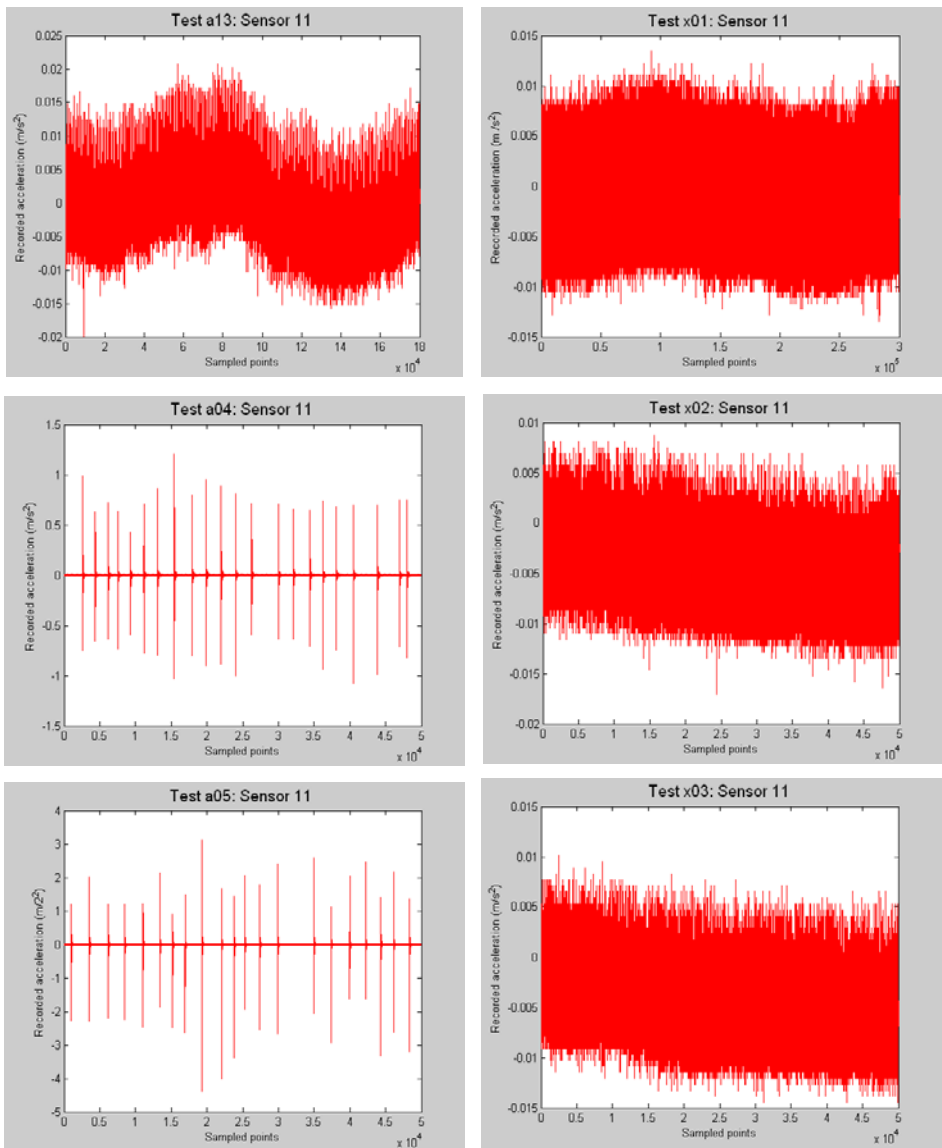


Figure 9.9 Accelerations recorded by sensor 11 during the tests performed with different excitation methods on (a) the damaged state, and (b) the undamaged state of the structure.

9.4.1 Results from the Environmental Vibrations Tests

The tests with ambient excitation were performed using different durations and sampling frequencies on the damaged and the undamaged structure, respectively. As a result, the data in a13 (damaged) contain 180000 points measured at a rate of 200 samples per second (s.p.s.), while both the undamaged tests, x01 and x04, recorded 300000 points long time histories at a rate of 500 s.p.s. (see Table 9.IV). To build a global linear regression model on the damaged and undamaged sets of data, for then comparing its *SSE*-histograms with twice those obtained by considering the undamaged state alone, the response time histories need, of course, to be of the same length. Therefore, time histories of length equal to the maximum common denominator of 60000 points were extracted from the original ones with sampling rates of 1 every 2 and 1 every 5 points, respectively. The points were sampled from a fixed window of the original signals, which included the points from 1001 to $(60000*2)+1$ and to $(60000*5)+1$, respectively.

For each test, the resulting signals of $N_p = 60000$ points each were filtered as previously described, and then collected in an acceleration matrix of size $N_p \times N_s$, where $N_s = 9$. The method defined in section 6.4 was then applied to the two matrices obtained from each couple of tests, with a parameter $\gamma = 40$ resulting into 166 undamaged response surface models built on $n = 360$ points each, at each sensor location. The corresponding *SSE*-histograms are multiplied by two and compared with those obtained from the global set of measurements, i.e., from the 166 global response surface models built on $n = 720$ points each, at each sensor location.

The absolute value of the damage index, *ADM*, defined as the non-dimensional difference between the means of each pair of histograms (Equation

6.36), is computed in Table 9.V for each sensor location and undamaged test. These values are compared to the maximum $ADM_u = 0.0663$ obtained by applying the SHM-RSM method to the measurements from the two undamaged tests x04 and x01.

Both the comparisons of the undamaged tests with the global one including also the damaged test, highlight sensors 5 and 8 as the ones closest to the most relevant damage.

A structural change is also clearly recognized at sensors 2 and 12, which are close to cracks that have been repaired. In particular, sensor 2 is the only one on the left hand side of the structure to be close to a repaired crack. Sensors 9 and 1 are on the right hand side of the structure, where most of the cracks are located, and therefore they are correctly included into the damaged set. The remaining sensors 6, 7, and 10 are instead located on the left hand side, where no repair was needed. Therefore, they are correctly classified as undamaged by the comparison with the undamaged test x04. However, when considering x01 as reference undamaged case, the ADM value computed at sensor 7 is greater than the threshold value, ADM_u , by a small amount. Therefore, when using this damage detection method in practical applications, we should consider the sensors whose ADM values differ the most from the threshold value as the most reliable of damage, while those which show slighter deviations should undergo further investigations.

TABLE 9.V RESULTS FROM THE AMBIENT EXCITATION TESTS(THE DASHED LINE CORRESPONDS TO $ADMu = 0.0663$).

| a13-x01 | | a13-x04 | |
|---------------|-----------|---------------|-----------|
| abs(ADM) | SENSOR | abs(ADM) | SENSOR |
| 0.0153 | 10 | 0.0034 | 10 |
| 0.0379 | 6 | 0.0183 | 6 |
| 0.0778 | 1 | 0.0519 | 7 |
| 0.0902 | 7 | 0.0818 | 1 |
| 0.1779 | 9 | 0.1970 | 9 |
| 0.2178 | 12 | 0.2068 | 12 |
| 0.3472 | 2 | 0.3668 | 2 |
| 0.9323 | 5 | 0.9325 | 5 |
| 0.9584 | 8 | 0.9602 | 8 |

9.4.2 Results from the Tests with the Hammer

Of the measurements recorded during the tests with the hammer in Table 9.IV, we consider only the ones that were collected with the same duration and sampling rate, which result in a common number of points equal to 50000. However, the several tests of same duration were performed by inferring to the structure with the hammer a different number of strokes, of different highest intensity. Note that, in this case, the excitation is an impact load whose expiration time is very short, almost instantaneous. Therefore, not enough points could be obtained by considering only the parts of the signals recorded when the excitation was active, as it was done for the BABYFRAME specimen in Chapter 8 when the excitation was instead applied by the shaker for a certain duration. Hence, to make the measurements collected during different tests

comparable with each other, the spikes need, in this case, to be eliminated from the signals. For this purpose, every peak is extracted together with the 50 points before it, and the 850 points after it. The total number of points of the resulting signal is obtained by subtracting $900S$ from the original 50000 points, where S is the number of spikes in the signal and its value depends on the test being considered. Therefore, the obtained signals have different lengths according to the value of S corresponding to the test during which they were measured. The lowest length is assumed as common number of points, N_p . In particular, N_p is equal to 16818 for the tests with the hammer in 5, and to 26265 for the tests with the hammer in 6.

The sensors located close to the hammer impacts recorded accelerations of too high intensities to be considered in the analyses. Therefore, sensors 5 and 8, and sensors 6 and 7 were not included in the analyses of the tests with the hammer in 5 and 6, respectively. In both cases, the total number of sensors is $N_S = 7$. Assuming again a parameter $\gamma = 40$, the acceleration time histories were divided into 60 and 93 clusters for the tests with hammer in 5 and 6, respectively, of $n = 280$ points each.

Tables 9.VI and 9.VII report the results obtained from the tests with the hammer in 5 and 6, respectively. Sensors 2 and 12 are clearly identified as damaged in both cases, probably because they are the ones that are the least influenced by the hammer position due to their central locations. In particular, sensor 2 shows the most significant structural change with respect to the other sensors, because it is the only one on the left hand side of the structure to be close to a repaired crack. The sensors on the right hand side of the structure are then identified by values of the damage index greater than the threshold computed from the pairs of undamaged tests.

The results from the tests a04 and x05 (hammer in 5) correctly classify as undamaged the sensors 6, 7, and 10, which are located on the left hand side where no repair was needed. The same consideration drawn for sensor 7 when using x01 as reference undamaged case for the ambient tests, needs to be done also when comparing the tests of the hammer in 5 with the undamaged case x02.

The results from the tests with the hammer in 6 successfully capture the presence of damage close to sensor 5, but sensor 8 is too faraway from the impact location to be recognized as damaged.

In conclusion, the results obtained from the tests with the hammer in different positions are consistent among each others, and with those obtained from the environmental vibration tests. In particular, sensor 2 is always recognized as the only one on the left hand side of the structure to be close to a repaired crack, and the right hand side is identified as damaged with respect to the remaining sensors on the other side. The environmental vibration tests are the easiest ones to analyze and they provide a rather complete and precise description of the actual damaged state of the structure. The obtained results are optimal in view of applying this excitation method for the continuous, long-term structural health monitoring of civil infrastructure pursued in Chapter 3.

TABLE 9.VI RESULTS FROM THE TESTS WITH HAMMER IN 5
 (THE DASHED LINE CORRESPONDS TO $ADMu = 0.0923$).

| a04-x02 | | a04-x05 | |
|---------------|-----------|---------------|-----------|
| abs(ADM) | SENSOR | abs(ADM) | SENSOR |
| 0.0228 | 10 | 0.0246 | 7 |
| 0.0497 | 6 | 0.0536 | 10 |
| 0.1053 | 7 | 0.0832 | 6 |
| 0.1848 | 1 | 0.1702 | 1 |
| 0.2014 | 9 | 0.2297 | 12 |
| 0.2271 | 12 | 0.2333 | 9 |
| 0.3958 | 2 | 0.3780 | 2 |

TABLE 9.VII RESULTS FROM THE TESTS WITH HAMMER IN 6
 (THE DASHED LINE CORRESPONDS TO $ADMu = 0.1563$).

| a05-x03 | | a05-x06 | |
|---------------|-----------|---------------|-----------|
| abs(ADM) | SENSOR | abs(ADM) | SENSOR |
| 0.0076 | 10 | 0.0493 | 10 |
| 0.0421 | 8 | 0.1026 | 8 |
| 0.1661 | 5 | 0.1374 | 1 |
| 0.1682 | 1 | 0.1805 | 5 |
| 0.2055 | 9 | 0.2019 | 12 |
| 0.2137 | 12 | 0.2280 | 9 |
| 0.4112 | 2 | 0.4065 | 2 |

References for Chapter 9

- Beni F. (2000). *Indagini diagnostiche e tecniche di identificazione strutturale per la conservazione dei monumenti* (in Italian), Master Degree Thesis, University of Genoa, Italy.
- Beni F., Lagomarsino S., Marazzi F., Magonette G., and Podestà S. (2002). “Structural Monitoring through Dynamic Identification”, in F. Casciati (ed.), *Proceedings 3rd World Conference on Structural Control*, John Wiley & Sons, Chichester, Vol.3, 139-152.

Chapter 10

Conclusions and Future Developments

The author presented her first results in the area of structural damage detection two years ago [Casciati and Faravelli, 2002]. They were obtained in a traditional way, by identifying the system eigenvalues and by comparing the associated eigenmodes. Despite the widely distributed cracks across the investigated system (the Memnon Colossi, in Luxor, Egypt), the results were barely satisfactory in terms of damage detection and quite null in terms of damage localization.

The subsequent attempt to build a more efficient procedure also had to satisfy some mandatory requirements in present international research toward the realization of smart sensors [ESF, 2004]. In extreme synthesis, the demand was to do the job relying on limited computational capacities, i.e., forget those methods pursuing a peculiar local description (as based on finite element

schemes) of the structural systems. Thence, the results achieved throughout the study were pursued with the final objective of implementing them in a software simple enough to be downloaded in the micro-processor which, coupled with the sensor, realizes the smart sensor device.

This remark led the research to be focused on the methods that work in the space of the observed variables, where global information measures are used to detect damage. This is a quite innovative approach which

- 1) only needs the availability of measured responses (in the form of multivariate time series) in the original undamaged state and in the current one of potential damage;
- 2) does not require any structural system identification;
- 3) shows an accuracy which strongly depends on the density of the sensor array deployed on the structural system.

Damage detection is here demanded to global measures as entropy or Lyapunov exponents, which showed to be quite efficient. It must be said that not all their potentiality toward damage localization was exploited within the reported activity. For this purpose two aspects could be pursued in view of further developments

- i) to compute these global measures in subspaces of the observed variables; this would allow to perform a sort of sensibility analysis on the role of the variables which were in turn removed;
- ii) to repeat the analysis conducted on the space of the observed variables, in larger spaces which account for an embedding dimension larger than 1, for instance 2. Also in this case, successive sub-structuring of this enlarged space could be the way toward a sensitivity analysis.

As an alternative to such developments, the relationships among these observed variables are approximated by response surface techniques, which also allow to localize the damage. This new damage detection method showed to be reliable and robust when applied to both the results of numerical simulation and experimental data. The global measures discussed above help in the extent that they preliminarily state whether or not the problem is well posed, i.e., whether the set of measured quantities are able to detect the specific damage to be localized. A fascinating future development along this track is that of building a sensor placement policy driven by such considerations.

It must be underlined that the numerical study case of Chapter 7 and the experiments which provided the data for Chapter 8 and 9 are so rich of information that there will always be room for further adjustments and investigations. In particular the ASCE benchmark studied in Chapter 7 can be used to generate always new situations of damage and of monitored response. It will certainly provide a gymnasium to further test and improve the robustness of the approach developed and implemented along the thesis.

The results of Chapter 9 are quite impressive. The ability to identify crack locations on a continuous wall opens the way to the new generation of sensors for which accuracy (but not sensitivity) is traded off by extremely low cost, which is the first requisite toward the availability of dense sensor arrays [Faravelli and Shoureshi, 2003]. The second requisite, of course, is their wireless nature which represents the necessary future development of the proposed approach for its application to structural health monitoring. The process can be easily downloaded in the microprocessor coming with the sensor and driving its activity, including its trans-receiver ability.

References for Chapter 10

- Casciati S. and Faravelli L. (2002). “Structural Damage Detection Based on Dynamic Response Identification”, *Structural Health Monitoring 2002*, D. Balageas (ed.), DEStech Publications Inc., Lancaster, ,1081-1090
- ESF, EUROCORES (2004). *Programme Smart Structural Systems Technologies (S3T)*, Call for Outline Proposals.
- Faravelli L. and Shoureshi R. (2003). *Proceedings of the ESF-NSF Workshop on Advancing Technological Frontiers for Feasibility of Ageless Structures*, Strasbourg, France, (CD available on request at ESF).

Appendix A

Multivariate Regression Analysis

In the presence of measured values y and $x_j, j=1, \dots, k$, the linear model

$$y = \beta_0 + \beta_1 x_1 + \beta_2 x_2 + \dots + \beta_k x_k + \varepsilon \quad (\text{A.1})$$

is guessed. Multivariate linear regression analysis pursues the estimation of the model parameters.

A.1 Estimation of the Parameters in Linear Regression Models

The least squares method is typically used to estimate the regression coefficient in a multiple linear regression model. Suppose that $n > k$ observations on the response variable are available, say y_1, y_2, \dots, y_n . Along with each observed response y_i , an observation on each regressor variables is recorded. Let x_{ij}

denote the i -th observation or level of variable x_j . The data will appear as in Table A.I.

We assume that the error term ε in the model has $E(\varepsilon) = 0$ and $\text{Var}(\varepsilon) = \sigma^2$, and that the $\{\varepsilon_i\}$ are uncorrelated random variables. We may write the model in Equation (A.1) in terms of the observations in Table 7.I as

TABLE A.I DATA FOR MULTIPLE LINEAR REGRESSION

| y | x₁ | x₂ | ... | x_k |
|----------|----------------------|----------------------|------------|----------------------|
| y_1 | x_{11} | x_{12} | \dots | x_{1k} |
| y_2 | x_{21} | x_{22} | \dots | x_{2k} |
| \vdots | \vdots | \vdots | | \vdots |
| y_n | x_{n1} | x_{n2} | \dots | x_{nk} |

$$\begin{aligned}
 y_i &= \beta_0 + \beta_1 x_{i1} + \beta_2 x_{i2} + \dots + \beta_k x_{ik} + \varepsilon_i \\
 &= \beta_0 + \sum_{j=1}^k \beta_j x_{ij} + \varepsilon_i, \quad i = 1, 2, \dots, n
 \end{aligned}
 \tag{A.2}$$

The method of the least squares chooses the β 's in Equation (A.2) so that the sums of the squares of errors, ε_i , are minimized. The least squares function is

$$\begin{aligned}
 L &= \sum_{i=1}^n \varepsilon_i^2 \\
 &= \sum_{i=1}^n \left(y_i - \beta_0 - \sum_{j=1}^k \beta_j x_{ij} \right)^2
 \end{aligned} \tag{A.3}$$

The function L is to be minimized with respect to $\beta_0, \beta_1, \dots, \beta_k$. The least squares estimators, say b_0, b_1, \dots, b_k , must satisfy

$$\left. \frac{\partial L}{\partial \beta_0} \right|_{b_0, b_1, \dots, b_k} = -2 \sum_{i=1}^n \left(y_i - \beta_0 - \sum_{j=1}^k \beta_j x_{ij} \right) = 0 \tag{A.4a}$$

and

$$\left. \frac{\partial L}{\partial \beta_{ij}} \right|_{b_0, b_1, \dots, b_k} = -2 \sum_{i=1}^n \left(y_i - \beta_0 - \sum_{j=1}^k \beta_j x_{ij} \right) x_{ij} = 0, \tag{A.4b}$$

where $j = 1, 2, \dots, k$.

Simplifying Equation (A.4), we obtain

In general, \mathbf{y} is an $n \times 1$ vector of the observations, \mathbf{A} is an $n \times p$ matrix of the levels of the regressor variables, $\boldsymbol{\beta}$ is a $p \times 1$ vector of the regression coefficients, and $\boldsymbol{\varepsilon}$ is an $n \times 1$ vector of the total errors.

We wish to find the vector of least squares estimators \mathbf{b} , that minimizes

$$L = \sum_{i=1}^n \varepsilon_i^2 = \boldsymbol{\varepsilon}^T \boldsymbol{\varepsilon} = (\mathbf{y} - \mathbf{A}\boldsymbol{\beta})^T (\mathbf{y} - \mathbf{A}\boldsymbol{\beta}) \quad (\text{A.7})$$

Note that L may be expressed as

$$\begin{aligned} L &= \mathbf{y}^T \mathbf{y} - \boldsymbol{\beta}^T \mathbf{A}^T \mathbf{y} - \mathbf{y}^T \mathbf{A} \boldsymbol{\beta} + \boldsymbol{\beta}^T \mathbf{A}^T \mathbf{A} \boldsymbol{\beta} \\ &= \mathbf{y}^T \mathbf{y} - 2\boldsymbol{\beta}^T \mathbf{A}^T \mathbf{y} + \boldsymbol{\beta}^T \mathbf{A}^T \mathbf{A} \boldsymbol{\beta} \end{aligned} \quad (\text{A.8})$$

since $\boldsymbol{\beta}^T \mathbf{A}^T \mathbf{y}$ is a 1×1 matrix, or scalar, and its transpose $(\boldsymbol{\beta}^T \mathbf{A}^T \mathbf{y})^T = \mathbf{y}^T \mathbf{A} \boldsymbol{\beta}$ is the same scalar. The least squares estimators must satisfy

$$\left. \frac{\partial L}{\partial \boldsymbol{\beta}} \right|_{\mathbf{b}} = -2\mathbf{A}^T \mathbf{y} + 2\mathbf{A}^T \mathbf{A} \mathbf{b} = \mathbf{0} \quad (\text{A.9})$$

which simplifies to

$$\mathbf{A}^T \mathbf{A} \mathbf{b} = \mathbf{A}^T \mathbf{y} \quad (\text{A.10})$$

Equation (A.10) is the set of least squares normal equations in matrix form. It is identical to Equation (A.5). To solve the normal equations, multiply both sides of Equation (A.10) by the inverse of $\mathbf{A}^T \mathbf{A}$. Thus, the least squares estimator of $\boldsymbol{\beta}$ is

$$\mathbf{b} = (\mathbf{A}^T \mathbf{A})^{-1} \mathbf{A}^T \mathbf{y} \quad (\text{A.11})$$

It is easy to see that the matrix form of the normal equations is identical to the scalar form. Writing out Equation (A.10) in detail, we obtain

$$\begin{bmatrix} n & \sum_{i=1}^n x_{i1} & \sum_{i=1}^n x_{i2} \dots & \sum_{i=1}^n x_{ik} \\ \sum_{i=1}^n x_{i1} & \sum_{i=1}^n x_{i1}^2 & \sum_{i=1}^n x_{i1} x_{i2} \dots & \sum_{i=1}^n x_{i1} x_{ik} \\ \vdots & \vdots & \vdots & \vdots \\ \sum_{i=1}^n x_{ik} & \sum_{i=1}^n x_{ik} x_{i1} & \sum_{i=1}^n x_{ik} x_{i2} \dots & \sum_{i=1}^n x_{ik}^2 \end{bmatrix} \begin{bmatrix} b_0 \\ b_1 \\ \vdots \\ b_k \end{bmatrix} = \begin{bmatrix} \sum_{i=1}^n y_i \\ \sum_{i=1}^n x_{i1} y_i \\ \vdots \\ \sum_{i=1}^n x_{ik} y_i \end{bmatrix} \quad (\text{A.12})$$

If the indicated matrix multiplication is performed, the scalar form of the normal equations, i.e., Equation (A.5), will result. In this form it is easy to see that $\mathbf{A}^T \mathbf{A}$ is a $p \times p$ symmetric matrix and $\mathbf{A}^T \mathbf{y}$ is a $p \times 1$ column vector. Note the special structure of the matrix $\mathbf{A}^T \mathbf{A}$. The diagonal elements of $\mathbf{A}^T \mathbf{A}$ are the sums of squares of the elements in the columns of \mathbf{A} , and the off-diagonal elements are the sums of the cross-products of the elements in the columns of \mathbf{A} . Furthermore, note that the elements of $\mathbf{A}^T \mathbf{y}$ are the sums of the cross-products of the elements of the columns of \mathbf{A} and the observations $\{y_i\}$.

The fitted regression model is

$$\hat{\mathbf{y}} = \mathbf{A}\mathbf{b} \quad (\text{A.13})$$

In scalar notation, the fitted model is

$$\hat{y}_i = b_0 + \sum_{j=1}^k b_j x_{ij}, \quad i = 1, 2, \dots, n \quad (\text{A.14})$$

The difference between the observation y_i and the fitted value \hat{y}_i is a residual, say $e_i = y_i - \hat{y}_i$. The $n \times 1$ vector of the residual is denoted by

$$\mathbf{e} = \mathbf{y} - \hat{\mathbf{y}} \quad (\text{A.15})$$

A.2 Properties of the Least Squares Estimators and Estimation of σ^2

The least squares method produces an unbiased estimator of the parameter $\boldsymbol{\beta}$ in the multiple linear regression model. This property may be easily demonstrated by finding the expected value of \mathbf{b} as follows

$$\begin{aligned} E(\mathbf{b}) &= E[(\mathbf{A}^T \mathbf{A})^{-1} \mathbf{A}^T \mathbf{y}] \\ &= E[(\mathbf{A}^T \mathbf{A})^{-1} \mathbf{A}^T (\mathbf{A}\boldsymbol{\beta} + \boldsymbol{\varepsilon})] \\ &= E[(\mathbf{A}^T \mathbf{A})^{-1} \mathbf{A}^T \mathbf{A}\boldsymbol{\beta} + (\mathbf{A}^T \mathbf{A})^{-1} \mathbf{A}^T \boldsymbol{\varepsilon}] \\ &= \boldsymbol{\beta} \end{aligned} \quad (\text{A.16})$$

because $E(\boldsymbol{\varepsilon}) = 0$ and $(\mathbf{A}^T \mathbf{A})^{-1} \mathbf{A}^T \mathbf{A} = \mathbf{I}$. Thus, \mathbf{b} is an unbiased estimator of $\boldsymbol{\beta}$. The variance property of \mathbf{b} is expressed by the covariance matrix

$$\begin{aligned} \text{Cov}(\mathbf{b}) &= E\{[\mathbf{b} - E(\mathbf{b})][\mathbf{b} - E(\mathbf{b})]^T\} \\ &= \sigma^2 (\mathbf{A}^T \mathbf{A})^{-1} \end{aligned} \quad (\text{A.17})$$

The covariance matrix of \mathbf{b} is a $p \times p$ symmetric matrix, whose (j, j) -th element is the variance of b_j and whose (i, j) -th element is the covariance between b_i and b_j .

It is also necessary to estimate σ^2 . To develop an estimator of this parameter consider the sum of squares of the residuals,

$$SSE = \sum_{i=1}^n (y_i - \hat{y}_i)^2 = \sum_{i=1}^n e_i^2 = \mathbf{e}^T \mathbf{e}$$

Substituting $\mathbf{e} = \mathbf{y} - \hat{\mathbf{y}} = \mathbf{y} - \mathbf{A}\mathbf{b}$, we have

$$\begin{aligned} SSE &= (\mathbf{y} - \mathbf{A}\mathbf{b})^T (\mathbf{y} - \mathbf{A}\mathbf{b}) \\ &= \mathbf{y}^T \mathbf{y} - \mathbf{b}^T \mathbf{A}^T \mathbf{y} - \mathbf{y}^T \mathbf{A}\mathbf{b} + \mathbf{b}^T \mathbf{A}^T \mathbf{A}\mathbf{b} \\ &= \mathbf{y}^T \mathbf{y} - 2\mathbf{b}^T \mathbf{A}^T \mathbf{y} + \mathbf{b}^T \mathbf{A}^T \mathbf{A}\mathbf{b} \end{aligned}$$

Because $\mathbf{A}^T \mathbf{A}\mathbf{b} = \mathbf{A}^T \mathbf{y}$, this last equation becomes

$$SSE = \mathbf{y}^T \mathbf{y} - \mathbf{b}^T \mathbf{A}^T \mathbf{y} \quad (\text{A.18})$$

Equation (A.18) is called the error or residual sum of squares, and it has $n - p$ degrees of freedom associated with it. It can be shown that

$$E(SSE) = \sigma^2(n - p)$$

so an unbiased estimator of σ^2 is given by

$$\sigma^2 = \frac{SSE}{n - p} \quad (\text{A.19})$$

The estimate of σ^2 produced by Equation (A.19) is model-dependent. That is, its value depends on the form of the model that is fit to the data. For example, if we fit a quadratic model to the data, the estimate of σ^2 may result to be larger than the estimate obtained from a first-order model, suggesting that the first-order model is superior than the quadratic in that there is less unexplained variability resulting from the first-order fit. If replicate runs are available (that is, more than one observation on y at the same x -levels), then a model-independent estimate of σ^2 can be obtained.

A.3 Hypothesis Testing in Multiple Regression

In multiple linear regression problems, certain tests of hypotheses about the model parameters are helpful in measuring the usefulness of the model. In this section we describe several important hypothesis-testing procedures. These

procedures require that the errors ε_i in the model are normally and independently distributed with mean zero and variance σ^2 , abbreviated $\varepsilon_i \sim N(0, \sigma)$. As a result of this assumption, the observations y_i are normally and independently distributed with mean $\beta_0 + \sum_{j=1}^k \beta_j x_{ij}$ and variance σ^2 .

A.4 Test for Significance of Regression

The test for significance of regression is a test to determine if there is a linear relationship between the response variable y and a subset of the regressor variables x_1, x_2, \dots, x_k . The appropriate hypotheses are

$$H_0 : \beta_1 = \beta_2 = \dots = \beta_k = 0 \tag{A.20}$$

$$H_1 : \beta_j \neq 0 \quad \text{for at least one } j$$

Rejection of H_0 in (7.30) implies that at least one of the regressor variables x_1, x_2, \dots, x_k contributes significantly to the model. The test procedure involves partitioning the total sum of squares $SST = \sum_{i=1}^n (y_i - \bar{y})^2$ into a sum of squares due to the model (or to regression) and a sum of squares due to residual (or error),

$$SST = SSR + SSE \tag{A.21}$$

If the null hypothesis $H_0 : \beta_1 = \beta_2 = \dots = \beta_k = 0$ is true, then SSR/σ^2 is distributed as χ_k^2 , where the number of degrees for χ^2 is equal to the number of regressor variables in the model. Also, we can show that SSR/σ^2 is distributed as χ_{n-k-1}^2 and that SSE and SSR are independent.

The test procedure for $H_0 : \beta_1 = \beta_2 = \dots = \beta_k = 0$ is to compute

$$F_0 = \frac{SSR/k}{SSE/(n-k-1)} = \frac{MSR}{MSE} \quad (\text{A.22})$$

and to reject H_0 if F_0 exceeds $F_{\alpha,k,n-k-1}$. Alternatively, one could use the P -value approach to hypothesis testing and, thus, reject H_0 if the P -value for the statistic F_0 is less than α . The test is usually summarized in a table such as Table A.II. This test procedure is called analysis of variance because it is based on a decomposition of the total variability in the response variable y .

TABLE A.II ANALYSIS OF VARIANCE FOR SIGNIFICANCE OF REGRESSION

| SOURCE OF VARIATION | SUM OF SQUARES | DEGREES OF FREEDOM | MEAN SQUARE | F_0 |
|---------------------|----------------|--------------------|-------------|-------------|
| Regression | SSR | k | MSR | MSR / MSE |
| Error or residual | SSE | $n - k - 1$ | MSE | |
| Total | SST | $n - 1$ | | |

A computational formula for SSR may be found easily. We have derived a computational formula for SSE in Equation (A.18), that is

$$SSE = \mathbf{y}^T \mathbf{y} - \mathbf{b}^T \mathbf{A}^T \mathbf{y}$$

Now because the total sum of squares is

$$SST = \sum_{i=1}^n y_i^2 - \left(\sum_{i=1}^n y_i \right)^2 / n = \mathbf{y}^T \mathbf{y} - \left(\sum_{i=1}^n y_i \right)^2 / n \quad (\text{A.23})$$

we may rewrite the Equation (A.18) as

$$SSE = \mathbf{y}^T \mathbf{y} - \left(\sum_{i=1}^n y_i \right)^2 / n - \left[\mathbf{b}^T \mathbf{A}^T \mathbf{y} - \left(\sum_{i=1}^n y_i \right)^2 / n \right]$$

or

$$SSE = SST - SSR \quad (\text{A.24})$$

Therefore, the regression sum of squares is

$$SSR = \mathbf{b}^T \mathbf{A}^T \mathbf{y} - \left(\sum_{i=1}^n y_i \right)^2 / n \quad (\text{A.25})$$

The coefficient of multiple determination R^2 is defined as

$$R^2 = \frac{SSR}{SST} = 1 - \frac{SSE}{SST} \quad (\text{A.26})$$

R^2 is a measure of the amount of reduction in the variability of y obtained by using the regressor variables x_1, x_2, \dots, x_k in the model. From inspection of the analysis of variance identity equation [Equation (A.21)], we see that $0 \leq R^2 \leq 1$. However, a large value of R^2 does not necessarily imply that the regression model is good. Adding a variable to the model will always increase R^2 , regardless whether the additional variable is statistically significant or not. Thus it is possible for models that have large values of R^2 to yield poor predictions of new observations or estimates of the mean response.

For example, if we add quadratic terms to a first-order model, we can show that the value of R^2 increases. However, if this increase in R^2 is relatively small, it suggests that the quadratic terms do not really improve the model.

Because R^2 always increases as we add terms to the model, some regression model builders prefer to use an adjusted R^2 statistic defined as

$$R_{\text{adj}}^2 = 1 - \frac{SSE/(n-p)}{SST/(n-1)} = 1 - \frac{n-1}{n-p}(1-R^2) \quad (\text{A.27})$$

In general, the adjusted R^2 statistic will not always increase as variables are added to the model. In fact, if unnecessary terms are added, the value of R_{adj}^2 will often decrease.

For the same first-order model, the adjusted R^2 will be very closed to the ordinary R^2 . When R^2 and R_{adj}^2 differ dramatically, there is a good chance that non significant terms have been included in the model. If the adjusted R^2 actually decreases when the quadratic terms are added to the model, this is a strong indication that the quadratic terms are unnecessary.

Appendix B

The Palazzo Geraci Façade Specimen

B.1 The Construction of the Specimen

The laboratory specimen was built by four workers in twenty days, trying to follow the same construction technique used to actually build the palace in the seventeenth century. The masonry was made of squared ashlar of limestone and sand. The dry ashlar were grooved laterally and at the base, and the liquid mortar was poured only after each course was emplaced. The mortar was poured from the top into the vertical joints and then it spread along the grooves on the horizontal surfaces. In this way, the mortar joints between the ashlar rows are not visible from the exterior.

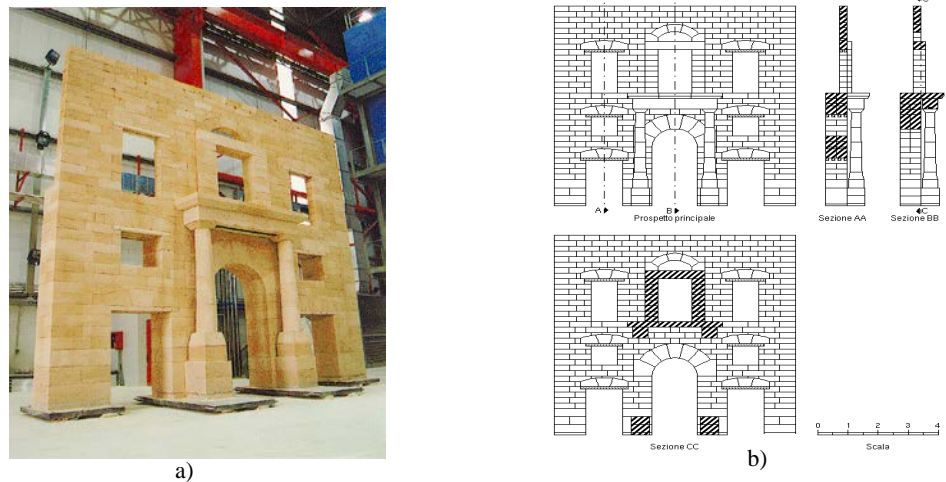


Figure B.1 (a) The original 1:2 scale model of the Palazzo Geraci façade built at the ELSA Laboratory, in Ispra. (b) Front prospect and sections of the original model.

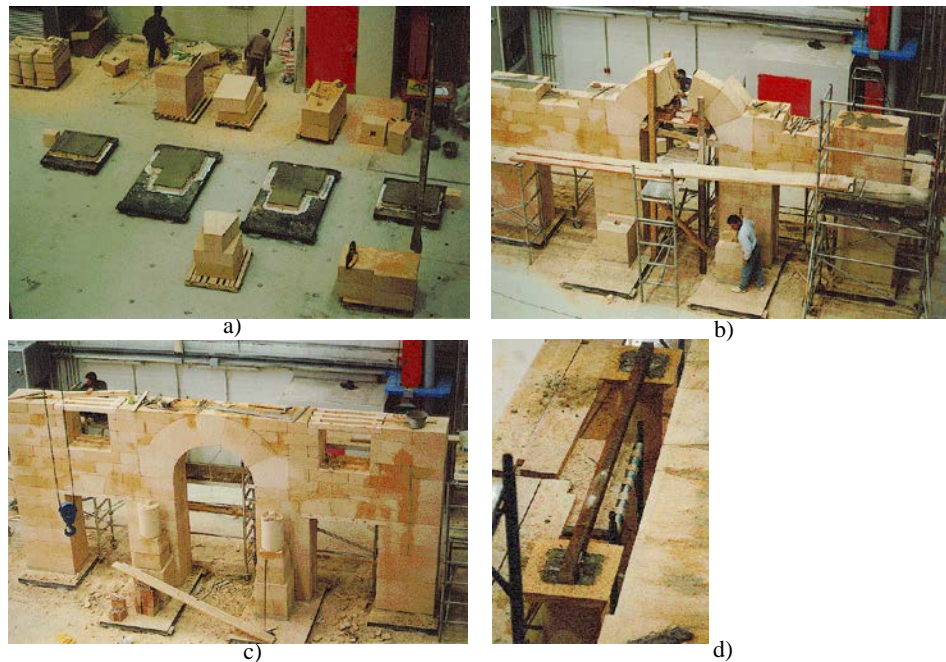


Figure B.2 Construction phases of the specimen: (a) support plane; (b) round-headed arch; (c) wooden beams at the intrados of the platbands above the lateral openings; (d) steel anchored to the top of the column capitals.

A first plate of stone ashlar, of 100 mm thickness, was glued to the abraded surfaces of four steel plates, two central ones of dimensions 2.3 x 2.3 x 100 mm and weight 2.33 tons each, and two lateral ones of dimensions 1.25 x 1.25 x 100 mm and weight 1.218 tons each. The four steel plates were placed on steel elements at 60 mm height from the ground level, to allow the future insertion of pressure cells. The support plane, shown in Figure B.2a, was finally levelled by a layer of bastard mortar, which was let to set.

The first three layers of stone ashlar are 330 mm high, while the following ones are 225 mm high (see Figure B.1). The base layers were made of thick stone ashlar, previously wetted and sealed by a thin layer of mortar; the liquid mortar was then poured from the top into the vertical grooves to form the vertical joints. All the other courses of stone ashlar were instead emplaced in completely drained conditions according to the construction technique of the time.

Until the height of 4.6 m, the wall was made of head and fillet stone ashlar, staggered of 175 mm with respect to the previous row. At the end of each layer, the irregular horizontal surfaces were levelled to allow the emplacement of the next layer. The verticality of the stone ashlar and the horizontality of the layers were checked by rods, levels, and a plumb-line.

The upper part of the façade was made of one head masonry. The stone ashlar were 250 mm thick and they were shaped with not parallel, but slightly convergent, horizontal surfaces, resulting in a height of 225 mm in the front and of 220 mm in the rear. The support of the next row of stone ashlar was granted exteriorly by the refinement of the ashlar edges, and interiorly by small lateritious flakes. The joints of the rear side were then sealed with mortar. Once

the mortar started to set, the liquid mortar was poured through the lateral grooves of the stone ashlar.

The original 1:2 scale model included several components whose main characteristics and construction techniques are briefly described below.

The central round arch of the ground floor is made of wedge-shaped ashlar (quoins) of limestone and sand, it spans 1.5 m, and it is about 0.6 m high. The total thickness of 700 mm was achieved by building two laterally adjacent arches (Figure B.2b). The arches were set up on two dosserets (pulvins). Each arch was made of six stone ashlar, which were emplaced in drained condition using a centre. At the middle height of the dosserets, four wooden posts were jointed together to hold a leaning floor, which offered support for the objects holding the stone ashlar during the emplacement. Once the emplacement was completed, the liquid mortar was poured into the grooves on the interior faces of the ashlar. The centres were then removed, and the lateral surfaces, the intrados, and the extrados of the arch were regularized by removing the excess of material.

The central opening of the noble floor, above the portal frame in Figure B.1, is surmounted by a lintel and a lowered arch of unloading (sordino). This structure, together with the two piers, is 0.4 m thick. The lowered arch was built in a manner similar to the one used for the round arch of the ground floor. In this case, the operation was facilitated by the presence of the monolithic lintel, at whose edges the arch was set up.

Six lateral openings are located at three different levels (0, 2.8, and 4.6 m above the ground level), and they are surmounted by platbands (flat arches) made of three shaped ashlar each. Two wooden beams were observed at the intrados of the platband of one of the highest windows (the other was destroyed

during the war), and therefore they were included in the model. In particular, beams of second class fir-wood (of section 100 x 100 mm) were installed in designated spaces drawn at the top of the openings (Figure B.2c). Four wooden beams were placed, with a 10 mm spacing, at the top of each of the openings of the ground floor. The above platband was then emplaced using two orders of ashlar, a front one and a rear one. The liquid mortar was finally poured into the grooves on the interior faces of the ashlar. Because of the reduced (250 mm) thickness of the upper wall, only two wooden beams and one course of ashlar were used for each of the platbands above the highest windows of the noble floor.

The afore-standing portal frame is composed by the two columns and the above lintel. The monolithic columns have a base diameter of 0.4 m and a top diameter of 0.3 m. Each column stands on a basement made of two parallelepiped blocks, of 0.5 m height each and square bases of sides 0.6 m and 0.5 m from bottom to top. The columns were constructed by assembling frustum-conic blocks with groove-and-tongue joints (Figure B.3), and by sealing the whole with mortar. The lintel is 0.5 m thick, 0.45 m high, and 2.8 m long. An iron of the same length and 6-9 cm thickness was observed at the intrados along the lintel centre axis (Figure B.2d). To include this element into the model, two steel plates (250 x 250 x 10 mm) were cemented in designated spaces at the top of the capitals. Each edge of the steel element, of section 80 x 80 mm and of 2.6 m length, was then anchored with bolts to two welded steel angles set ajar (Figure B.4). The steel element was then embedded in a groove at the intrados of lintel. The axial joint with the portal frame was realized pouring liquid mortar in the designated lateral grooves. The portal frame was

completed by three large plates embedded in the masonry and supported by the lintel.

The resulting structure in Figure B.1 was 8 m long and 8.2 m high, with a total of eight openings. The wall thickness varied from 0.7 m for the first 4.6 m of height above the ground level, to 0.25 m for the remaining height.

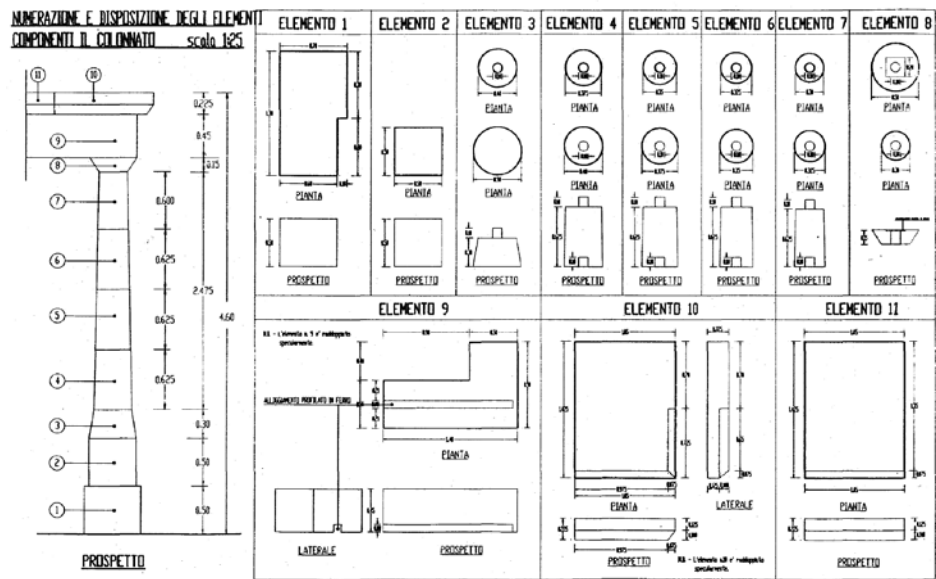


Figure B.3 Structural details of the columns.

Three different types of tests were carried out using different structural configurations, and each test was repeated for different intensities of the reference earthquake: (1) model with base isolation, and reference earthquake at 100% and 200%; (2) model without base isolation, and reference earthquake at 20%, 100%, and 200%; (3) repaired model without base isolation, and reference earthquake at 100% and 200%.

In the first case, the base isolation consisted of a mechanic isolator with elastoplastic response, and it was made of eight radial C-steel elements between two support plates. After this first series of tests, no cracks were evident on the structure and the stiffness matrix, measured before and after the tests, showed only slight changes.

The second series of tests caused damage to the structure. After the test at 100%, two vertical cracks formed in the lower parts of the right central foot and of the column support. The test at 200% damaged all four feet of the structure, where sub-vertical cracks appeared not necessarily following the vertical joints of the masonry (Figure B.7a).

For the third series of tests, the damaged model was consolidated to avoid that the cracked stone blocks could be pulled out of their locations by the large horizontal displacements. The repair consisted of confining the cracked stones of the low parts of the feet of the model, by adding steel brackets at different levels. The limits of this retrofitting technique were shown after the repetition of the test at 200%; indeed, the feet protection transferred the damage to the upper part of the structure (Figure B.7b).

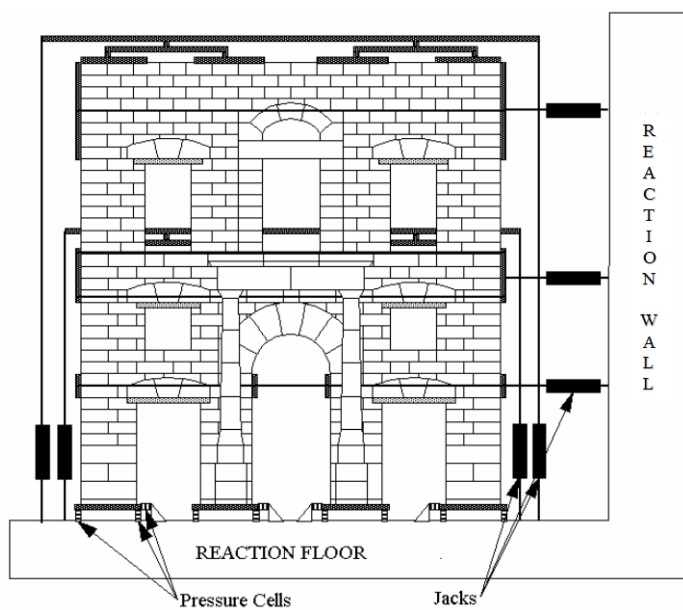


Figure B.5 Pseudo-dynamic tests of the specimen.

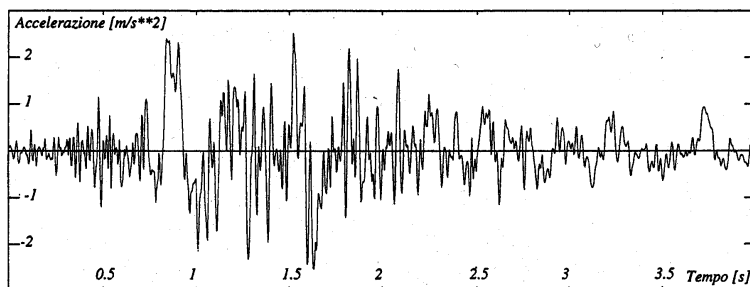


Figure B.6 Reference earthquake used for the pseudo-dynamic tests.

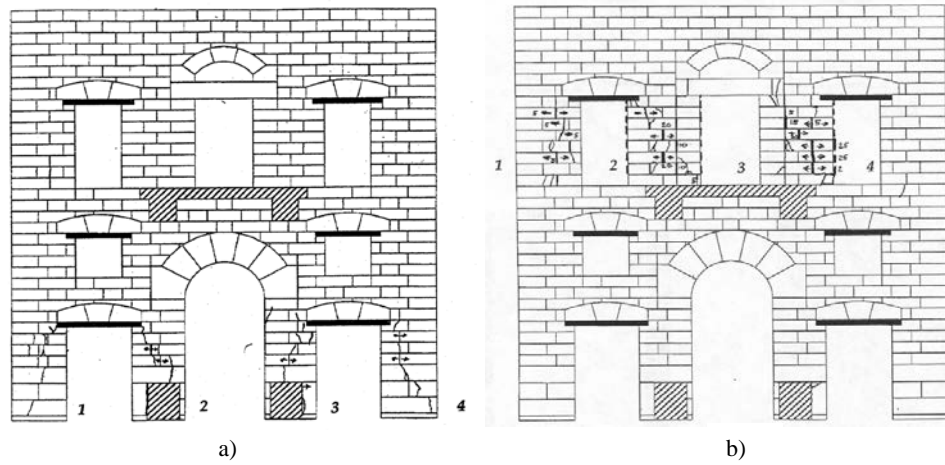


Figure B.7 Cracks formed into the structure following the pseudo-dynamic tests. (a) Model without the base isolation after the test at 200%. (b) Repaired model (without base isolation) after the test at 200%.

References

Despite each chapter contains its own reference list, for sake of fast consultation the reference list is reported in alphabetical order below. The list not only assembles all the chapters' references, but several reports, paper and book relevant to the thesis topic are also added.

- Aktan A.E. and Faust D., A Holistic Integrated Systems Approach to Assure the Mobility, Efficiency, Safety and Integrity of Highway Transportation, *Structural Health Monitoring and Intelligent Infrastructures*, Z. Wu and M. Abe (eds.), Balkema, Lisse, The Netherlands, Vol. 1, 2003, 7-18.
- Box G.E.P. and Wilson K.B., The Exploration and Exploitation of Response Surfaces: Some General Considerations and Examples, *Biometrics*, 10, 1954, 16-60.
- Breitung K. and Faravelli L., Response Surface Methods and Asymptotic Approximations, Chapter 6 in F. Casciati and J.B. Roberts (eds.), *Mathematical Models for Structural Reliability Analysis*, CRC Press, Boca Raton, USA, 1996, 227-285.

- Bucher C.G. and Borgund U.A., A Fast and Efficient Response Surface Approach for Structural Reliability Problems, *Structural Safety*, 7, 1990, 57-66
- Casciati F., Casciati S. and Faravelli L., Damage Detection via Response Surface Approximations, *Proceedings ICASP9*, A. Der Kiureghian et al. (eds.), Millpress, Rotterdam, The Netherlands, 2003, 511-516.
- Casciati F. and Faravelli L., *Fragility Analysis of Complex Structural Systems*, Research Studies Press, Taunton, UK, 1991..
- Casciati F., Rossi R., Fuzzy Chip Controllers and Wireless Links in Smart Structures, in *Keynote Lectures in SMART03*, Springer Verlag, 2003.
- Casciati S. and Faravelli L., Structural Damage Detection Based on Dynamic Response Identification, *Structural Health Monitoring 2002*, D. Balageas (ed.), DEStech Publications Inc., Lancaster, 2002, 1081-1090
- Casciati S., Colabrese E. and Magonette G. Damage Detection and Localization by Statistical Comparison of Response Time Histories, *Structural Health Monitoring 2003*, F-K.. Chang (ed.), DEStech, Lancaster, 2003a, 733-741
- Casciati S., Colabrese E. and Magonette G., Monitoring and Response Surface Methodology to detect and Locate Structural Damage, *Structural Health Monitoring and Intelligent Infrastructures*, Z. Wu and M. Abe (eds.), Balkema, Lisse, The Netherlands, Vol., 2003b, 423-429.
- Chang P., The Role of Health Monitoring in Infrastructure Management, *Structural Health Monitoring 2002*, D. Balageas (ed.), DEStech Publications Inc., Lancaster, 2002, 21-30
- Chase S.B. and Washer G., Nondestructive Evaluation for Bridge Management in the Next Century, *Public Roads*, , July-August, 1997, 16-25

- Chou and Ghaboussi, Genetic Algorithm in Structural Damage Detection, *Computers & Structures*, 79, 2001, 1335-1353.
- Der Kiureghian A., Madanat S. and Pestana J.M., *Proceedings ICASP9*, Millpress, Rotterdam, The Netherlands, 2003.
- Doebling S.W., Farrar C.R., Prime M.B., Shevitz D.W., Damage Identification and Health Monitoring of Structural and Mechanical Systems for Changes in Their Vibration Characteristics: a Literature Review, LA-13070-MS Report, Los Alamos National Laboratory, 1996.
- Doebling S.W., Farrar C.R., Prime M.B., Shevitz D.W., Damage Identification and Health Monitoring of Structural and Mechanical Systems for Changes in Their Vibration Characteristics, *Shock and Vibration Digest*, 30, 2, 1999.
- Draper, N. & Smith, H., *Applied Regression Analysis*, Wiley, New York, 1981.
- Faber M.H., Englund S. and Racwitz R., Aspect of Parallel Wire Cable Reliability, *Structural Safety*, 25, 2, 2003, 201-225
- Faravelli L., Response Surface Approach for Reliability Analysis, *J. Eng. Mech., ASCE*, 115, (12), 1989, 2763-2781
- Faravelli L., Structural Reliability via Response Surface, *Proc. IUTAM Symposium on Nonlinear Stochastic Mechanics*, N. Bellomo and F. Casciati (eds.), Springer Verlag, 1992, 213-223.
- Faravelli L., Blocking Problems in the Analysis of Random Fields, *Probabilities and Materials*, D. Breyse (ed.), NATO-ASI Series 269, Kluwer Academic Publishers, Dordrecht, The Netherlands, 1994, 177-196.
- Faravelli L., Modelling the Response of an Elastomeric Base Isolator, *Journal of Structural Control*, 8, 1, 2000, 17-30

- Faravelli L. and Pisano A., Damage Assessment Toward Performance Control, *Proceedings of DAMAS'97*, University of Sheffield, UK, 1997, 185-198.
- Faravelli L., Rossi R, Wireless communication between sensor/device stations, *Proceedings ICES02*, Rome, Balkema, 2003.
- Faravelli L. and Spencer J.B. (eds.), *Proceedings of the US-Europe Workshop on Sensor and Smart Structures Technology*, John Wiley & Sons, Chichester, UK, 2003.
- Farrar C.R. and Robertson A.N., An Introduction to the Los Alamos Damage Prognosis Project, *Structural Health Monitoring 2003*, F-K. Chang (ed.), DEStech Publications Inc, Lancaster, 2003,561-566.
- Frangopol D.M. and Neves L.C, Integrating Lifetime Performance and Life-cycle cost in Management of Civil Infrastructures, *Structural Health Monitoring and Intelligent Infrastructures*, Z. Wu and M. Abe (eds.), Balkema, Lisse, The Netherlands, Vol. 2, 2003,1097-1102.
- Fu G. and Moosa A.G., Structural Damage Diagnosis using High Resolution Images, *Structural Safety*, 23, 4, 2001, 281-295
- Gayton N., Bourinet J.M. and Lemaire M., CQ2RS: a New Statistical Approach to the Response Surface Method for Reliability Analysis, *Structural Safety*, 25, 1, 2003, 99-121
- Gen M. and Cheng R., *Genetic Algorithms and Engineering Optimization*, John Wiley and Sons, New York, 2000,.
- Gomes H.M. and Awruch A.M., Comparison of Response Surface and Neural Network with Other Methods for Structural Reliability Analysis, *Structural Safety*, 26, 1, 2004, 49-58

- Guan X.L. and Melchers R.E., Effect of Response Surface Parameters Variation on Structural Reliability Estimation, *Structural Safety*, 23, 4, 2001, 429-444
- Gupta S. and Manohar C.S., An Improved Response Surface Method for the Determination of Failure Probability and Importance Measures, *Structural Safety*, 26, 2, 2004, 123-139
- Hemez F.M, Robertson A.N. and Cundy A.L, Uncertainty Quantification and Model Validation for Damage Prognosis, *Structural Health Monitoring 2003*, F-K. Chang (ed.), DEStech Publications Inc, Lancaster, 2003,575-582.
- Inada T., Shimamura Y., Todoroki A., Kobayashi H and Nakamura H., Damage Identification Method for Smart Composite Cantilever Beam with Piezoelectric Materials, *Proceedings Structural Health Monitoring 2000*, F-K. Chang (ed.), DEStech, Lancaster, 2000, 986-994.
- Iwasaki, A., Todoroki, A. and Sugiyu, T. Remote Smart Damage Detection via Internet with Unsupervised Statistical Diagnosis, *Proc. IUTAM Symposium on Dynamics of Advanced Material and Smart Structures*, K. Watanabe and F. Ziegler (eds.), Kluwer Academic Publisher, Dordrecht, The Netherlands, 2002, 157-166.
- Johnson E.A., Lam H.F., Katafygiotis L.S. and Beck J.L., A Benchmark Problem for Structural Health Monitoring and Damage Detection, *Proc. 14th Engineering Mechanics Conference*, Austin Texas, 2000.
- Khuri A.I. and Cornell J.A., *Response Surfaces: Design and Analyses*, Marcel and Decker, New York, 1987,.
- Kim S-H. and Na S-W., Response Surface Method Using Vector Projected Sampling Points, *Structural Safety*, 19, 1, 1997, 3-19

- Kleinbaum, D.G. and Kupper, L.L., *Applied Regression Analysis and Other Multivariable Methods*, Duxbury Press, Boston, USA, 1978.
- Krawczuc M. and Ostachowicz W., Spectral Beam Finite Element and Genetic Algorithm for Crack Detection in Beams, *Structural Health Monitoring 2001*, F-K. Chang (ed.), DEStech Publications Inc., 2001, Lancaster, 889-898.
- Liu Y.W. and Moses F.A., A Sequential Response Surface Method and its Application in the Reliability Analysis of Aircraft Structural Systems, *Structural Safety*, 16, 1994, 39-46
- Marwala T., Probabilistic Fault Identification using a Committee of Neural Networks and Vibration Data, *AIAA, Journal of Aircraft*, 38, 2001, 138-146.
- Masri S.F., Smyth A.W., Chassiakos A.G., Caughey T.K. and Hunter N.F., Application of Neural Networks for Detection of Changing in Nonlinear Systems, *J. Eng. Mech., ASCE*, 126, 7, 2000, 666-683.
- Melchers R.E., *Structural Reliability Analysis and Prediction*, 2nd Edition, John Wiley & Sons, Chichester, UK, 1999.
- Myers R.H., *Response Surface Methodology*, Allyn and Bacon, Boston, 1971
- Myers R.H. and Montgomery D.C., *Response Surface Methodology: Process and Product Optimization using Design Experiments*, John Wiley & Sons, 1995.
- Nakamura M., Masri S.F., Chassiakos A.G. and Caughey T.K., A Method for Non-parametric Detection through the Use of Neural Networks, *Earthquake Engineering and Structural Dynamics*, 27, 1998, 997-1010.
- Peeters B., System Identification and Damage Detection in Civil Engineering, PhD Thesis, K.U. Leuven Civil Engineering Department, 2000.

- Petersen R.G., *Design and Analysis of Experiments*, Marcel Decker, New York, 1985.
- Pisano A., *Structural System Identification: Advanced Approaches and Applications*, PhD Thesis, University of Pavia, Dept. of Structural Mechanics, 1997.
- Rajashekhar M.R. and Ellingwood B.R., A New Look at the Response Surface Approach for Reliability Analysis, *Structural Safety*, 12, 1993, 205-220
- Romero V.J., Swiler L.P. and Giunta A.A., Construction of Response Surfaces Based on Progressive-Lattice-Sampling Experimental Design with Application to Uncertainty Propagation, *Structural Safety*, 26, 2, 2004, 201-219
- Shinozuka M, Homeland security and safety, *Structural Health Monitoring and Intelligent Infrastructures*, Z. Wu and M. Abe (eds.), Balkema, Lisse, The Netherlands, Vol. 2, 2003,1139-1145.
- Sohn H., Farrar C.R., Hemez F.M., Czamecki J.J., Shunk D. D., Stinemates D.W. and Nadler B.R., A Review of Structural Health Monitoring Literature: 1996-2001, LA-MS Report, Los Alamos National Laboratory. Distributed at the SAMCO Summer School, Cambridge, 2003.
- Stahl F.L. and Gagnon C.C., *Cable Corrosion in Bridges and Other Structures*, ASCE Press, 1995.
- Van der Auweraer H. and Peeters B., International Research Projects on Structural Health Monitoring: an Overview, *Structural Health Monitoring*, 2 (4), 2003, 341-358.
- Wong F.S., Uncertainties in Dynamic Soil-Structure Interaction, *J. Eng. Mech.*, ASCE, 110, 1984, 308-324

- Wong F.S., Slope Reliability and Response Surface Method, *J. Geo Eng., ASCE*, 111, 1985, 32-53
- Wong K-Y., Instrumentation and Health Monitoring of Cable-Supported Bridges, *Journal of Structural Control and Health Monitoring*, 11, 2, 2004.
- Xu B., Wu Z.S. and Yokoyama K., Response Time Series Based Structural Parametric Assessment Approach with Neural Networks, *Structural Health Monitoring and Intelligent Infrastructures*, Z. Wu and M. Abe (eds.), Balkema, Lisse, The Netherlands, Vol. 1, 2003, 601-609.
- Yi J-H. and Feng M.Q., Stochastic Optimization Techniques for NDE of Bridges using Vibration Signatures, *Smart Structures and Materials 2003*, SPIE 5057, S-C. Liu (ed.), SPIE, Bellingham, 2003, 582-593.
- Zheng H.T., Xue S.T., Qian Y.Y., Xie L.Y. and Mita A, Structural Damage Identification by Neural Networks and Modal Analysis, *Structural Health Monitoring and Intelligent Infrastructures*, Z. Wu and M. Abe (eds.), Balkema, Lisse, The Netherlands, Vol. 1, 2003, 635-639.

Other Theses

Dottorandi del X Ciclo

1. Marco Battaini "Sistemi strutturali controllati: progettazione e affidabilità" (Febbraio 1998).
2. Claudia Mariani "Problemi di ottimizzazione per strutture bidimensionali anisotrope" (Febbraio 1998).
3. Antonella Negri "Stima delle perdite idrologiche nei bacini di drenaggio urbani" (Febbraio 1999).

Dottorandi dell' XI Ciclo

4. Aurora Angela Pisano "Structural System Identification: Advanced Approaches and Applications" (Febbraio 1999).
5. Carla Saltalippi "Preannuncio delle piene in tempo reale nei corsi d'acqua naturali" (Febbraio 1999).

- 6.** Eugenio Barbieri “Thermofluid dynamics and topology: optimisation of an active thermal insulation structure (Ottobre 1999).

Dottorandi del XII Ciclo

- 7.** Massimiliano Barbolini “Dense snow avalanches: computational models, hazard mapping and related uncertainties” (Ottobre 1999).
- 8.** Paolo Espa “Moti atmosferici generati da forze di galleggiamento: simulazioni numeriche e studio su modello fisico” (Ottobre 1999)
- 9.** Lorenza Petrini “Shape memory alloys: modelling the martensitic phase behaviour for structure engineering exploitation” (Ottobre 1999).

Dottorandi del XIII Ciclo

- 10.** Stefano Podestà “Risposta sismica di antichi edifici religiosi in muratura: una nuova proposta per un modello di vulnerabilità” (Ottobre 2001).
- 11.** Daniele Sturla “Simulazioni lagrangiane di flussi rapidamente variati nell’approssimazione di acque poco profonde” (Ottobre 2002).

Dottorandi del XV Ciclo

- 12.** Francesco Marazzi “Semi-active control of civil structures: implementation aspects” (Ottobre 2002).
- 13.** Roberto Nascimbene “Sail modelling for maximal speed optimum design” (Ottobre 2002).

Dottorandi del XVI Ciclo

- 14.** Massimo Giudici “Progettazione in regime non lineare di strutture in CAP a cavi aderenti e non aderenti” (Ottobre 2003).
- 15.** Matteo Mutti “Stability analysis of stratified three-phase flows in pipes” (Ottobre 2003).
- 16.** Gabriella Petaccia “Propagazione di onde a fronte ripido per rottura di sbarramenti in alvei naturali” (Ottobre 2003).
- 18.** Tiziana D’Amico “Ricerca e Sviluppo di Metodologie Diagnostiche per il Recupero di Edifici Monumentali: Prove Vibroacustiche sul Tufo” (Ottobre 2004).

Dottorandi del XVII Ciclo

- 17.** Sara Casciati “Damage Detection and Localization in the Space of the Observed Variables” (Ottobre 2004).